Development of Design Methods for Geosynthetic Reinforced Flexible Pavements

FHWA Report Reference:
DTFH61-01-X-00068

Final Report

Prepared for the
U.S. DEPARTMENT OF TRANSPORTATION
FEDERAL HIGHWAY ADMINISTRATION

May 25, 2004

Prepared by

Dr. Steven W. Perkins
Associate Professor
Department of Civil Engineering
Western Transportation Institute
Montana State University – Bozeman
Bozeman, Montana 59717
Office Telephone: 406-994-6119
Fax: 406-994-6105
E-Mail: stevep@ce.montana.edu

AND

Dr. Barry R. Christopher
Christopher and Associates
210 Boxelder Lane
Roswell, Georgia, USA

Mr. Eli L. Cuelho
Research Engineer
Western Transportation Institute
Montana State University – Bozeman
Bozeman, Montana USA

Dr. Gudmund R. Eiksund
Senior Research Engineer
SINTEF Civil and Environmental Engineering
Trondheim, Norway

Dr. Inge Hoff
Senior Research Engineer
SINTEF Civil and Environmental Engineering
Trondheim, Norway

Dr. Charles W. Schwartz
Associate Professor
University of Maryland
College Park, Maryland USA

Dr. Geir Svanø
Senior Research Engineer
SINTEF Civil and Environmental Engineering
Trondheim, Norway

Mr. Arnstein Watn
Research Director
SINTEF Civil and Environmental Engineering
Trondheim, Norway

TECHNICAL REPORT STANDARD PAGE

1. Report No. **DTFH61-01-X-00068**	2. Government Accession No.	3. Recipient's Catalog No.
4. Title and Subtitle **Development of Design Methods for Geosynthetic Reinforced Flexible Pavements**	5. Report Date **May 25, 2004** 6. Performing Organization Code **MSU G&C #426202**	
7. Authors **Steven W. Perkins, Ph.D., P.E.** **Barry R. Christopher, Ph.D., P.E.** **Eli L. Cuelho, P.E.** **Gudmund R. Eiksund, Ph.D.** **Inge Hoff, Ph.D.** **Charles W. Schwartz, Ph.D.** **Geir Svanø, Ph.D.** **Arnstein Watn**	8. Performing Organization Report No.	
9. Performing Organization Name and Address **Department of Civil Engineering** **205 Cobleigh Hall** **Montana State University** **Bozeman, Montana 59717**	10. Work Unit No. 11. Contract or Grant No. **DTFH61-01-X-00068**	
12. Sponsoring Agency Name and Address **Federal Highway Administration** **400 Seventh Street, S.W. Room 4410** **Washington D.C. 20590**	13. Type of Report and Period Covered **Final: August 30, 2001 – January 31, 2004** 14. Sponsoring Agency Code **FHWA-HIPT**	
15. Supplementary Notes		

16. Abstract

Base reinforcement in pavement systems using geosynthetics has been found under certain conditions to provide improved performance. Current design methods for flexible pavements reinforced with a geosynthetic in the unbound aggregate base layer are largely empirical methods based on a limited set of design conditions over which test sections have been constructed. These design methods have been limited in use due to the fact that the methods are not part of a nationally recognized pavement design procedure, the methods are limited to the design conditions in the test sections from which the method was calibrated, and the design methods are often times proprietary and pertain to a single geosynthetic product.

The first U.S. nationally recognized mechanistic-empirical design guide for flexible pavements is currently under development and review (NCHRP Project 1-37A, NCHRP 2003). The purpose of this project was to develop design methods for geosynthetic reinforced flexible pavements that are compatible with the methods being developed in NCHRP Project 1-37A. The methods developed in this project, while compatible with the NCHRP 1-37A Design Guide, are sufficiently general so as to allow the incorporation of these methods into other mechanistic-empirical design methods.

The design components addressed in this project include material and damage models for the different layers of the pavement cross section, incorporation of reinforcement into a finite element response model, and the development of response model modules that account for fundamental mechanisms of reinforcement. Mechanistic material models are required for all components of the pavement cross section included in the finite element response model. Material models from the NCHRP 1-37A Design Guide for the asphalt concrete, and the unbound aggregate and subgrade layers are used in this study. Additional material models for the unbound aggregate layer are also examined. Material models for components associated with the reinforcement are developed in this project. These include a material model for the reinforcement itself, and an interface shear interaction model for the reinforcement-aggregate and reinforcement-subgrade interaction surfaces. Along with these material models, testing methods providing parameters for use in the material

models have been examined and preliminarily evaluated. These testing methods include tension tests for evaluating non linear direction dependent elastic constants for the reinforcement and cyclic pullout tests for evaluating a stress dependent interface shear resilient modulus. These tests have been devised to provide parameters pertinent to small strain and displacement conditions present in pavement applications.

Empirical damage models from the NCHRP 1-37A Design Guide for asphalt concrete fatigue and permanent deformation of asphalt concrete, and unbound aggregate and subgrade layers have been used in this project. A damage model for permanent deformation of unbound aggregate within a zone influenced by the reinforcement was developed and is based on the NCHRP 1-37A Design Guide model for unbound aggregate but with parameters adjusted by reinforcement ratios. Large-scale reinforced repeated load triaxial tests have been performed on aggregate materials to provide methods for assessing reinforcement ratios and the zone of reinforcement over which these ratios apply.

An additional empirical model was developed to describe the growth of permanent interface shear stress with traffic passes on a reinforced pavement. Theoretical considerations are made to relate the permanent shear stress to permanent and resilient strains seen in the reinforcement. Normalized relationships between the permanent to resilient reinforcement strain ratio and traffic passes are developed for three reinforcement materials from reinforcement strain data from previously constructed test sections. The permanent interface shear stress is used in response model modules to account for confinement effects of the reinforcement on base aggregate materials during vehicular loading of the pavement.

Finite element response models for unreinforced pavement cross sections were developed following guidelines in the NCHRP 1-37A Design Guide. Reinforcement was added to the response model by including a layer of membrane elements for the reinforcement and contact interface surfaces for both sides of the reinforcement. Evaluation of reinforced response models by simply including a reinforcement sheet with interface surfaces clearly showed the inability of such a simple static single load cycle analysis for predicting performance of reinforced pavements. This exercise indicated that fundamental mechanisms and processes involved in reinforced pavements are missing from such an approach and that auxiliary response model modules were needed to account for these mechanisms.

Additional models included a response model module created to account for effects of the reinforcement on the aggregate layer during construction. This compaction model describes the increase in confinement of the aggregate layer as lateral movement of the aggregate is restrained during compaction through shear interaction with the reinforcement. Modeling of this process within the context of a finite element response model consisted of the application of a shrinkage strain to the reinforcement and the monitoring of increased lateral stress in the aggregate. Pavement load is not applied in this model. The lateral stresses in the aggregate arising from this analysis are used as initial stresses in subsequent response model modules.

A second response model module (traffic I model) of the reinforcement pavement is then created by using the initial stresses from the compaction model. Pavement load is applied to this model with the distribution of interface shear stress between the reinforcement and the surrounding materials being extracted from the model. The interface shear stresses are taken as resilient values and used in the interface shear stress growth model to determine a permanent interface shear stress distribution for different periods in the life of the pavement. A finite number (typically 6) of distributions are created for different periods and used to compute equivalent lateral force distributions acting horizontally on the aggregate layer.

A third response model module (traffic II model) is created by applying the force distribution arising from the traffic I model to nodes at the level of the reinforcement in an otherwise unreinforced pavement cross section. This analysis is repeated for the number of force distributions created from the traffic I model. For each analysis, the lateral stresses in the base aggregate layer are extracted and used as initial stresses in subsequent response models. This step describes the influence of traffic loading on the increase in confinement of the aggregate layer as shear interaction occurs between the aggregate and the reinforcement.

A fourth response model module (traffic III model) of the reinforced pavement is created by using the initial stresses from the traffic II model. Pavement load is applied to this model and is repeated for each of the initial stress conditions corresponding to different periods in the life of the pavement. From these analyses, vertical strain in the pavement layers and tensile strain in the asphalt concrete layer are extracted as response measures and used in damage models to compute permanent surface deformation of the pavement as a function of traffic passes and fatigue life of the asphalt concrete. The damage model for permanent deformation of aggregate within a zone of reinforcement is used to compute permanent surface deformation.

The unreinforced models were field calibrated from test sections constructed in two pavement test facilities. One facility involved the use of full scale tests loaded by a heavy vehicle simulator. The second facility involved the use of

large-scale laboratory model tests. Reinforced models were then compared to test sections from these same two facilities. In general, favorable agreement was seen between predictions from the models and results from pavement test sections.

A sensitivity study was performed to examine the effect of reinforcement for a range of pavement cross sections. In general, the effects of reinforcement on permanent surface deformation are consistent with observed results from pavement test sections. Modest benefits were observed for thick pavement cross sections and pavement sections on a firm subgrade while test sections are not available to confirm these results. In terms of fatigue life, significant effects from the reinforcement were observed. Since the distress feature of rutting has been readily observed in reinforced pavement test sections while asphalt concrete fatigue life has been more difficult to observe and quantify, experimental support for these predictions is lacking.

In general, the methods developed in this project appear to describe reinforced pavement performance generally observed in test sections constructed to date. Significant improvement in terms of the number of traffic passes needed to reach a specified pavement surface deformation was observed for pavements constructed over relatively weak subgrades. The method has been formulated to be generic such that properties of the reinforcement established from different test methods are used as input. Steps needed for implementation of these procedures in the NCHRP 1-37A Design Guide software are provided in this report.

17. Key Words		18. Distribution Statement	
Pavements, Highways, Geogrid, Geotextile, Geosynthetic, Reinforcement, Base Course, Finite Element Modeling, Mechanistic-Empirical Modeling		**Unrestricted. This document is available through the National Technical Information Service, Springfield, VA 21161.**	
19. Security Classif. (of this report) **Unclassified**	20. Security Classif. (of this page) **Unclassified**	21. No. of Pages **263**	22. Price

PREFACE

DISCLAIMER STATEMENT

This document is disseminated under the sponsorship of the United States Federal Department of Transportation in the interest of information exchange. The United States Government assumes no liability of its contents or use thereof.

The contents of this report reflect the views of the authors, who are responsible for the facts and accuracy of the data presented herein. The contents do not necessarily reflect the official policies of the United States Department of Transportation

The United States Government does not endorse products of manufacturers. Trademarks or manufacturers' names appear herein only because they are considered essential to the object of this document

This report does not constitute a standard, specification, or regulation.

ALTERNATIVE FORMAT STATEMENT

The Federal Highway Administration attempts to provide reasonable accommodations for any known disability that may interfere with a person participating in any service, program, or activity of the Department. Alternative accessible formats of this document will be provided upon request.

ACKNOWLEDGMENTS

The author gratefully acknowledges the financial and technical support of the principal sponsor, the U.S. Federal Highway Administration, and the supporting sponsors including the Finnish, Norwegian and Swedish National Road Administrations, Bidim Geosynthetics, TeleTextiles, ASA, and Tensar Earth Technologies, Inc. The author acknowledges the shared responsibilities and technical contributions from the partners and subcontractors constituting the project team including the Western Transportation Institute (Mr. Eli Cuelho), SINTEF Civil and Environmental Engineering, Trondheim, Norway (Dr. Gudmund Eiksund, Dr. Inge Hoff, Dr. Geir Svanø and Mr. Arnstein Watn), Christopher Consultants, Atlanta, Georgia (Dr. Barry Christopher), and the University of Maryland, College Park, Maryland (Dr. Charles Schwartz).

TABLE OF CONTENTS

LIST OF TABLES

LIST OF FIGURES

CONVERSION FACTORS

The following conversion factors are required for interpretation of results contained in this report.

1 m = 3.28 ft
1 mm = 0.0394 in
1 kN = 225 lb
1 kN/m = 68.6 lb/ft
1 kPa = 0.145 psi
1 kN/m^3 = 6.37 lb/ft^3

EXECUTIVE SUMMARY

Base reinforcement in pavement systems using geosynthetics has been found under certain conditions to provide improved performance. Current design methods for flexible pavements reinforced with a geosynthetic in the unbound aggregate base layer are largely empirical methods based on a limited set of design conditions over which test sections have been constructed. These design methods have been limited in use due to the fact that the methods are not part of a nationally recognized pavement design procedure, the methods are limited to the design conditions in the test sections from which the method was calibrated, and the design methods are often times proprietary and pertain to a single geosynthetic product.

The first U.S. nationally recognized mechanistic-empirical design guide for flexible pavements is currently under development and review (NCHRP Project 1-37A, NCHRP 2003). The purpose of this project was to develop design methods for geosynthetic reinforced flexible pavements that are compatible with the methods being developed in NCHRP Project 1-37A. The methods developed in this project, while compatible with the NCHRP 1-37A Design Guide, are sufficiently general so as to allow the incorporation of these methods into other mechanistic-empirical design methods.

The design components addressed in this project include material and damage models for the different layers of the pavement cross section, incorporation of reinforcement into a finite element response model, and the development of response model modules that account for fundamental mechanisms of reinforcement. Mechanistic material models are required for all components of the pavement cross section included in the finite element response model. Material models from the NCHRP 1-37A Design Guide for the asphalt concrete, and the unbound aggregate and subgrade layers are used in this study. Additional material models for the unbound aggregate layer are also examined. Material models for components associated with the reinforcement are developed in this project. These include a material model for the reinforcement itself, and an interface shear interaction model for the reinforcement-aggregate and reinforcement-subgrade interaction surfaces. Along with these material models, testing methods providing parameters for use in the material models have been examined and preliminarily evaluated. These testing methods include tension tests for evaluating non linear direction dependent elastic constants for the reinforcement and cyclic pullout tests for evaluating a stress dependent interface shear resilient modulus. These tests have been devised to provide parameters pertinent to small strain and displacement conditions present in pavement applications.

Empirical damage models from the NCHRP 1-37A Design Guide for asphalt concrete fatigue and permanent deformation of asphalt concrete, and unbound aggregate and subgrade layers have been used in this project. A damage model for permanent deformation of unbound aggregate within a zone influenced by the reinforcement was developed and is based on the NCHRP 1-37A Design Guide model for unbound aggregate but with parameters adjusted by reinforcement ratios. Large-scale reinforced repeated load triaxial tests have been performed on aggregate materials to provide methods for assessing reinforcement ratios and the zone of reinforcement over which these ratios apply.

An additional empirical model was developed to describe growth of permanent interface shear stress with traffic passes on a reinforced pavement. Theoretical considerations are made to relate the permanent shear stress to permanent and resilient strains seen in the reinforcement. Normalized relationships between the permanent to resilient reinforcement strain ratio and traffic passes are developed for three reinforcement materials from reinforcement strain data from previously constructed test sections. The permanent interface shear stress is used in response model modules to account for confinement effects of the reinforcement on base aggregate materials during vehicular loading of the pavement.

Finite element response models for unreinforced pavement cross sections were developed following guidelines in the NCHRP 1-37A Design Guide. Reinforcement was added to the response model by including a layer of membrane elements for the reinforcement and contact interface surfaces for both sides of the reinforcement. Evaluation of reinforced response models by simply including a reinforcement sheet with interface surfaces clearly showed the inability of such a simple static single load cycle analysis for predicting performance of reinforced pavements. This exercise indicated that fundamental mechanisms and processes involved in reinforced pavements are missing from such an approach and that auxiliary response model modules were needed to account for these mechanisms.

Additional models include a response model module created to account for effects of the reinforcement on the aggregate layer during construction. This compaction model describes the increase in confinement of the aggregate layer as lateral movement of the aggregate is restrained during compaction through shear interaction with the reinforcement. Modeling of this process within the context of a finite element response model consisted of the application of a shrinkage strain to the reinforcement and the monitoring of increased lateral stress in the aggregate. Pavement load is not applied in this model. The lateral stresses in the aggregate arising from this analysis are used as initial stresses in subsequent response model modules.

A second response model module (traffic I model) of the reinforcement pavement is then created by using the initial stresses from the compaction model. Pavement load is applied to this model with the distribution of interface shear stress between the reinforcement and the surrounding materials being extracted from the model. The interface shear stresses are taken as resilient values and used in the interface shear stress growth model to determine a permanent interface shear stress distribution for different periods in the life of the pavement. A finite number (typically 6) of distributions are created for different periods and used to compute equivalent lateral force distributions acting horizontally on the aggregate layer.

A third response model module (traffic II model) is created by applying the force distribution arising from the traffic I model to nodes at the level of the reinforcement in an otherwise unreinforced pavement cross section. This analysis is repeated for the number of force distributions created from the traffic I model. For each analysis, the lateral stresses in the base aggregate layer are extracted and used as initial stresses in subsequent response models. This step describes the influence of traffic loading on the increase in confinement of the aggregate layer as shear interaction occurs between the aggregate and the reinforcement.

A fourth response model module (traffic III model) of the reinforced pavement is created by using the initial stresses from the traffic II model. Pavement load is applied to this model and is repeated for each of the initial stress conditions corresponding to different periods in the life of the pavement. From these analyses, vertical strain in the pavement layers and tensile strain in the asphalt concrete layer are extracted as response measures and used in damage models to compute permanent surface deformation of the pavement as a function of traffic passes and fatigue life of the asphalt concrete. The damage model for permanent deformation of aggregate within a zone of reinforcement is used to compute permanent surface deformation.

The unreinforced models were field calibrated from test sections constructed in two pavement test facilities. One facility involved the use of full scale tests loaded by a heavy vehicle simulator. The second facility involved the use of large-scale laboratory model tests. Reinforced models were then compared to test sections from these same two facilities. In general, favorable agreement was seen between predictions from the models and results from pavement test sections.

A sensitivity study was performed to examine the effect of reinforcement for a range of pavement cross sections. In general, the effects of reinforcement on permanent surface deformation are consistent with observed results from pavement test sections. Modest benefits were observed for thick pavement cross sections and pavement sections on a firm subgrade while test sections are not available to confirm these results. In terms of fatigue life, significant effects from the reinforcement were observed. Since the distress feature of rutting has been readily observed in reinforced pavement test sections while asphalt concrete fatigue life has been more difficult to observe and quantify, experimental support for these predictions is lacking.

In general, the methods developed in this project appear to describe reinforced pavement performance generally observed in test sections constructed to date. Significant improvement in terms of the number of traffic passes needed to reach a specified pavement surface deformation was observed for pavements constructed over relatively weak subgrades. The method has been formulated to be generic such that properties of the reinforcement established from different test methods are used as input. Steps needed for implementation of these procedures in the NCHRP 1-37A Design Guide software are provided in this report.

1.0 INTRODUCTION

Existing design methods for flexible pavements reinforced with a geosynthetic in the unbound base aggregate layer are largely empirically based (Berg et al., 2000). These existing design methods have been limited in use by many state departments of transportation due to several factors, namely:

1. Design methods are not part of a nationally recognized pavement design procedure
2. Design methods are often times applicable to a narrow range of design conditions
3. Design methods are often times proprietary, making it difficult to directly compare the cost-benefit of several reinforcement products from different manufacturers

The first nationally recognized mechanistic-empirical design guide for flexible pavements in the United States being developed under NCHRP Project 1-37A (NCHRP 2003), herein referred to as the NCHRP 1-37A Design Guide, presents a unique opportunity to provide a design method that overcomes the problems noted above. A significant motivation for the development of the NCHRP 1-37A Design Guide was to provide the ability to evaluate new pavement materials for which a significant historical data base of performance is not available. This is accomplished by the use of mechanics-based pavement response models and sufficiently descriptive material models for the various pavement layers that provide a rigorous means of assessing pavement response measures (i.e. vertical strain in all pavement layers and tensile strain in the asphalt concrete layer), which are later used in empirical damage models to assess long term pavement performance. Given the complex nature of a geosynthetic reinforced flexible pavement and the introduction of a host of new variables associated with the reinforcement, a mechanistic procedure is ideally suited and even essential for providing a design method that is both generic and comprehensive.

The purpose of this project was to develop design procedures that, in general, fall within the category of mechanistic-empirical methods and, in particular, are compatible with procedures developed under the NCHRP 1-37A Design Guide. As such, many of the response model, material model and damage model procedures incorporated in the NCHRP 1-37A Design Guide are used as a starting point in this project. To include the reinforcement in the pavement design cross section, new material models associated with the reinforcement and its shear interaction with surrounding materials were introduced. The pavement response model (in this project a finite element model is used) was also modified to include a layer of reinforcement with contact interfaces between the reinforcement and the surrounding materials. Several additional response modeling steps or modules were introduced to account for the mechanical action of the reinforcement on the pavement system during construction and loading by vehicular traffic. Lastly, the damage model for permanent strain in the unbound aggregate layer was reevaluated to account for the influence of reinforcement on the development of permanent vertical strain.

This report first describes the material models that are used for the pavement layers. Several of these models are identical to those used in the NCHRP 1-37A Design Guide. New models are introduced for the new components of the system associated with the reinforcement. Additional models for the base aggregate layer are introduced and later used in response models to evaluate the importance of this selection. The tests needed to define material properties associated with these models are described. Some of these tests are those developed for the NCHRP 1-37A Design Guide while others associated with the reinforcement are extensions of tests previously developed for reinforcement materials. A summary of material parameters is given for actual pavement materials tested in this project. These materials correspond to those used in previously constructed test sections to which this design procedure is calibrated against.

Section 4 provides a description of the procedures followed to set up finite element pavement response models of unreinforced pavement cross sections, where these procedures follow those contained in the NCHRP 1-37A Design Guide. Given the need to introduce new components associated with the reinforcement layer, a general purpose finite element package (Abaqus, Hibbitt et al., 2002) was used. Steps taken to verify the set up and calculations of the response models are provided. Section 5 details procedures established for the set up of response models for reinforced cross sections.

Section 6 describes how the response and damage models were field calibrated from the unreinforced test sections. Results from models of the reinforced test sections are then compared to rutting measurements from those sections. These test sections include full-scale indoor test sections loaded by a heavy vehicle simulator (Perkins, 2002) and large-scale box test sections cyclically loaded by a stationary circular plate (Perkins, 1999). Results from other test sections reported by other studies were not used due to the absence of material properties for the pavement layers needed in the models used in this project

Section 7 provides results from a sensitivity study where a range of pavement cross sections, geosynthetic types and subgrade types were used in models. Section 8 provides results from a study where the material model type used for the base aggregate layer was varied. Section 9 provides a summary and discussion of the methods developed in this project, while Section 10 discusses research that is needed to address issues raised in this project.

2.0 BACKGROUND

Geosynthetic materials have been used in the aggregate base course layer of flexible pavements for the past 25 years. Research studies conducted over this period have demonstrated the ability of the reinforcement to reduce the rate of permanent surface deformation (rutting) due to the accumulation of permanent strain in the unbound layers (i.e. base and subgrade layers). Berg et al. (2000) provided a summary of experimental, modeling and design development work up to the year 2000. The majority of the test sections evaluated to date have been relatively thin pavement sections on weak subgrade materials. The effect of the reinforcement has been evaluated mainly in terms of its ability to reduce the rate of rutting. Since the performance of the majority of these pavement sections appeared to be controlled by rutting, the effect of reinforcement on the fatigue life of the asphalt concrete layer has not been experimentally established.

Berg et al. (2000) also describes several empirical design techniques that were developed from the results of constructed test sections. Most of these design solutions were developed for a particular reinforcement product and have been used successfully for projects where conditions were similar to those in the test sections from which the solution was developed.

Numerical modeling studies of reinforced pavements were also summarized in Berg et al. (2000). The majority of these studies used finite element techniques and treated the problem by simply including a reinforcement layer with contact interfaces between the reinforcement and the pavement layers into the finite element response model. With a single vehicular load applied to these models, the models tended to show a response improvement as compared to an unreinforced section that was significantly lower than that observed in experimental test sections. These studies point to the need for additional modeling steps and considerations that account for the fundamental mechanisms of reinforcement operating in reinforced pavements. In this project, the models developed are used to illustrate this point and to provide these additional steps that account for these mechanisms.

3.0 MATERIAL MODELS, TESTS AND PARAMETERS

The finite element response model and damage models used in this study were selected to match those anticipated for use in the NCHRP 1-37A Design Guide corresponding to NCHRP Project 1-37A (NCHRP 2003). In this project, material models from the NCHRP 1-37A Design Guide for the asphalt concrete and unbound aggregate and subgrade soils were used. Damage models from the NCHRP 1-37A Design Guide for permanent deformation in the asphalt concrete and unbound layers, and for fatigue in the asphalt concrete were used. In addition to these models, several additional material models were used for the unbound aggregate. These additional models were examined in order to provide guidance on whether the type of unbound aggregate material model influenced the ability of the method to predict base-reinforced pavement performance.

The addition of reinforcement to the pavement system required the introduction of several material models for components associated with the reinforcement. These included a material model for the reinforcement sheet, a material model for the reinforcement-aggregate interaction, a revised damage model for permanent deformation for aggregate influenced by the reinforcement and an interface shear stress growth model that is used to describe the effect of restraining shear stresses acting on the aggregate by the reinforcement on confinement of the aggregate layer. Table 3.0.1 provides a list of the various material and damage models that have been used in this project.

3.1 Asphalt Concrete

Test sections previously reported by Perkins (1999, 2002) and used in this project for purposes of model comparison and validation used two different asphalt concrete mixes. Dynamic modulus tests were performed on these mixes to provide input parameters for elastic modulus and Poisson's ratio as a function of temperature and load frequency. Default damage models for asphalt concrete permanent deformation and fatigue from the NCHRP 1-37A Design Guide were used and are described below.

Table 3.0.1 Material and damage models used in this study

	Mechanistic Models		Empirical Models	
	NCHRP 1-37A Material Models	Additional Material Models	NCHRP 1-37A Damage Models	Other Models
Asphalt Concrete	• Dynamic Modulus		• Permanent Deformation • Fatigue	
Unbound Aggregate	• Isotropic Non-Linear Elastic with Tension Cutoff	• Isotropic Linear Elastic • Isotropic Linear Elastic with Tension Cutoff • Anisotropic Linear Elastic • Anisotropic Linear Elastic with Tension Cutoff • Anisotropic Non-Linear Elastic	• Permanent Deformation of Unreinforced Aggregate	• Permanent Deformation of Reinforced Aggregate
Reinforcement-Aggregate Interaction		• Coulomb Friction		• Interface Shear Stress Growth
Reinforcement		• Isotropic Linear Elastic		
Subgrade Soil	• Isotropic Non-Linear Elastic with Tension Cutoff		• Permanent Deformation	

3.1.1 Dynamic Modulus

Asphalt concrete material testing was conducted at the University of Maryland to determine dynamic modulus master curves and temperature shift relationships for two asphalt concrete mixes used in previously constructed test sections. The testing approach for this study followed recommendations from the NCHRP 1-37A Design Guide (NCHRP 2003) draft for instrumentation and testing details, which are based on those developed for the Superpave Simple Performance Test (NCHRP Project 9-19). Since all asphalt materials in this study were provided as field cores, it was impossible to fabricate specimens conforming exactly to the NCHRP 1-37A Design Guide due to the limited height of the field cores.

Two asphalt concrete mixtures from previous large-scale laboratory and field tests of pavements with geosynthetic base layer reinforcement were tested and included:

- MSU (laboratory box tests performed at Montana State University, Perkins 1999)
- CRREL (indoor field tests performed at the U.S. Army Corps of Engineers Cold Regions Research and Engineering Laboratory, Perkins 2002)

Volumetric and binder information for these two mixtures is summarized in Table 3.1.1. Aggregate grain size distributions are summarized in Figures 3.1.1 and 3.1.2.

Table 3.1.1 Properties of asphalt mixtures

Material	Binder Viscosity (CTS)	Air Voids (%)	Rice Gravity	Asphalt Content (%)
MSU	350	3.3 – 5.6	2.43	6.5
CRREL	NA	13.2 – 18.9	2.62	5.0

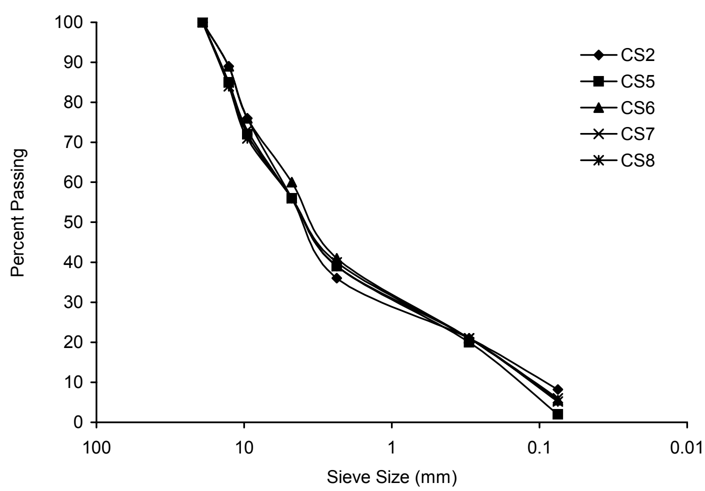

Figure 3.1.1 Aggregate gradation for MSU asphalt mixture

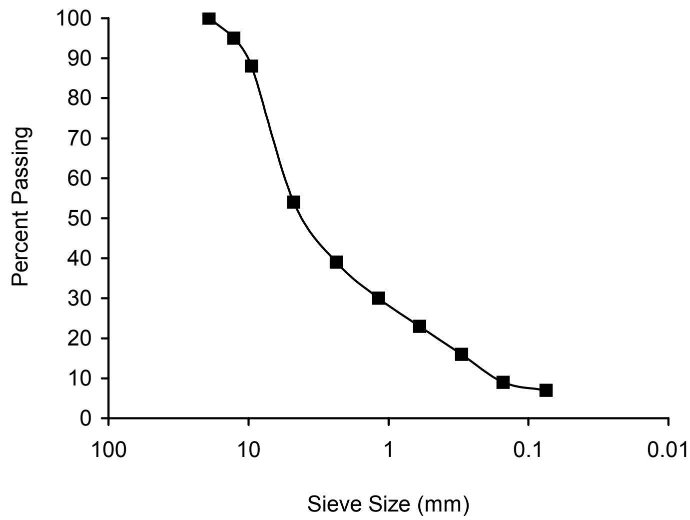

Figure 3.1.2 Aggregate gradation for CRREL asphalt mixture

The asphalt mixtures were provided in the form of field cores from the test sections. The numbers of cores provided for each mixture are summarized in Table 3.1.2. All cores were 150 mm in diameter and ranged between 50 and 100 mm in thickness. Visual inspection of the cores found some to have unacceptably rough faces or other defects such as cracks or raveling aggregate; these cores were removed from consideration for testing. All of the remaining acceptable cores were tested for bulk density; statistics on the measured bulk density values are also summarized in Table 3.1.2. Cores having density values near the middle of the measured range for each mixture were selected for specimen fabrication and testing.

Table 3.1.2 Statistics for asphalt cores

Material	Number of Cores	Number Acceptable	Bulk Specific Gravity		
			Mean	Std. Dev.	Range
MSU	30	14	2.368	0.0261	2.316 – 2.412
CRREL	12	9	2.367	0.0292	2.321 – 2.404

The NCHRP 1-37A Design Guide dynamic modulus test protocols call for compressive testing of 100 mm diameter by 150 mm tall cylindrical specimens. Additionally, the protocols state test specimens should meet certain geometric qualities to reduce testing variability. The specimens should be cored and cut smooth without any bumps and ridges in the surfaces and the ends of the test specimens must be perpendicular to the vertical axis within a tolerance of no more than 0.5 degrees.

Since all asphalt materials in this study were provided as field cores, it was impossible to fabricate specimens conforming exactly to the NCHRP 1-37A Design Guide protocols. Various options were considered, including reheating and recompacting the asphalt and stacking of trimmed field cores to obtain a cylinder of sufficient dimensions. The final best judgment of the testing team was to test prismatic specimens cut from the field cores. The target dimensions of the prismatic specimens were 50 mm by 50 mm square and 100 mm long for a length-to-width ratio of 2. Variability in the dimensions of the field cores required small adjustments to the dimensions in some cases.

Specimen instrumentation and the test setup followed the NCHRP 1-37A Design Guide protocols to the best extent possible, given the different specimen geometry. Axial LVDTs were mounted to test specimens using studs glued directly to the sample. Axial gage length for all tests was 50 mm (equivalent to the specimen width) centered on the midheight of the specimen.

NCHRP 1-37 Draft Test Method A1 for dynamic modulus $|E^*|$ was used as the guideline for the dynamic modulus tests. Testing was performed at frequencies of 25Hz, 10Hz, 5Hz, 1Hz, 0.5Hz, and 0.1Hz at target temperatures of $-6\ ^oC$, $4\ ^oC$, $20\ ^oC$, $40\ ^oC$, and $54\ ^oC$. Dynamic modulus testing was performed in compression with the stress applied in haversine form at multiple temperatures and frequencies. Temperature was verified with a dummy sample having an embedded thermocouple. The sequence for testing was from lowest to highest temperature and highest to lowest frequency. No preconditioning of the specimen was performed before the start of the dynamic modulus test because of concerns regarding excessive unrecoverable deformations. The dynamic strains during the test were limited to 150 $\mu\varepsilon$ to ensure linear viscoelastic response. Three replicate specimens were tested for each mixture. A preliminary test was performed at the beginning of the test series for each mixture to determine the appropriate stress levels required to keep the dynamic strains within the 150 $\mu\varepsilon$ limit.

Actual dynamic strains for the dynamic modulus tests ranged between 70$\mu\varepsilon$ and 150$\mu\varepsilon$. An average strain was computed from the average of the 4 axial LVDTs. The dynamic modulus $|E^*|$ is then computed in the usual way for each temperature and frequency combination as:

$$|E^*| = \frac{\sigma_o}{\varepsilon_o} \tag{3.1.1}$$

in which σ_o is the peak dynamic stress and ε_o is the corresponding peak dynamic strain.

It was discovered during testing that it was impossible to test the small prismatic specimens at the highest temperature of 60°C. Because of the small cross-section area of these specimens and the very soft state of the asphalt mixture at this temperature, the dynamic load required to limit the dynamic strains to within 150 με was less than the smallest load that the 100 kN testing machine could apply with adequate control.

It was also observed that the CRREL specimens deformed significantly at the 40°C loading. Some cracking of the specimen and shifting of the aggregates was also evident. This behavior was not observed for the MSU material.

The dynamic modulus data at all temperatures and frequencies were combined to form a master curve and temperature shift factor for each mixture. The master curve is constructed by determining the temperature shift factors $a(T)$ giving the best-fit relationship between dynamic modulus E^* versus reduced frequency ω_R for the sigmoidal form:

$$\log E^* = a_1 + \frac{a_2}{1 + e^{(-a_3 \log \omega_R - a_4)}} \tag{3.1.2}$$

where:

E^* = complex modulus (MPa)

a_1, a_2, a_3, a_4 = material constants

$\omega_R = a(T)\ \omega$

$\omega = 2\pi/t$ (t = loading time, seconds)

and

$$a(T) = 10^{\left(b_1 T^2 + b_2 T + b_3\right)} \tag{3.1.3}$$

where:

T = temperature of AC (°C)

b_1, b_2, b_3 = temperature shift factors

Poisson's ratio is given by Equation 3.1.4 (NCHRP 2003).

$$\nu = 0.15 + \frac{0.35}{1 + e^{\left(-12.452 + 2.291 \log E^*\right)}} \tag{3.1.4}$$

where:

ν = Poisson's ratio

E^* = complex modulus (psi)

The master curves and temperature shift relations determined via this procedure for each of the asphalt mixtures resulted in the calibration of the parameters given in Table 3.1.3. The values of ω listed in Table 3.1.3 were determined for the loading time for the loading device used in each pavement test facility.

Table 3.1.3 Dynamic modulus equation parameters for asphalt mixes

	a_1	a_2	a_3	a_4	b_1	b_2	b_3	ω (rad/s)
MSU	2.373	2.168	0.6157	-0.2789	1.8×10^{-3}	-0.21	3.44	2.5π
CRREL	3.150	1.243	0.8259	-1.511	9.96×10^{-4}	-0.155	2.63	14.4π

3.1.2 Permanent Deformation

The empirical equation for the asphalt concrete damage model for permanent deformation in the NCHRP 1-37A Design Guide is:

$$\log\left(\frac{\varepsilon_p}{\varepsilon_r}\right) = k_1\beta_1 + k_2\beta_2 \log T + k_3\beta_3 \log N \tag{3.1.5}$$

where

ε_p = permanent vertical strain as a function of N

ε_r = resilient vertical strain from the response model taken along the model centerline

k_1, k_2, k_3 = laboratory material properties

β_1, β_2, β_3, = field calibration coefficients

T = temperature of AC (°F)

N = traffic repetitions

Values for k_1, k_2 and k_3 were taken as default values from the NCHRP 1-37A Design Guide and are listed in Table 3.1.4. Values for β_1, β_2 and β_3 were not taken as the field calibration values from NCHRP 1-37A but were calibrated directly from the test sections used in this project. These values were initially taken equal to 0.6, 1.0 and 1.1, respectively, and allowed to vary between 0.5 and 2.0 times these values during field calibration, with resulting values listed in Table 3.1.4. The values of 0.6, 1.0 and 1.1 are default values used in the NCHRP 1-37A Design Guide as of May 2003. Field calibration consisted of a comparison of model predictions to results from test sections and is described in greater detail in Section 5.0.

Table 3.1.4 Asphalt concrete permanent deformation damage model parameters

	k_1	k_2	k_3	β_1	β_2	β_3
MSU	-3.3426	1.734	0.4392	0.15	0.892	0.275
CRREL	-3.3426	1.734	0.4392	0.19	0.85	0.38

3.1.3 Fatigue

The empirical equation for the asphalt concrete damage model for fatigue in the NCHRP 1-37A Design Guide is given by Equation 3.1.6:

$$N_f = k_1\beta_1\left(\frac{1}{\varepsilon_t}\right)^{k_2\beta_2}\left(\frac{1}{E}\right)^{k_3\beta_3} \tag{3.1.6}$$

where:

N_f = traffic repetitions to AC fatigue

k_1, k_2, k_3 = laboratory material properties

β_1, β_2, β_3, = field calibration coefficients

ε_t = resilient horizontal tensile strain from the response model taken as the maximum tensile value within the AC layer

E = AC dynamic modulus used in response model (psi)

Values for k_1, k_2, k_3, β_1, β_2 and β_3 were taken as default values from the NCHRP 1-37A Design Guide and are listed in Table 3.1.5. Values for β_1, β_2 and β_3 were not field calibrated from test sections due to the lack of a clear definition of fatigue failure of the asphalt concrete in these test sections. The predominant observable mode of failure in these test sections was permanent deformation.

Table 3.1.5 Asphalt concrete fatigue damage model parameters

	k_1	k_2	k_3	β_1	β_2	β_3
MSU	1.0	3.9492	1.281	1.0	1.2	1.5
CRREL	1.0	3.9492	1.281	1.0	1.2	1.5

3.2 Unbound Materials

Test sections previously reported by Perkins (1999, 2002) and used in this project for model comparison and validation, used three different unbound aggregates and three different subgrade soils. Resilient modulus tests were performed on these materials to calibrate an isotropic non linear elastic with tension cutoff material model. Repeated load triaxial tests were performed on these materials to calibrate a damage model for permanent deformation of unbound materials. These tests were performed at the University of Maryland.

Table 3.2.1 lists the aggregates used in this study. Figure 3.2.1 shows the grain size distribution curves for these three aggregates. Table 3.2.2 lists the three subgrades used. Table 3.2.3 lists the target water content and dry density for the prepared specimens. These target values were based on average values obtained in test sections where these materials were used.

Table 3.2.1 Aggregate material properties

	Aggregate		
	MSU	GA	CRREL
Classification[1]	A-1-a GW	A-1-a GW-GM	A-1-a SM
Maximum dry density (kN/m^3)[2]	21.5	21.4	23.6
Optimum moisture content (%)[2]	7.2	6.6	5.3
Specific gravity[3]	2.63	2.64	2.94
At least one fractured face (%)[4]	73	100	100
At least two fractured faces (%)[4]	70	100	100

[1]Per AASHTO M145-87 and ASTM D2487
[2]Per ASTM D1557
[3]Per ASTM D854
[4]Per ASTM D5821

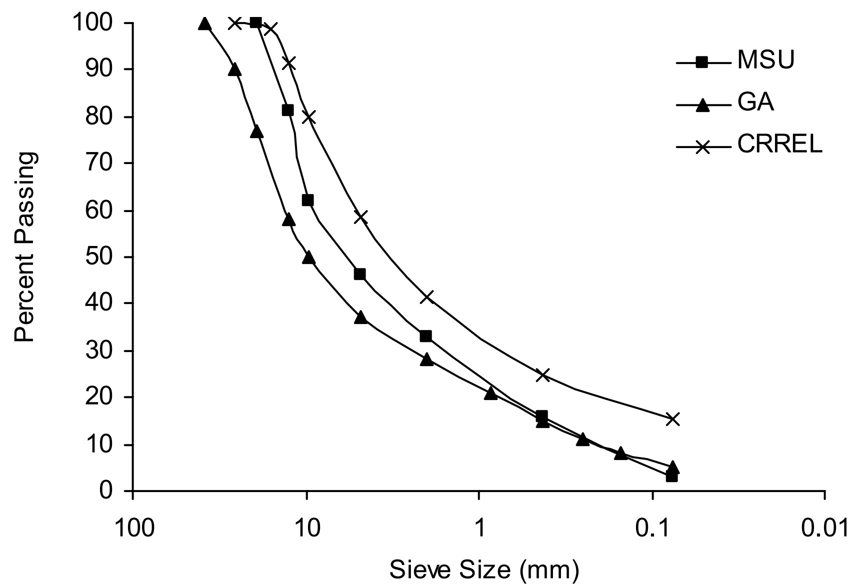

Figure 3.2.1 Grain size distribution of aggregates

Table 3.2.2 Subgrade material properties

	Subgrade		
	CS	SSS	CRREL
Classification[1]	A-7 (6) CH	A-4 SM	A-7 (6) CH
Maximum dry density (kN/m^3)[2]	16.0	18.2	17.6
Optimum moisture content (%)[2]	20.0	11.5	17.9
Specific gravity[3]	2.70	2.68	2.76
Liquid limit (%)[4]	73	NP[6]	56
Plastic limit (%)[4]	28	NP[6]	20
Plasticity Index (%)[4]	45	NP[6]	36
Passing # 200 Sieve (%)[5]	100	40	86

[1]Per AASHTO M145-87 and ASTM D2487
[2]Per ASTM D1557
[3]Per ASTM D854
[4]Per ASTM D4318
[5]Per ASTM D1140
[6] NP=Non Plastic

Table 3.2.3 Target moisture content and dry density of prepared specimens

Unbound Material	ID	w (%)	γ_d (kN/m3)
Aggregates	MSU	6.0	20.7
	CRREL	4.1	20.8
	GA	7.5	22.2
Subgrades	CS	45.0	11.4
	CRREL	28.5	15.0
	SSS	14.0	14.8

Test specimens for both the resilient modulus and repeated load permanent deformation tests were prepared following the recommendations in NCHRP Project 1-28A (NCHRP, 2000; Andrei, 1999). All materials were remolded and compacted by the impact method in specimen molds to the target moisture content and dry density values listed in Table 3.2.3. For the subgrades and the MSU and CRREL aggregates, specimens were prepared to a diameter of 102 mm and a height of 204 mm. Due to the larger particle size in the GA aggregate, specimens were prepared to a sample size of 152 mm by 304 mm.

Specimens were contained in rubber membranes having a thickness of 0.635 mm. Specimens were tested in a MTS TestStar closed loop, electro-hydraulic triaxial testing machine. Air was used as the confining fluid to the specimens. Axial displacement measurements were made with two LVDT's placed 180 degrees from each other. The LVDT's were attached to the specimens to measure displacement within the center one-half of the specimen. This was accomplished by attaching the LVDT's to clamps placed around the specimen at the upper and lower one-quarter points. Figure 3.2.2 shows a specimen set up prior to testing.

3.2.1 Resilient Modulus

Resilient modulus tests were performed according to the protocol established in NCHRP Project 1-28A (NCHRP 2000). In this protocol, a series of steps consisting of different levels of confining pressure and cyclic axial stress are followed such that resilient modulus is measured for varying confinement and shear stress levels. Tables 3.2.4 and 3.2.5 list the stress sequences followed for the aggregate and subgrade materials. Confining pressure is held constant within each load step.

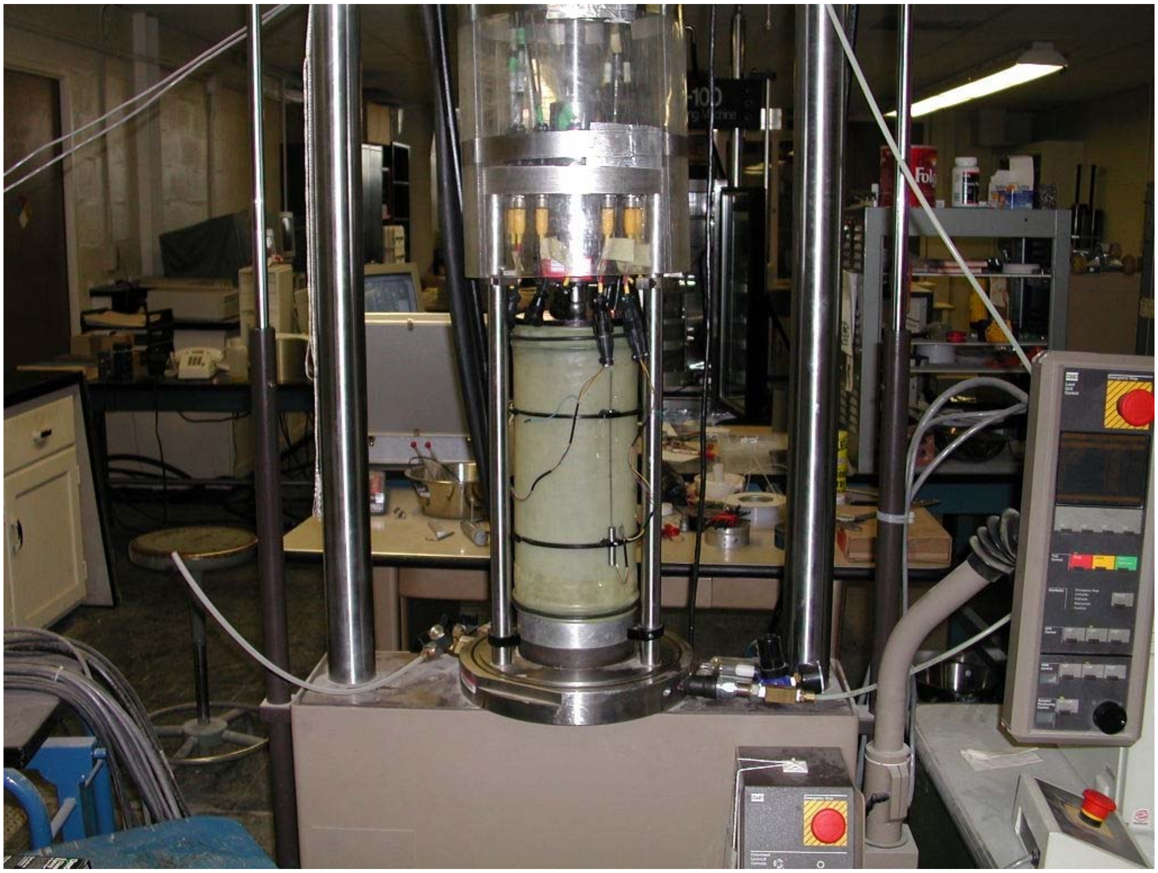

Figure 3.2.2 Triaxial test set up

Cyclic loading consists of repeated cycles of a haversine shaped load-pulse. These load pulses had a 0.1 sec load duration and 0.9 sec rest period for aggregate materials and a 0.2 sec load duration and 0.8 sec rest period for subgrade materials. These loading and the rest times are intended to simulate field loading conditions.

Resilient modulus was calculated as the change in axial stress divided by the change in axial strain for the last 10 cycles of each step and averaged. Equation 3.2.1 was then used to determine material properties k_1, k_2, k_3 for each material with these properties listed in Table 3.2.6.

$$M_R = p_a k_1 \left(\frac{\theta}{p_a} \right)^{k_2} \left(\frac{\tau_{oct}}{p_a} + 1 \right)^{k_3} \qquad (3.2.1)$$

In Equation 3.2.1

M_R = resilient modulus

p_a = atmospheric pressure (101.3 kPa)

θ = bulk stress = $\sigma_1 + 2\sigma_3$

τ_{oct} = octahedral shear stress = $\sqrt{2}/3(\sigma_1 - \sigma_3)$

k_1, k_2, k_3 = material properties

Table 3.2.4 Resilient modulus test protocol for aggregate materials

Sequence	Confining Pressure (psi)	Contact Stress (psi)	Cyclic Stress (psi)	N_{rep}
Conditioning	15.0	3.0	30.0	1000
1	3.0	0.6	1.5	100
2	6.0	1.2	3.0	100
3	10.0	2.0	5.0	100
4	15.0	3.0	7.5	100
5	20.0	4.0	10.0	100
6	3.0	0.6	3.0	100
7	6.0	1.2	6.0	100
8	10.0	2.0	10.0	100
9	15.0	3.0	15.0	100
10	20.0	4.0	20.0	100
11	3.0	0.6	6.0	100
12	6.0	1.2	12.0	100
13	10.0	2.0	20.0	100
14	15.0	3.0	30.0	100
15	20.0	4.0	40.0	100
16	3.0	0.6	9.0	100
17	6.0	1.2	18.0	100
18	10.0	2.0	30.0	100
19	15.0	3.0	45.0	100
20	20.0	4.0	60.0	100
21	3.0	0.6	15.0	100
22	6.0	1.2	30.0	100
23	10.0	2.0	50.0	100
24	15.0	3.0	75.0	100
25	20.0	4.0	100.0	100
26	3.0	0.6	21.0	100
27	6.0	1.2	42.0	100
28	10.0	2.0	70.0	100
29	15.0	3.0	105.0	100
30	20.0	4.0	140.0	100

Table 3.2.5 Resilient modulus test protocol for subgrade materials

Sequence	Confining Pressure (psi)	Contact Stress (psi)	Cyclic Stress (psi)	N_{rep}
Conditioning	4.0	0.8	7.0	1000
1	8.0	1.6	4.0	100
2	6.0	1.2	4.0	100
3	4.0	0.8	4.0	100
4	2.0	0.4	4.0	100
5	8.0	1.6	7.0	100
6	6.0	1.2	7.0	100
7	4.0	0.8	7.0	100
8	2.0	0.4	7.0	100
9	8.0	1.6	10.0	100
10	6.0	1.2	10.0	100
11	4.0	0.8	10.0	100
12	2.0	0.4	10.0	100
13	8.0	1.6	14.0	100
14	6.0	1.2	14.0	100
15	4.0	0.8	14.0	100
16	2.0	0.4	14.0	100

Table 3.2.6 Unbound materials resilient modulus model parameters

	k_1	k_2	k_3
Unbound Aggregates			
MSU	957	0.906	-0.614
CRREL	662	1.010	-0.585
GA	741	1.091	-0.653
Subgrade Soils			
CS	139	0.187	-3.281
SSS	449	1.030	-1.856
CRREL	170	0.450	-16.39

Figures 3.2.3 – 3.2.8 provide a comparison of the predicted values of resilient modulus from Equation 3.2.1 to the measured values. Measured values for each test replication are shown as different symbols. From these results it is seen that Equation 3.2.1 generally provides an excellent fit to the data and that little data scatter is seen between test replicates for most materials.

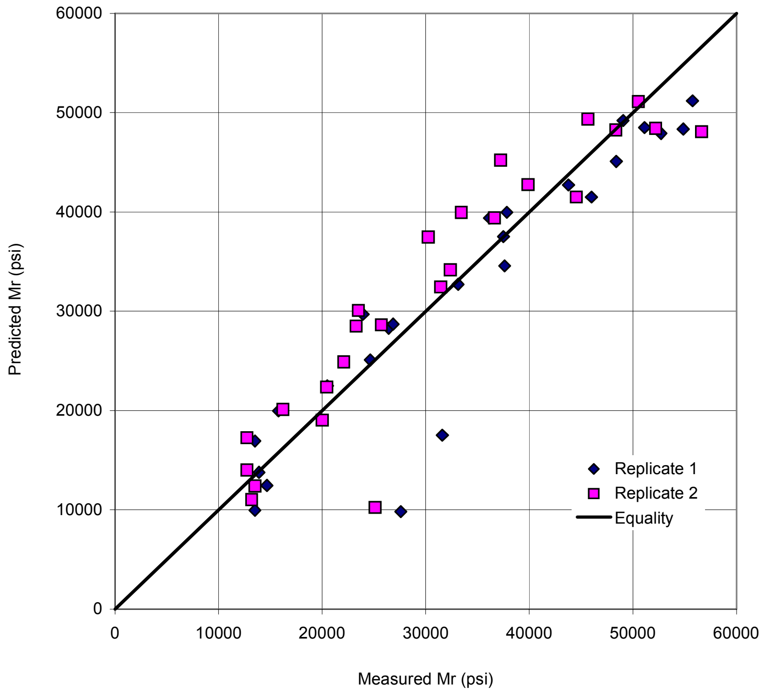

Figure 3.2.3 Predicted versus measured resilient modulus for MSU aggregate

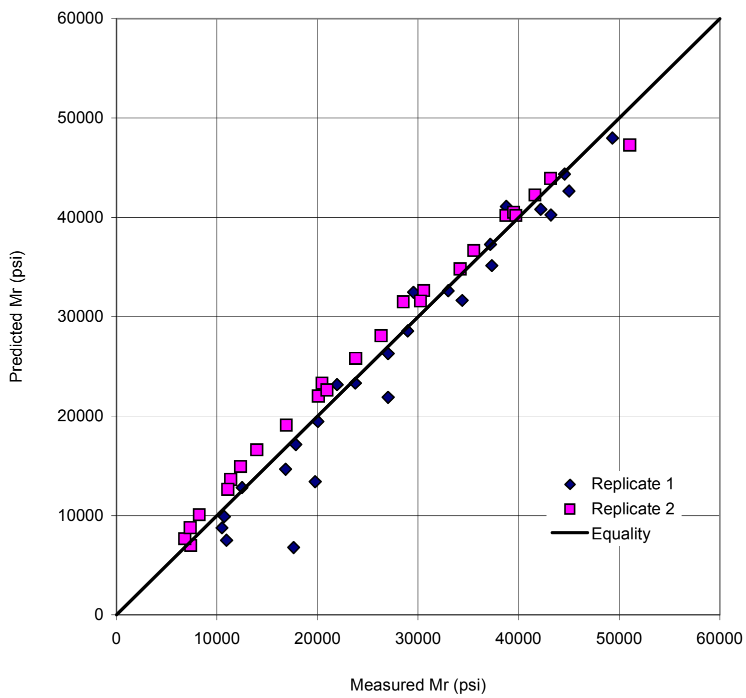

Figure 3.2.4 Predicted versus measured resilient modulus for CRREL aggregate

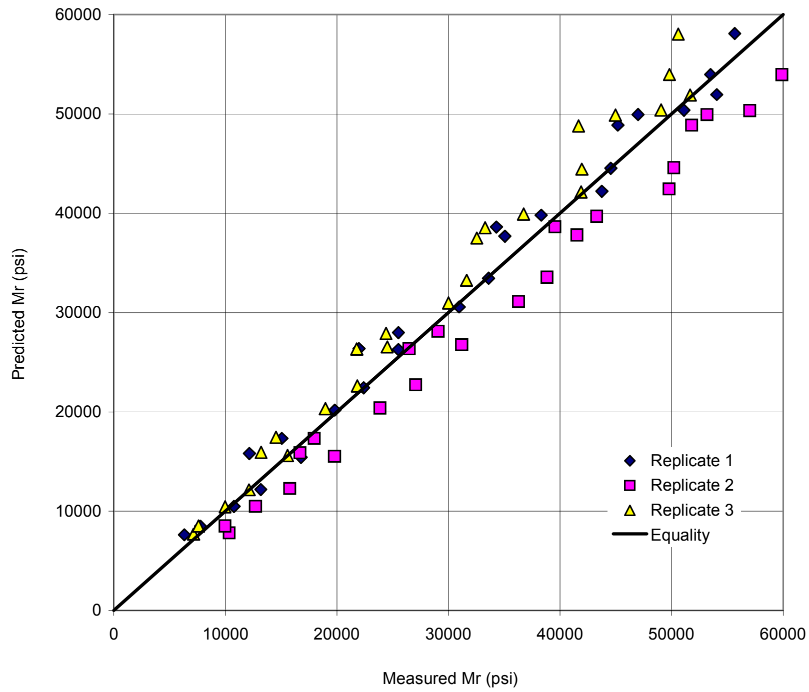

Figure 3.2.5 Predicted versus measured resilient modulus for GA aggregate

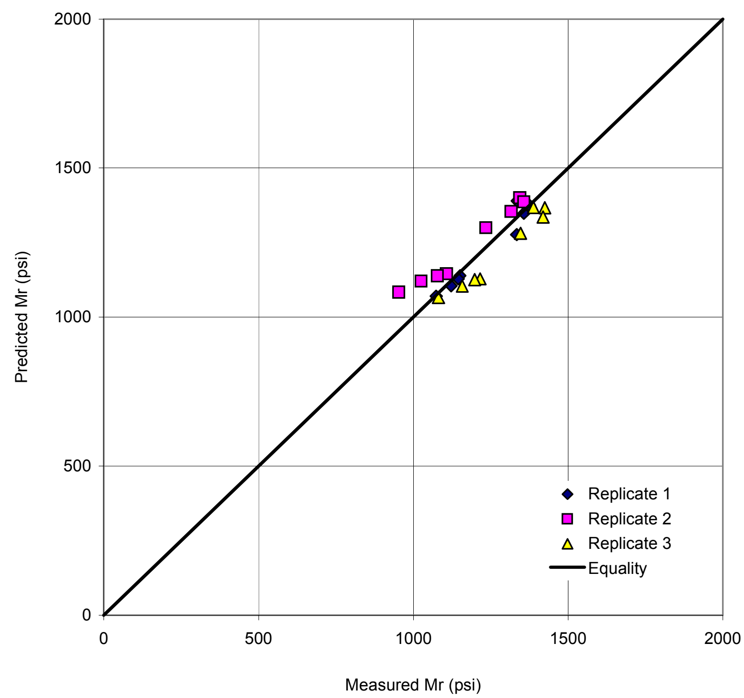

Figure 3.2.6 Predicted versus measured resilient modulus for CS subgrade

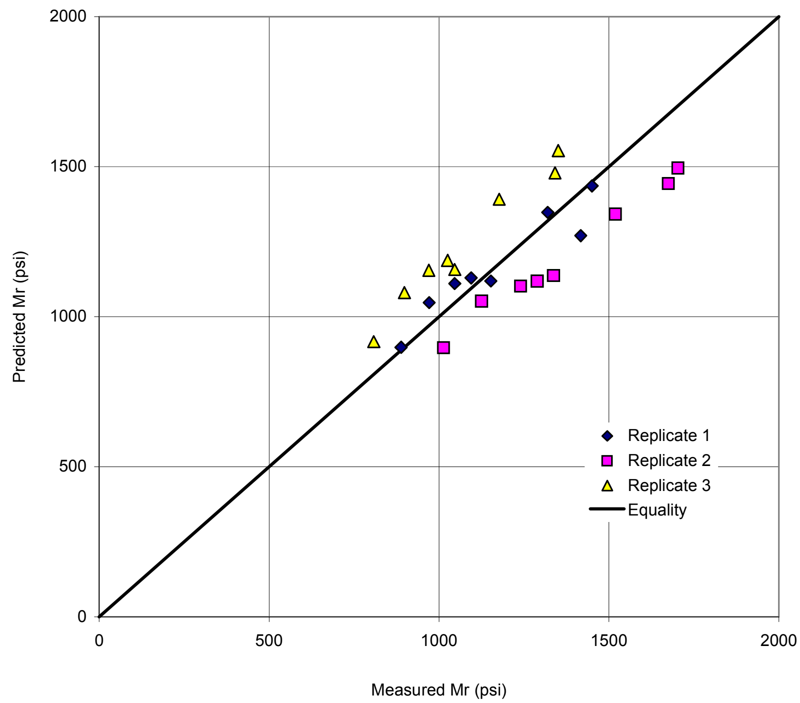

Figure 3.2.7 Predicted versus measured resilient modulus for CRREL subgrade

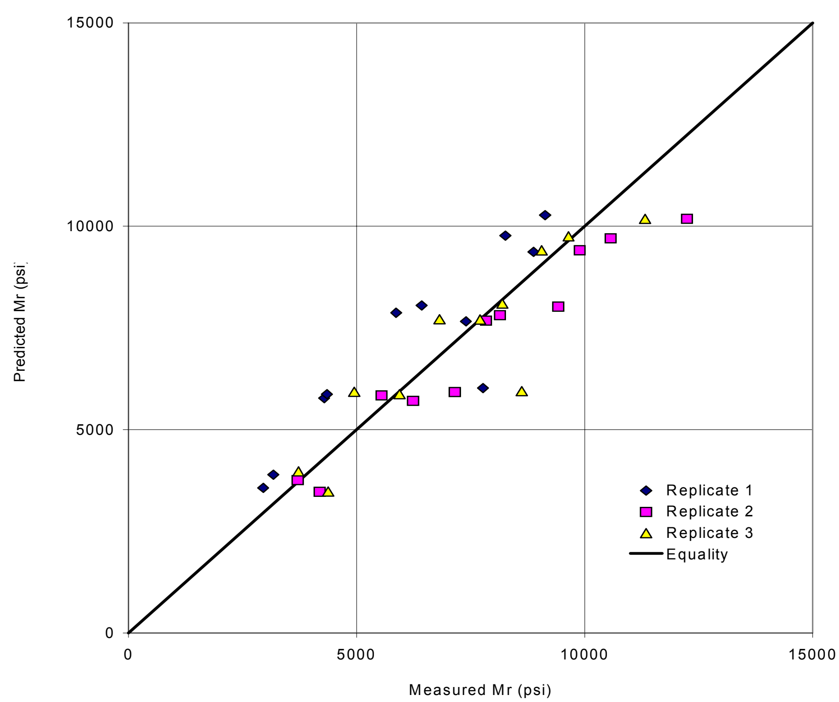

Figure 3.2.8 Predicted versus measured resilient modulus for SSS subgrade

3.2.2 Permanent Deformation

Repeated load permanent deformation tests followed the protocols developed by Yau (1999). The same MTS triaxial testing machine used for the resilient modulus tests was also used to conduct the repeated load permanent deformation tests. The repeated load permanent deformation tests were performed by applying a large number of loading cycles at a single stress level. For aggregate materials, the repeated loading consisted of a haversine stress pulse of 0.1 sec duration followed by a 0.9 sec rest period. For subgrade materials, the repeated loading consisted of a haversine stress pulse of 0.45 sec duration followed by 1 sec rest period. The tests were targeted at 100,000 load repetitions. Some tests were terminated prematurely when the LVDTs reached their range limits. Air was used as the confining fluid, and all tests were performed undrained.

Two different stress states were initially selected to be used for loading specimens. The first consisted of a cyclic stress of 655 kPa, a contact stress of 23.8 kPa, and a confining stress of 103 kPa. The second stress state consisted of a cyclic stress of 345 kPa, a contact stress of 4.1 kPa, and a confining stress of 20.7 kPa. These two stress states were first applied to aggregate material. However, the first stress state often produced displacements in aggregate materials that were too small to be detected by LVDTs due to the high stiffness from the high confining pressure. Consequently, the second stress state was applied to all aggregate material test specimens.

The appropriate stress state for each subgrade material was determined by conducting a monotonic loading triaxial test using a constant rate of strain. The cyclic stress used in the repeated load triaxial test was then taken as the deviatoric stress necessary to reach 65 % of the failure stress in the monotonic test for each subgrade. Contact stress was determined as 10 % of the cyclic stress and confining stress as 20.7 kPa for each subgrade soil tested.

Figures 3.2.9 – 3.2.14 show the ratio of permanent to resilient strain ratio versus number of load cycles for each of the three aggregates and three subgrades tested. Data is plotted as a strain ratio for consistency with models for permanent deformation shown later in this report. The figures contain replicate samples tested for each of the six materials, which are denoted in the figures using different data point symbols. The results show reasonably good repeatability for the tests with the subgrades but poor repeatability with the aggregates. In general, repeated load triaxial tests on aggregate materials are generally characterized by poor repeatability. The results also show some inconsistencies with some of the weaker subgrade materials giving a higher number of load cycles to a particular strain ratio as compared to the stronger aggregate materials. This may be due to the use of averaged results from two replicate tests on the aggregate materials that did not show good repeatability.

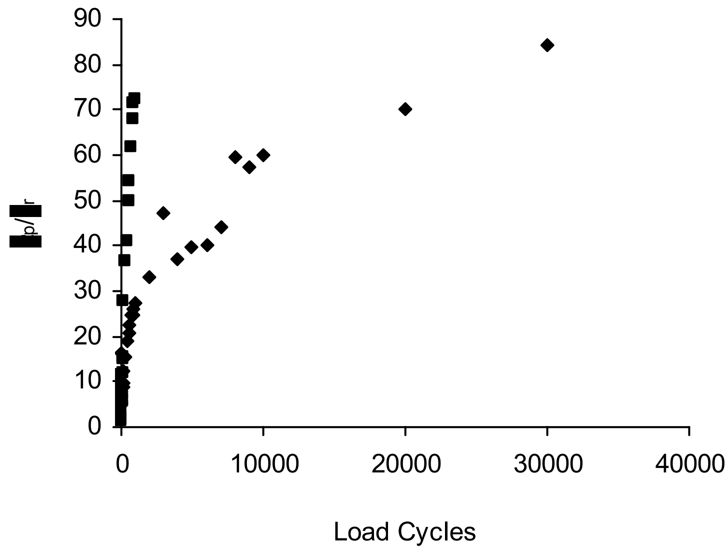

Figure 3.2.9 Permanent to resilient strain ratio versus load cycles from permanent deformation tests on MSU aggregate

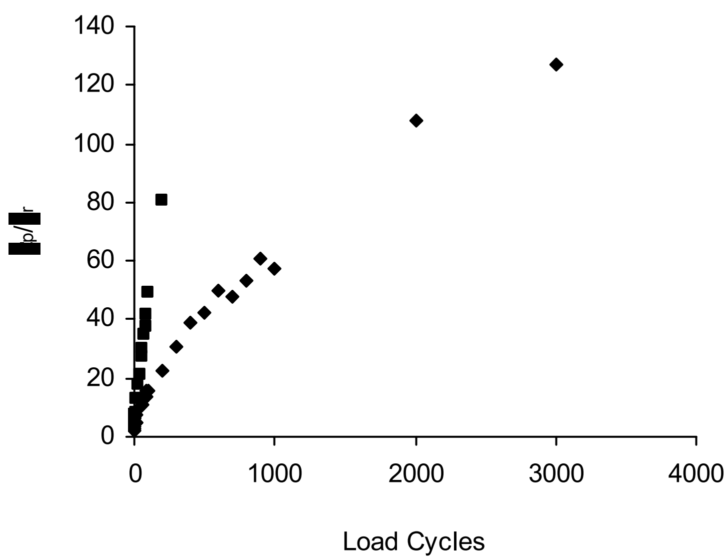

Figure 3.2.10 Permanent to resilient strain ratio versus load cycles from permanent deformation tests on CRREL aggregate

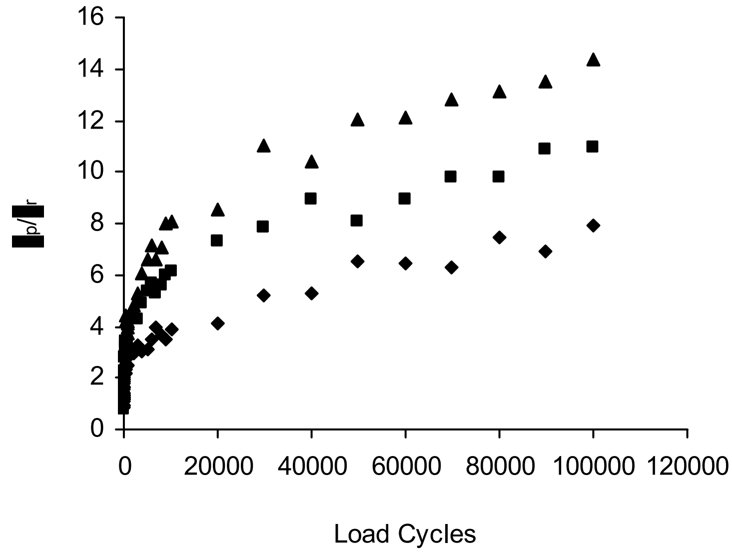

Figure 3.2.11 Permanent to resilient strain ratio versus load cycles from permanent deformation tests on GA aggregate

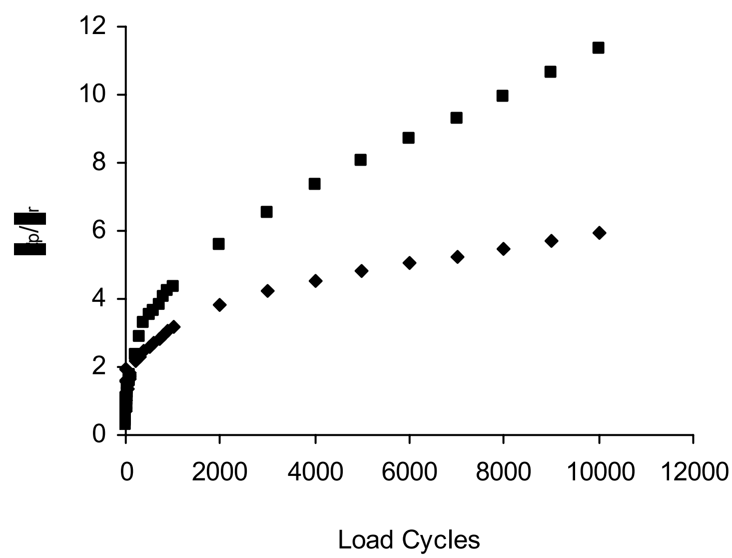

Figure 3.2.12 Permanent to resilient strain ratio versus load cycles from permanent deformation tests on CS subgrade

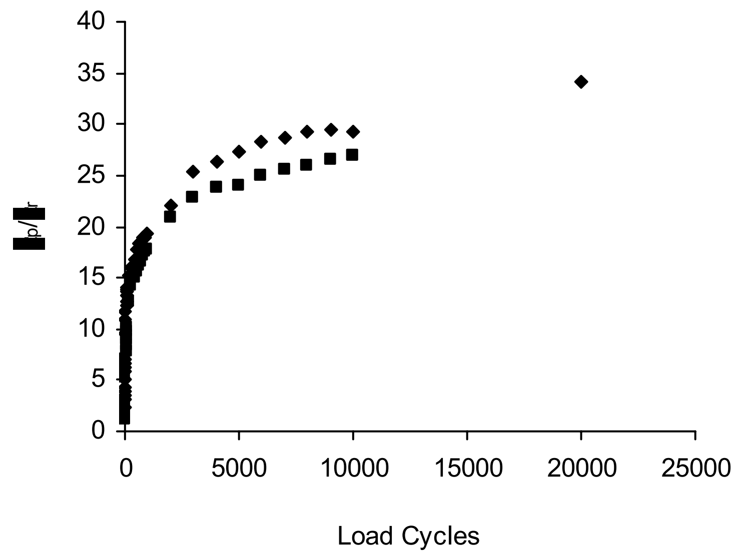

Figure 3.2.13 Permanent to resilient strain ratio versus load cycles from permanent deformation tests on CRREL subgrade

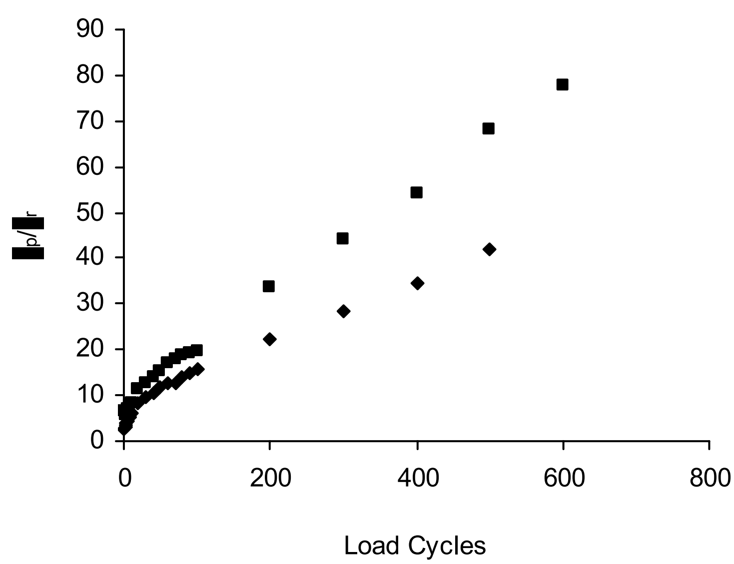

Figure 3.2.14 Permanent to resilient strain ratio versus load cycles from permanent deformation tests on SSS subgrade

A model for permanent deformation based on modifications of work by Tseng and Lytton (1989) has been used to interpret permanent deformation results from the repeated load triaxial tests (NCHRP 2003). This model is given by Equation 3.2.2,

$$\delta_a(N) = \xi_1\left(\frac{\varepsilon_o}{\varepsilon_r}\right)e^{-\left(\frac{\rho}{N}\right)^{\xi_2\beta}}\varepsilon_v h \qquad (3.2.2)$$

where

δ_a = permanent deformation of a layer

N = number of traffic repetitions

ε_o,β,ρ = material parameters

ε_r = resilient strain imposed in a laboratory test

ε_v = average vertical resilient strain in a layer

h = layer thickness

ξ_1,ξ_2 = field calibration functions

For the triaxial test, Equation 3.2.2 can be rewritten by Equation 3.2.3.

$$\frac{\varepsilon_p}{\varepsilon_v} = \xi_1\frac{\varepsilon_0}{\varepsilon_r}e^{-\left(\frac{\rho}{N}\right)^{\xi_2\beta}} \qquad (3.2.3)$$

where ε_p is the permanent strain and ε_v is the resilient strain measured in the triaxial test. When interpreting the triaxial tests, the field calibration functions ξ_1 and ξ_2 are set to 1.0. Equation 3.2.4 was used to determine the parameter ρ in terms of the water content W_c (NCHRP 2003). The parameters ($\varepsilon_o/\varepsilon_r$) and β were then taken as material properties calibrated from the test. Table 3.2.7 presents the calibration parameters contained in Equation 3.2.3 for all the six materials tested, where these values are for the average of the replicates tested.

$$\rho = 10^{(0.622685+0.541524W_c)} \qquad (3.2.4)$$

Table 3.2.7 Permanent deformation model parameters for unbound materials

	ρ	$\varepsilon_o/\varepsilon_r$	β
Aggregate			
MSU	7440	88.7	0.127
CRREL	789	82.6	0.165
GA	789	12.2	0.242
Subgrade			
CS	4.13E+26	4690	0.0361
CRREL	4.75E+15	839	0.0455
SSS	2.33E+08	1420	0.0979

3.3 Additional Aggregate Material Models

In addition to the isotropic non linear elastic with tension cutoff model used for the unbound aggregate described in Section 3.2.1, six additional material models were used for the unbound aggregate. These additional models were examined in order to provide guidance on whether the unbound aggregate material model type influenced the ability of the method to predict base-reinforced pavement performance. Each material model is described in the following sections. The calibration parameters for each model were selected in part based on the results of the tests described in Section 3.2.1 and additional tests described in the sections below. These properties were adjusted in some cases to provide for a comparable level of permanent surface deformation in the pavement model used to compare the material models. Further details concerning the pavement model used for this comparison are provided in Section 8.0.

3.3.1 Isotropic Linear Elastic

In order to evaluate the simplest material model that could be used for the unbound aggregate, an isotropic linear elastic model was used having an elastic modulus and a Poisson's ratio as input parameters. Table 3.3.1 lists these values resulting from the adjustment process described in Section 8.0 taken to have comparison between models.

Table 3.3.1 Isotropic linear elastic material model parameters

Material Model	Elastic Modulus (MPa)	Poisson's Ratio
Isotropic Linear Elastic	43.0	0.25

3.3.2 Isotropic Linear Elastic with Tension Cutoff

To examine the separate effects of a model with tension cutoff versus one having tension cutoff and non linear elastic properties, an isotropic linear elastic with tension cutoff model was created. This model used the same material model described in Section 3.2.1 but with parameters selected to provide linear elastic behavior. The parameters used in this model are listed in Table 3.3.2, where T_c is the maximum tensile stress that the material can carry. In this model, the elastic modulus used was 38 % greater than that used in the isotropic linear elastic model without tension cutoff. This value was selected in order to provide similar surface deformation response for the pavement model described in Section 8.0.

Table 3.3.2 Isotropic linear elastic with tension cutoff material model parameters

Material Model	k_1	k_2	k_3	p_a (kPa)	ν	T_c (kPa)
Isotropic Linear Elastic with Tension Cutoff	592.3	0.0	0.0	101.3	0.25	0.001

3.3.3 Anisotropic Non Linear Elastic with Tension Cutoff

An anisotropic non linear elastic with tension cutoff model was developed based on the isotropic version described in Section 3.2.1. Whereas the model described in Section 3.2.1 uses Equation 3.2.1 to calculate the elastic modulus for a particular stress state, the anisotropic model also uses Equation 3.2.1 to calculate an elastic modulus that is taken as the modulus in the vertical direction (E_v) of the unbound aggregate. The anisotropic model has a second modulus for all horizontal directions of the material (E_h). The model also requires the input of a shear modulus pertinent to any vertical plane (G_v), a Poisson's ratio defining lateral expansion due to vertical stress (ν_{vh}), and a Poisson's ratio in the horizontal plane of the material (ν_h). The constitutive matrix for the material model is given by Equation 3.3.1.

$$\begin{pmatrix} \tilde{\varepsilon}_x \\ \tilde{\varepsilon}_y \\ \tilde{\varepsilon}_z \\ \tilde{\gamma}_{xy} \\ \tilde{\gamma}_{yz} \\ \tilde{\gamma}_{zx} \end{pmatrix} = \begin{pmatrix} 1/E_h & -\nu_h/E_h & -\nu_{vh}/E_v & 0 & 0 & 0 \\ -\nu_h/E_h & 1/E_h & -\nu_{vh}/E_v & 0 & 0 & 0 \\ -\nu_{hv}/E_h & -\nu_{hv}/E_h & 1/E_v & 0 & 0 & 0 \\ 0 & 0 & 0 & 1/G_h & 0 & 0 \\ 0 & 0 & 0 & 0 & 1/G_v & 0 \\ 0 & 0 & 0 & 0 & 0 & 1/G_v \end{pmatrix} \begin{pmatrix} \tilde{\sigma}_x \\ \tilde{\sigma}_y \\ \tilde{\sigma}_z \\ \tilde{\tau}_{xy} \\ \tilde{\tau}_{yz} \\ \tilde{\tau}_{zx} \end{pmatrix} \quad (3.3.1)$$

where:

$$\nu_{hv} = \nu_{vh} \frac{E_h}{E_v} \tag{3.3.2}$$

$$G_h = \frac{E_h}{2(1+\nu_h)} \tag{3.3.3}$$

The model is formulated by requiring input of the parameters listed in Table 3.3.3. The values for k_1, k_2, k_3 were chosen to match those of the MSU unbound aggregate. Values of E_h/E_v and G_v/E_v were selected based on typical values from triaxial compression and extension tests reported by Adu-Osei et al. (2001). Values of ν_h and ν_{vh} were taken as 0.25 in the absence of any other supporting data.

Table 3.3.3 Anisotropic non linear elastic with tension cutoff material model parameters

Material Model	k_1	k_2	k_3	p_a (kPa)	T_c (kPa)	E_h/E_v	G_v/E_v	ν_h	ν_{vh}
Anisotropic Non Linear Elastic with Tension Cutoff	957	0.906	-0.614	101.3	0.001	0.35	0.25	0.25	0.25

3.3.4 Anisotropic Linear Elastic

The model described in Section 3.3.3 was used with the material properties listed in Table 3.3.4 to model anisotropic linear elastic behavior.

Table 3.3.4 Anisotropic linear elastic material model parameters

Material Model	k_1	k_2	k_3	p_a (kPa)	T_c (kPa)	E_h/E_v	G_v/E_v	ν_h	ν_{vh}
Anisotropic Linear Elastic	503.46	0.0	0.0	101.3	100,000	0.35	0.25	0.25	0.25

3.3.5 Anisotropic Linear Elastic with Tension Cutoff

The model described in Section 3.3.3 was used with the material properties listed in Table 3.3.5 to model anisotropic linear elastic with tension cutoff behavior.

Table 3.3.5 Anisotropic linear elastic with tension cutoff material model parameters

Material Model	k_1	k_2	k_3	p_a (kPa)	T_c (kPa)	E_h/E_v	G_v/E_v	ν_h	ν_{vh}
Anisotropic Linear Elastic with Tension Cutoff	552.8	0.0	0.0	101.3	0.001	0.35	0.25	0.25	0.25

3.4 Reinforced Aggregate

Unbound aggregate located within a zone above and, in cases where the reinforcement is contained within the aggregate layer, below the reinforcement is influenced by the reinforcement. Pavement test sections have clearly shown that aggregate within these zones experiences less horizontal and vertical strain as compared to aggregate in similar locations in test sections without reinforcement. To help identify the causes for this reduction of strain, large-scale cyclic triaxial tests were performed on reinforced and unreinforced specimens. The specimens measured 600 mm in height and 300 mm in diameter. For the reinforced specimens, a single layer of reinforcement was placed mid-height in the sample. Specimens were instrumented to delineate the zone of reinforcement above and below the reinforcement layer. Resilient modulus tests were performed following the protocol described in Section 3.2.1. Repeated load permanent deformation tests were then performed on the same samples following procedures for the tests described in Section 3.2.2. These tests were performed to assess the following:

1. Changes in resilient modulus behavior.
2. Changes in permanent deformation behavior.
3. Thickness of the zone of influence of the reinforcement on the unbound aggregate.
4. Stress state, or degree of friction mobilization, necessary to see changes in resilient modulus and/or permanent deformation behavior.

The tests were performed using equipment for large-scale triaxial testing at the Norwegian University of Science and Technology (NTNU) and the Norwegian Foundation for Industrial and Technical Research (SINTEF) in Trondheim, Norway. The facility is described in detail by Skoglund (2002).

3.4.1 Test Setup

Specimens measuring 600 mm in height and 300 mm in diameter were compacted inside a rigid compaction mould using a vibrating plate compactor. The compactor was set to give the same density as measured in the pavement test sections for which the same unbound aggregate was used. A sketch of the compactor is shown in Figure 3.4.1 with data for the compactor listed in Table 3.4.1. Figure 3.4.2 shows the density achieved in the 15 specimens tested using the CRREL aggregate. The range in density was within 0.7 % of the target density.

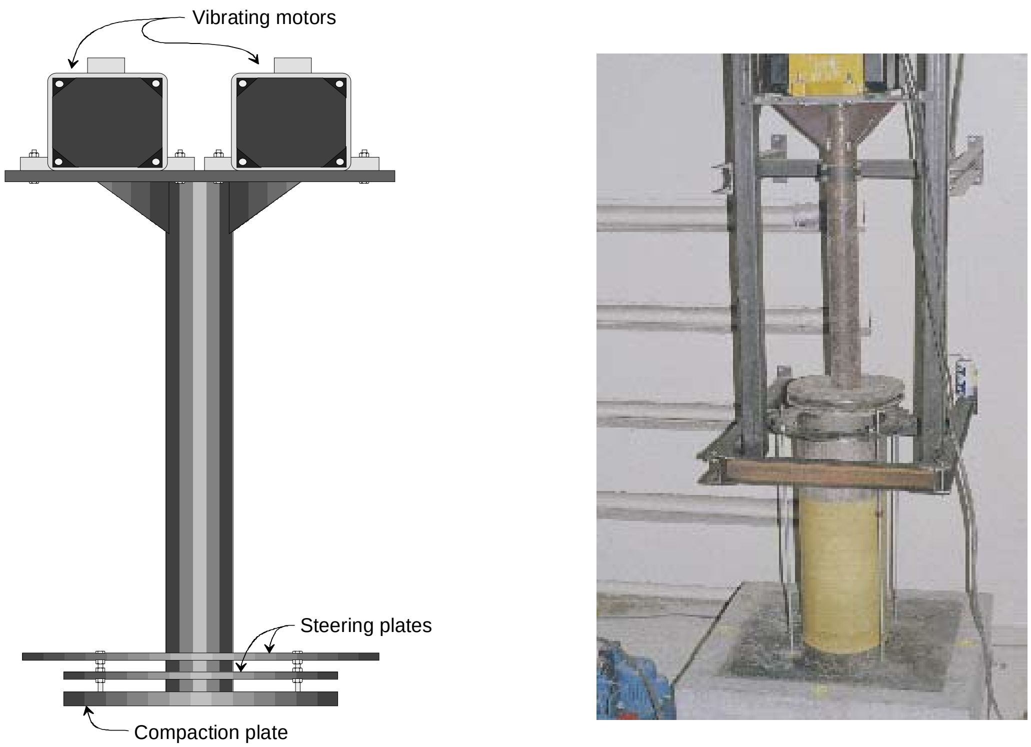

Figure 3.4.1 Vibrating plate compactor and support frame

Table 3.4.1 Specifications for the triaxial compaction equipment

Total weight	224 kg
Working frequency	2870 rpm (48 Hz)
Centripetal force	2 x 6 kN
Power consumption	2 x 1500 W
Compaction time per layer	120 sec

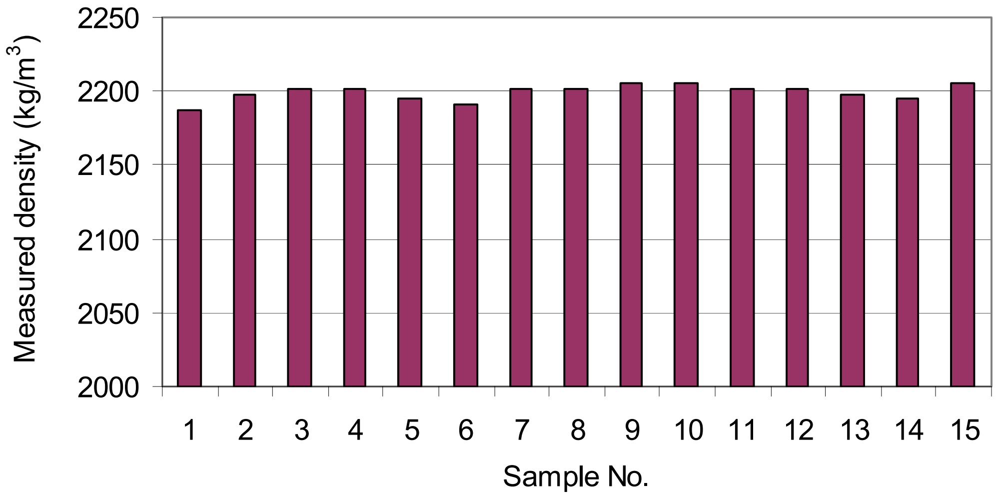

Figure 3.4.2 Compacted density of large-scale triaxial specimens using the CRREL aggregate

To transfer the sample from the compaction mold to the latex membrane with a minimum of disturbance, special equipment has been constructed. This equipment allows the sample to be extruded from the mold and contained in the latex membrane while an internal vacuum is maintained in the sample. Figure 3.4.3 shows a photo of a sample during extrusion and transfer to the membrane.

A sketch of the triaxial testing equipment is shown in Figure 3.4.4. The equipment applies variable axial loads with the confining pressure held constant. In Figure 3.4.4, typical on-sample instrumentation is shown. This instrumentation includes two LVDTs for measuring axial deformation between the end plates and six LVDTs mounted on calipers for measurement of radial deformations.

In this project eight additional sensors for local measurements of axial deformation were included. The axial LVDT was attached to the sample by glue on the rubber membrane at the middle of the sample. The LVDT cores were attached to pieces of metal glued to the membrane at different distances from the center. The measuring distances were 75, 100, 200 and 300 mm. The last measurement of 300 mm spanned from the middle of the sample to the top platen. This additional instrumentation was used to investigate the influence zone of the reinforcement.

Figure 3.4.3 Triaxial specimen during extrusion and transfer to membrane

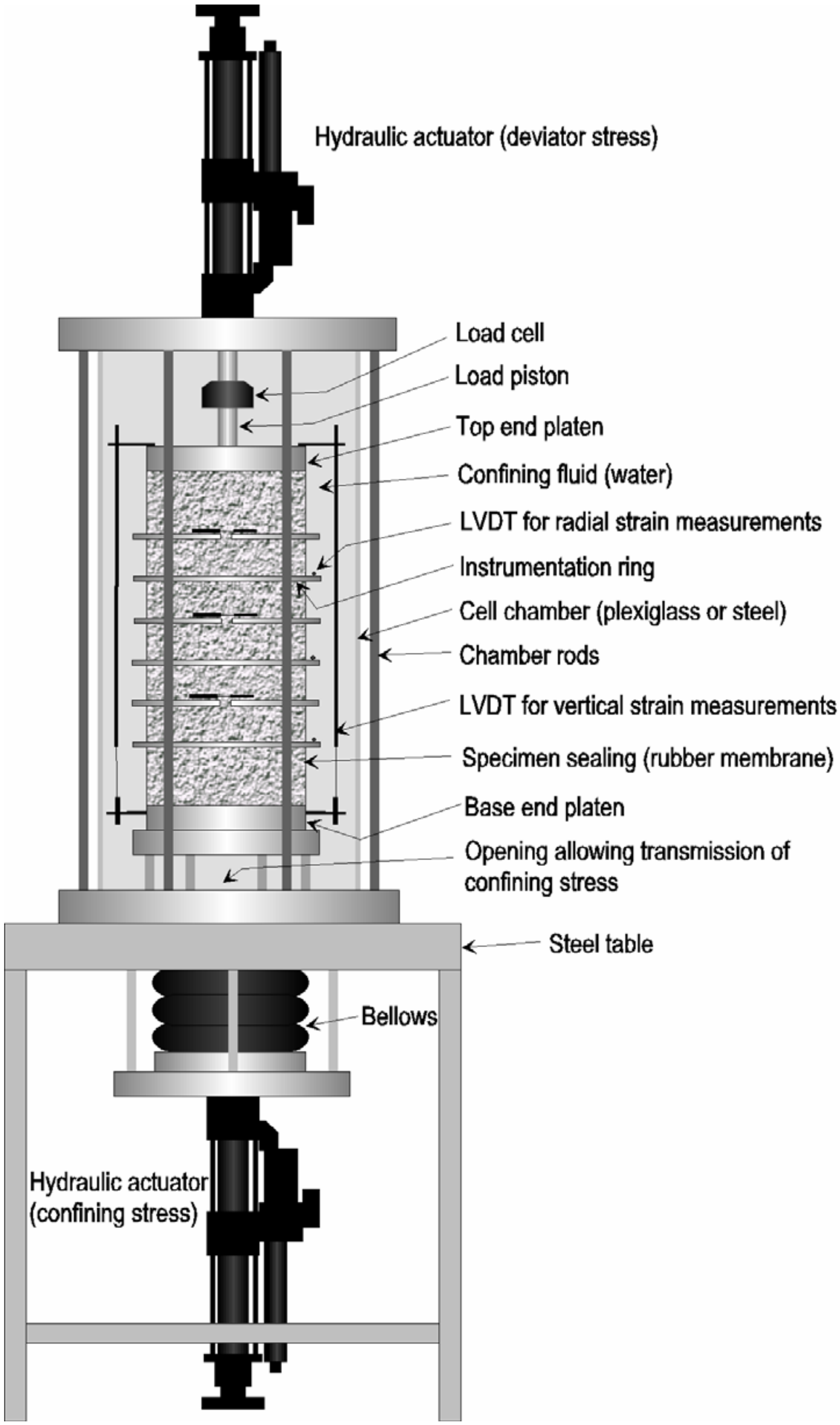

Figure 3.4.4 Schematic of the large-scale triaxial testing equipment

3.4.2 Materials

Tests were performed on the CRREL and GA unbound aggregate materials described in Section 3.2. Grain size distributions for these aggregates are given in Figure 3.2.1 while index properties are given in Table 3.2.1. These materials were compacted to dry densities and at water contents used in test sections using these materials and are listed in Table 3.4.2.

Table 3.4.2 Compaction dry density and water content for large-scale triaxial specimens

Material	Dry Density (kN/m^3)	Water Content (%)
GA	22.0	6.5
CRREL	21.6	3.6

Four different types of reinforcement were used in the tests (two geogrids, one geotextile and one geocomposite). These products are identified in Table 3.4.3 along with properties reported by the manufacturers.

Table 3.4.3 Reinforcement products used in large-scale triaxial tests

Name	Type	Aperture size mm MD, XMD	Strength at failure kN/m MD, XMD	Strength kN/m at x % strain x, MD, XMD
Amoco ProPex 2006	Polypropylene woven, slit film	NA	30.7, 30.7	2%, 4.3,13.6 5%, 10.0, 22.0
Polyfelt PEC 35/35	Composite of PP non-woven and grid of polyester yarns	40 x 40	36.0, 36.0	2%, 4.4 5%, 12.9
Teletextiles 30/30	Woven polyester grid PVC coated	25 x 25	45.5, 32.0	2%, 11.9, 5.0 5%, 20.2, 8.3
Tensar BX 1200	Polypropylene grid	25 x 36	21.0, 31.0	2%, 6.4, 10.5 5%, 12.5, 23.0

3.4.3 Resilient Modulus and Permanent Deformation Testing Procedures

The procedure used for the resilient modulus portion of the test followed that described in Section 3.2.1. The six different sequence groups resulted in a mobilized friction angle ranging from 15 to 51.5 degrees. Resilient modulus testing was stopped once the sample reached an accumulated permanent vertical strain of 1 %. This was done such that samples could then be used for permanent deformation testing. Stopping at 1 % permanent axial strain resulted in a different number of load cycles applied to the specimens prior to the initiation of the subsequent permanent deformation test.

The permanent deformation tests should ideally be performed on samples not exposed to any prior stress sequencing. Due to the large size of the samples and the excessive time required for sample preparation, permanent deformation tests were performed on samples exposed to the resilient modulus test sequencing. In order to make the different samples as comparable as possible the resilient tests where stopped at a total strain of 1%. Table 3.4.4 lists the loading conditions used in the permanent deformation tests performed on the CRREL aggregate. Figure 3.4.5 shows the stress state used for the permanent deformation tests in relation to the stress states used in the resilient modulus tests. The range of stress states shown in Table 3.4.4 and Figure 3.4.5 permit drawing conclusions regarding the degree of friction mobilization needed before reinforcement effects are seen.

Table 3.4.4 Loading conditions used in large-scale permanent deformation tests

Stress set	Test number	Deviatoric stress (kPa)		Confining stress (kPa)	Stop criterion number of pulses/ total vertical strain
		min	max		
1	Tests 1, 2	4.7	345	20.7	100,000 or 5 %
2	Tests 3-7, 11-15	4.7	281	20.7	100,000 or 5 %
3	Tests 8, 9, 10	25.0	680	103.0	100,000 or 5%

The need to perform permanent deformation tests following resilient modulus tests creates a need to correct for the effect of resilient modulus conditioning on the results from the permanent deformation test. Specimens experiencing resilient modulus test conditioning will effectively show less permanent strain in the subsequent permanent deformation test due to the accumulation of some permanent strain during resilient modulus conditioning. To develop correction techniques, supplemental tests were performed at the University of Maryland on the GA aggregate using the equipment described in Section 3.2. Permanent deformation tests were performed on resilient modulus conditioned and non-conditioned specimens (two replicates each) using a confining stress of 20.7 kPa, a maximum cyclic deviatoric stress of 345 kPa and a minimum cyclic stress of 4.1 kPa.

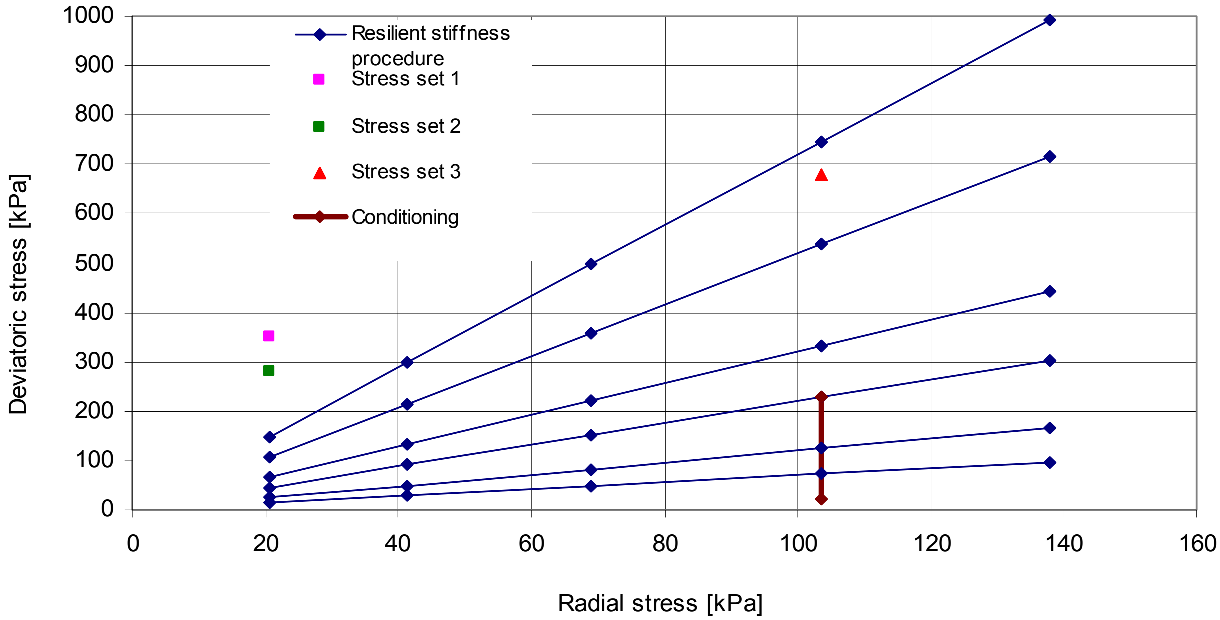

Figure 3.4.5 Stress states for permanent deformation tests relative to resilient modulus tests

Figure 3.4.6 shows the results of permanent strain (ε_p) normalized by the resilient strain (ε_r) seen in the stress cycle for the four tests performed and plotted against the number of load cycles in the permanent deformation test (N). The data shown in Figure 3.4.6 was fit to an equation having the form given by Equation 3.4.1 with the values of a and b shown on Figure 3.4.6.

$$\log \frac{\varepsilon_p}{\varepsilon_r} = a + b \log(N) \tag{3.4.1}$$

From Figure 3.4.6 it is seen that the M_R conditioning has an effect on the overall magnitude of the permanent deformation response. Both the slope and intercept terms in Equation 3.4.1 differs significantly between the unconditioned and conditioned specimens. To account for these differences the M_R conditioning can be interpreted as applying some initial number of load cycles ΔN that induces some initial permanent strain $\Delta\varepsilon_p$ prior to the start of the actual permanent deformation loading. In other words, the N and ε_p measured in the conditioned tests are not the same N and ε_p measured in the unconditioned tests, but instead can be expressed as follows:

$$N_{equiv} = N + \Delta N \tag{3.4.2}$$

$$(\varepsilon_p)_{equiv} = \varepsilon_p + \Delta\varepsilon_p \tag{3.4.3}$$

in which N_{equiv} and $(\varepsilon_p)_{equiv}$ are the equivalent total number of load cycles and permanent strain including the loading cycles during the initial M_R sequence and where ΔN and $\Delta\varepsilon_p$ can be viewed as horizontal and vertical shift factors for the conditioned permanent deformation test results.

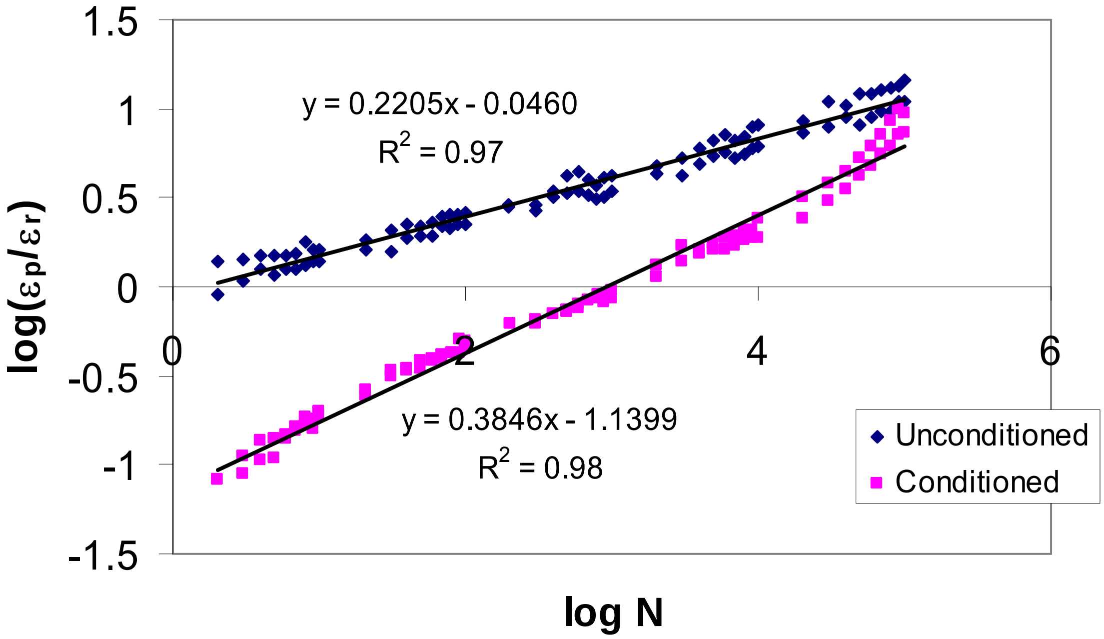

Figure 3.4.6 Resilient modulus conditioned and unconditioned permanent deformation test results

It should be noted that the loading cycles during the initial M_R sequence are at various stress conditions, all of which are different from the stress conditions in the permanent deformation loading. However, the model form of Equation 3.4.1 is designed to account for different stress conditions through normalization by the resilient strain term in the denominator.

The unknown ΔN and $\Delta\varepsilon_p$ values in Equations 3.4.2 and 3.4.3 can be determined via nonlinear optimization by requiring that both the unconditioned and conditioned permanent deformation results conform to the same linear trend in log-log space, with these equations expressed by Equations 3.4.4 and 3.4.5 and in which the regression coefficients *a* and *b* are required to be the same for both equations.

Unconditioned: $$\log \frac{\varepsilon_p}{\varepsilon_r} = a + b \log N \qquad (3.4.4)$$

Conditioned: $$\log \frac{\varepsilon_p + \Delta\varepsilon_p}{\varepsilon_r} = a + b \log(N + \Delta N) \qquad (3.4.5)$$

In actuality, the ΔN and $\Delta\varepsilon_p$ values in Equations 3.4.4 and 3.4.5 are not completely unknown. The M_R test sequence consists of 4000 load cycles and the permanent strain at end of the M_R test sequence is also measured during the conditioned tests. The permanent strains at the end of the M_R test sequence for these two replicates were 0.0033 and 0.0043.

The nonlinear optimization of Equations 3.4.4 and 3.4.5 was performed for two cases: (a) no constraint on the horizontal shift ΔN; and (b) ΔN constrained to a value of 4000 (i.e. the number of load cycles in the M_R sequence). The vertical shift $\Delta\varepsilon_p$ was unconstrained in both cases.

Results from the unconstrained nonlinear optimization case are shown in Figure 3.4.7. The best-fit line through the unconditioned and shifted conditioned data occurred for values of the shift factors ΔN=615 and $\Delta\varepsilon_p$=2.87E-3.

The low standard error ratio seen in Figure 3.4.7 indicates a good statistical fit. However, close examination of the shifted conditioned data in Figure 3.4.7 suggests that there may be some bias; the shifted conditioned data are slightly overpredicted, then slightly underpredicted, and then slightly overpredicted again as *N* increases, suggesting that the shifted conditioned data are not as well represented by a power law model as are the unconditioned data. This behavior was also evident in the unshifted conditioned data in Figure 3.4.6; it is simply amplified by the shifting procedure.

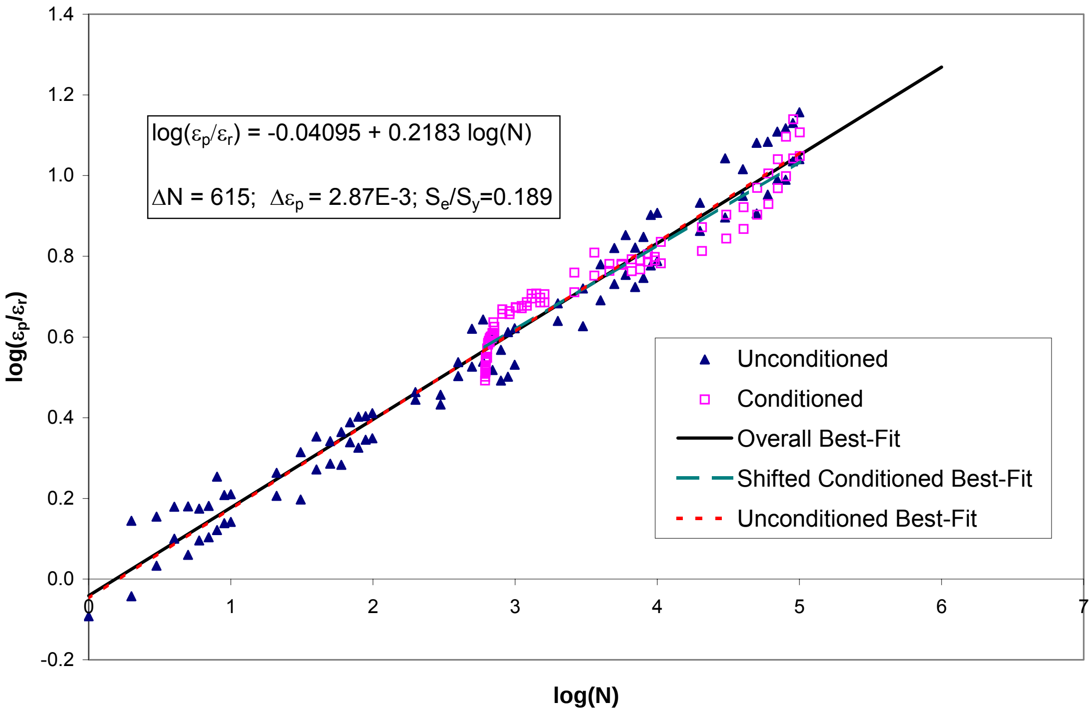

Figure 3.4.7 Unconstrained non linear optimization results

Individual best-fit lines through the unconditioned and shifted conditioned data are also shown on Figure 3.4.7 and are given by Equations 3.4.6 and 3.4.7.

Unconditioned: $$\log\frac{\varepsilon_p}{\varepsilon_r} = -0.0483 + 0.2211\log N \qquad R^2 = 0.97 \qquad (3.4.6)$$

Shifted Conditioned: $$\log\frac{\varepsilon_p}{\varepsilon_r} = -0.0061 + 0.2081\log N \qquad R^2 = 0.92 \qquad (3.4.7)$$

The slope coefficients for both of these equations are comparable and similar to the value for the combined results. The intercept coefficients in Equations 3.4.6 and 3.4.7 differ by approximately one order of magnitude, however.

Results from the nonlinear optimization case with ΔN constrained to a value of 4000 are shown in Figure 3.4.8. The best-fit line through the unconditioned and shifted conditioned data occurred at a vertical shift factor value $\Delta\varepsilon_p$=3.93E-3.

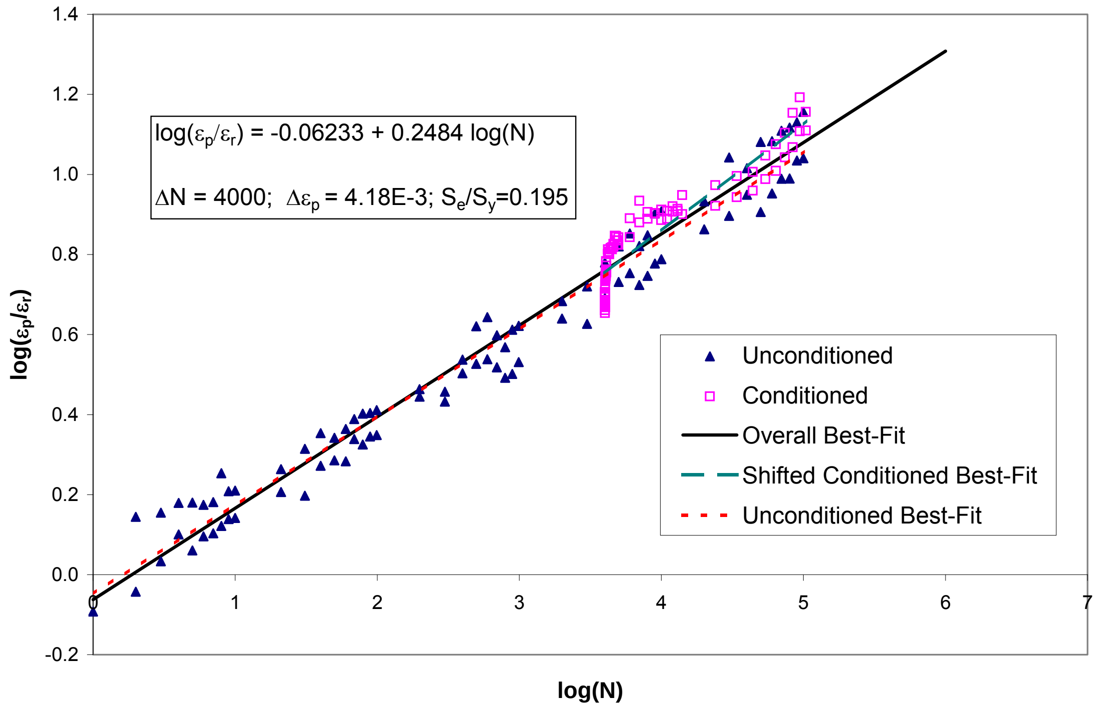

Figure 3.4.8 Constrained non linear optimization results

The standard error ratio for the equation shown on Figure 3.4.8 is again quite low, but the bias in the shifted conditioned data is more pronounced. Note that the vertical shift factor $\Delta\varepsilon_p$=4.18E-3 for the best-fit condition lies almost in the middle of the measured range of 3.3E-3 to 4.3E-3 for the two replicates.

Individual best-fit lines through the unconditioned and shifted conditioned data are also shown on Figure 3.4.8 and are given by Equations 3.4.8 and 3.4.9.

Unconditioned: $$\log\frac{\varepsilon_p}{\varepsilon_r} = -0.0483 + 0.2211 \log N \qquad R^2 = 0.97 \qquad (3.4.8)$$

Shifted Conditioned: $$\log\frac{\varepsilon_p}{\varepsilon_r} = -0.2185 + 0.2697 \log N \qquad R^2 = 0.85 \qquad (3.4.9)$$

The slope coefficients for both of these equations are comparable and similar to the value for the combined results shown on Figure 3.4.8. The intercept coefficients in Equations 3.4.8 and 3.4.9 now differ only by about a factor of 4 and bracket the intercept coefficient for the combined regression in Figure 3.4.8.

In summary, treating the effects of the M_R conditioning as initial horizontal (N) and vertical (ε_p) offsets of the subsequent permanent deformation test results is arguably appropriate in concept and appears acceptable in practice. The ΔN shift can be taken as the total number of cycles during specimen conditioning (4000 for M_R conditioning using the NCHRP 1-28A protocols) and $\Delta\varepsilon_p$ can be set equal to the measured accumulated permanent strain at the end of the specimen conditioning. The shifted M_R-conditioned permanent deformation data follow the same overall trend (i.e., similar slope and intercept coefficients in log-log space) as the unshifted unconditioned data. There is a systematic bias in the measured vs. predicted unconditioned data that is magnified by the shifting procedure, suggesting that a linear fit (in log-log space, or power law in arithmetic space) is perhaps not the most appropriate model form for the shifted conditioned data. Nonetheless, the linear fit is judged sufficiently accurate for comparative analysis and prediction purposes. The data presented below for the permanent deformation tests from the large-scale triaxial device has been corrected using a similar procedure. Details concerning the procedure used are described in Section 3.4.5.

3.4.4 Resilient Modulus Results

Resilient modulus was calculated for each of the loading steps in the same manner as that described in Section 3.2.1. Resilient modulus results were then fit to the non linear elastic model given by Equation 3.4.10. Table 3.4.5 lists the values of k_1, k_2, k_3 resulting from the calibration process. In Table 3.4.5, reinforcement products are identified by a number ranging from 1 to 4. These numbers do not correspond to the sequence of products listed in Table 3.4.3.

$$M_R = p_a k_1 \left(\frac{\theta}{p_a}\right)^{k_2} \left(\frac{\tau_{oct}}{p_a}+1\right)^{k_3} \tag{3.4.10}$$

Table 3.4.5 shows the deviation in parameter values between the different samples is relatively insignificant. The standard deviations for k_1, k_2, k_3 are 50, 0.04 and 0.07 respectively. In addition to the R^2 values shown in Table 3.4.5, Figure 3.4.9 shows the average resilient moduli for each step from all the samples. The variation between the samples is indicated with ± two times the standard deviation (≈ 95 % confidence). This data together shows a good fit of the data to Equation 3.4.10 and a negligible difference between reinforced and unreinforced specimens. Comparison of values of k_1, k_2, k_3 for the CRREL aggregate to results obtained on conventional sized specimens (Section 3.2.1), where values of k_1 = 662, k_2 = 1.010, and k_3 = -0.585 were obtained, shows good agreement to the unreinforced large-scale tests.

Table 3.4.5 Resilient modulus properties for CRREL aggregate from large-scale triaxial tests

Sample	Reinforcement & ID	k_1	k_2	k_3	R^2
1	No	725	0.97	-0.589	0.984
2	Yes (1)	681	1.00	-0.520	0.985
3	No	670	0.945	-0.666	0.982
4	Yes (1)	718	1.008	-0.561	0.981
5	Yes (2)	683	1.040	-0.591	0.981
6	Yes (2)	797	0.996	-0.637	0.944
7	Yes (3)	722	1.04	-0.632	0.978
8	Yes (3)	682	1.078	-0.616	0.978
9	Yes (1)	687	1.041	-0.555	0.966
10	No	695	1.080	-0.604	0.979
11	No	714	1.060	-0.653	0.981
12	Yes (1)	671	0.983	-0.450	0.987
13	Yes (4)	828	0.965	-0.574	0.985
14	Yes (4)	740	1.020	-0.694	0.982
15	Yes (1)	746	0.961	-0.506	0.989

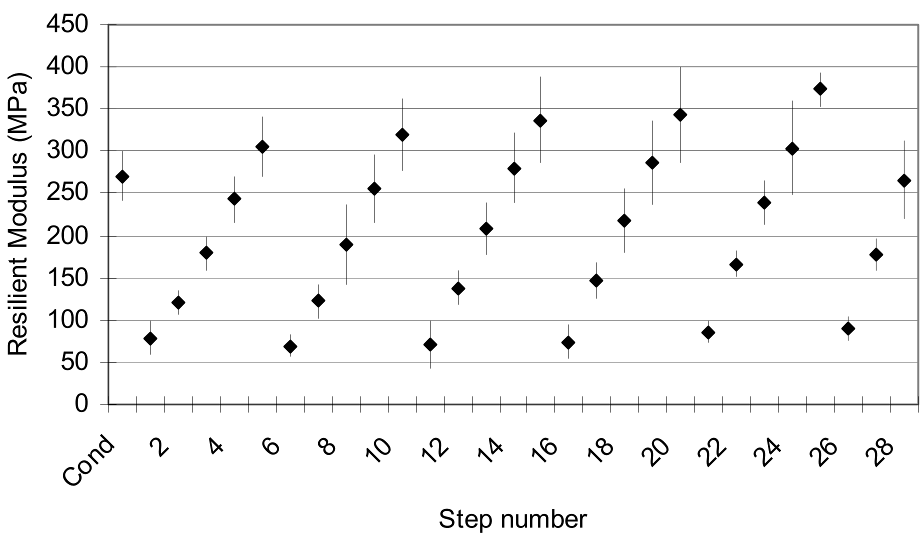

Figure 3.4.9 Resilient modulus for each load step for all CRREL tests

Figure 3.4.10 shows resilient modulus calculated for the second stress state used in the permanent deformation tests (i.e. $(\sigma_1\text{-}\sigma_3)_{max}$ = 281 kPa, σ_3 = 20.7 kPa) using the values of k_1, k_2, k_3 listed in Table 3.4.5 and Equation 3.4.10. Test 16 corresponds to results obtained from conventional sized specimens (Section 3.2.1). The unnumbered lightly shaded boxes correspond to unreinforced tests. Different reinforcement types are denoted by a number from 1 to 4 for the reinforced tests denoted by shaded boxes. The data shown in Figure 3.4.10 tends to support the conclusion that only minor differences in resilient modulus behavior is seen between reinforced and unreinforced specimens and that all results compare well to those obtained from conventional sized specimens. The majority of the tests show values of resilient modulus within 5 % of the mean value. Test 13 was slightly high and yielded a value 10% greater than the mean. Test 3 on an unreinforced specimen gave a comparatively low value being 20 % below the mean.

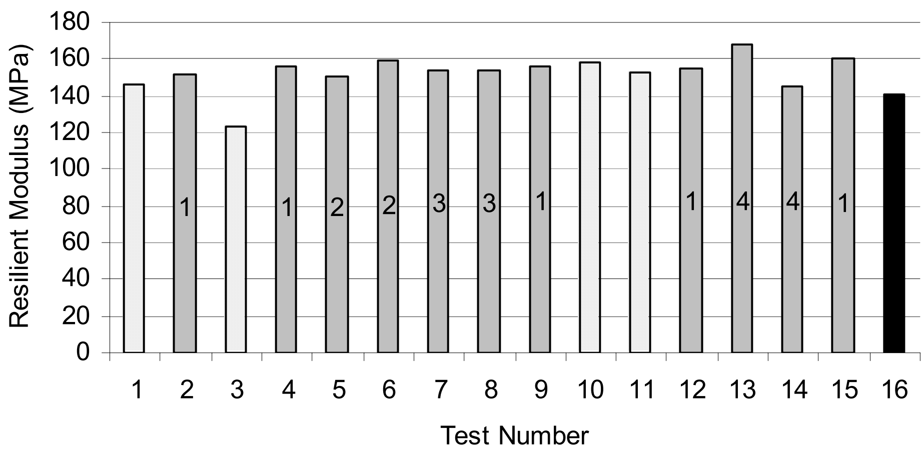

Figure 3.4.10 Calculated resilient modulus for the 2nd permanent deformation test stress state

Table 3.4.6 shows results from tests performed on the GA aggregate. The resilient modulus properties are listed for an average of 3 unreinforced specimens and 3 reinforced specimens using the reinforcement product 1 from the large-scale triaxial tests. Values from conventional sized specimens from Section 3.2.1 are also listed. Resilient modulus listed in Table 3.4.6 is calculated for the 2nd stress state used in the permanent deformation tests. The results show a reduction in resilient modulus between the unreinforced and reinforced large-scale triaxial tests. Comparison of the large-scale and conventional sized unreinforced tests shows an even greater disparity of resilient modulus properties. A comparison of density between the samples shows a lower density in the reinforced large-scale samples as compared to the unreinforced large-scale samples. The conventional sized samples had a higher water content but also a higher density. Resilient modulus tests on the CRREL aggregate gave consistent results between large and conventional sized specimens, indicating that there is not a specimen size effect on resilient modulus properties. Results on the CRREL aggregate also gave consistent results between large scale reinforced and unreinforced tests.

Table 3.4.6 Resilient modulus properties for GA aggregate

Sample	Reinforcement & ID	Density (kN/m^3)	k_1	k_2	k_3	M_R (MPa)
Large-Scale	No	21.8	1136	0.871	-0.489	221
Large-Scale	Yes (1)	21.6	886	0.953	-0.528	185
Conventional Sized	No	22.3	741	1.091	-0.653	165

3.4.5 Permanent Deformation Results

Figure 3.4.11 shows the development of permanent deformation for the CRREL aggregate for tests 1 and 2 conducted under the 1st stress state listed in Table 3.4.4. The reinforced specimen is seen to produce approximately half the permanent deformation for a given number of load cycles.

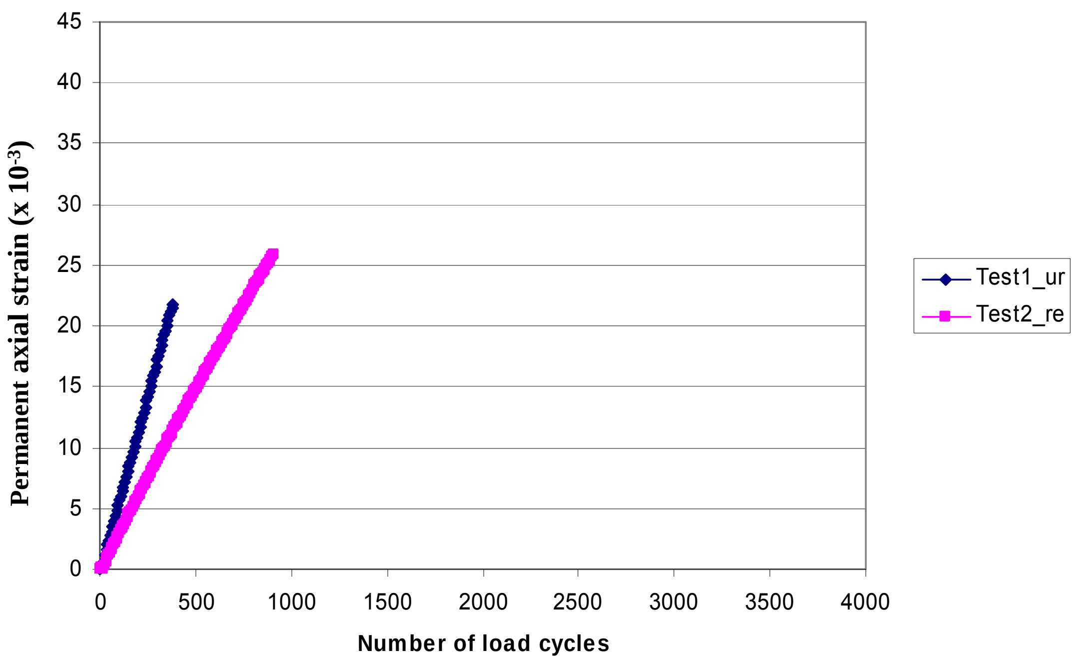

Figure 3.4.11 Permanent deformation versus load cycles for tests 1 and 2 on CRREL aggregate

Figure 3.4.12 shows combined results from tests 1, 2, 3, 4 and 11. Tests 1, 3 and 11 were unreinforced, while tests 3 and 11 were performed at the same stress state. The results show a reasonable comparison between unreinforced tests 3 and 11 despite the fact that the resilient modulus portion of these tests indicated that sample 3 was somewhat less stiff than sample 11 The order of the results does, however, reflect this condition with test 3 giving slightly greater permanent strain. Sample 11 contained one membrane, while sample 3 contained two membranes, however the additional confinement provided by two membranes did not appear to affect either the resilient modulus or permanent deformation results. Test 1 shows less permanent strain than tests 3 and 11, which was not anticipated since test 1 was conducted under a higher degree of mobilization. These results point to the difficulty in repeatability and consistency of results for this type of test, which was also seen in the results in Section 3.2.2 for conventional sized specimens. The scatter in these results, however, is well within the scatter seen from test replicates on conventional sized specimens (Section 3.2.2). Comparison of results from reinforced test 4 to unreinforced tests 3 and 11 shows a significant reduction in permanent strain by a factor of approximately 8.

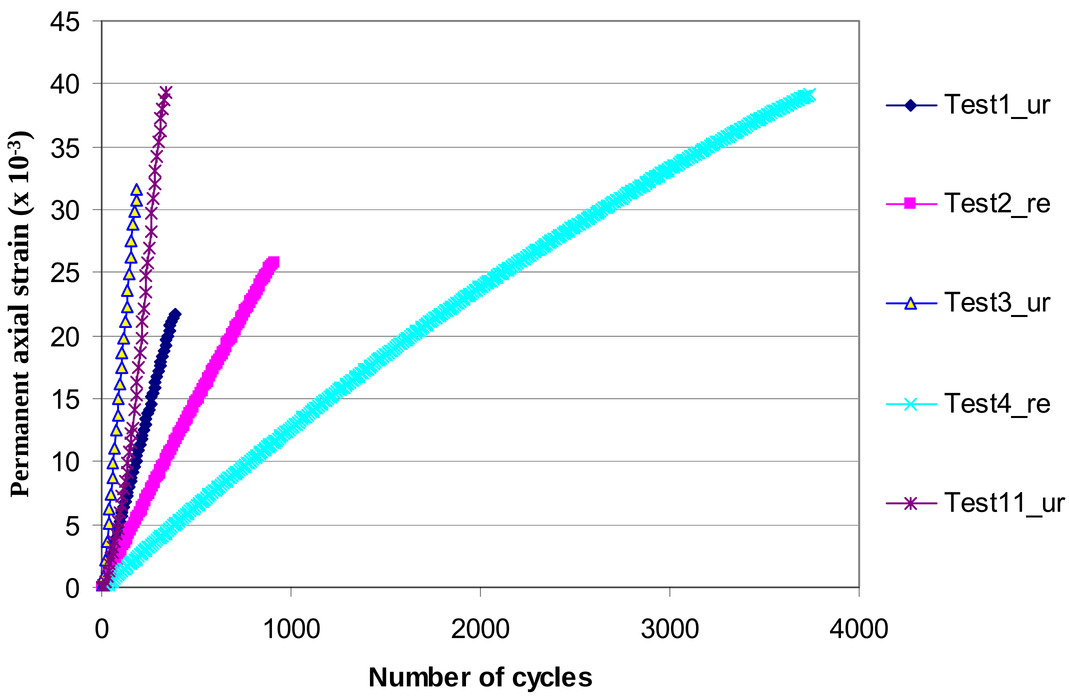

Figure 3.4.12 Permanent deformation versus load cycles for tests 1, 2, 3, 4 and 11 for CRREL aggregate

Figure 3.4.13 shows additional results from tests using reinforcement number 1. Tests 12 and 15 were conducted with only one membrane, whereas the other tests had two membranes. While it might be suspected that the additional confinement provided by two membranes in test 4 was the cause of this difference, comparison of unreinforced tests 3 and 11 that had either one or two membranes does not provide support for this argument.

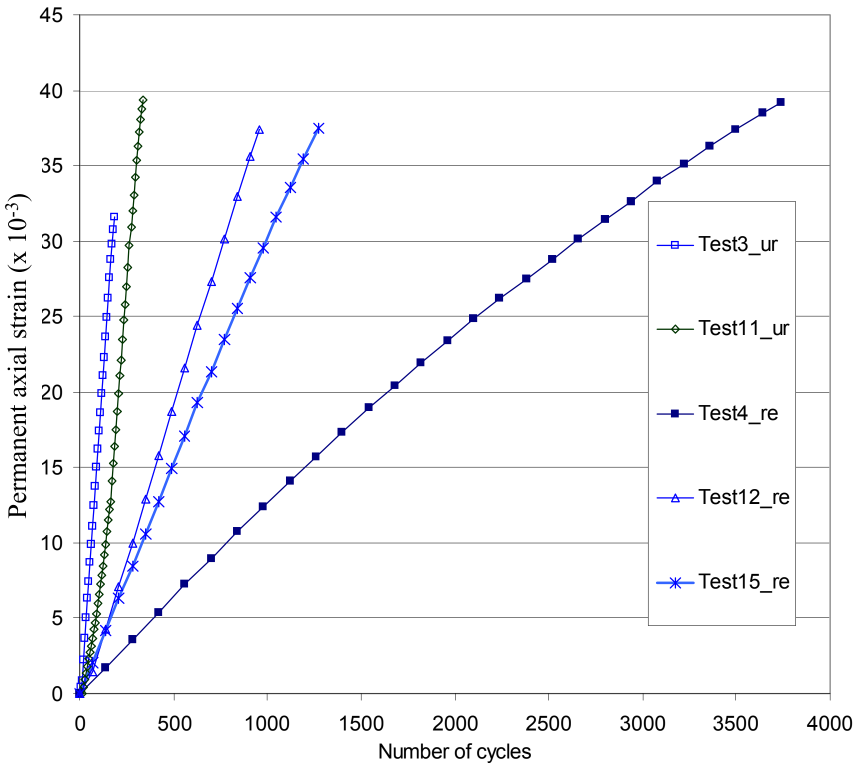

Figure 3.4.13 Permanent deformation versus load cycles for tests 3, 4, 11, 12 and 15 for CRREL aggregate

Figure 3.4.14 shows results from the tests performed under the 2nd stress state. The results show poor performance from test 14, however in this test a local failure in the top of the specimen was noted. Tests 5-7 using reinforcements 2 and 3 performed approximately the same and good repeatability was seen between tests 5 and 6 using reinforcement 2. Test 13 used the same reinforcement as test 14 and developed more permanent deformation as compared to the other reinforcements. Test 13 performed nearly the same, however, as test 15 using reinforcement 1. These results indicate that the scatter in results between reinforced tests is as great as any differences between reinforcement products. All reinforcement products, however, displayed substantially less permanent strain than unreinforced specimens.

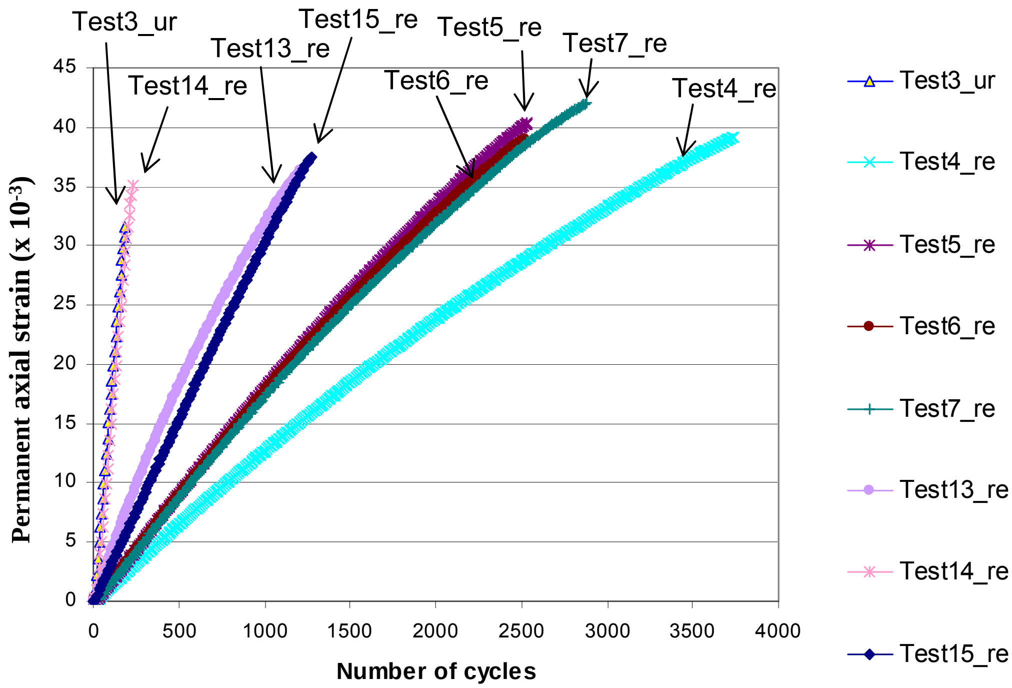

Figure 3.4.14 Permanent deformation versus load cycles for tests 3-7 and 13-15 for CRREL aggretate

Figure 3.4.15 shows results from tests 8-10 where stress state 3 was used. The results show no significant effects of reinforcement for tests conducted at a relatively high confinement of 103 kPa.

Figure 3.4.16 provides a summary of the results presented in Figures 3.4.11 – 3.4.15 by showing the number of cycles necessary to reach 2 % permanent strain. The results clearly show the effect of the reinforcement for stress state 1 and 2. Making clear distinctions between reinforcement products does not appear to be warranted from the results.

The results shown in Figure 3.4.16 do not include the cycles that were necessary to reach 1 % permanent strain in the resilient modulus portion of the test. Figure 3.4.17 provides this data where there is seen to be a similar correlation to the order of results seen in Figure 3.4.16. This suggests that if an equivalent number of cycles from the resilient modulus test were added into that observed from the permanent deformation test, this would only serve to further distinguish the trends seen in Figure 3.4.16.

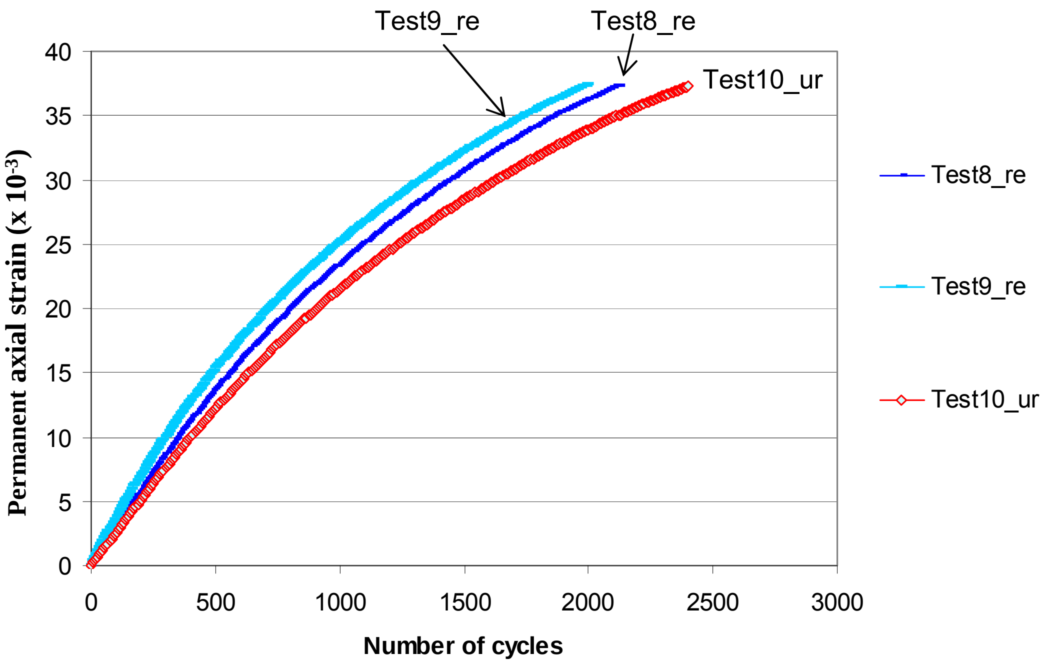

Figure 3.4.15 Permanent deformation versus load cycles for tests 8-10 for CRREL aggregate

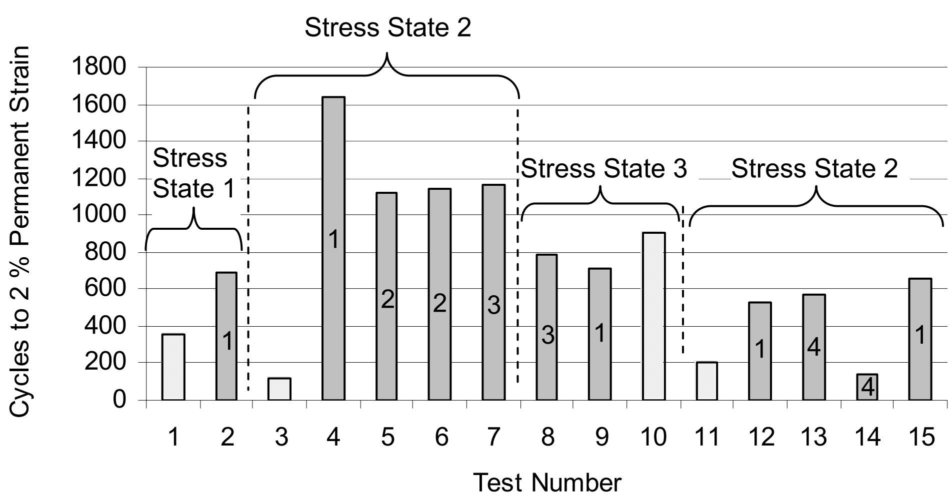

Figure 3.4.16 Cycles to 2 % permanent strain in the permanent deformation tests for CRREL aggregate

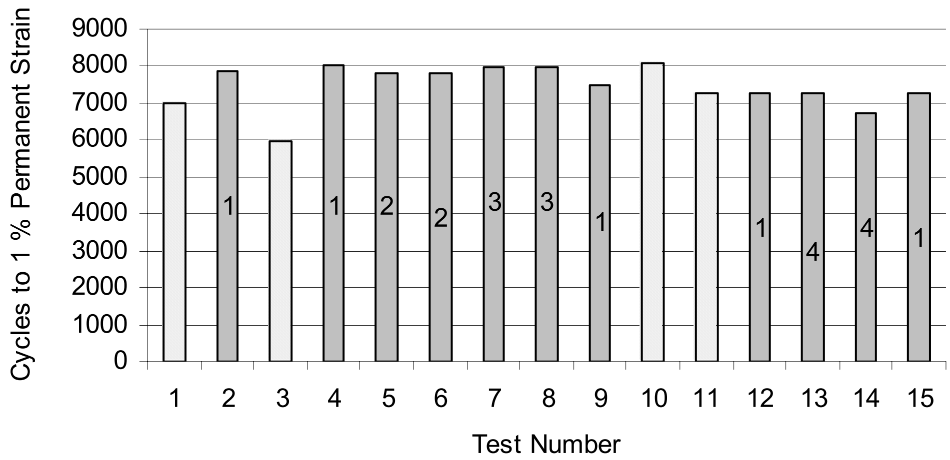

Figure 3.4.17 Cycles to 1 % permanent strain in the resilient modulus tests for CRREL aggregate

Figure 3.4.18 shows the permanent strains developed during the resilient modulus portion of the tests. These results show that significant permanent strain and noticeable differences between reinforced and unreinforced specimens does not occur until step 3 where the mobilized friction angle is 31.5 degrees.

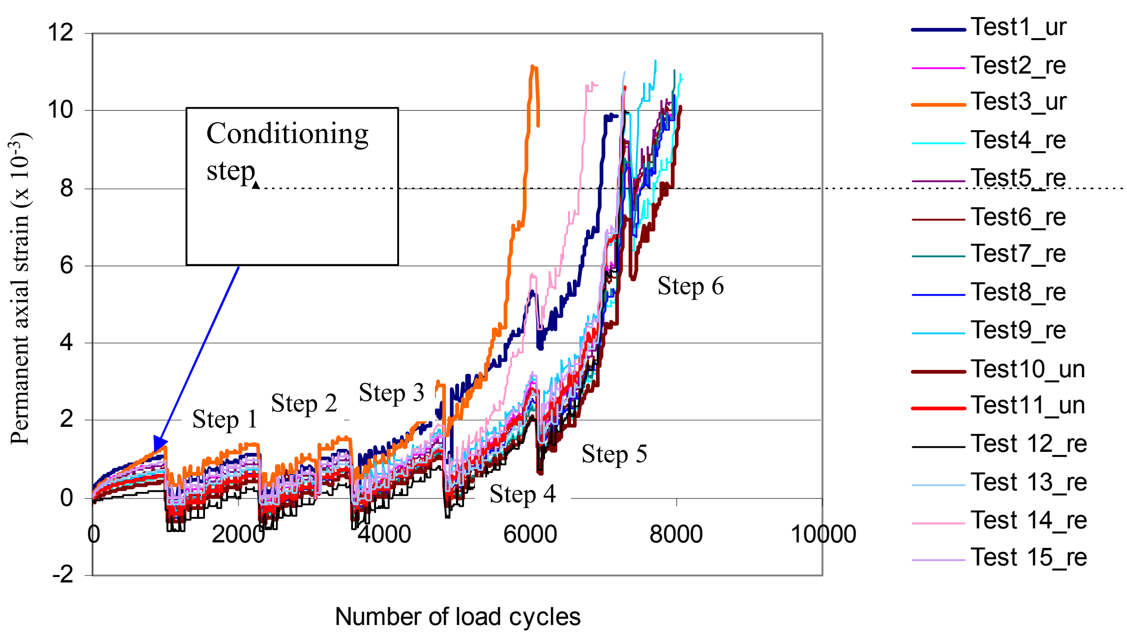

Figure 3.4.18 Permanent strains developed in the resilient modulus tests for CRREL aggregate

The modified Tseng and Lytton (1989) model presented in Section 3.2.2 has been used to interpret permanent deformation results from the large-scale triaxial tests. This model is given by Equation 3.4.11.

$$\delta_a(N) = \xi_1 \left(\frac{\varepsilon_o}{\varepsilon_r} \right) e^{-\left(\frac{\rho}{N} \right)^{\xi_2 \beta}} \varepsilon_v h \qquad (3.4.11)$$

where

δ_a = permanent deformation of a layer

N = number of traffic repetitions

$\varepsilon_o, \beta, \rho$ = material parameters

ε_r = resilient strain imposed in a laboratory test

ε_v = average vertical resilient strain in a layer

h = layer thickness

ξ_1, ξ_2 = field calibration functions

For the triaxial test, Equation 3.4.11 can be rewritten by Equation 3.4.12.

$$\frac{\varepsilon_p}{\varepsilon_v} = \xi_1 \frac{\varepsilon_0}{\varepsilon_r} e^{-\left(\frac{\rho}{N} \right)^{\xi_2 \beta}} \qquad (3.4.12)$$

where ε_p is the permanent strain and ε_v is the resilient strain. Equation 3.4.12 can be rewritten to account for the load cycles and permanent strain developed during the resilient modulus portion of the test (see Section 3.4.3)

$$\frac{\left(\varepsilon_p + \varepsilon_{p-shift} \right)}{\varepsilon_v} = \xi_1 \frac{\varepsilon_0}{\varepsilon_r} e^{-\left(\frac{\rho}{N + N_{shift}} \right)^{\xi_2 \beta}} \qquad (3.4.13)$$

where $\varepsilon_{p-shift}$ and N_{shift} represent the permanent strain and equivalent number of load cycles imposed during the resilient modulus test. When interpreting the triaxial tests the field calibration functions ξ_1 and ξ_2 are set to 1.0. Equation 3.4.14 developed in NCHRP 1-37A was used to determine the parameter β in terms of the water content W_c. For the specimen water content of 3.6 %, a value of β of 0.2115 was obtained. The parameters ($\varepsilon_o/\varepsilon_r$), ρ and N_{shift} were then taken as material parameters calibrated from the test. The value of $\varepsilon_{p\text{-}shift}$ was taken as the actual value of permanent strain induced during the resilient modulus testing procedure (approximately 1 %). The parameter N_{shift} was calibrated from Equation 3.4.13 due to the fact that the stress state in the resilient modulus test was varied with the lower stress levels not producing any permanent strain in the aggregate. N_{shift} had calibrated values ranging from 200 to 500. This procedure is similar in concept but differs slightly in detail from that described in Section 3.2.2. The modifications in this approach were made in order to provide a better fit to the experimental data.

$$\beta = 10^{(-0.6119 - 0.017638 W_c)} \tag{3.4.14}$$

Table 3.4.7 shows the results of the modified Tseng and Lytton calibration for each permanent deformation test. Average calibration parameters were determined by fitting Equation 3.4.12 to an average of test results. Tests 3 and 11 were used to determine average values for unreinforced material. Given the lack of clear distinction between the reinforcement products, tests at stress state 2 were averaged to provide values taken as pertinent to any reinforcement product. It should be noted that values for the reinforced samples are for deformation measurements made for the entire height of the sample. These measurements include aggregate that was not influenced by the reinforcement. This fact is taken into account in Section 3.4.7 to derive parameters pertinent to the aggregate within the zone of reinforcement.

Results from the tests performed using the GA aggregate were inconclusive regarding the effect of reinforcement on permanent strain development. Results from two large-scale unreinforced tests, three reinforced large-scale tests and results from the unreinforced conventional sized tests presented in Section 3.2.2 are given in Figure 3.4.19. The tests on the large-scale specimens were conducted under a confinement of 20.7 kPa, and a deviatoric stress of 345 kPa. The test on the conventional sized specimen was also conducted under a confinement of 20.7 kPa but with a deviatoric stress of 111 kPa. The conventional sized specimen had experienced resilient modulus testing prior to permanent deformation testing. The results show good agreement between the two unreinforced large-scale tests. The unreinforced conventional sized test shows less permanent strain as compared to the large-scale unreinforced tests, which is expected since the deviatoric stress state was less for the conventional sized specimen. A large amount of scatter exists between the three reinforced tests. The shape of two of the curves is not characteristic of typical results from this test.

Table 3.4.7 Permanent deformation parameters for modified Tseng and Lytton model

Sample	Reinforcement	$\varepsilon_0/\varepsilon_r$	β	ρ
1	No	911	0.2115	567358
2	Yes	607	0.2115	700417
3	No	1797	0.2115	418260
4	Yes	492	0.2115	989006
5	Yes	550	0.2115	912953
6	Yes	529	0.2115	796869
7	Yes	578	0.2115	881877
8	Yes	253	0.2115	134570
9	Yes	221	0.2115	87297
10	No	299	0.2115	187797
11	No	17006724	0.2115	177327550
12	Yes	3730	0.2115	3036275
13	Yes	549	0.2115	383507
14	Yes	25926	0.2115	4639519
15	Yes	2640	0.2115	2893046
Average	Unreinforced Test 3, 11	3086	0.2115	338012
Average	Reinforced Test 4-7,13,15	2142	0.2115	1363802

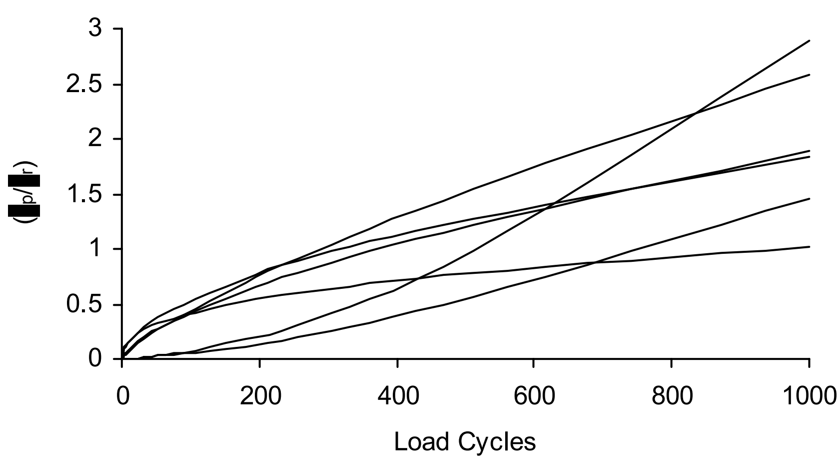

Figure 3.4.19 Normalized permanent strains in reinforced and unreinforced tests with GA aggregate

3.4.6 Zone of Influence

Radial displacement measurements were made along 6 levels of the CRREL aggregate specimens in the repeated load permanent deformation tests and were used to determine radial strain. Figure 3.4.20 shows the distribution of normalized radial strain along the specimen for the average of the reinforced and unreinforced CRREL tests. Radial strain has been normalized by dividing each reading by the average of all six readings. The data shows that the reinforcement has the effect of restraining radial movement of the aggregate. The zone of influence is approximately equal to 150 mm above and below the reinforcement.

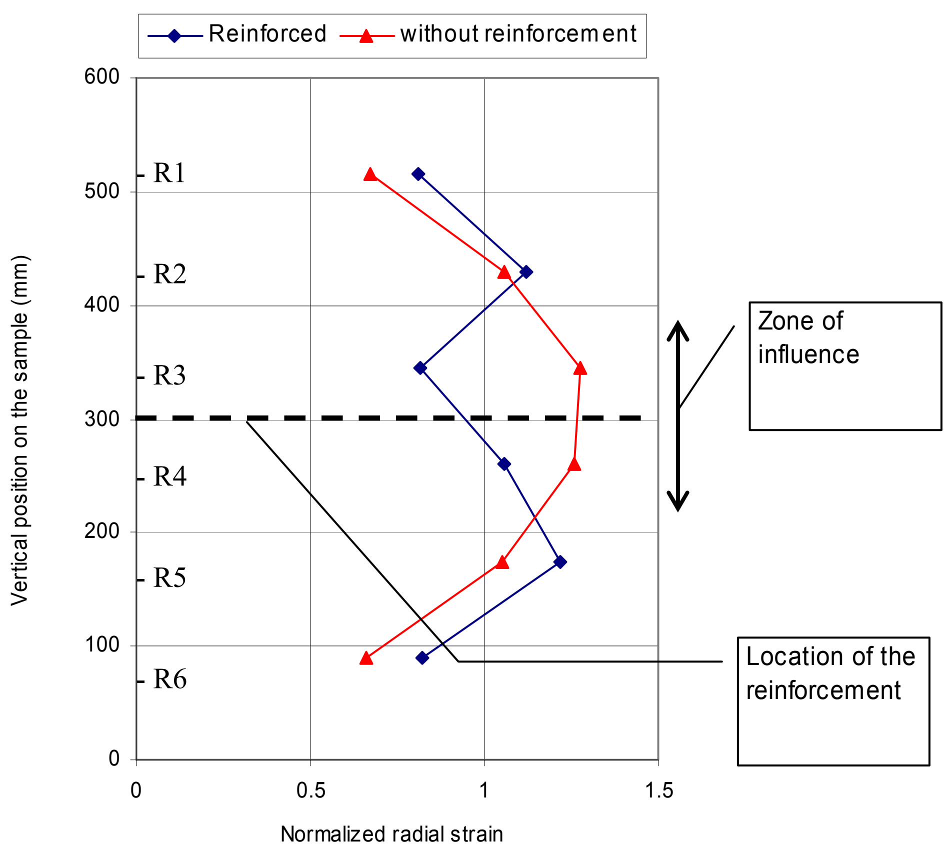

Figure 3.4.20 Average radial strain for permanent deformation tests

3.4.7 Summary and Discussion

From the results presented in Section 3.4 the following points can be made:

1. Reinforcement does not have an effect on the resilient modulus properties of unbound aggregates as seen in triaxial resilient modulus tests.

2. Reinforcement has an appreciable effect on the permanent deformation properties of unbound aggregate as seen in repeated load permanent deformation tests.
3. The relatively poor repeatability seen in permanent deformation tests makes it difficult to distinguish between tests with different reinforcement products.
4. Permanent deformation properties contained in the modified Tseng and Lytton model were determined as average values for reinforced specimens as a group and for unreinforced specimens. The values for reinforced aggregate are in fact average values for both the aggregate within and outside the zone of reinforcement.
5. Reinforcement is not seen to have an appreciable effect on permanent deformation until a mobilized friction angle of approximately 30 degrees is reached.
6. The zone of influence of the reinforcement on the unbound aggregate is equal to the radius of the specimen (150 mm) above and below the reinforcement.

The conclusions made above are supported by recent work reported by Moghaddas-Nejad and Small (2003) where similar tests were reported using two granular materials (a silica sand and 5 mm aggregate) and one geogrid product in samples measuring 200 mm by 400 mm. Specimens contained one layer of reinforcement. They also observed that reinforcement had a negligible effect on resilient modulus but a significant effect on permanent deformation. Reductions in permanent deformation depended on the stress state applied to the sample, with greater reductions seen for low confining pressures and high deviatoric stress (i.e. higher levels of mobilization). Figure 3.4.21 shows the reduction of permanent strain as a function of deviator stress and confining stress, where lines of degree of friction mobilization have been superimposed. The data lines shown in Figure 3.4.21 were generated from a permanent deformation model calibrated from the results of the reinforced and unreinforced tests and therefore do not show the scatter characteristic of actual test data. These results show that reductions in permanent strain do not become appreciable until a mobilized friction angle of approximately 30 degrees is reached. These results also indicate that the reduction of permanent strain in reinforced aggregate is a continuous function of the stress state in the aggregate.

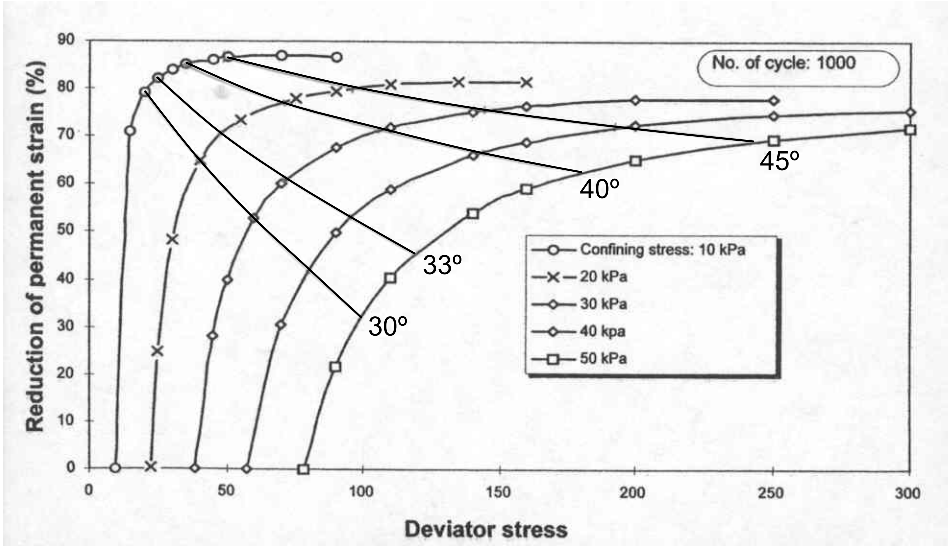

Figure 3.4.21 Reduction in permanent strain at cycle number 1000 versus deviator stress (adapted from Moghaddas-Nejad and Small, 2003)

The permanent deformation parameters determined for reinforced aggregate specimens pertain to a composite sample involving material within and outside the zone of reinforcement. To determine the parameters pertaining only to the material within the zone of reinforcement, the total axial deformation of the sample (Δ_T) for any given cycle number is expressed as the sum of the part within the zone of reinforcement (Δ_R) and the part outside this zone (Δ_U).

$$\Delta_T = \Delta_R + \Delta_U \tag{3.4.15}$$

These deformations can be expressed in terms of strains and sample height over which the strain is assumed to occur (Equations 3.4.16-3.4.18). These equations assume that the reinforced zone corresponds to 150 mm above and below the reinforcement (i.e. ½ of the sample) as was observed in the tests.

$$\Delta_T = \varepsilon_{P_T} H \tag{3.4.16}$$

$$\Delta_R = \varepsilon_{P_R} \frac{H}{2} \tag{3.4.17}$$

$$\Delta_U = \varepsilon_{P_U} \frac{H}{2} \tag{3.4.18}$$

Inserting Equations 3.4.16-3.4.18 into Equation 3.4.15 and dividing by a resilient strain, which is assumed to be constant within each zone, results in Equation 3.4.19. The assumption of constant resilient strain is supported by the observation of constant resilient modulus between reinforced and unreinforced specimens.

$$\frac{\varepsilon_{p_T}}{\varepsilon_r} = \frac{1}{2}\frac{\varepsilon_{p_R}}{\varepsilon_r} + \frac{1}{2}\frac{\varepsilon_{p_U}}{\varepsilon_r} \tag{3.4.19}$$

Equation 3.4.12 is then inserted into Equation 3.4.19 for each $\varepsilon_p/\varepsilon_r$ term, resulting in Equation 3.4.20.

$$\left(\frac{\varepsilon_o}{\varepsilon_r}\right)_T e^{-\left(\frac{\rho_T}{N}\right)^{0.2115}} = \frac{1}{2}\left(\frac{\varepsilon_o}{\varepsilon_r}\right)_U e^{-\left(\frac{\rho_U}{N}\right)^{0.2115}} + \frac{1}{2}\left(\frac{\varepsilon_o}{\varepsilon_r}\right)_R e^{-\left(\frac{\rho_R}{N}\right)^{0.2115}} \tag{3.4.20}$$

The parameters for the "total" specimen are taken as those in Table 3.4.7 for the reinforced specimens, which represent the total deformation of composite samples having reinforced and unreinforced zones. The parameters for "unreinforced zone" are taken as those in Table 3.4.7 for the unreinforced specimens. These parameters are summarized below.

$$\left(\frac{\varepsilon_o}{\varepsilon_r}\right)_T = 2142, \quad \rho_T = 1{,}363{,}802$$

$$\left(\frac{\varepsilon_o}{\varepsilon_r}\right)_U = 3086, \quad \rho_U = 338{,}012$$

Equation 3.4.20 was then solved for the two parameters pertaining to the reinforced zone ($(\varepsilon_o/\varepsilon_r)_R$ and ρ_R) by nonlinear optimization, resulting in the following parameters for the aggregate within the reinforced zone.

$$\left(\frac{\varepsilon_o}{\varepsilon_r}\right)_R = 3560, \quad \rho_R = 6.247\times 10^8$$

Figure 3.4.22 shows the normalized strain ratio $\varepsilon_p/\varepsilon_r$ plotted against load cycles for each of the components in Equation 3.4.20, where it is seen that the sum of the reinforced and unreinforced parts approximates well the total strain measured for the specimens.

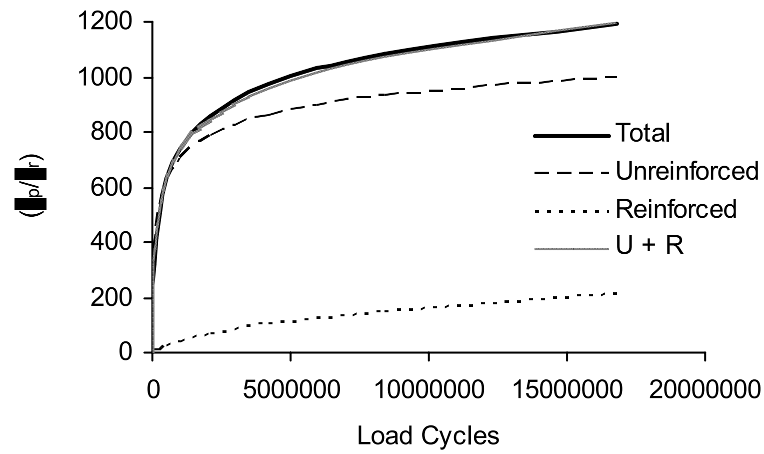

Figure 3.4.22 Normalized permanent strain versus load cycles for reinforced and unreinforced zones of samples containing reinforcement

Table 3.4.8 provides ratios of the parameters between reinforced and unreinforced aggregate. These ratios will be used in later sections to modify permanent deformation properties determined from conventional tests reported in Section 3.2.2 for aggregate in pavements within a zone of influence of the reinforcement

Table 3.4.8 Ratio between permanent deformation model parameters for reinforced and unreinforced aggregate

Parameter	$\varepsilon_0/\varepsilon_r$	ρ	β
Reinforced/unreinforced	1.15	1850	1.0

3.5 Reinforcement Materials

The response model used in this study is a 2-D axisymmetric finite element model based on that contained in the NCHRP 1-37A Design Guide. The use of a 2-D axisymmetric response model requires that the reinforcement be described by an isotropic material model, which by definition is incapable of describing direction dependent (i.e. machine versus cross-machine) material properties. Given that the material models for the remaining pavement layers are elastic, a model of similar complexity is desired and therefore chosen for the reinforcement. While many reinforcement materials exhibit non linear behavior, this behavior is ignored for the sake of simplicity with an attempt, however, made to select properties pertinent to the stress or strain range anticipated for the material. Hence, an isotropic linear elastic model is used for the reinforcement within the finite element response model, where required input parameters consist of an elastic modulus, E, and a Poisson's ratio, ν.

Testing described in this section and in Section 3.6 was performed using three geosynthetic reinforcement materials. These materials were selected because they were used in pavement test sections previously reported by Perkins (1999, 2002). The properties for these materials are also used in later sections pertaining to the development of response models for reinforced pavements. Table 3.5.1 lists these materials and properties reported by the manufacturers. The product ID assigned to the material is used throughout the remainder of this report.

Table 3.5.1 Reinforcement materials used in testing and modeling

Name	Product ID	Type	Aperture size mm MD, XMD	Strength at failure kN/m MD, XMD	Strength kN/m at x % strain x, MD, XMD
Amoco ProPex 2006	A	Polypropylene woven, slit film	NA	30.7, 30.7	2%, 4.3,13.6 5%, 10.0, 22.0
Tensar BX 1100	B	Polypropylene grid	25 x 36	13.0, 20.0	2%, 5.0, 8.1 5%, 9.0, 15.8
Tensar BX 1200	C	Polypropylene grid	25 x 36	21.0, 31.0	2%, 6.4, 10.5 5%, 12.5, 23.0

3.5.1 Orthotropic Linear Elastic Material Model

It is well-known that reinforcement materials exhibit direction dependent properties. Most notably, the elastic modulus differs between the machine and cross-machine directions of the material. An orthotropic material model best describes the direction dependent properties of reinforcement materials but cannot be used directly in a 2-D axisymmetric finite element model. An orthotropic linear elastic material model contains 9 independent elastic constants, of which the four describing behavior within the plane of the material (E_{xm}, E_m, $\nu_{xm\text{-}m}$, $G_{xm\text{-}m}$) are pertinent to a reinforcement sheet modeled by membrane elements. These parameters are defined as:

E_{xm}: Elastic modulus in the cross-machine direction

E_m: Elastic modulus in the machine direction

$\nu_{xm\text{-}m}$: Poisson's ratio in the cross-machine/machine plane

$G_{xm\text{-}m}$: Shear modulus in the cross-machine/machine plane

The use of an elastic model that allows for the specification of different moduli in the two principal directions of the material thus requires specification of Poisson's ratio and shear modulus in the plane of the material. Section 3.5.5 discusses the development of equations used to calculate equivalent isotropic properties (E and ν) for use in the finite element response model from the four orthotropic properties listed above. The indirect properties needed for the response model therefore consist of E_{xm}, E_m, $\nu_{xm\text{-}m}$ and $G_{xm\text{-}m}$.

3.5.2 Elastic Moduli from Cyclic Tension Tests

Elastic moduli in the two principal directions of the reinforcement material can be determined from tension tests. Presently in the U.S., standards ASTM D4595 and ASTM D6637 (ASTM, 2003) are used for conducting tension tests on geotextiles and geogrids, respectively. These tests are performed on samples of prescribed dimensions and at a prescribed strain rate (typically 10 ± 3 %/min) and temperature (typically 20°C). Loading in these tests is monotonic. Ideally, these same tests would be used to determine elastic moduli in the machine and cross-machine material directions, thus providing input parameters for E_{xm}, E_m. Conditions pertinent to the reinforced pavement application that may not be accounted for in these tests include:

1. Cyclic loading
2. Temperature
3. Strain rate
4. Normal stress confinement
5. Sample size

Work has been performed by WTI external to this project to provide information and data for the effect of cyclic loading. A literature review has been performed to examine and comment on the possible influence of temperature, strain rate and normal stress confinement. A literature review on the effect of sample size was conducted, however no clear conclusions could be made.

In a reinforced pavement, permanent strain in the reinforcement is seen to increase with increased traffic passes while dynamic strain for each traffic pass of constant load magnitude remains relatively constant. For non linear reinforcement materials, the modulus will be dependent on the current strain or load at which a cycle of load is applied, which is in turn dependent on the number of traffic passes that have been applied. Creep and/or stress relaxation during repeated loading also leads to changes in material stiffness as the material is reloaded. Conditioning of the material during construction may also be a factor especially for materials whose load-strain curve is convex.

To examine these issues, a series of cyclic tension tests was performed. These tests were performed on standard sized wide-width specimens (200 mm in width by 100 mm in length). Loading was performed by loading up to a prescribed axial strain followed by the application of 1000 load cycles where the axial strain varied between prescribed limits having a cyclic strain amplitude of 0.2 %. The seating strain was applied at a rate of 50 %/min while the cyclic strain was applied at a rate of 16 %/min. Table 3.5.2 provides a schedule of target strain values used in the tests. Temperature during testing was room temperature (20 °C). The tests performed in this way were cyclic stress-relaxation tests in that load was allowed to decrease as the strain was cycled between set limits.

Table 3.5.2 Loading steps for cyclic wide-width tension tests

Step	Static Strain (%)	Cyclic Strain (%)
1	0.5	0.2
2	1.0	0.2
3	1.5	0.2
4	2.0	0.2
5	3.0	0.2
6	4.0	0.2

Results for the three materials listed in Table 3.5.1 in each material direction are shown in Figures 3.5.1 – 3.5.6. In these figures, data from the cyclic test is compared to results from a monotonic loading test performed at a strain rate of 10 %/min. The results show that the initial parts of the two curves are nearly identical even though the strain rate is 5 times faster for this part of the curve for the cyclic test. Once cycling begins, stress relaxation is seen to occur in the material. The amount of stress relaxation tends to grow with increasing step number. When reloading occurs at the end of cyclic loading to the next target strain level, the load-strain curve has a slope that is steeper than the tangent to the monotonic curve at this same strain. This results in the tendency for the cyclic curve to rejoin the monotonic. The slopes of the cyclic curves also tend to increase moderately with increasing cycle number.

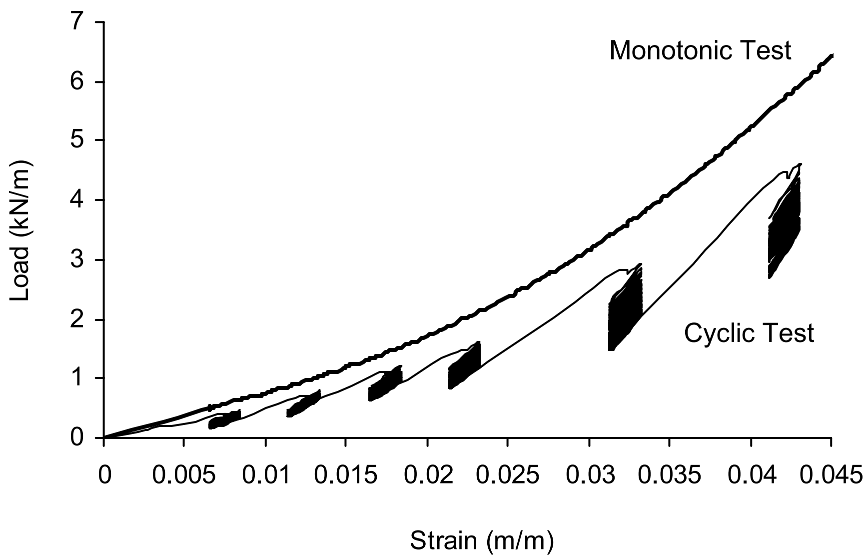

Figure 3.5.1 Cyclic wide-width tension tests on geosynthetic A machine direction

Tables 3.5.3 – 3.5.5 list tensile modulus values determined from the end of cyclic loading for each step, the corresponding tangent modulus from the monotonic curve and the initial modulus from the monotonic curve for all tests performed. For the two geogrids (geosynthetics B and C), this data shows that the modulus after cyclic loading at any step tends to approximate the initial modulus of the load-strain curve and is equal for all step levels. Some of the tests tend to show a modest decrease in cyclic modulus with increased step number, however the decrease is negligible.

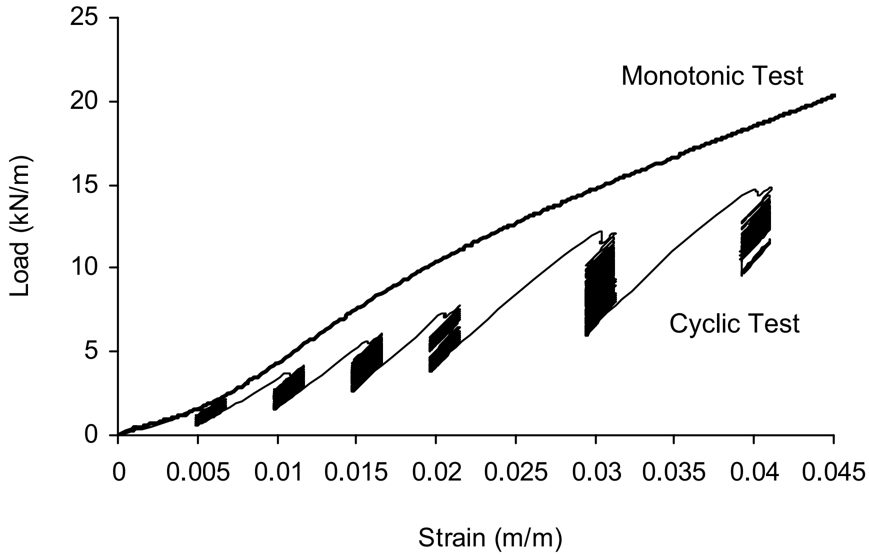

Figure 3.5.2 Cyclic wide-width tension tests on geosynthetic A cross-machine direction

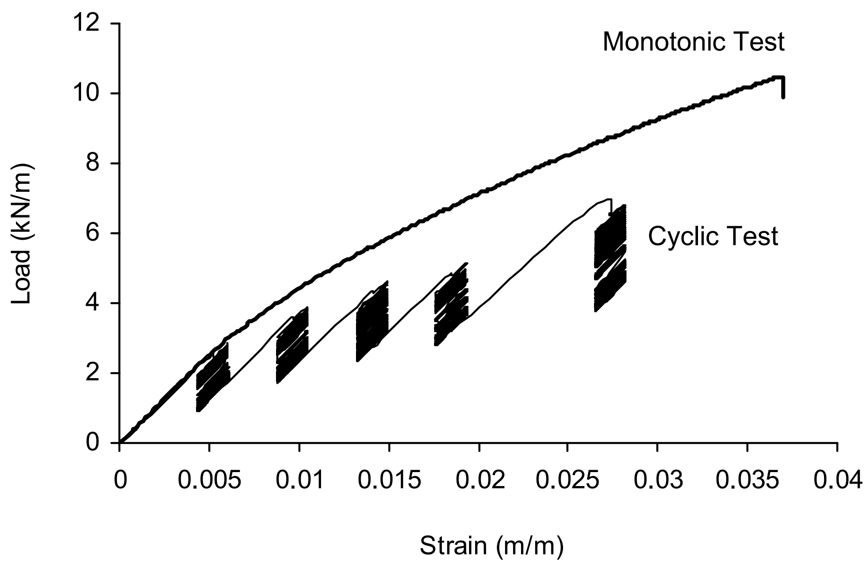

Figure 3.5.3 Cyclic wide-width tension tests on geosynthetic B machine direction

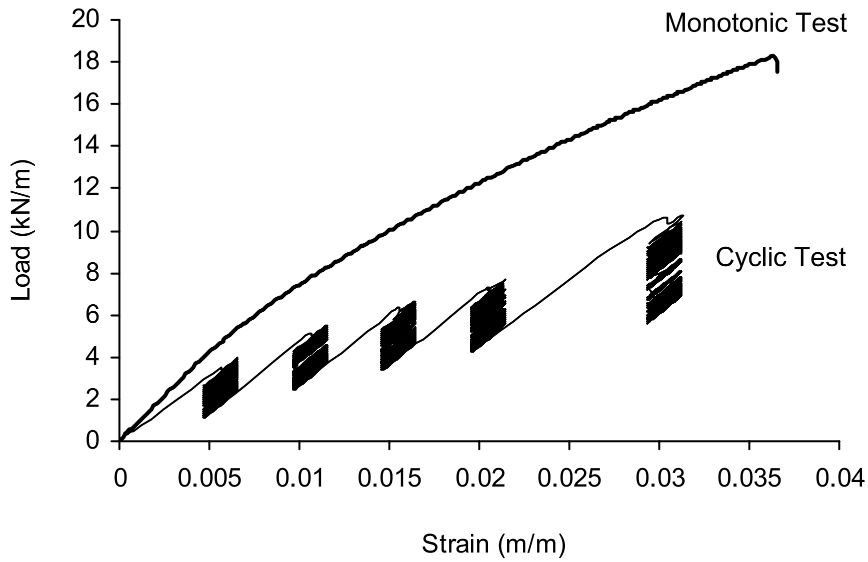

Figure 3.5.4 Cyclic wide-width tension tests on geosynthetic B cross-machine direction

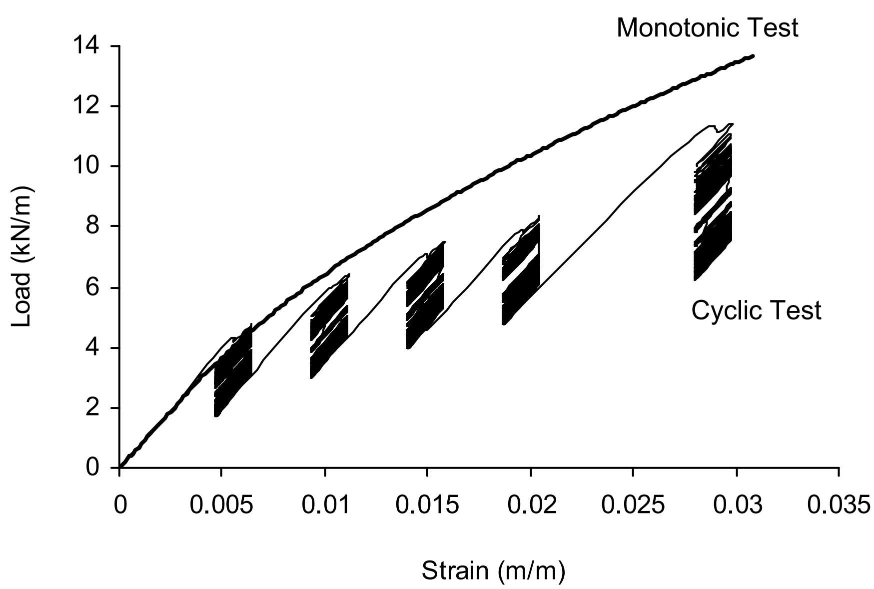

Figure 3.5.5 Cyclic wide-width tension tests on geosynthetic C machine direction

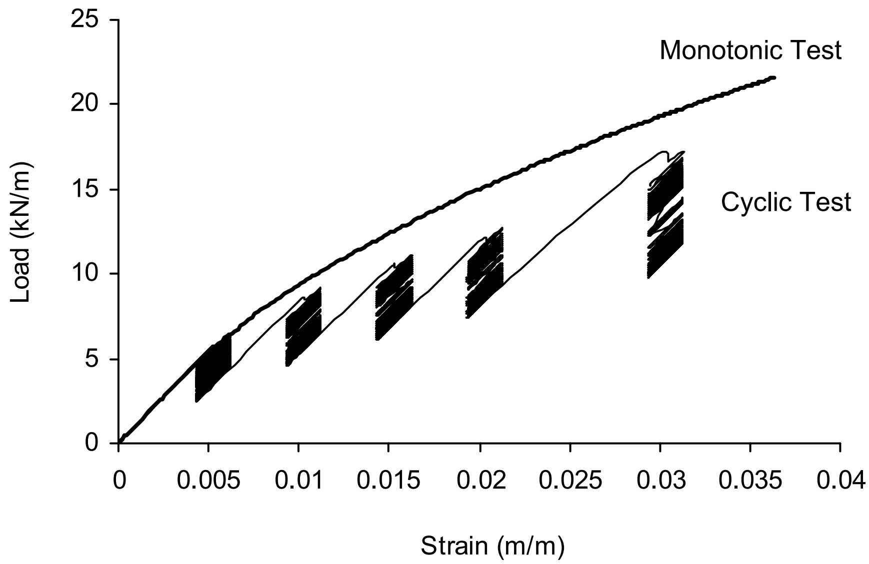

Figure 3.5.6 Cyclic wide-width tension tests on geosynthetic C cross-machine direction

Table 3.5.3 Tensile modulus values for geosynthetic A

<table>
<tr><th rowspan="5">Step</th><th colspan="12">Tensile Modulus (kN/m)</th></tr>
<tr><th colspan="12">geosynthetic A</th></tr>
<tr><th colspan="6">Machine Direction</th><th colspan="6">Cross Machine Direction</th></tr>
<tr><th colspan="3">Test 1</th><th colspan="3">Test 2</th><th colspan="3">Test 1</th><th colspan="3">Test 2</th></tr>
<tr><th>Cyc</th><th>Tan</th><th>Ini</th><th>Cyc</th><th>Tan</th><th>Ini</th><th>Cyc</th><th>Tan</th><th>Ini</th><th>Cyc</th><th>Tan</th><th>Ini</th></tr>
<tr><td>1</td><td>97</td><td>82</td><td rowspan="6">71</td><td>164</td><td>63</td><td rowspan="6">61</td><td>533</td><td>486</td><td rowspan="6">224</td><td>540</td><td>383</td><td rowspan="6">150</td></tr>
<tr><td>2</td><td>160</td><td>101</td><td>202</td><td>81</td><td>743</td><td>578</td><td>948</td><td>533</td></tr>
<tr><td>3</td><td>175</td><td>126</td><td>246</td><td>102</td><td>930</td><td>576</td><td>1053</td><td>569</td></tr>
<tr><td>4</td><td>222</td><td>155</td><td>287</td><td>124</td><td>982</td><td>527</td><td>1067</td><td>541</td></tr>
<tr><td>5</td><td>319</td><td>213</td><td>397</td><td>166</td><td>1137</td><td>402</td><td>1067</td><td>422</td></tr>
<tr><td>6</td><td>452</td><td>248</td><td>490</td><td>198</td><td>1151</td><td>336</td><td>1123</td><td>339</td></tr>
</table>

Table 3.5.4 Tensile modulus values for geosynthetic B

Step	Tensile Modulus (kN/m)											
	geosynthetic B											
	Machine Direction						Cross Machine Direction					
	Test 1			Test 2			Test 1			Test 2		
	Cyc	Tan	Ini	Cyc	Tan	Ini	Cyc	Tan	Ini	Cyc	Tan	Ini
1	537	419	535	553	415	524	739	711	840	725	709	840
2	549	312		553	313		724	557		711	554	
3	532	258		553	259		724	473		710	473	
4	527	233		548	234		726	429		710	431	
5	532	182		553	182		724	343		710	336	

Table 3.5.5 Tensile modulus values for geosynthetic C

Step	Tensile Modulus (kN/m)											
	geosynthetic C											
	Machine Direction						Cross Machine Direction					
	Test 1			Test 2			Test 1			Test 2		
	Cyc	Tan	Ini	Cyc	Tan	Ini	Cyc	Tan	Ini	Cyc	Tan	Ini
1	900	618	667	859	623	740	1171	895	1115	1147	856	1040
2	884	494		828	474		1113	681		1103	665	
3	833	389		794	378		1099	550		1103	547	
4	836	332		796	334		1099	473		1112	474	
5	819	282		796	240		1099	384		1089	386	

For the geotextile (geosynthetic A), the initial load-strain behavior is the least stiff part of the curve, meaning the initial modulus is the lowest of all cyclic or tangent values. Little stress-relaxation is seen for the lower steps and less is seen in the machine direction as compared to the cross machine direction. This results in cyclic modulus values for the lower steps that are more close to the tangent modulus values. As stress-relaxation increases for the higher steps, the cyclic modulus becomes greater.

The results shown above have the following implications for the project and reinforced pavement modeling. For materials like geosynthetics B and C, cyclic loading tends to create a state in the material where the stiffness of small-strain amplitude load cycles is equal to a constant for any level of permanent strain. These results suggest that a constant elastic modulus should be used for the reinforcement for any level of pavement load application. This constant modulus value can be approximated from the average of the cyclic modulus values.

For materials like geosynthetic A, the cyclic modulus tends to increase significantly with increased strain level. Figures 3.5.7 and 3.5.8 show the cyclic modulus values listed in Table 3.5.3 plotted against permanent strain level. The points at zero strain are taken as the initial modulus of the curves. In the absence of strain induced in the material during compaction, these results would suggest that the values at zero strain be used for early load applications. It might also be argued that values for the early load cycles be evaluated for a small value of strain (say 0.2 %) to represent the dynamic strain in the material during load application.

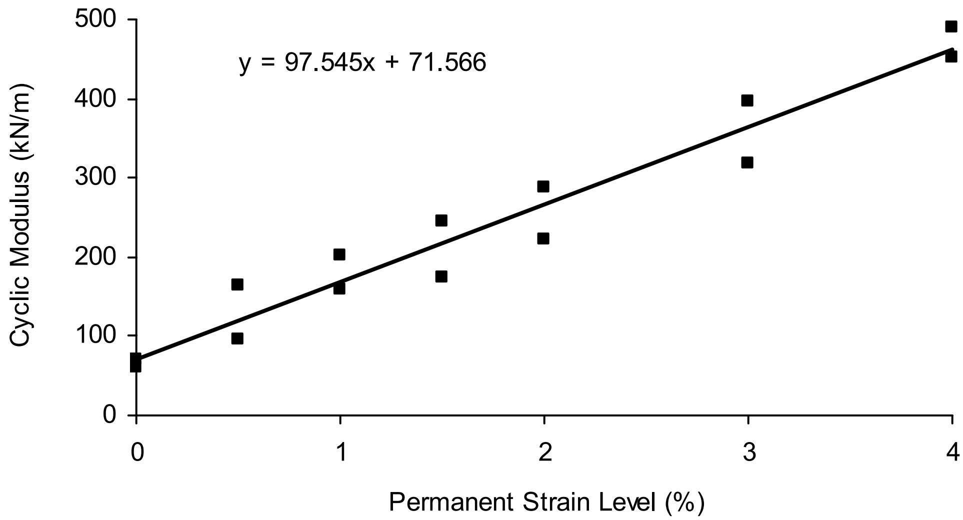

Figure 3.5.7 Cyclic tensile modulus versus permanent strain, geosynthetic A, machine direction

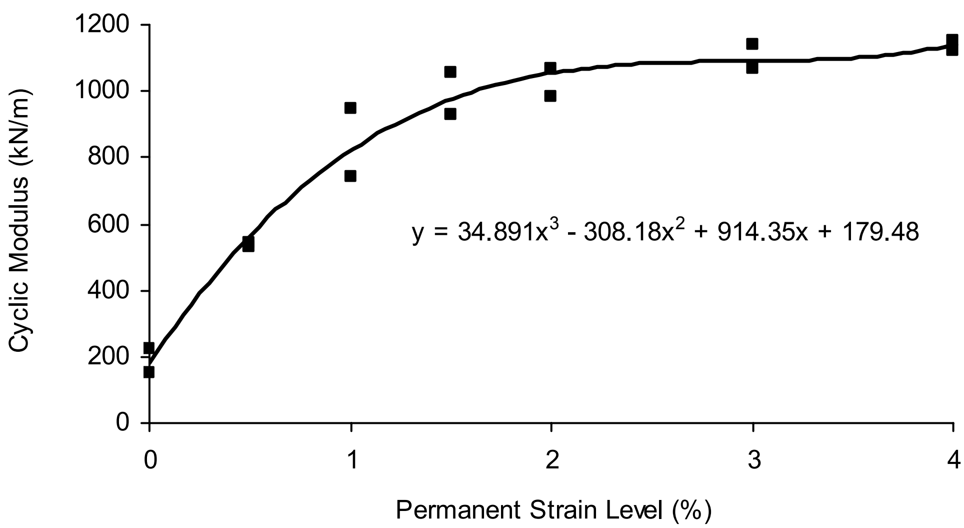

Figure 3.5.8 Cyclic tensile modulus versus permanent strain, geosynthetic A, cross-machine direction

Temperatures within the base aggregate of most pavements are below room temperature. Since most laboratory tension tests are conducted at room temperature, temperature may be a consideration for materials whose elastic modulus is dependent on temperatures colder than room temperature. Table 3.5.6 presents a summary of 11 studies where the mechanical properties of geosynthetics were examined as a function of temperature. Five of these studies used HDPE geomembranes. Of the remaining studies, only one examined the effect of temperature on tensile modulus. Austin et al. (1993) showed a 12 % increase in modulus as temperature was lowered from 32 to 23 ºC. For HDPE geomembranes, Tsuboi et al. (1998) showed an approximate 75 % increase in secant modulus at 1 % strain as temperature decreased from 20ºC to 0. Soong and Lord (1998) showed a 45 % increase in secant modulus at 0.3 % strain for this same temperature decrease. These results suggest modest yet important effects of temperature on modulus but are not sufficiently complete to allow modifications to the tensile modulus values reported in Tables 3.5.3 – 3.5.5 for the three geosynthetics used in this study for anticipated temperatures in roadways.

The strain rate in standard tension tests is relatively slow in comparison to that experienced in the field. As an example, consider a road where the reinforcement develops a dynamic strain of 0.2 % and where a wheel-path travel distance of 0.333 m is required for the dynamic strain to fully develop. For a vehicle traveling at 100 km/hr, the strain rate will be 1000 %/min, which is 100 times faster than the strain rate used in current ASTM testing standards. While many studies have examined the effect of strain rate on tensile modulus and ultimate strength, the majority of these studies have focused on strain rates slower than 10 %/min. For strain rates slower than 10 %/min, creep strains develop and lead to the observation of decreasing modulus with decreasing strain rate. Extrapolation of these results to strain rates faster than 10 %/min will most likely be misleading due to the non linear dependency of creep strains on loading rate.

Table 3.5.6 Literature review of temperature effects in geosynthetics

Study	Temperature (°C)	Geosynthetic	Polymers Type and Number of Products	Material Property of Interest
Calhoun (1972)	-18,23,43,66,82	Geotextile	PP (6)	Tensile strength Strain at failure
			vinylidene chloride(1)	
Allen et al. (1983)	-12, 22	Geotextile	PP (3)	Tensile strength Strain at failure Breaking strength Secant modulus at 10% strain
			PET (2)	
McGown et al. (1985)	0,10,20, 30,40	Geogrid	PP (1)	Tensile strength
Bush (1990)	10,20,40	Geogrid	HDPE (3)	Long-term strength
Austin et al. (1993)	23,27,32	Geogrid	PP (1)	Tensile modulus at 1%, 2% and 5% strain
Budiman (1994)	-20,-10,0,20	Geomembrane	HDPE (1)	Stress/strain behavior
Soong et al. (1994)	-10,10,30, 50,70	Geomembrane	HDPE (1)	Stress relaxation Stress relaxation modulus
Soong and Lord (1998)	-10,10,30,50, 70	Geomembrane	HDPE (1)	Secant modulus at 0.3 % strain
Hsuan (1998)	20,30,40,50, 60,70,80	Geoemebrane	HDPE (2)	Tensile strength Stress/strain behavior
Tsuboi et al. (1998)	-25,0,20, 40,60	Geomembrane	HDPE (1)	Tensile strength Secant modulus at 1% strain
			Ethylene Rubber (1)	
			Thermo Plastic Olefin (1)	
			Poly Vinyl Chloride (1)	
Cazzuffi (1999)	10,20,30	Geogrid	HDPE (1)	Tensile creep behavior
			PET (1)	
		Geotextile	PP/PET (1)	

Of the studies available for strain rates faster than 10 %/min, Van Zanten (1986) showed that tensile strength for different geosynthetic polymers increased with increasing strain rates up to 100 %/min with HDPE giving the greatest increase and with nylon, polyester, and polypropylene giving comparable increases. Raumann (1979) conducted tests on woven polypropylene and polyester materials at strain rates up to 100 %/min and showed that elongation at failure decreased with increasing strain rate with the effect being most significant for polypropylene materials. McGown et al. (1985) also showed that strength increased with increasing strain rate up to 100 %/min and decreasing temperature for HDPE and polypropylene geogrids. Bathurst and Cai (1994) presented load-strain curves for HDPE and polyester geogrids at strain rates up to 1050 %/min (Figure 3.5.9) and showed that stiffness was only slightly influenced by strain rate for polyester materials but was much more significant for polypropylene geogrids. As with temperature effects, these results indicate an important effect of strain rate on modulus, however the existing information is not sufficient to allow for modifications to be made to the modulus values reported in Tables 3.5.3 – 3.5.5 for the three geosynthetics used in this project.

McGown et al. (1982) has shown that normal stress confinement of certain geosynthetics has an influence on tensile modulus with modulus increasing as normal load is applied to the material. FHWA performed an extensive evaluation on the effects of confinement and developed protocols for evaluating confined extension and creep (Elias et al., 1998). In general, effects of confinement are most appreciable for nonwoven geotextiles, of some importance for woven geotextiles and woven geogrids, and not a factor for extruded geogrids. Confined tension tests have not been conducted in this study to examine these effects for the materials used.

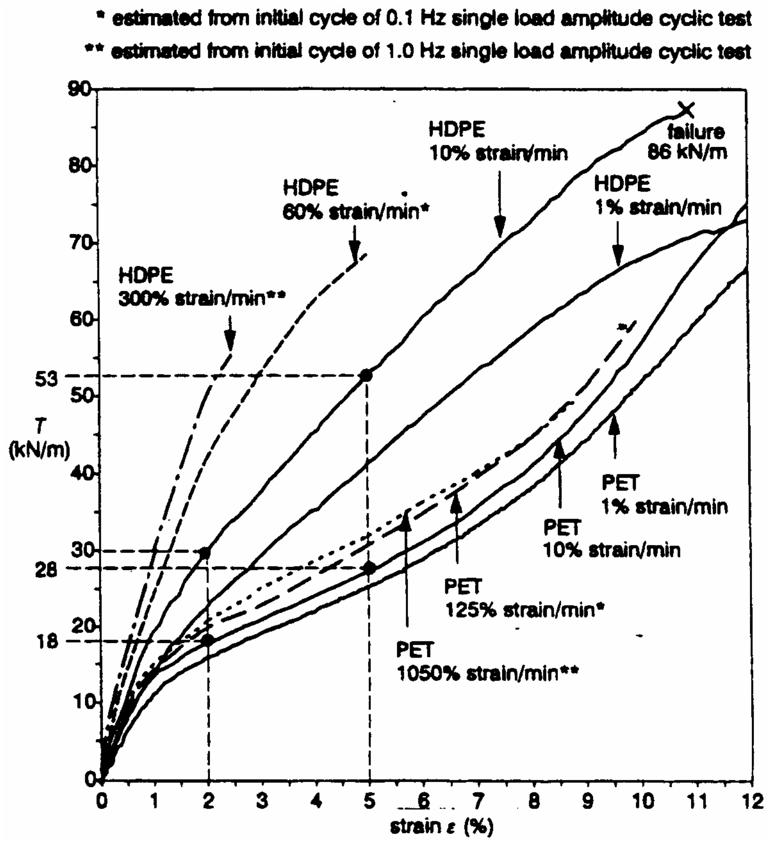

Figure 3.5.9 Load-strain curves at different strain rates (Bathurst and Cai, 1998)

3.5.3 In-Plane Poisson's Ratio from Biaxial Tension Tests

The in-plane Poisson's ratio $\nu_{xm\text{-}m}$ describes the ratio of the compressive transverse strain in the machine direction to the tensile axial strain in the cross-machine direction when the material is loaded uniaxially in the cross-machine direction. Poisson's ratio is commonly determined on continuous materials by measuring the transverse strain and axial strains during a uniaxial loading test where samples are free to contract as axial load is applied. It is unclear whether this type of test would be appropriate for discontinuous materials such as geosynthetic sheets. Conversely, Poisson's ratio can be calculated from a plane-strain tension test when the sample is sufficiently wide to ensure plane strain conditions over the majority of the sample. Samples need to be excessively wide in order to accurately determine Poisson's ratio from this type of test.

Poisson's ratio can also be determined by conducting biaxial loading tests on reinforcement materials. Such a test has been reported by McGown et al. (2002) and McGown and Kupec (2004). The tests are performed by applying an equal constant rate of strain to both principal directions of the material. Load-strain curves are then plotted for each material direction. From the linear elastic portions of the curve, corresponding load (stress) and strain are noted for each material direction. Poisson's ratio $\nu_{xm\text{-}m}$ is then calculated from either Equation 3.5.1 or 3.5.2.

$$\nu_{xm-m} = \frac{E_{xm}}{\sigma_m}\left(\frac{\sigma_{xm}}{E_{xm}} - \varepsilon_{xm}\right) \tag{3.5.1}$$

$$\nu_{xm-m} = \frac{E_{xm}}{\sigma_{xm}}\left(\frac{\sigma_m}{E_m} - \varepsilon_m\right) \tag{3.5.2}$$

where:

E_{xm}: Elastic modulus in the cross-machine direction measured in a corresponding uniaxial test

E_m: Elastic modulus in the machine direction measured in a corresponding uniaxial test

σ_m: Stress in the machine direction from the biaxial test

σ_{xm}: Stress in the cross-machine direction from the biaxial test

ε_m: Strain in the machine direction from the biaxial test

ε_{xm}: Strain in the cross-machine direction from the biaxial test

Data has been reported by McGown and Kupec (2004) on a biaxial geogrid product similar to the geogrids used in this study. This material appears to be approximately isotropic with E_{xm}= E_m= 1580 kN/m. Analyzing the data provided, Poisson's ratio $\nu_{xm\text{-}m}$ calculated from Equation 3.5.1 is equal to 0.5 to 0.7 depending on how the data is interpreted. Similar results were reported for polypropylene and polyester geogrids. Further results from the project are not currently available but are anticipated with the completion of a Ph.D. thesis in 2004. These results suggest that relatively high Poisson's ratios may be used for biaxial geogrids. Since geotextiles have not been tested in this device, it is not clear what values of Poisson's ratio would be obtained.

3.5.4 In-Plane Shear Modulus from Aperture Stability Modulus Tests

The in-plane shear modulus ($G_{xm\text{-}m}$) of sheet reinforcement materials is a parameter for which tests have not been specifically developed. A test has been developed to determine a parameter called the aperture stability modulus, which will be shown below to be related to the in-plane shear modulus of the material. This test was developed in an attempt to explain differences in reinforcement benefit between different geogrid reinforcement materials in test sections conducted by the US Army Corp of Engineers. The test involves clamping a square specimen between a fixed frame having an internal opening of 405 mm by 405 mm. Two 50.8 mm diameter cylinders are clamped to the center of the sample and located directly over the middle of a junction. A torque of 2000 N-mm is applied to the axis of the clamped cylinder and the angle of rotation, θ, (in degrees) is measured. The aperture stability modulus (*ASM*) is then calculated by Equation 3.5.3 and has units of N-mm/degree.

$$ASM = \frac{2000}{\theta} \tag{3.5.3}$$

A theoretical solution for the angle of rotation of a rigid plug fixed to the center of a circular sheet having isotropic linear elastic properties and fixed along its perimeter from rotation (but not from radial movement) (Figure 3.5.10) is:

$$\theta = \frac{T}{4\pi b G R_{in}}\left(\frac{1}{R_{in}} - \frac{R_{in}}{R^2{}_{out}}\right)\frac{180}{\pi} \tag{3.5.4}$$

where:

θ = rotation (degrees)

T = torque

b = sheet thickness

G = in-plane shear modulus

R_{in} = radius of inner rigid plug

R_{out} = radius of circular clamped sheet

Solving Equation 3.5.4 for G results in Equation 3.5.5. Recognizing that the term $T/\theta = ASM$, Equation 3.5.5 is rewritten as Equation 3.5.6.

$$G = \frac{T}{4\pi b \theta R_{in}}\left(\frac{1}{R_{in}} - \frac{R_{in}}{R^2{}_{out}}\right)\frac{180}{\pi} \tag{3.5.5}$$

$$G = ASM\,\frac{180}{4\pi^2 b R_{in}}\left(\frac{1}{R_{in}} - \frac{R_{in}}{R^2{}_{out}}\right) \tag{3.5.6}$$

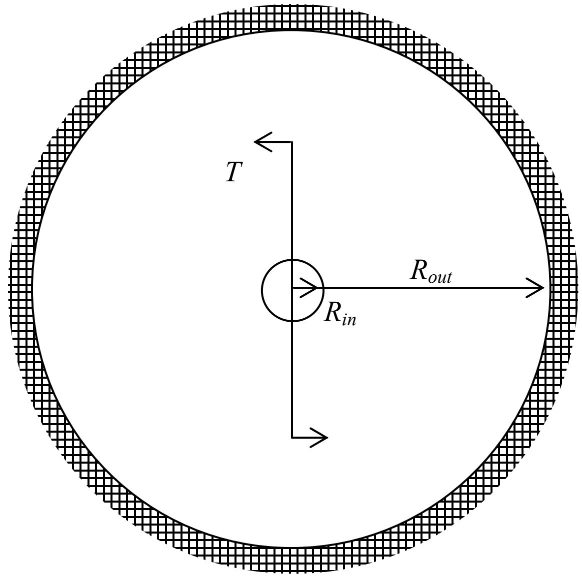

Figure 3.5.10 Orientation of fixed sheet for Equation 3.5.4

Equation 3.5.6 is then applied to conditions in the aperture stability modulus test where R_{in} = 0.0508 m. The outer radius is set equal to a value producing an equivalent area as a square having sides of 0.405 m, and produces a value of R_{out} = 0.2286 m. Assuming that b =0.001 m for reinforcement sheets, Equation 3.5.6 reduces to Equation 3.5.7, where G has units of kPa when ASM has units of N-mm/degree.

$$G = 7ASM \tag{3.5.7}$$

It should be noted that this solution pertains to a reinforcement sheet assumed to have isotropic linear elastic properties, yet is being used to provide a shear modulus that will be used along with other orthotropic linear elastic properties to calculate an equivalent elastic modulus for an isotropic linear elastic material.

Aperture stability modulus tests performed on geosynthetics A, B and C produced values of 260, 135 and 417 N-mm/degree. From Equation 3.5.7, values of in-plane shear modulus are 1.82, 0.945, 2.919 MPa for geosynthetics A, B and C. The results appear to be reasonable for the two geogrid materials (geosynthetics B and C), but excessively high for the geotextile (geosynthetics A). The geotextile value is high because the circular plug engages the tensile properties of the strands as torque is applied. It is unclear how this test or any other test can be used to identify appropriate values for a geotextile. Intuitively, it might be argued that values of shear modulus for woven geotextiles be set to values near zero. The equations developed below in Section 3.5.5 to convert orthortropic to isotropic linear elastic properties will show, however, that setting values of shear modulus close to zero has a significant and unrealistic impact on equivalent isotropic elastic properties. Further work is needed to establish reasonable values for use with geotextiles.

3.5.5 Conversion of Orthotropic to Isotropic Linear Elastic Properties

The constitutive equation for an orthotropic linear-elastic material containing the elastic constants described in Section 3.5.1 is given by Equation 3.5.8.

$$\begin{Bmatrix} \varepsilon_{xm} \\ \varepsilon_{m} \\ \varepsilon_{n} \\ \gamma_{xm-m} \\ \gamma_{xm-n} \\ \gamma_{m-n} \end{Bmatrix} = \begin{bmatrix} 1/E_{xm} & -\nu_{m-xm}/E_m & -\nu_{n-xm}/E_n & 0 & 0 & 0 \\ -\nu_{xm-m}/E_{xm} & 1/E_m & -\nu_{n-m}/E_n & 0 & 0 & 0 \\ -\nu_{xm-n}/E_{xm} & -\nu_{m-n}/E_m & 1/E_n & 0 & 0 & 0 \\ 0 & 0 & 0 & 1/G_{xm-m} & 0 & 0 \\ 0 & 0 & 0 & 0 & 1/G_{xm-n} & 0 \\ 0 & 0 & 0 & 0 & 0 & 1/G_{m-n} \end{bmatrix} \begin{Bmatrix} \sigma_{xm} \\ \sigma_{m} \\ \sigma_{n} \\ \tau_{xm-m} \\ \tau_{xm-n} \\ \tau_{m-n} \end{Bmatrix} \tag{3.5.8}$$

where the subscripts *xm* and *m* denote the in-plane cross-machine and machine directions, and *n* denotes the direction normal to the plane of the geosynthetic. The model contains 9 independent elastic constants, of which 4 (E_{xm}, E_m, ν_{xm-m}, G_{xm-m}) are pertinent to a reinforcement sheet modeled by membrane elements in a pavement response model. Sections 3.5.2 – 3.5.4 discussed testing methods to determine these parameters. Poisson's ratio, ν_{m-xm}, is related to ν_{xm-m} through Equation 3.5.9.

$$\nu_{m-xm} = \nu_{xm-m} \frac{E_m}{E_{xm}} \tag{3.5.9}$$

When using membrane elements, values for the remaining elastic constants can be set to any values that ensure stability of the elastic matrix. Stability requirements for the elastic constants are given by Equations 3.5.10 – 3.5.14.

$$E_{xm}, E_m, E_n, G_{xm-m}, G_{xm-n}, G_{m-n} > 0 \tag{3.5.10}$$

$$\left|\nu_{xm-m}\right| = \left(\frac{E_{xm}}{E_m}\right)^{1/2} \tag{3.5.11}$$

$$\left|\nu_{xm-n}\right| = \left(\frac{E_{xm}}{E_n}\right)^{1/2} \tag{3.5.12}$$

$$\left|\nu_{m-n}\right| = \left(\frac{E_m}{E_n}\right)^{1/2} \tag{3.5.13}$$

$$1 - \nu_{xm-m}\nu_{m-xm} - \nu_{m-n}\nu_{n-m} - \nu_{xm-n}\nu_{n-xm} - 2\nu_{m-xm}\nu_{n-m}\nu_{xm-n} > 0 \tag{3.5.14}$$

The constitutive matrix for an isotropic linear-elastic constitutive matrix is given by Equation 3.5.15 and contains 2 (E, ν) independent elastic constants. The third elastic constant in Equation 3.5.15 (G) is expressed in terms of E and ν by Equation 3.5.16.

$$\begin{Bmatrix} \varepsilon_{xm} \\ \varepsilon_m \\ \varepsilon_n \\ \gamma_{xm-m} \\ \gamma_{xm-n} \\ \gamma_{m-n} \end{Bmatrix} = \begin{bmatrix} 1/E & -\nu/E & -\nu/E & 0 & 0 & 0 \\ -\nu/E & 1/E & -\nu/E & 0 & 0 & 0 \\ -\nu/E & -\nu/E & 1/E & 0 & 0 & 0 \\ 0 & 0 & 0 & 1/G & 0 & 0 \\ 0 & 0 & 0 & 0 & 1/G & 0 \\ 0 & 0 & 0 & 0 & 0 & 1/G \end{bmatrix} \begin{Bmatrix} \sigma_{xm} \\ \sigma_m \\ \sigma_n \\ \tau_{xm-m} \\ \tau_{xm-n} \\ \tau_{m-n} \end{Bmatrix} \tag{3.5.15}$$

$$G = \frac{E}{2(1+\nu)} \tag{3.5.16}$$

Equivalency of measured orthotropic elastic constants (E_{xm}, E_m, ν_{xm-m}, G_{xm-m}) to isotropic constants (E, ν) is established using a work-energy equivalency formulation. It is assumed that two materials, one containing orthotropic properties and the second containing isotropic properties, experience an identical general state of stress given in Figure 3.5.11.

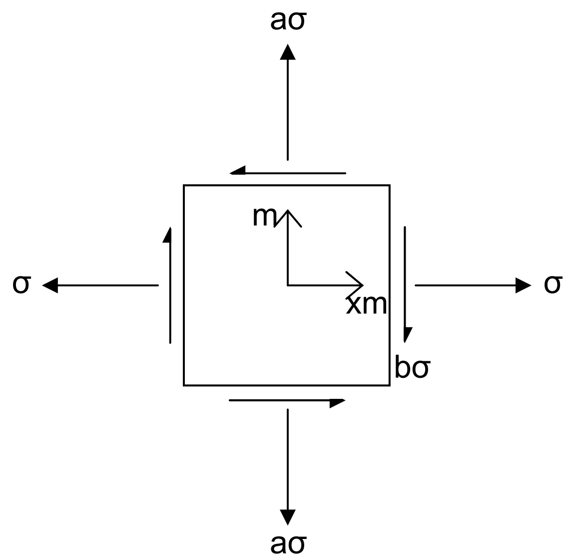

Figure 3.5.11 General state of stress experienced by a reinforcement element

According to Equations 3.5.8 and 3.5.15, the three in-plane strains produced by this stress state in the orthotropic material are given by Equations 3.5.17 – 3.5.19 and by Equations 3.5.20 – 3.5.22 for the isotropic material.

$$\varepsilon_{xm} = \sigma\left(\frac{1}{E_{xm}} - a\frac{\nu_{m-xm}}{E_m}\right) \tag{3.5.17}$$

$$\varepsilon_{m} = \sigma\left(\frac{a}{E_{m}} - \frac{\nu_{m-xm}}{E_m}\right) \tag{3.5.18}$$

$$\gamma_{xm-m} = \frac{b\sigma}{G_{xm-m}} \tag{3.5.19}$$

$$\varepsilon_{xm} = \frac{\sigma}{E}(1 - a\nu) \tag{3.5.20}$$

$$\varepsilon_{m} = \frac{\sigma}{E}(a - \nu) \tag{3.5.21}$$

$$\gamma_{xm-m} = 2b\sigma\frac{(1+\nu)}{E} \tag{3.5.22}$$

The work energy produced by the application of the stress state shown in Figure 3.5.11 is given in general by Equation 3.5.23. Substitution of Equations 3.5.17 – 3.5.19 and 3.5.20 – 3.5.22 into Equation 3.5.23 results in the work energy for the orthotropic and isotropic materials given by Equations 3.5.24 and 3.5.25, respectively.

$$W = \frac{1}{2}\left(\sigma\varepsilon_{xm} + a\sigma\varepsilon_{m} + b\sigma\gamma_{xm-m}\right) \tag{3.5.23}$$

$$W = \frac{\sigma^2}{2}\left(\frac{1}{E_{xm}} + \frac{a^2}{E_m} - \frac{2a\nu_{m-xm}}{E_m} + \frac{b^2}{G_{xm-m}}\right) \tag{3.5.24}$$

$$W = \frac{\sigma^2}{2E}\left(1 - 2a\nu + a^2 + 2b^2(1+\nu)\right) \tag{3.5.25}$$

Equivalent isotropic elastic constants are chosen to produce equivalent work energy by the orthotropic and isotropic materials given by Equations 3.5.24 and 3.5.25. Since an infinite number of combinations of the two isotropic elastic constants (E, ν) to establish equivalency between Equations 3.5.24 and 3.5.25 are possible, a value for the isotropic Poisson's ratio, ν, is assumed such that the value of isotropic elastic modulus, E, can be calculated. Setting Equations 3.5.24 and 3.5.25 equal to each other and solving for E results in Equation 3.5.26. Assuming a value of $\nu = 0.25$ and substitution of Equation 3.5.9 into Equation 3.5.26 results in Equation 3.5.27.

$$E = \frac{1 - 2a\nu + a^2 + 2b^2(1+\nu)}{\frac{1}{E_{xm}} + \frac{a^2}{E_m} - 2a\frac{\nu_{m-xm}}{E_m} + \frac{b^2}{G_{xm-m}}} \tag{3.5.26}$$

$$E = \frac{1 - 0.5a + a^2 + 2.5b^2}{\frac{1}{E_{xm}} + \frac{a^2}{E_m} - 2a\frac{\nu_{xm-m}}{E_{xm}} + \frac{b^2}{G_{xm-m}}} \tag{3.5.27}$$

Equation 3.5.27 provides a means of establishing an equivalent isotropic elastic modulus (E) for an assumed value of isotropic Poisson's ratio (ν) for a single state of stress given in Figure 3.5.11. In Figure 3.5.11, the stress factors a and b describe the magnitude of normal stress in the machine direction and the magnitude of shear stress acting on the reinforcement element. The stress state in a reinforcement layer in a pavement system varies from point to point, meaning that values of *a* and *b* vary from point to point. This situation creates the need to assess values of *a* and *b* in an average sense for the entire reinforcement layer. Since pavement response models are ultimately used for the prediction of pavement performance, the true test of equivalency lies in the comparison of performance predictions between response models using orthotropic and isotropic elastic constants. The stress factors *a* and *b* are estimated using the following procedure:

1. A 3-dimensional model of a reinforced pavement system was created. The pavement cross-section consisted of three layers (75 mm of asphalt concrete, 300 mm of base aggregate, 3.435 m of subgrade) with the reinforcement placed between the base and subgrade layers. The distance from the pavement load centerline to the edge of the model was 2.4384 m.

   A linear elastic model was used for the asphalt concrete layer. The non-linear elastic model with tension cutoff described in Section 3.2.1 was used for the base and subgrade layers. Three sets of material properties were used and are given in Tables 3.5.7 – 3.5.9. Properties given in Table 3.5.7 represent the materials used in the MSU test sections using the MSU base and CS subgrade. A temperature of 21.5ºC was assumed for the AC material.

Table 3.5.7 Material property set 1 for the 3D model

Layer	Unit Weight (kN/m^3)	Poisson's Ratio, ν	Elastic Modulus (kPa)				
Asphalt Concrete	23	0.2762	3,337,169				
				g_1^P	k_1^P	τ_1	
Base (overlay)	0	0.25	16,320	1.0	1.0	0.01	
Subgrade (overlay)	0	0.25	12,940	1.0	1.0	0.01	
			p_a (kPa)	k_1	k_2	k_3	T_c (kPa)
Base (finite)	20	0.25	101.3	957	0.906	-0.614	0.001
Subgrade(finite)	18	0.25	101.3	139	0.187	-3.281	0.001

Table 3.5.8 Material property set 2 for the 3D model

Layer	Unit Weight (kN/m^3)	Poisson's Ratio, ν	Elastic Modulus (kPa)				
Asphalt Concrete	23	0.49	3,337,169				
				g_1^P	k_1^P	τ_1	
Base (overlay)	0	0.25	16,320	1.0	1.0	0.01	
Subgrade (overlay)	0	0.25	12,940	1.0	1.0	0.01	
			p_a (kPa)	k_1	k_2	k_3	T_c (kPa)
Base (finite)	20	0.25	101.3	957	0.906	-0.614	0.001
Subgrade(finite)	18	0.25	101.3	139	0.187	-3.281	0.001

Table 3.5.9 Material property set 3 for the 3D model

Layer	Unit Weight (kN/m^3)	Poisson's Ratio, ν	Elastic Modulus (kPa)				
Asphalt Concrete	23	0.49	3,337,169				
				g_1^P	k_1^P	τ_1	
Base (overlay)	0	0.25	16,320	1.0	1.0	0.01	
Subgrade (overlay)	0	0.25	12,940	1.0	1.0	0.01	
			p_a (kPa)	k_1	k_2	k_3	T_c (kPa)
Base (finite)	20	0.25	101.3	957	0.906	-6.14	0.001
Subgrade(finite)	18	0.25	101.3	139	0.187	-3.281	0.001

Rough contact was used between the reinforcement and the base, and between the reinforcement and the subgrade. The model with each set of material properties listed in Tables 3.5.7 – 3.5.9 was analyzed using two sets of orthotropic elastic properties for the reinforcement layer (Table 3.5.10). Each set of reinforcement properties approximates the behavior of two common geogrid types.

Table 3.5.10 Orthotropic linear-elastic properties for the reinforcement layer

Case	E_{xm} (kPa)	E_m (kPa)	E_n (kPa)	$\nu_{xm\text{-}m}$	$\nu_{xm\text{-}n}$	$\nu_{m\text{-}n}$	$G_{xm\text{-}m}$ (kPa)	$G_{xm\text{-}n}$ (kPa)	$G_{m\text{-}n}$ (kPa)
1	595,000	365,925	595,000	0.813	0.25	0.25	2919	2919	2919
2	325,000	220,000	325,000	0	0	0	987	987	987

2. The 3-D model described above with each set of material properties listed in Tables 3.5.7 – 3.5.9 was analyzed using an isotropic linear-elastic model for the reinforcement with

Poisson's ratio set equal to 0.25 for all analyses and elastic modulus varied between 50,000 and 1,000,000 kPa.

3. Two sets of response parameters were extracted from each of the analyses described in steps 1 and 2. One set of parameters consisted of the maximum horizontal tensile strain in the asphalt concrete layer, which was then used to determine the number of cycles to fatigue failure according to Equation 3.5.28.

$$N_f = k_1 \beta_1 \left(\frac{1}{\varepsilon_t} \right)^{k_2 \beta_2} \left(\frac{1}{E} \right)^{k_3 \beta_3} \tag{3.5.28}$$

where:

N_f = traffic repetitions to AC fatigue

k_1, k_2, k_3 = laboratory material properties, taken as the May 2003 draft NCHRP 1-37A default values equal to:

k_1 = 1.0

k_2 = 3.9492

k_3 = 1.281

β_1, β_2, β_3, = field calibration coefficients, taken as the May 2003 draft NCHRP 1-37A default values equal to:

β_1 = 1.0

β_2 = 1.2

β_3 = 1.5

ε_t = resilient horizontal tensile strain from the response model taken as the maximum tensile value with the AC layer

E = AC complex modulus used in response model (psi)

The second set of parameters consisted of the vertical strain extrapolated to each node along the model centerline, which was then used to determine the number of cycles needed to reach 25 mm of permanent surface deformation. Permanent strain in the AC layer was determined according to Equation 3.5.29 while permanent deformation in the base and subgrade layers was determined according to Equation 3.5.30.

$$\log\left(\frac{\varepsilon_p}{\varepsilon_r}\right) = k_1\beta_1 + k_2\beta_2 \log T + k_3\beta_3 \log N \tag{3.5.29}$$

where:

ε_p = permanent vertical strain as a function of N

ε_r = resilient vertical strain from the response model taken along the model centerline

k_1, k_2, k_3 = laboratory material properties, taken as the May 2003 draft NCHRP 1-37A default values equal to:

k_1 = -3.3426

k_2 = 1.734

k_3 = 0.4392

β_1, β_2, β_3, = field calibration coefficients, taken as the May 2003 draft NCHRP 1-37A default values equal to:

β_1 = 0.8369

β_2 = 0.5

β_3 = 2.2

T = temperature of AC (°F)

N = traffic repetitions

$$\delta_a = \xi_1\left(\frac{\varepsilon_o}{\varepsilon_r}\right)e^{-\left(\frac{\rho}{N}\right)^{\xi_2\beta}}\varepsilon_v\, h \tag{3.5.30}$$

δ_a = permanent deformation for the layer/sublayer

N = traffic repetitions

ε_o, β, ρ = material properties (Table 3.5.11)

ε_r = resilient strain imposed in laboratory test to obtain material properties ε_o, β, and ρ

ε_v = average vertical resilient strain in the layer/sublayer as obtained from the response model

h = thickness of the layer/sublayer

ξ_1, ξ_2 = field calibration coefficients (Table 3.5.11)

Table 3.5.11 Permanent deformation properties for base and subgrade materials

Material	$(\varepsilon_o/\varepsilon_r)$	ρ	β	ξ_1	ξ_2
MSU Aggregate	88.58	7342	0.1271	0.4318	1.336
CS Subgrade	4683	4.13×10^{26}	0.03614	2.500	1.089

4. For each of the models analyzed using isotropic linear-elastic properties, the values of elastic modulus used in these analyses for the reinforcement were plotted against the number of cycles to fatigue and the number of cycles to 25 mm surface deformation. Figures 3.5.12 and 3.5.13 provide these plots for the model material parameters listed in Table 3.5.7.

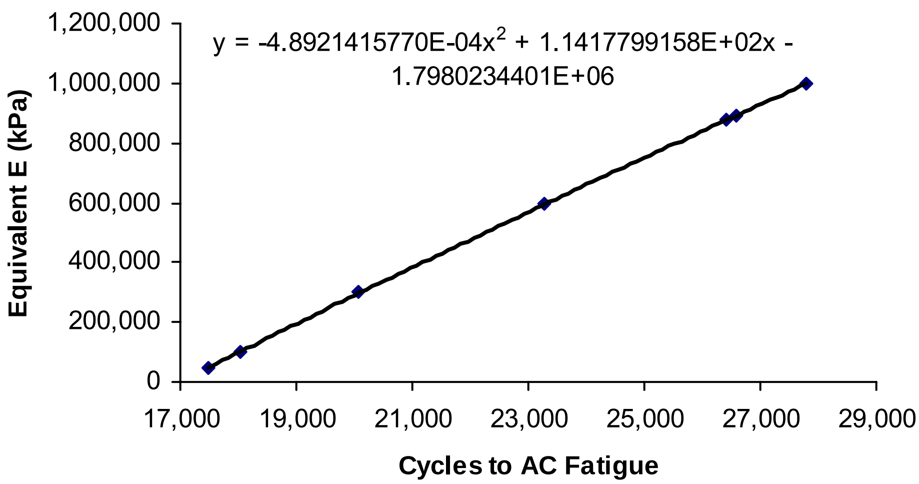

Figure 3.5.12 Cycles to AC fatigue versus isotropic reinforcement elastic modulus for model parameters listed in Table 3.5.7

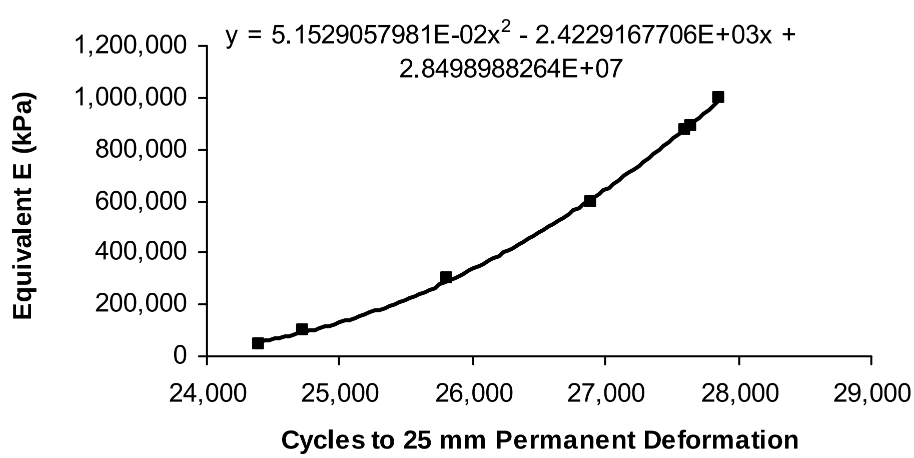

Figure 3.5.13 Cycles to 25 mm permanent surface deformation versus isotropic reinforcement elastic modulus for model parameters listed in Table 3.5.7

5. For the 3D analyses with the two sets of orthotropic properties listed in Table 3.5.10, the number of cycles to fatigue and the number of cycles to 25 mm surface deformation were calculated using Equations 3.5.28 – 3.5.30 for each of the 3 sets of model material properties, with values listed in Table 3.5.12.

Table 3.5.12 Cycles to AC fatigue and 25 mm permanent surface deformation for orthotropic reinforcement cases 1 and 2

Model Material Property Set	Reinforcement Case	Cycles to AC Fatigue	Cycles to 25 mm permanent surface deformation
1	1	23,318	27,131
1	2	19,200	25,252
2	1	31,393	46,417
2	2	26,137	42,372
3	1	9314	12,116
3	2	9128	11,745

6. With the values listed in Table 3.5.12, figures similar to Figures 3.5.12 and 3.5.13 were used for each material property set to determine the equivalent value of isotropic elastic modulus, with values given in Table 3.5.13.

Table 3.5.13 Equivalent isotropic elastic modulus for reinforcement cases 1 and 2

		Equivalent isotropic elastic modulus (kPa)	
Model Material Property Set	Reinforcement Case	AC Fatigue	25 mm permanent surface deformation
1	1	598,464	692,917
1	2	213,850	173,694
2	1	657,909	663,647
2	2	198,903	237,810
3	1	569,260	678,139
3	2	158,197	186,954

Equation 3.5.27 was solved for parameters *a* and *b* to minimize the difference between equivalent *E* values predicted by Equation 3.5.27 and those listed in Table 3.5.13. This resulted in values of $a = 0.35$ and $b = 0.035$. With these values of *a* and *b*, Figure 3.5.14 shows equivalent *E* values predicted by Equation 3.5.27 versus those given in Table 3.5.13.

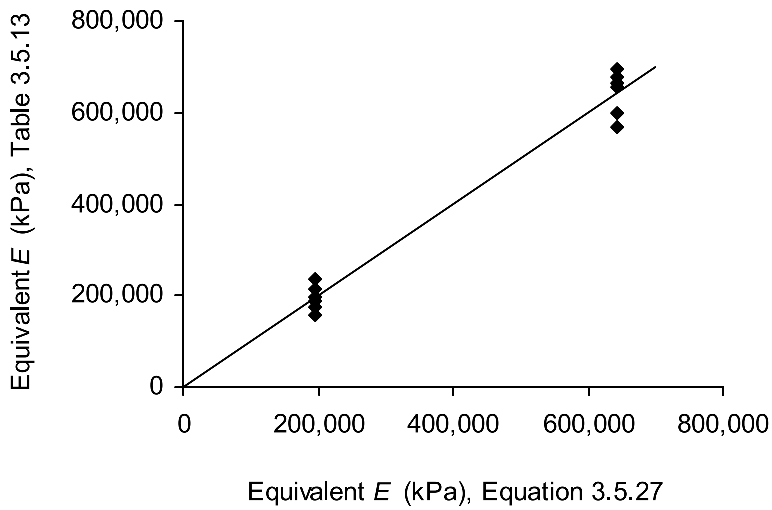

Figure 3.5.14 Comparison of predicted and analyzed equivalent *E* values

7. Geogrid strain data from the CRREL test sections was analyzed to evaluate the appropriateness of the value used for *a*. Under a moving wheel load situation, it is expected that load induced in the reinforcement layer will be different in the longitudinal versus the transverse directions for a point directly under the wheel. The differences between the stress or load in the reinforcement layer in these two directions can be used to determine a value for the stress parameter *a*. Results from traffic trials performed with a heavy vehicle simulator (HVS) reported by Perkins (2002) are used to establish the differences in load between these two directions. In these test trials, two geogrid reinforcement materials were used in two different test sections. Bonded resistance strain gauges were attached to the geogrid in the longitudinal and transverse directions along the travel path of the wheel to measure dynamic strain. The ratio of strain in the machine (longitudinal) to the cross-machine (transverse) directions was on the average of 0.74 to 0.88 for the two geogrid materials. The ratio of tensile modulus between the machine and cross-machine directions for these two materials was 0.595 and 0.615. This results in a ratio of stress between machine and cross-machine directions of 0.44 and 0.54 for the two materials, resulting in an average ratio of 0.5. This value is reasonably close to the value of *a* from the above analysis.

3.5.6 Summary Tensile Properties

Table 3.5.14 summarizes tensile properties measured and selected for the three geosynthetics used in this project. Values of tensile modulus in the machine and cross-machine directions (E_m, E_{xm}) for geosynthetic A were determined from the equations provided in Figures 3.5.12 and 3.5.13 at a strain of 0.2 %. These values will be used in later sections as values appropriate for the entire life of the pavement. Values for geosynthetics B and C correspond to the average of the cyclic values listed in Tables 3.5.4 and 3.5.5. Values of Poisson's ratio (ν_{xm-m}) for geosynthetics B and C were assumed to be 0.7 based on limited data discussed in Section 3.5.3. Test data to base a selection of Poisson's ratio for geosynthetic A is not available. A value of 0.25 was assumed for this material. The in-plane shear modulus (G_{xm-m}) was calculated from measured values of aperture stability modulus from Equation 3.5.7. The value shown for geosynthetic A is most likely unrealistically high but is used in the absence of any other data. Values of equivalent isotropic modulus (E) are then calculated for an assumed value of isotropic Poisson's ratio (ν) from Equation 3.5.27. While there are a number of uncertainties associated with the determination of several parameters contained in Table 3.5.13, particularly for geosynthetic A, due to the need to further develop several test methods, the values for equivalent isotropic elastic modulus appear reasonable. Section 7.0 examines the influence of changes in values of isotropic elastic modulus on pavement performance.

Table 3.5.14 Geosynthetic tensile properties

Property	Geosynthetic		
	A	B	C
E_{xm} (MPa)	389	720	1114
E_m (MPa)	96	544	835
ν_{xm-m}	0.25	0.7	0.7
G_{xm-m} (MPa)	1.820	0.945	2.919
E (kPa)	234	426	928
ν	0.25	0.25	0.25

3.6 Reinforcement-Aggregate Interaction Properties

In a reinforced pavement, the amount of relative movement between the aggregate and the reinforcement is relatively small for a single application of traffic load and is most likely predominately a recoverable displacement. As such, a resilient interface shear stiffness or modulus is an appropriate material property that should be used to describe reinforcement-aggregate interaction for use in an elastic response model. Equation 3.6.1 provides a general definition of resilient interface shear modulus and is seen to have units of force/distance^3.

$$G_I = \frac{\tau_I}{\Delta_I} \tag{3.6.1}$$

where:

G_I = resilient interface shear modulus

τ_I = shear stress applied to the interface

Δ_I = relative displacement between the aggregate and reinforcement for the shear stress applied

It might also be expected that the resilient interface shear modulus is dependent on the level of normal confinement on the interface and the amount of applied shear stress.

To develop a means of assessing resilient interface shear modulus, cyclic pullout tests were performed by WTI as a project external to this study. The results from this work are used to select parameters for an interface interaction model for the finite element response model used in this project.

3.6.1 Cyclic Pullout Tests

Given the expectation that resilient interface shear modulus is dependent on normal stress and applied shear stress on the interface, cyclic pullout tests were conducted. The testing protocol developed was based on resilient modulus tests for unbound aggregate (NCHRP 1-28A). Conducting cyclic pullout tests according to a resilient modulus protocol also helps reduce the sensitivity of the results to changes in specimen preparation techniques by the stress conditioning that is applied to the specimen at the beginning of the test.

The pullout box used for cyclic testing is a full-sized box built to guidelines provided in ASTM D6706 (ASTM 2003). Details concerning construction of the box are given in Perkins and Cuelho (1999). The inside dimensions of the box are 1.10 m high by 0.90 m wide by 1.25 m long. The load actuator is connected to the load frame at the front of the box. The actuator extends through the load frame and is connected to the sample using pinned connections. The embedded geosynthetic is glued between two pieces of sheet metal (load transfer sheets) using a rigid epoxy to transfer the point load from the actuator into a uniform line load at the edge of the geosynthetic. A slit at the front of the pullout box accommodates the sample with minimal friction. A similar slit exists at the back of the pullout box to allow the wires connected to the rear of the geosynthetic sample to be connected to linearly varying differential transducers (LVDTs) mounted externally (Figure 3.6.1).

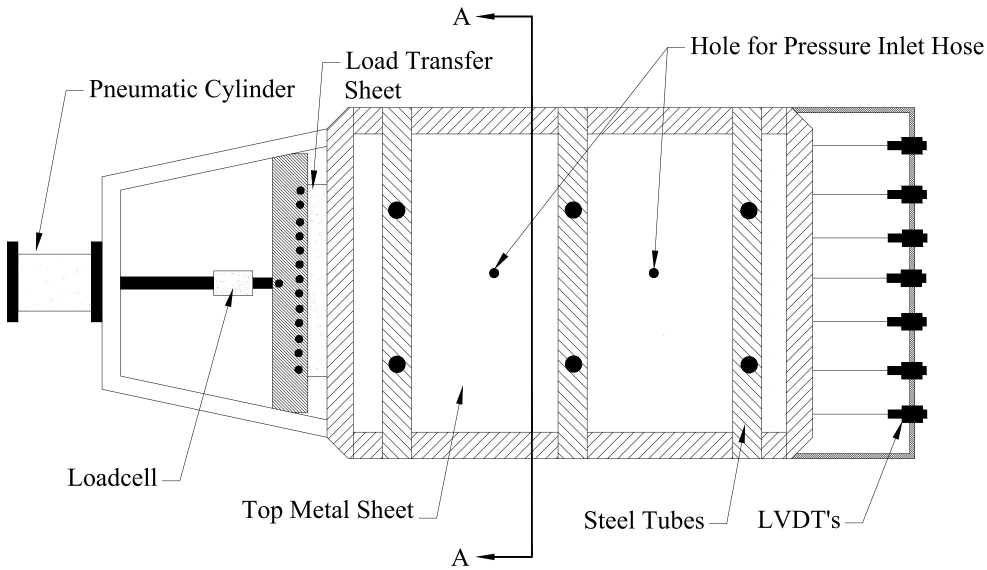

Figure 3.6.1 Plan view of pullout box

Normal confinement is provided using a flexible pneumatic bladder on top of the soil. This bladder reacts against a flat, rigid steel plate held in place by steel tubes bolted to the sidewalls of the pullout box. A cutaway view of Figure 3.6.1 (see Figure 3.6.2) shows this arrangement. Shear load is delivered to the sample using a pneumatic cylinder connected to an automated binary regulator (ABR). The ABR is capable of splitting inlet air pressure into 15 equal divisions to allow various impulse shapes to be delivered to the geosynthetic during testing.

During testing, loads are transferred through the geosynthetic and into the soil. Increased bearing pressures from the front wall are minimized using load transfer sleeves on the inside of the front wall. These sleeves extend into the soil allowing dilation and excess bearing pressures to dissipate rather than increase confinement at the front of the sample. This provides uniform confinement across the area of the embedded geosynthetic.

To provide for a test where applied shear stresses were relatively uniform across the length of the geosynthetic, the length of the embedded geosynthetic was limited to approximately 50 to 80 mm. Longer specimens experience a decrease of pullout displacement with distance from the applied load and result in a non-uniform application of interface shear stress on the sample. Sample widths were generally 450 mm, depending on the geosynthetic type. Samples of this size made it possible to engage the entire sample during loading.

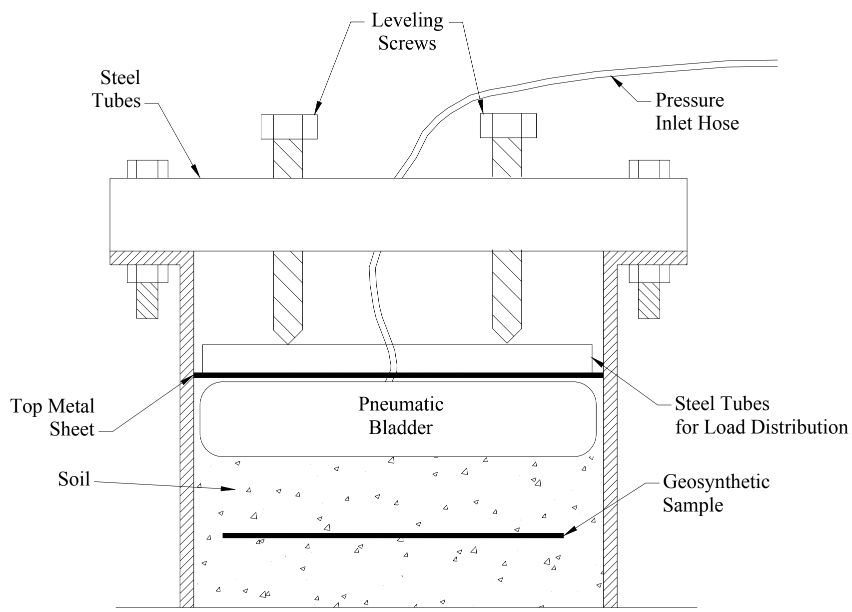

Figure 3.6.2 Pullout box end view (section A-A from Figure 3.6.1)

The limited size of the reinforcement reduced the size of the aggregate sample needed for testing. The aggregate sample was set to a size of 310 mm in height by 640 mm in length and 900 mm in width. The configuration of the aggregate sample relative to the box dimensions is shown in Figure 3.6.3. The additional space in the box not occupied by the aggregate sample was taken up by a reinforced wooden box, as shown in Figure 3.6.3.

The MSU aggregate (described in Section 3.2) was used in all tests and was compacted to a dry density and at a water content used in test sections reported by Perkins (1999). After the soil was compacted to the height of the bottom load transfer sleeve, the soil was slightly scarified and the geosynthetic sample was put into place such that the leading edge (front) of the sample was aligned with the embedded edge of the load transfer sleeve (Figure 3.6.4). Thin metal rollers between the load transfer sheets and the load transfer sleeves were used to minimize friction during testing.

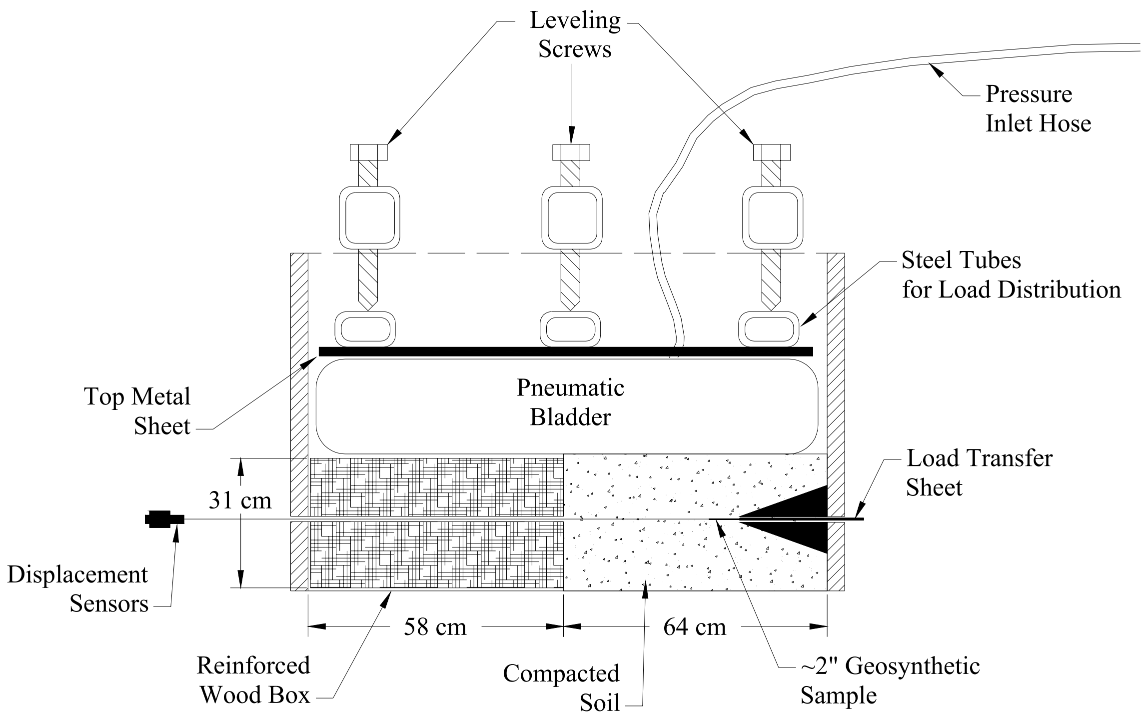

Figure 3.6.3 Configuration of pullout aggregate specimen

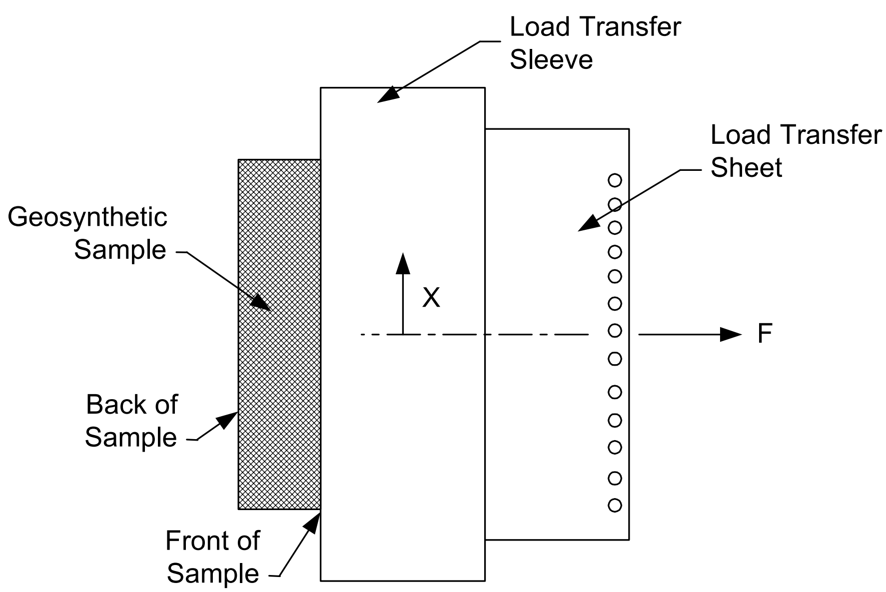

Figure 3.6.4 Plan view of sample arrangement

The sample was temporarily held in place while the lead wires, used to measure displacement of the sample, were connected and while the cover soil was being compacted. Thin wires, having a diameter of 0.381 mm, were used to provide this connection. For the geogrids, a small diameter drill bit was used to make a hole where the sensor wire was to be placed. The wire was inserted through the hole and bent over 180 degrees to minimize friction. For the geotextiles, the wire was simply inserted through the woven mesh of the fabric and bent 180 degrees. A small drop of glue was used to minimize local deformations at this location due to the presence of the lead wire. The wires were run through the soil and out the back of the pullout box through small-diameter brass tubes.

Applied loads were measured using a load cell attached between the pneumatic cylinder and the load transfer plates that has an accuracy of 0.004 kN. Displacements were measured using seven LVDTs and two extensometers that have an accuracy of 2.5 x 10^{-3} mm. LVDTs were used to measure the displacements on the geosynthetic and the extensometers were used to measure displacements of the sheet metal load transfer sheets. Maximum and minimum load and displacement values were collected from all sensors for all the cycles. A typical arrangement of the sensors is shown in Figure 3.6.5.

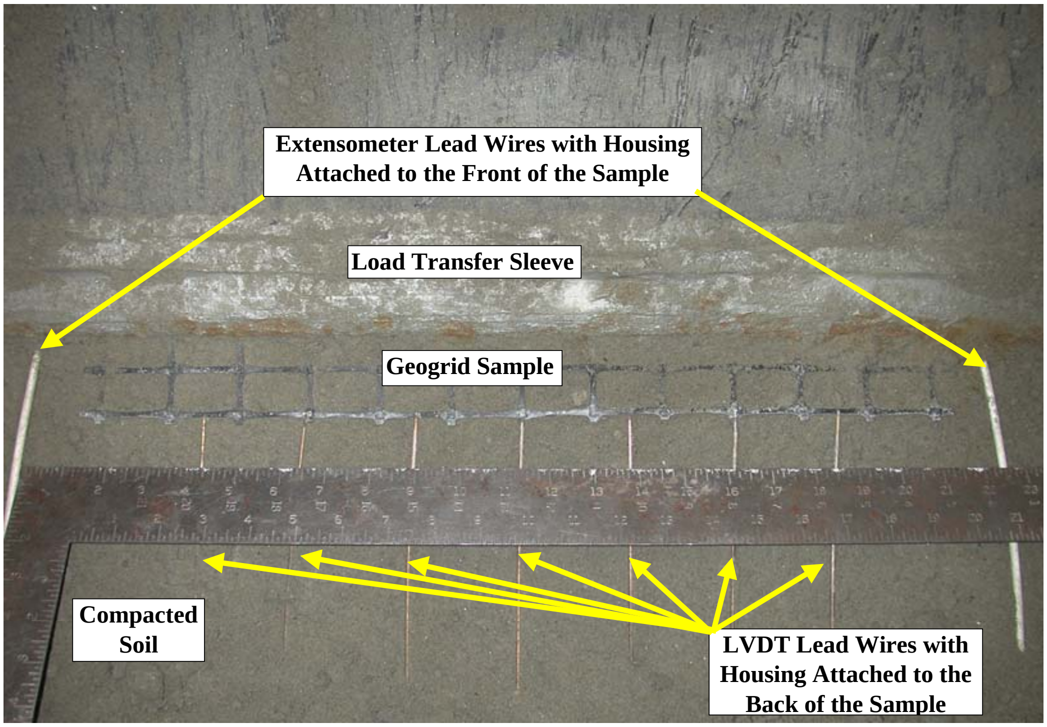

Figure 3.6.5 Typical displacement sensor arrangement

The loading protocol followed in the tests is illustrated in Figure 3.6.6 where the cyclic pullout load is plotted against the normal stress confinement used for each cyclic load level. The test begins with a conditioning step consisting of the application of 1000 cycles of shear load at a confinement of 51.7 kPa. This step is designed to erase specimen anomalies due to slight variations in specimen preparation. Following the conditioning step, six separate loading sequences, based on a theoretical failure line, are followed. The sixth load sequence represents a failure line and the remaining five are based on a percentage of the sixth. Five levels of confinement are used within each load sequence to define a line called a "sequence group," as illustrated in Figure 3.6.6. Testing begins with the first sequence group (SG-1) with the lower confinement steps being conducted first, and progresses to the sixth sequence group (SG-6) unless pullout failure occurs earlier. Cyclic shear load is applied between the values on the seating load line and the points for the sequence group. Maximum and minimum loads applied to the geosynthetic for a particular load step are determined from the sequence group and the seating load lines, respectively.

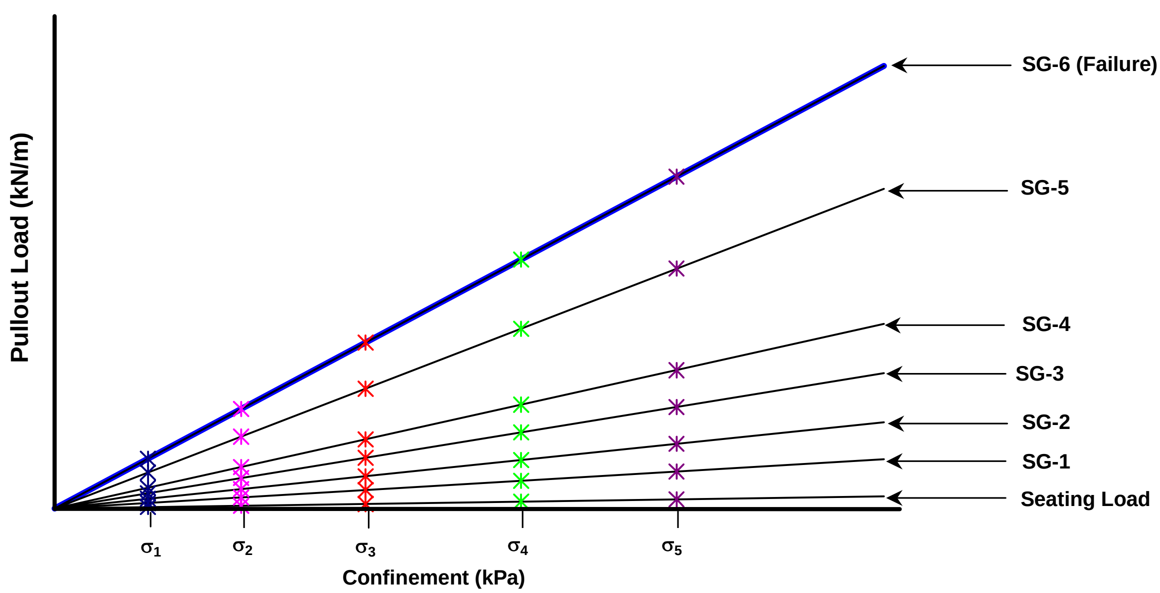

Figure 3.6.6 Cyclic pullout loading steps

The slope of the failure line is determined from the area of the geosynthetic sample and an assumed ultimate interaction friction angle between the soil and geosynthetic taken as 51.5 degrees. The slopes of the remaining five sequence groups and the seating load are determined using percentages of the failure line. Table 3.6.1 provides the load for each sequence group as a percentage of the failure line. For the first two confinement levels, 300 shear load cycles were applied to ensure that the resilient behavior stabilized. For the remaining confinements, 100 cycles of shear load were applied.

Table 3.6.1 Load percentage in relation to failure line for each sequence group

Load Level	Percentage of Failure Load
Seating Load	2.8%
SG 1	9.7%
SG 2	16.7%
SG 3	30.6%
SG 4	44.4%
SG 5	72.2%
SG 6	100.0%

The cyclic load pulse was designed to mimic a single wheel load experienced by a geosynthetic embedded in a roadway. Figure 3.6.7 illustrates this pulse shape showing the maximum load and minimum (seating) load. A single pullout pulse is delivered in 0.75 seconds and has 0.75 seconds between subsequent pulses.

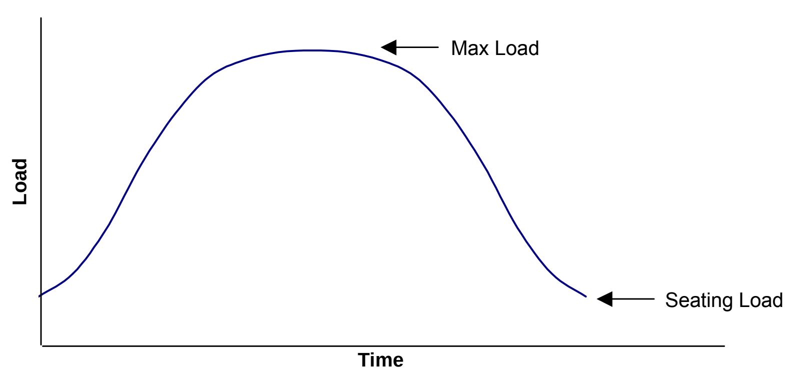

Figure 3.6.7 Cyclic shear load pulse

An average value of the resilient interface shear modulus was calculated according to Equation 3.6.1 as an average value for the last ten cycles for each confinement level within each sequence group. Figure 3.6.8 provides a graphical illustration of how G_I is determined from a single load pulse. The shear stress in Figure 3.6.8 is defined as the load applied to the sample divided by the engaged area of the sample, which includes both the top and bottom areas of the reinforcement.

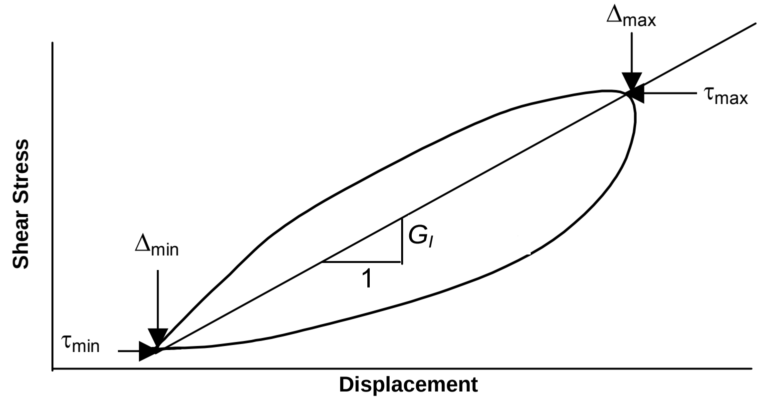

Figure 3.6.8 Definition of calculation of G_I

Even though short samples were used to provide for uniform pullout displacement across the length of the sample, small differences in displacement between the front and back of the samples were observed. This made it necessary to average the displacement across the length of the reinforcement by averaging front and rear displacements. The displacement at the front of the sample was measured using two extensometers attached to the sheet metal load transfer plate along the edge where the reinforcement met the plates. These two values were averaged to provide a front end displacement representative of the centerline of the reinforcement. The displacement at the back (embedded end) of the sample was recorded using LVDT's attached to 7 points along the reinforcement as shown in Figure 3.6.5. These displacements were averaged to provide for an average rear end displacement. The average front and rear displacements were then averaged to provide for an average displacement of the reinforcement sheet.

The resilient interface shear modulus was then calculated for the cycles defined above the difference between the maximum and minimum shear stress divided by the average midpoint displacement difference (Equation 3.6.2).

$$G_I = \frac{\tau_{\max} - \tau_{\min}}{\Delta_{\max_a} - \Delta_{\min_a}} \tag{3.6.2}$$

where τ_{max} is the maximum shear stress within that cycle, τ_{min} is the minimum shear stress within that cycle, and $\Delta_{max\ a}$ and $\Delta_{min\ a}$ are the average maximum and minimum displacement within the material and are defined as:

$$\Delta_{\max_a} = \frac{\Delta_{\max b} + \Delta_{\max f}}{2} \tag{3.6.3}$$

$$\Delta_{\min_a} = \frac{\Delta_{\min b} + \Delta_{\min f}}{2} \tag{3.6.4}$$

The shear stresses are calculated from Equation (3.6.5).

$$\tau = \frac{F}{2 * w * (l - \Delta_b)} \tag{3.6.5}$$

where F represents the load applied to the sample, 2 represents the two sides of the sample, w is the width of the sample, l is the length of the sample and Δ_b is the average displacement at the back of the sample, which is subtracted from the length of the sample to account for the loss of area during pullout. The displacements used in Equation 3.6.2 are those corresponding to the geosynthetic material, which are assumed to be equal to the relative displacement between the aggregate and the reinforcement. This implies zero displacement of the soil. This assumption results in upper bound values of displacement used in Equation 3.6.2 corresponding to lower bound values of resilient interface shear modulus.

3.6.2 Resilient Interface Shear Modulus

Resilient interface shear modulus results from the cyclic pullout tests described in Section 3.6.1 were fit to Equation 3.6.6, which was chosen because of its similarity to the equation used for the resilient modulus of unbound materials.

$$G_I = k_1 P_a \left(\frac{\sigma_I}{p_a}\right)^{k_2} \left(\frac{\tau_I}{p_a} + 1\right)^{k_3} \tag{3.6.6}$$

In Equation 3.6.6,

p_a = atmospheric pressure (101.3 kPa)

P_a = atmospheric pressure divided by a unit length of 1 m (101.3 kN/m^3)

σ_I = interface normal stress

τ_I = interface shear stress

k_1, k_2, k_3 = material properties

Table 3.6.2 lists values of k_1, k_2, k_3 for the three geosynthetics used in this study from tests with the MSU-aggregate. Figure 3.6.9 shows the variation of resilient interface shear modulus versus interface normal stress for the three materials given in Table 3.6.2 according to Equation 3.6.6. An interface shear stress of 10 kPa was used to generate data shown in this figure.

Table 3.6.2 Resilient interface shear modulus parameters from cyclic pullout tests

Geosynthetic	k_1	k_2	k_3
A	1069	0.407	-1.42
B	2609	0.508	-1.79
C	2761	0.518	-1.87

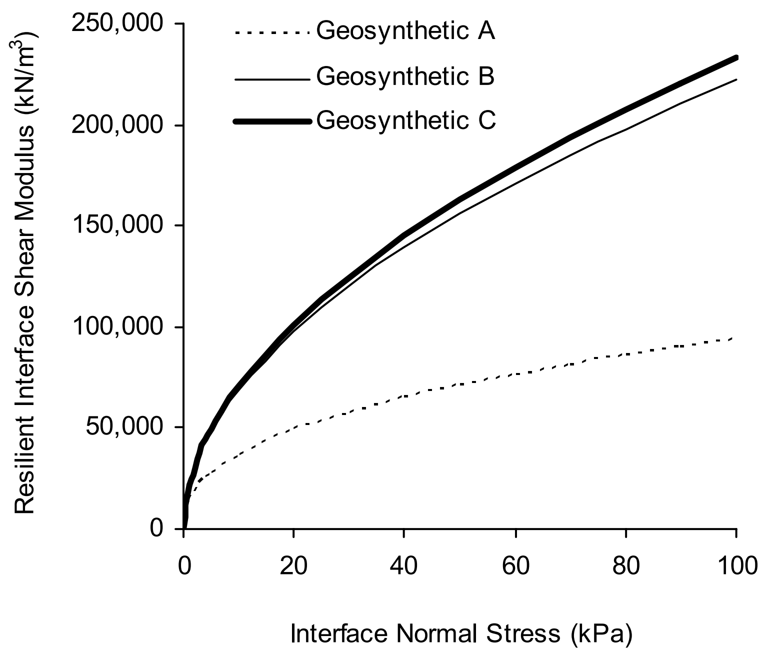

Figure 3.6.9 Resilient interface shear modulus versus interface normal stress for three geosynthetic materials

3.6.3 Coulomb Friction Model

The finite element response model for reinforced pavements (Section 4) uses a Coulomb friction model for the two interfaces on either side of the reinforcement. The shear stress versus shear displacement relationship for the interface is shown schematically in Figure 3.6.10. The relationship has an elastic region whose slope, G_I, is governed by a parameter E_{slip}. The peak shear stress is a function of the normal stress and is governed by a friction coefficient μ. Values of E_{slip} and μ are constant for an interface, meaning that the slope of the elastic part of the τ-Δ curve is a function of both E_{slip} and μ.

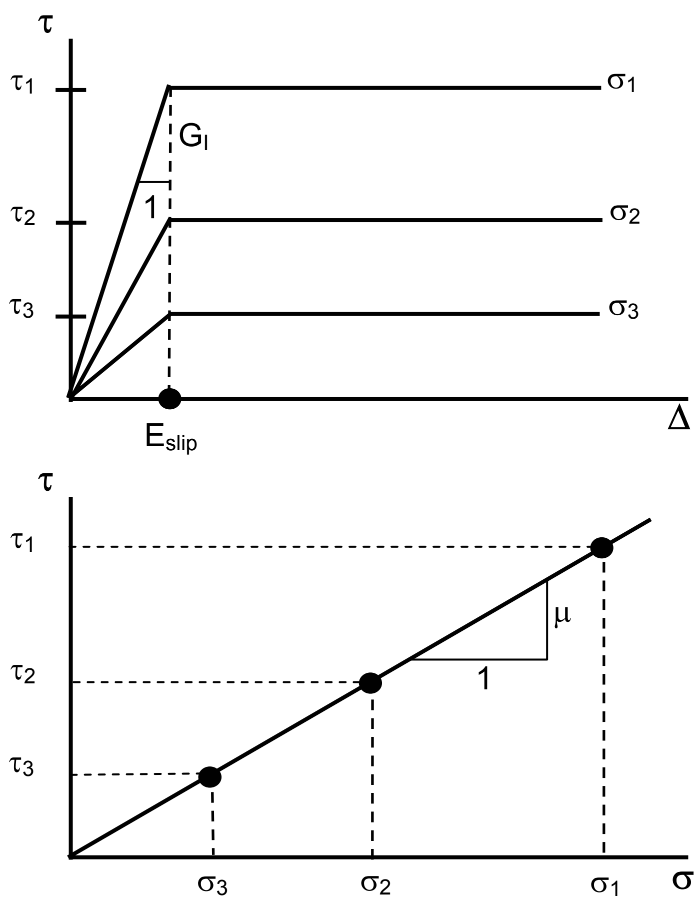

Figure 3.6.10 Schematic of the Coulomb interface friction model

The slope of the elastic portion of the τ-Δ curve is expressed by an interface shear modulus, G_I, which has units of kPa/m or force/distance^3. From Figure 3.6.10, G_I can be expressed by Equation 3.6.7, which shows the dependency on the parameters E_{slip} and μ, and the normal stress on the interface, σ_n.

$$G_I = \frac{\tau_{\max}}{E_{slip}} = \frac{\mu \sigma_n}{E_{slip}} \tag{3.6.7}$$

Comparison of Equation 3.6.7 to 3.6.6 shows that both equations show a dependency of resilient interface shear modulus on interface normal stress (σ_n). Equation 3.6.7 does not, however, show a dependency of resilient interface shear modulus on interface shear stress (τ_n). Figure 3.6.11 shows a comparison of Equations 3.6.6 and 3.6.7.

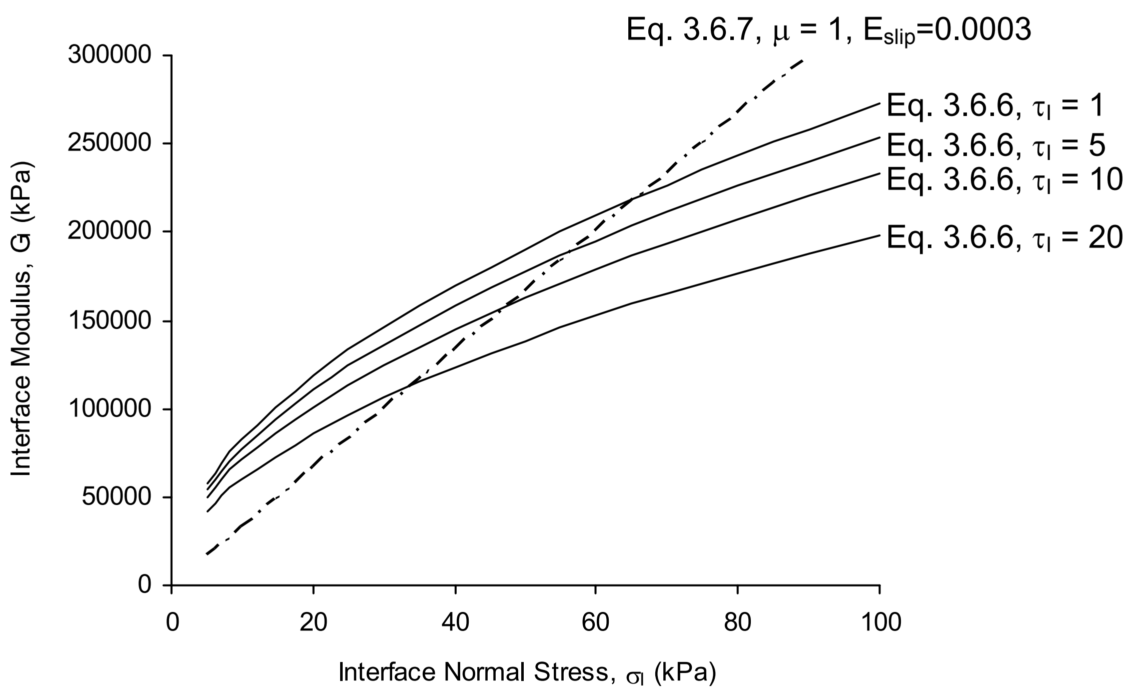

Figure 3.6.11 Variation of interface shear modulus, G_I, with interface normal stress, σ_I, according to Equations 3.6.6 and 3.6.7.

Cyclic pullout tests provide parameters k_1, k_2, k_3 such that G_I can be estimated from Equation 3.6.6. To select proper input values (μ and E_{slip}) for use in finite element response models, the following procedure is followed:

1. The coefficient of friction (μ) is determined from conventional pullout or direct shear tests.
2. Cyclic pullout tests are performed to calibrate constants k_1, k_2, k_3 in Equation 3.6.6.
3. Typical interface stress conditions are calculated for the pavement response model being analyzed. Selection of these typical stress conditions is discussed in Section 4.3.

4. Typical interface stresses are used in Equation 3.6.6 to determine G_I.
5. The parameter E_{slip} is determined from Equation 3.6.7 by setting G_I equal to that obtained in step 4, μ equal to that used in step 1, and σ_n equal to σ_I used in step 3.

3.7 Interface Shear Stress Growth

Experimental and theoretical studies on reinforcement of aggregate base layers in flexible pavements using geosynthetics have shown that the principal effect of the reinforcement is to provide lateral confinement of the aggregate (Bender and Barenberg, 1978; Kinney and Barenberg, 1982; Perkins 1999; Perkins and Edens, 2002). Lateral confinement is due to the development of interface shear stresses between the aggregate and the reinforcement, which in turn transfers load to the reinforcement. As a cycle of traffic load is applied, there is both a resilient or recoverable shear stress and a permanent shear stress that exists when the traffic load is removed. The permanent interface shear stress continues to grow as repeated traffic loads are applied, meaning that the lateral confinement of the aggregate base layer becomes greater with increasing traffic load repetitions.

The reinforced pavement response model described in Section 5 is formulated to account for the effect of increasing lateral confinement with increasing traffic load repetitions. This response model uses a relationship between increasing permanent interface shear stress and traffic pass level developed in this section. This relationship is obtained from field data by examining tensile strains developed in the reinforcement as a function of traffic passes and relating this development to interface shear stress through appropriate theoretical considerations.

3.7.1 Field Data

Previously reported test sections (Perkins 1999) showed the development of extensional horizontal strain at the bottom of the base aggregate layer under the area of the load, as shown for a typical test section in Figure 3.7.1, where extensional strain is taken as positive. The magnitude of strain is seen to increase with increasing traffic load repetitions. Relative motion is created between the aggregate and the relatively stiff reinforcement, which in turn creates interface shear stress. This shear stress induces load and strain in the reinforcement with the strain distribution shown in Figure 3.7.2 for a typical test section and where tensile strain is taken as positive.

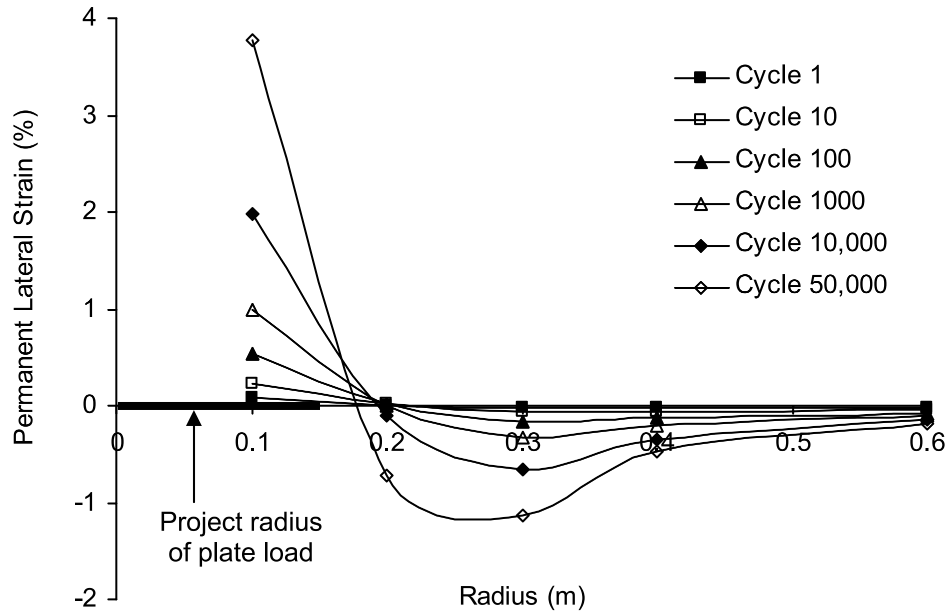

Figure 3.7.1 Development of lateral strain in the bottom of a base aggregate layer with traffic load repetitions

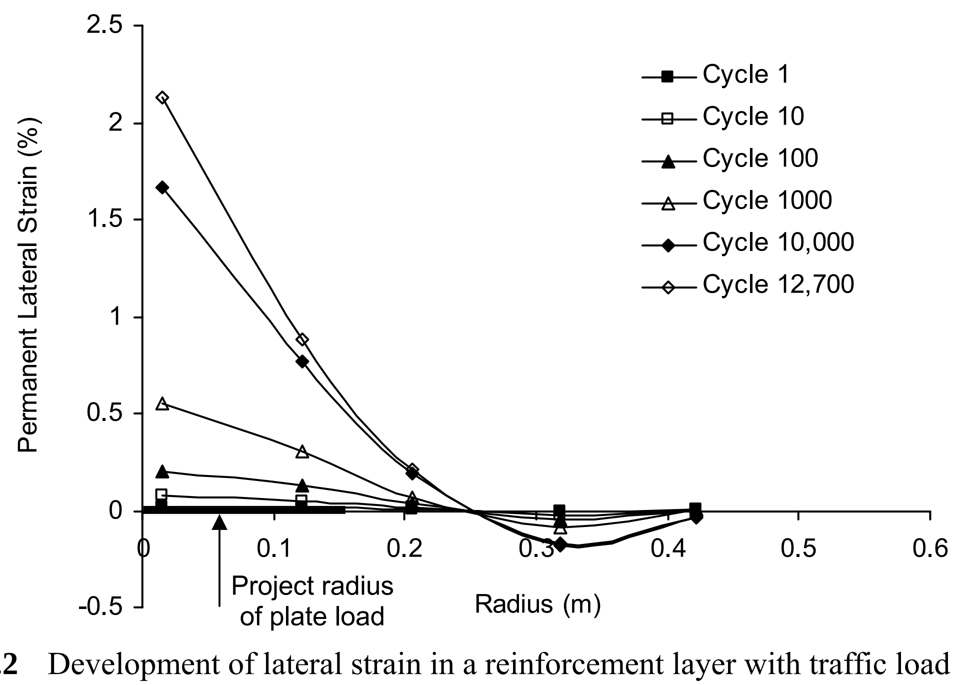

Figure 3.7.2 Development of lateral strain in a reinforcement layer with traffic load repetitions

Dynamic (resilient), ε_r, and permanent strain, ε_p, data was collected from strain gauges attached to the reinforcement sheets. Resilient strain for each strain gauge was nearly constant for all traffic pass levels. The permanent strain was normalized by the resilient strain for the corresponding traffic pass and plotted against a normalized traffic pass level. Expressing permanent reinforcement strain as a function of these variables is convenient when extending reinforcement strain to interface shear stress, as will be shown in the following section. Normalized traffic pass level ($N/N_{25\ mm}$) is the actual traffic pass level divided by the number of traffic passes necessary to achieve 25 mm of permanent surface deformation. Figures 3.7.3 – 3.7.5 show these results for test sections detailed in Table 3.7.1. The strain gauges were placed on ribs in either the machine or cross-machine direction of the geosynthetic and were oriented in a direction radial to the centerline of the load plate. The gauges were placed on the first rib from the centerline of the load plate, meaning that the center point of the gauge was between 15 to 20 mm from the centerline of the test section.

Table 3.7.1 Test sections and strain gauge locations

Test Section	Geosynthetic	AC Thickness (mm)	Base Thickness (mm)	Subgrade CBR (%)	Gauged Direction
1	B	75	300	1.5	(1) Cross-Machine
1	B	75	300	1.5	(2) Machine
2	C	75	300	1.5	(1) Cross-Machine
2	C	75	300	1.5	(2) Machine
3	A	75	300	1.5	(1) Cross-Machine
3	A	75	300	1.5	(2) Machine

The results shown in Figures 3.7.3 – 3.7.5 tend to suggest that the ratio of permanent to resilient strain differs between different reinforcement products and between different material directions. This relationship can be approximated by a logarithmic curve given by Equation 3.7.1 and shown as a “Trend Line” for each gauge. The curve fitting parameters A and B are listed in Table 3.7.2 for each test section.

$$\log\left(\frac{\varepsilon_p}{\varepsilon_r}\right) = \log(A) + B\log\left(\frac{N}{N_{25mm}}\right) \tag{3.7.1}$$

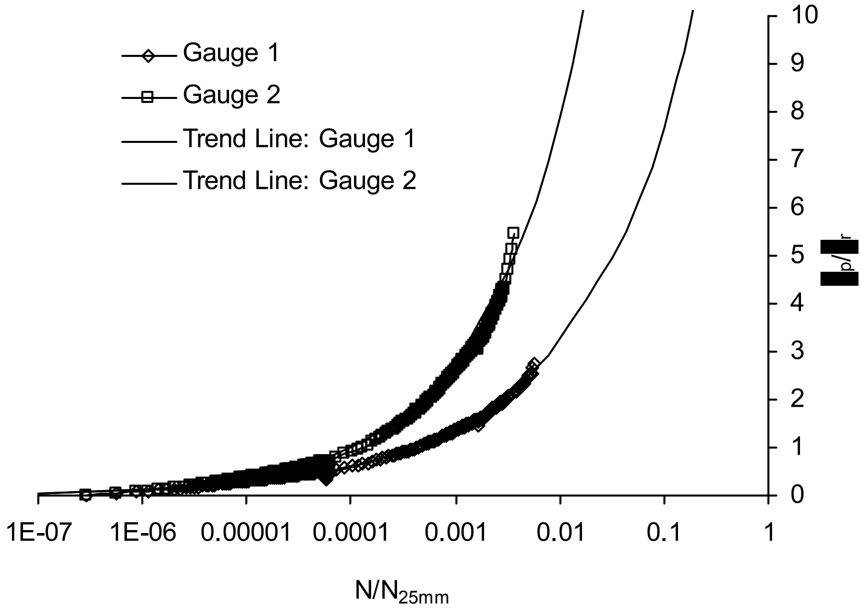

Figure 3.7.3 Permanent over resilient strain versus normalized traffic load passes for section 1

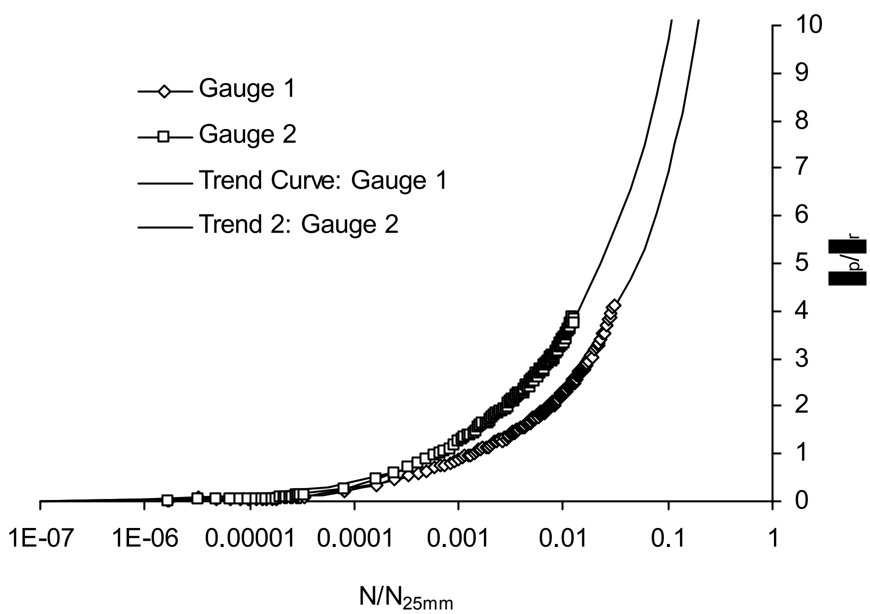

Figure 3.7.4 Permanent over resilient strain versus normalized traffic load passes for section 2

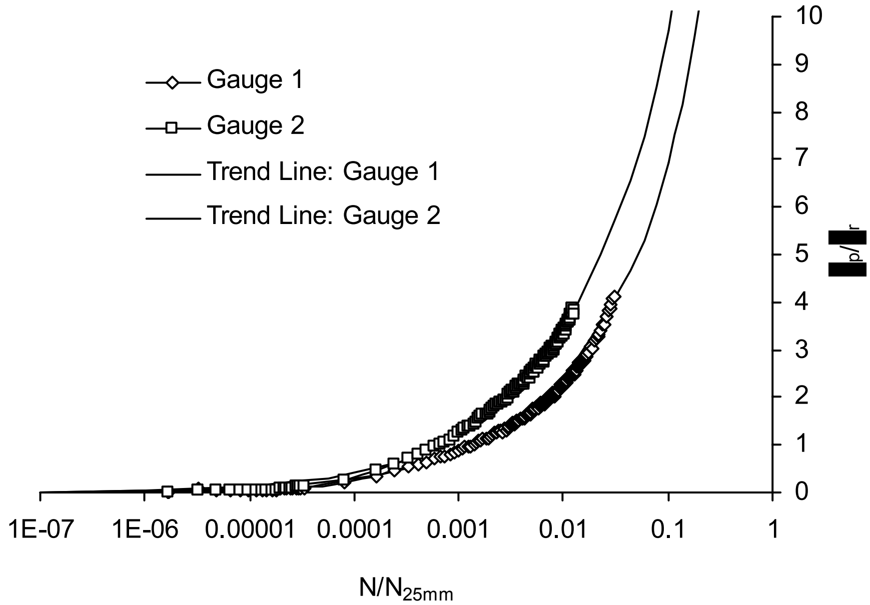

Figure 3.7.5 Permanent over resilient strain versus normalized traffic load passes for section 3

Table 3.7.2 Parameters A and B for equation 1 for test sections shown in Figures 3.7.3 – 3.7.5

Test Section	Strain Gauge	*A*	*B*
1	1	18	0.37
1	2	63	0.45
2	1	20	0.46
2	2	28	0.46
3	1	3.0	0.18
3	2	4.3	0.18

3.7.2 Theory

In order to relate measured reinforcement strain to interface shear stress, an infinitesimal axisymmetric element of the reinforcement is considered (Figure 3.7.6). The interface shear stress from relative movement of the base is considered as a unit shear stress, τ. Force equilibrium in the radial direction for an infinitesimal element is given by Equation 3.7.2.

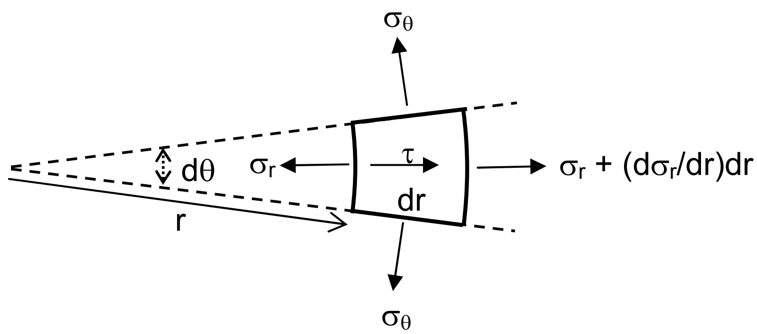

Figure 3.7.6 Infinitesimal reinforcement element

$$\frac{d\sigma_r}{dr} \, dr \; rd\theta d\theta + \sigma_r \; dr \; d\theta\theta d + \tau \; dr \; rd\theta d\theta - \sigma_\theta \; drd\theta rd = 0 \qquad (3.7.2)$$

Dividing Equation 3.7.2 by rdrdθdt yields Equation 3.7.3.

$$\frac{d\sigma_r}{dr} + \frac{\sigma_r - \sigma_\theta}{r} + \tau = 0 \qquad (3.7.3)$$

In cases where it is reasonable to assume that the difference in stresses between the radial and the ring directions is small, such as in the vicinity of the centerline of the test section, Equation 3.7.3 can be approximated by Equation 3.7.4. Since the majority of the reinforcement effect arises from an area centered under the wheel load, Equation 3.7.4 is used for the entire radius of the model.

$$\frac{d\sigma_r}{dr} + \tau = 0 \qquad (3.7.4)$$

Separating and integrating Equation 3.7.4 produces Equation 3.7.5.

$$\sigma_r = \int \tau \, dr \qquad (3.7.5)$$

If the reinforcement is assumed to correspond to an elastic material with an elastic modulus in any principal direction given by E, then the stress σ_r can be replaced by εE, where ε is the strain in the reinforcement in the radial direction. Equation 3.7.5 can then be expressed in terms of strain for the dynamic (resilient) state, ε_r, when a resilient interface shear stress, τ_r, acts on the reinforcement (Equation 3.7.6) and for the state when locked-in or permanent strain, ε_p, exists in the reinforcement when the pavement load is removed and a locked-in or permanent shear stress, τ_p, acts on the reinforcement (Equation 3.7.7).

$$\varepsilon_{\mathrm{r}} = \frac{\int \tau_r \; dr}{E} \tag{3.7.6}$$

$$\varepsilon_{\mathrm{p}} = \frac{\int \tau_p \; dr}{E} \tag{3.7.7}$$

If it is assumed that the shape of the functions for τ_r and τ_p are identical, then Equations 3.7.6 and 3.7.7 can be combined to yield Equation 3.7.8.

$$\tau_{\mathrm{p}} = \tau_r \, \frac{\varepsilon_p}{\varepsilon_r} \tag{3.7.8}$$

Equation 3.7.8 allows for the permanent shear stress on the interface to be estimated for any traffic pass level by using Equation 3.7.1 to estimate the permanent to resilient reinforcement strain ratio ($\varepsilon_p/\varepsilon_r$) provided the resilient or dynamic interface shear stress, τ_r, can be determined. Techniques for making this determination and its relationship to the development of a response model for reinforced pavements is presented in Section 5.

4.0 UNREINFORCED PAVEMENT RESPONSE MODELS

The pavement response model used in this study is a two-dimensional axisymmetric finite element model created using the commercial finite element package Abaqus (Hibbitt et al. NCHRP 1-37A Design). The model was set-up to match as closely as possible the set-up procedures used in the NCHRP 1-37A Design Guide (NCHRP 2003), where these procedures were provided by the University of Maryland. In this section, details concerning the set-up of response models for unreinforced and reinforced models are provided. Steps taken to verify the performance of unreinforced models as compared to other solutions are provided. Calibration and validation of the unreinforced and reinforced models is provided by comparing model predictions to results from test sections reported by Perkins (1999, 2002).

4.1 NCHRP 1-37A Design Guide Response Model Set-Up

4.1.1 Model Geometry and Meshing

The finite element pavement response model used in this study was a two dimensional axisymmetric model containing infinite elements along the two boundaries of the model. Meshing rules in the NCHRP 1-37A Design Guide have been established to provide adequate solution accuracy while minimizing computational time. Figure 4.1.1– 4.1.4 illustrate a mesh created for an unreinforced pavement cross section having three layers consisting of asphalt concrete, unbound base aggregate and subgrade soil. In Figure 4.1.1, the axis of symmetry of the model is noted. The bottom and right hand boundaries of the model contain infinite elements. The distance from the top of the axis of symmetry to the boundary between the finite and infinite elements (*rMax* and *zMax*) is determined from Equations 4.1.1 – 4.1.2.

$$rMax = MAX\,(0.6096\,m, 8 * tire\ radius, 1.2 * (tire\ radius + 0.8128\,m)) \tag{4.1.1}$$

$$zMax = MAX\,(0.9525\,m, 12.5 * tire\ radius, thickness\ above\ subgrade + 0.9144\,m) \tag{4.1.2}$$

For the example shown in Figures 4.1.1 – 4.1.4, the tire radius is 152.4 mm, leading to the values for *rMax* and *zMax* shown in Figure 4.1.1.

A minimum of four elements are needed through the thickness of any layer. In addition, the aspect ratio for the elements within a certain radius through the asphalt concrete and aggregate layers should be kept close to 1. For this problem with an asphalt concrete and aggregate thickness of 75 and 300 mm, respectively, and the need to fit a whole number of elements under the tire load having a radius of 152.4 mm, this required elements measuring 18.75 mm in height by 19.05 mm in width. The radius of the zone of uniform elements corresponds to a distance for 24 elements, as shown in Figure 4.1.2. Beyond the zone of uniform elements, the width of the elements can progressively grow by a maximum factor of 1.2 between any two elements and with a maximum aspect ratio for any element not to exceed 5. Within the subgrade (Figure 4.1.4), the uniform elements are continued down for 8 elements. Beyond this zone, the height of the elements can progressively grow by a maximum factor of 1.2 between any two elements and with a maximum aspect ratio for any element not to exceed 5. Four node quadrilateral elements were used for all the elements contained in the finite element region.

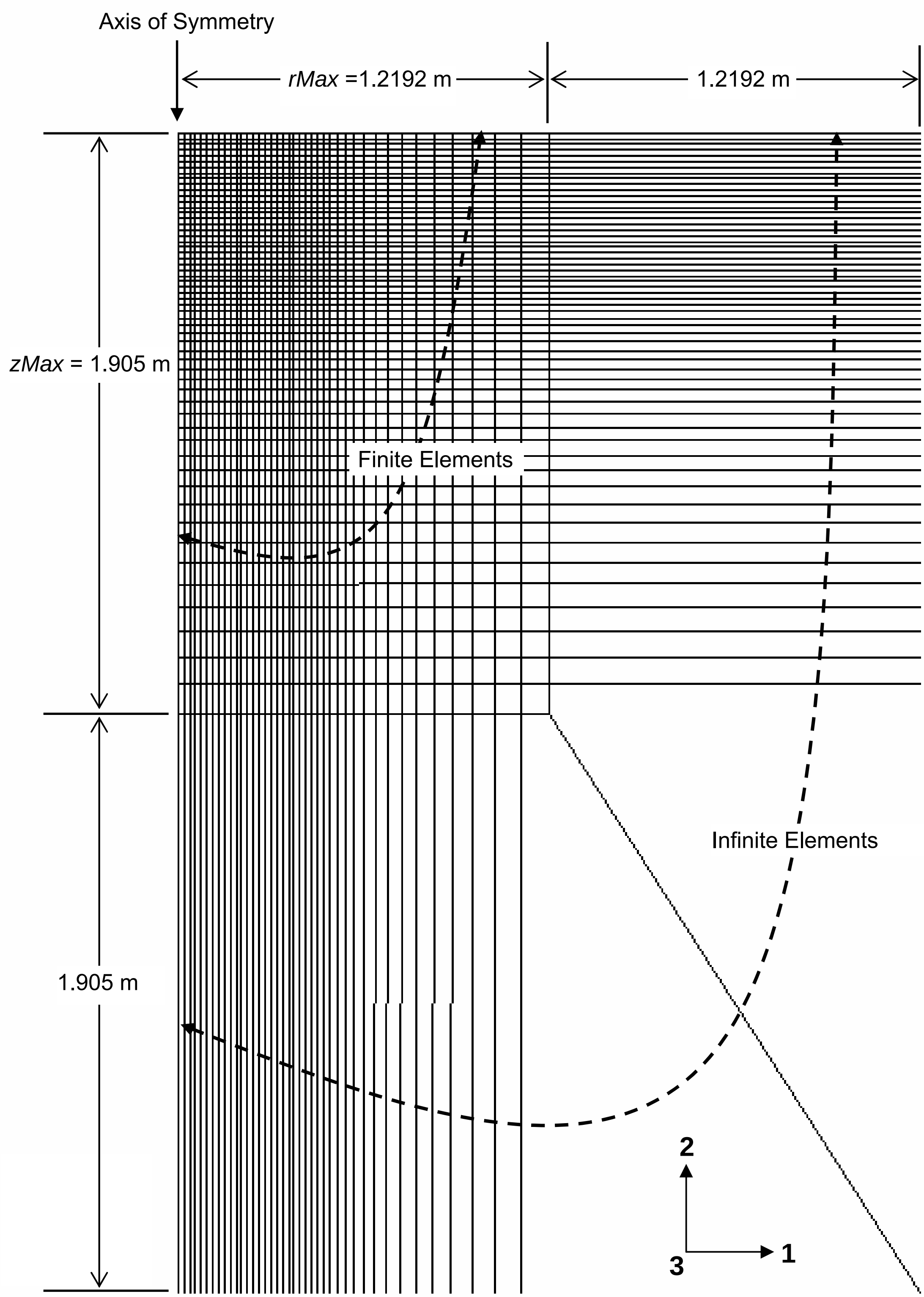

Figure 4.1.1 Geometry and meshing of finite element pavement response model

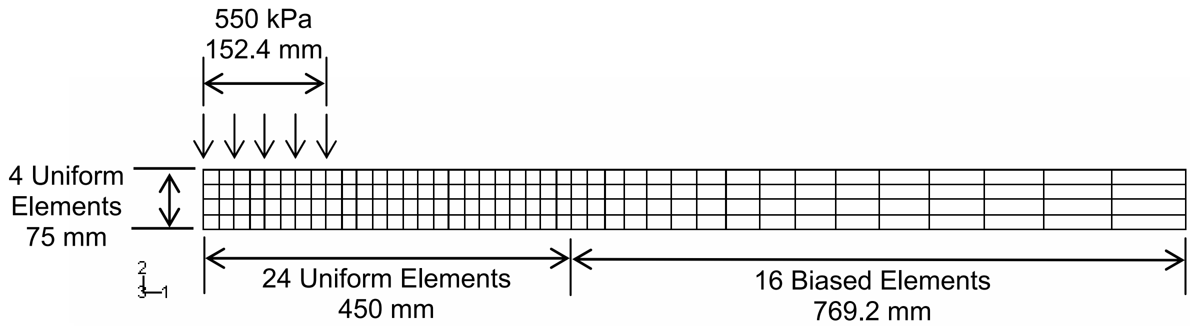

Figure 4.1.2 Geometry and meshing of asphalt concrete layer

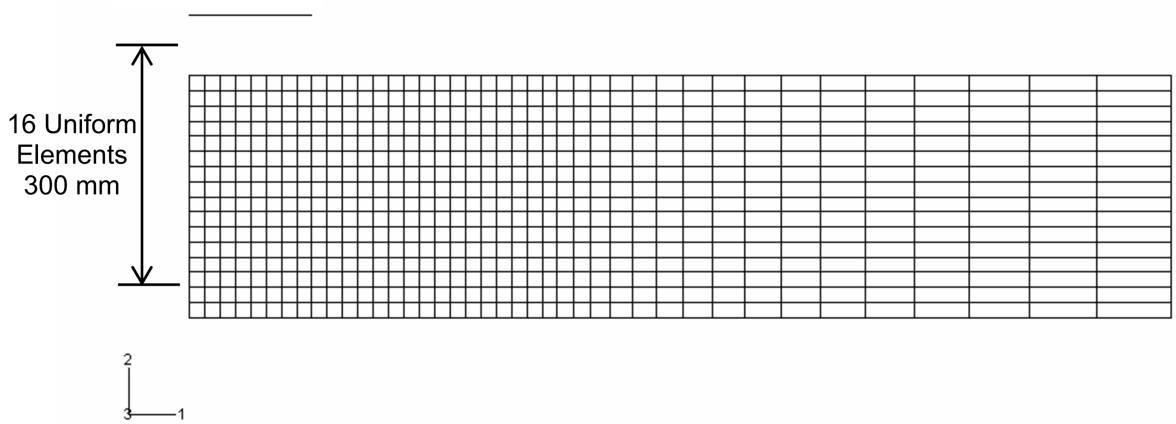

Figure 4.1.3 Geometry and meshing of unbound base aggregate layer

The linear isotropic model for the asphalt concrete described in Section 3.1.1 was used for the top layer. Elastic modulus and Poisson's ratio were chosen for a particular temperature and load frequency pertaining to the problem being analyzed. One of the material models for the unbound aggregate layer described in Section 3.2.1 or 3.3 was used for the finite element region of this layer. An isotropic linear elastic model was used for the infinite elements in this layer as this is the only material model allowed for infinite elements in Abaqus. Elastic modulus for the infinite elements in this layer was taken as the resilient modulus from Equation 3.2.1 calculated as a constant using the geostatic stresses at the mid-height of the layer. The non linear elastic with tension cutoff material model described in Section 3.2.1 was used for the finite element region of the subgrade. For the infinite elements along the vertical (right hand) boundary of the problem, isotropic linear elastic modulus was calculated from Equation 3.2.1 using the geostatic stresses at the mid-point of the subgrade layer. For the infinite elements along the bottom

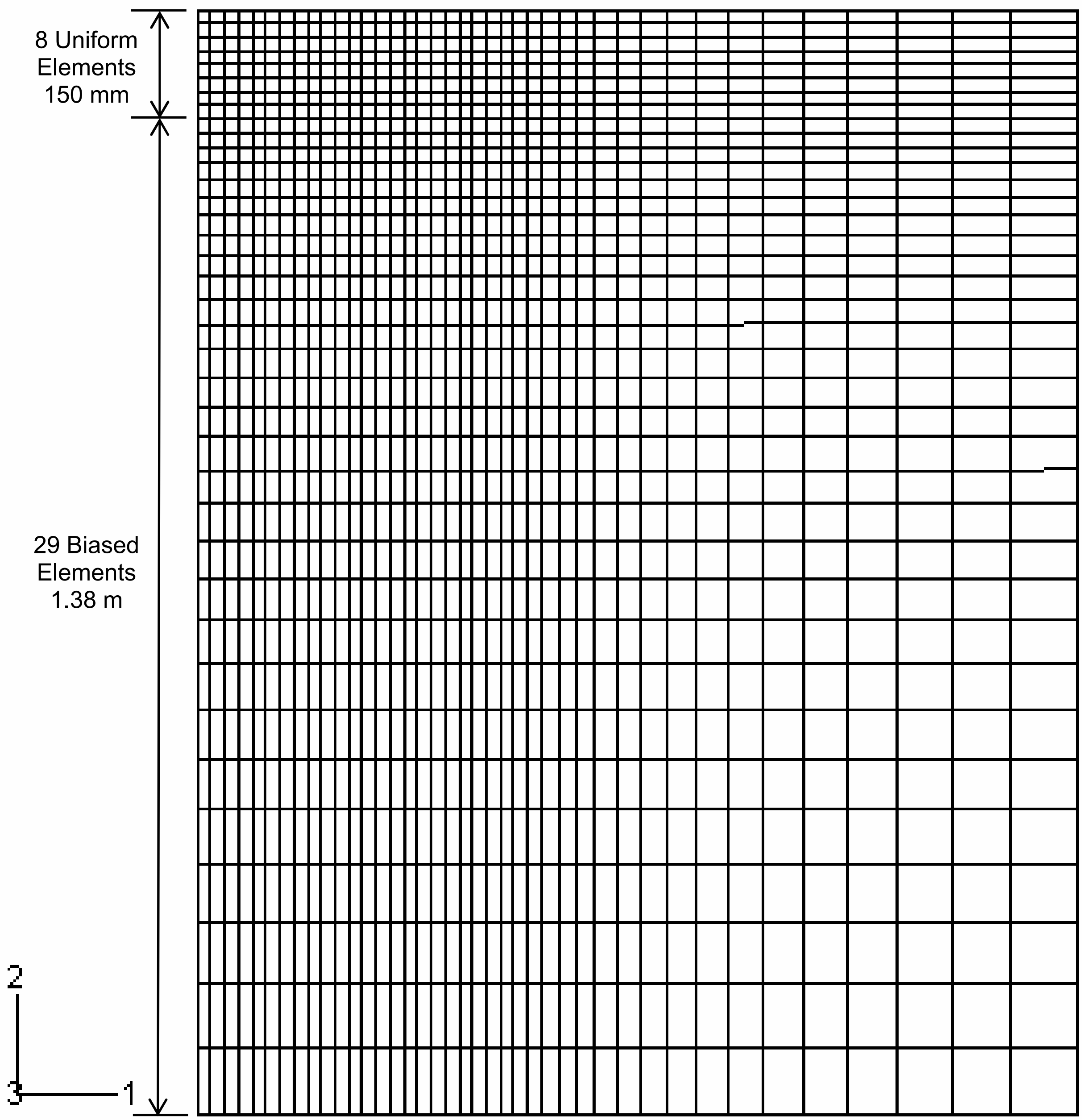
8 Uniform
Elements
150 mm
29 Biased
Elements
1.38 m
2
3
1

4.1.2 Overlay Elements

Preliminary work with response models having tension cutoff activated for the aggregate layer resulted in analyses that were typically unable to reach numerical convergence. Abaqus manuals indicate that numerical stability is commonly encountered with problems where tension cutoff is specified. The problem appears to be one where tension cutoff is activated within an increment leading to large localized accelerations. Overlay elements placed on top of elements having tension cutoff material behavior were used to provide numerical stability. Overlay elements are created by creating an additional set of elements having the same nodal connectivity as the original elements being overlain.

Since the numerical stability arises from sudden and potentially large displacements in regions experiencing tension cutoff, a viscoelastic material model was used for the overlay elements. The visoelastic model contains as few as 5 parameters, namely instantaneous (initial) elastic modulus (E), Poisson's ratio (ν) and Prony series parameters (g_1^P, k_1^P, τ_1). The parameters g_1^P, k_1^P can be thought of as parameters describing the long-term decay of the shear and bulk relaxation modui, respectively, while the parameter τ_1 describes the rate of decay. Equation 4.1.3 shows the use of parameters g_1^P and τ_1 to describe the variation of shear modulus with time, $G(t)$, as a function of the initial or instantaneous shear modulus, G_o. Setting parameters g_1^P and k_1^P to 1.0 results in values of elastic moduli that equal the instantaneous values at t=0 and become equal to zero for large values of time. Figure 1 shows $G(t)$ for G_o=1, g_1^P=1.0 and τ_1=0.01. Selection of τ_1=0.01 results in a relatively rapid decay of modulus for an analysis period of 1 second. The use of overlay elements allowed solutions to converge while not impacting the overall response of the model, which will be demonstrated in Section 4.2.

$$G(t) = G_o\left[1-\overline{g}_1^{\,P}\left(1-e^{\frac{-t}{\tau_1}}\right)\right] \tag{4.1.3}$$

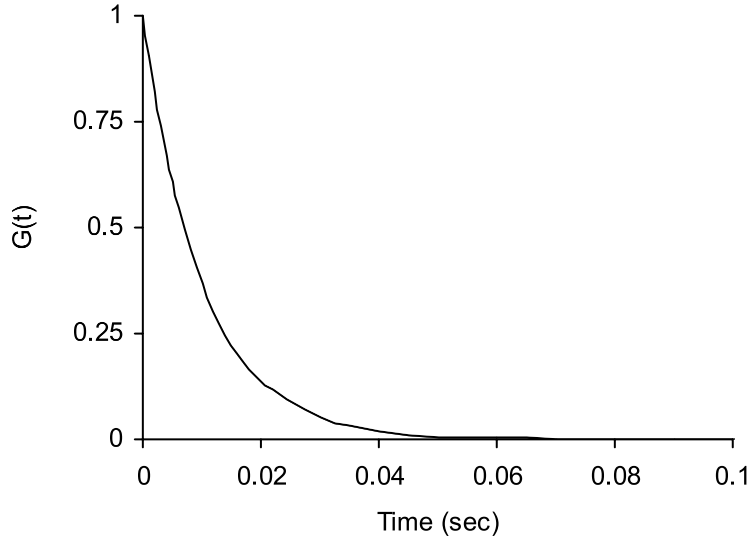

Figure 4.1.5 Example of decay of shear modulus with time for viscoelastic model

4.1.3 Initial Conditions and Load Steps

For all analyses, initial conditions in the form of geostatic stresses were specified by using the material densities and layer thickness (for establishing vertical stresses) and an earth pressure coefficient of 1.0 (for establishing horizontal stresses). Equilibrium of these stresses was established by specifying a geostatic load step as the first load step in the analysis. Execution of this step leaves the model in a strain and displacement free state prior to the application of pavement load. The second load step consisted of the application of the pavement pressure, which was taken as 550 kPa for most analyses. Since a viscoelastic material model was used in the analyses, the second step was a *Visco step where the pavement pressure was applied as a ramp load over typically 100 load increments.

4.1.4 Abaqus UMAT

The non linear elastic with tension cutoff material model described in Section 3.2.1 was implemented in Abaqus as a user defined material model (UMAT). Appendix A provides a copy of the code used for this model. The model is developed by treating the resilient modulus from Equation 3.2.1 as the elastic modulus for a particular state of stress.

For non linear problems, Abaqus applies the load in increments and a tangential formulation of the UMAT is required. A finite element in the soil mass will be in a general three dimensional state of stress. From this general stress tensor, values of θ and τ_{oct} are computed using Equations 4.1.4 – 4.1.6.

$$\theta = \left(\sigma_x + \sigma_y + \sigma_z\right) \tag{4.1.4}$$

$$\tau_{oct} = \sqrt{\frac{1}{3}\left(s_x^{\ 2} + s_y^{\ 2} + s_z^{\ 2} + 2\tau_{xy}^{\ 2} + 2\tau_{yz}^{\ 2} + 2\tau_{zx}^{\ 2}\right)} \tag{4.1.5}$$

$$\begin{aligned} s_x &= \sigma_x - \theta/3 \\ s_y &= \sigma_y - \theta/3 \\ s_z &= \sigma_z - \theta/3 \end{aligned} \tag{4.1.6}$$

In terms of principal stresses, Equation 4.1.5 can be written as:

$$\tau_{oct} = \tfrac{1}{3}\sqrt{\left(\sigma_1 - \sigma_3\right)^2 + \left(\sigma_2 - \sigma_3\right)^2 + \left(\sigma_1 - \sigma_2\right)^2} \tag{4.1.7}$$

The equivalent triaxial stresses σ_a and σ_r, that in a triaxial cell would correspond to the same values of θ and τ_{oct} are computed by first expressing values of θ and τ_{oct} in terms of triaxial stresses σ_a and σ_r.

$$\tau_{oct} = \sqrt{2}/3\,\left(\sigma_a - \sigma_r\right) \tag{4.1.8}$$

$$\theta = \sigma_a + 2\sigma_r \tag{4.1.9}$$

Solving for the equivalent triaxial stresses σ_a and σ_r:

$$\sigma_a = \tfrac{1}{3}\theta + \sqrt{2}\,\tau_{oct} \tag{4.1.10}$$

$$\sigma_r = \tfrac{1}{3}\theta - \tfrac{1}{\sqrt{2}}\,\tau_{oct} \tag{4.1.11}$$

Under these equivalent stresses, an equivalent strain ε_a under triaxial conditions is computed as:

$$\varepsilon_a = \frac{\sigma_a - \sigma_{a0}}{M_R} - \frac{2\nu}{M_R}\left(\sigma_r - \sigma_{r0}\right) \tag{4.1.12}$$

where the stresses σ_{a0} and σ_{r0} are the vertical and horizontal stresses in the pavement structure at no-wheel-load (geostatic) conditions. The equivalent axial strain $\varepsilon_a^{'}$ is not a strain that is found in the pavement layers under a general 3D stress condition, but is a strain that is compatible with the equivalent triaxial stresses σ_a and σ_r.

The equivalent tangential stiffness E_T for triaxial loading in the axial direction is defined as:

$$\frac{1}{E_T} = \frac{d\varepsilon_a}{d\sigma_a} \tag{4.1.13}$$

Substitution of Equation 4.1.12 into Equation 4.1.13 yields:

$$\frac{1}{E_T} = \frac{1}{M_R} - \frac{\varepsilon_a}{M_R}\frac{dM_R}{d\sigma_a} \tag{4.1.14}$$

Evaluation of the term $dM_R/d\sigma_a$ yields:

$$\frac{dM_R}{d\sigma_a} = k_1\, k_2 \left(\frac{\theta}{p_a}\right)^{k_2 - 1} \left(\frac{\tau_{oct}}{p_a} + 1\right)^{k_3} + k_1\, k_3 \left(\frac{\theta}{p_a}\right)^{k_2} \left(\frac{\tau_{oct}}{p_a} + 1\right)^{k_3 - 1} \frac{\sqrt{2}}{3} \tag{4.1.15}$$

Dividing through by M_R gives:

$$\frac{1}{M_R}\frac{dM_R}{d\sigma_a} = \frac{k_2}{\theta} + k_3 \frac{\sqrt{2}}{3}\frac{1}{\tau_{oct} + p_a} \tag{4.1.16}$$

The resulting equivalent tangential Young's modulus under triaxial testing conditions is therefore written as:

$$E_T = \frac{1}{\dfrac{d\varepsilon_a}{d\sigma_a}} = \frac{1}{\dfrac{1}{M_R} - \varepsilon_a\left(\dfrac{k_2}{\theta} + k_3\dfrac{\sqrt{2}}{3}\dfrac{1}{\tau_{oct} + p_a}\right)} \tag{4.1.17}$$

It should be remembered that the strain ε_a is not an actual pavement strain but is an equivalent strain computed from Equations 4.1.10 – 4.1.12. The tangential elastic Young's modulus, E_T, is then used to compute the stiffness matrix **E** for isotropic elastic conditions.

The input to a user material routine is the current strain increment $\Delta\varepsilon_i$, as well as the strain and stress "tensors" ε_{i-1} and σ_{i-1} at the previous equilibrium step. The routine responds with the corresponding stress "tensor" σ_i for the strain $\varepsilon_i = \varepsilon_{i-1} + \Delta\varepsilon_i$, and the tangent stiffness matrix **E**.

Since the model is stress dependent, it is easy to compute the strain due to a given stress, but to calculate the stress due to a given strain requires iterations. The scheme has been adopted to perform these calculations:

1) Input the strain increment ε_I from Abaqus
2) Use the stress σ_{i-1} from the previous load step to calculate the first estimate of M_R
3) Define a modulus iteration factor $f = 1.5$

Start iteration loop:

4) Calculate the constitutive secant stiffness matrix **E** for the current value of M_R
5) From the strain ε_i, compute the resulting stress $\sigma_i = \sigma_0 + \mathbf{E}\ \varepsilon_i$, where σ_0 is the initial geostatic stress
6) Apply tension cut-off if tensile strength is exceeded
7) Evaluate a new value M_{Res} of the modulus from the resulting stress σ_i
8) Compare M_R and M_{Res}.
   a) If $M_{Res} < M_R$, then *reduce* the modulus by a factor f : $M_R = M_R /f$
      (*Reduce* the factor f if $M_{Res} > M_R$ in the previous iteration loop.)
   b) If $M_{Res} > M_R$, then *increase* the modulus by a factor f : $M_R = M_R *f$
      (*Reduce* the factor f if $M_{Res} < M_R$ in the previous iteration loop.)
9) If the change in M_R is larger than a *criterion*, go back to Point 4.
10) The subroutine returns **E** and σ_i to the calling routines of the program (i.e. to Abaqus through the UMAT)

E is a *secant stiffness*, and σ_i is the stress, and both correspond to the strain ε_i. This process is illustrated in Figure 4.1.6.

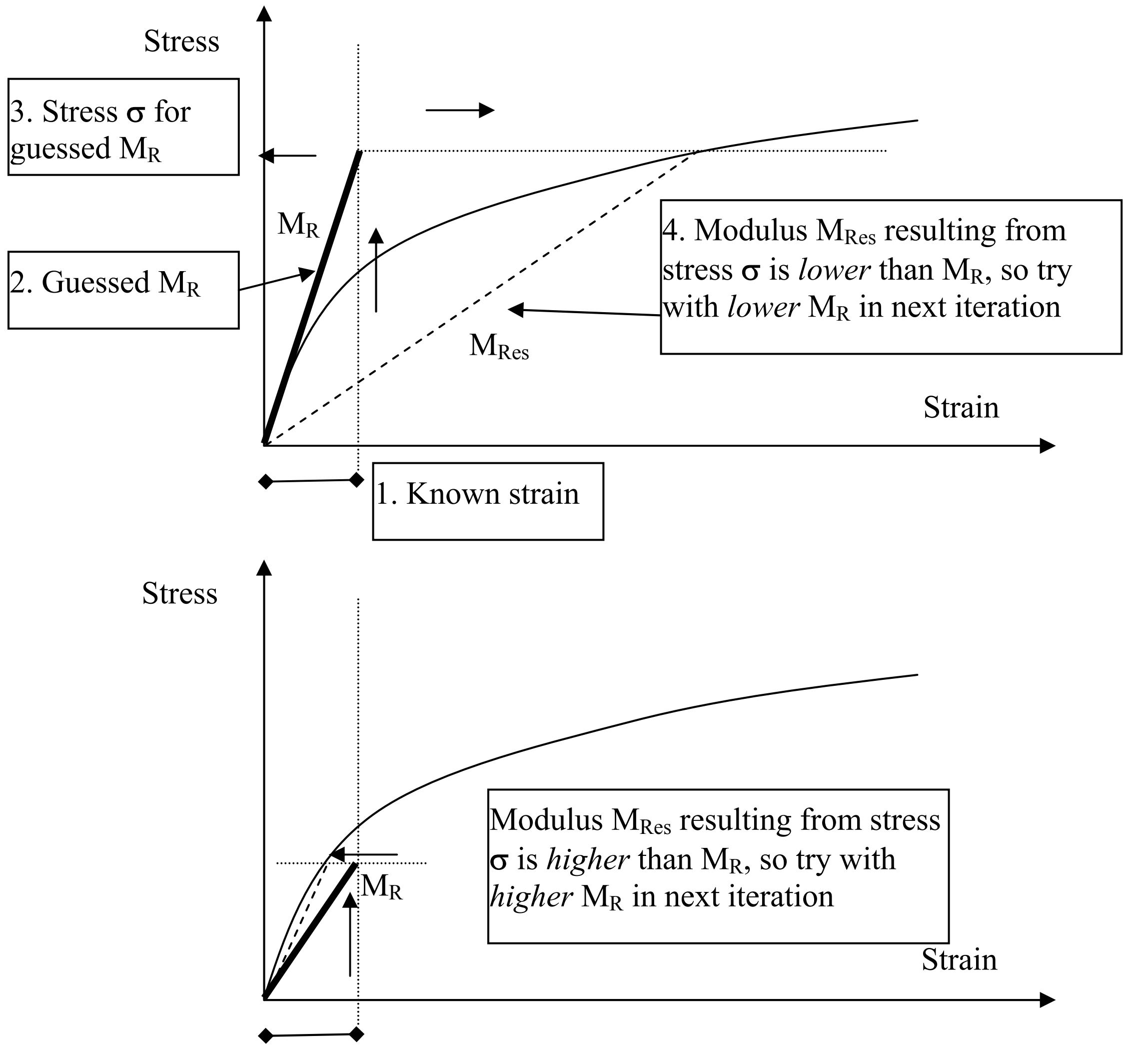

Figure 4.1.6 Stress iterations followed in UMAT

Tension cutoff is treated in a simple way by adjusting the stress σ_i so that tension does not occur. For any given state of stress, the three principal stresses and their associated unit vectors denoting their directions are computed. For each individual principal stress, if any are found to exceed the tensile strength of the material, specified as an input parameter, then the stress is set equal to the tensile strength. The new principal state of stress, assumed to have the same orientation, is then transformed back to the original xyx coordinate system. This process is done within equilibrium iterations so that at the end of the load increment the stress state has no tension and is in equilibrium with the applied loads.

4.2 Benchmark Tests

Benchmark tests were performed to verify proper performance of the finite element response model. The first series of tests correspond to simple 1-element tests performed to verify behavior of the UMAT described in Section 4.1.4. The second series of tests correspond to relatively small special models developed to evaluate the performance of the tension cutoff feature. The third series corresponds to pavement response models created according to the geometry and meshing described in Section 4.1.

4.2.1 One Element Tests

Single axisymmetric element models were created to mimic triaxial boundary and loading conditions. The isotropic non linear elastic model described in Section 3.2.1 was used with the different parameter sets shown in Table 4.2.1. The stress σ_c represents the lateral stress applied to the element, which was held constant. The stress $\Delta\sigma$ represents the difference between the axial stress and lateral stress. The first set of parameters exercises stress hardening behavior (increasing modulus during loading) by having $k_3 = 0$. The second set exercises stress softening behavior (decreasing modulus during loading) by having $k_2 = 0$. The third set corresponds to a mixture of hardening and softening.

Table 4.2.1 Material property and stress conditions for single element tests

Set	k_1	k_2	k_3	p_a	σ_c	$\Delta\sigma$
Hardening	10,000	1	0	14.7	1	50
Softening	2041	0	-4	14.7	1	50
Combined	4518	0.5	-1	14.7	1	50

Figures 4.2.1 – 4.2.3 show the response of the UMAT model described in Section 4.1.4 and the solution from the model used in the NCHRP 1-37A Design guide as compared to the analytical solution for 25, 50 and 100 steps during load and unload, respectively. These results show the UMAT and the NCHRP 1-37A Design Guide models tend to show slightly different predictions that both improve with increased number of load increments. Figure 4.2.4 shows the UMAT model compared to the analytical solution for a 1000 load and unload steps, where it is seen that the prediction is quite good.

It should be noted that the stress hardening loading where $k_1 = 1$ creates a situation where the axial strain goes to a value of $1/k_1$ as $\Delta\sigma$ goes to infinity. In other words, the strain becomes "locked" as loading continues to increase. This type of loading is very difficult to numerically predict.

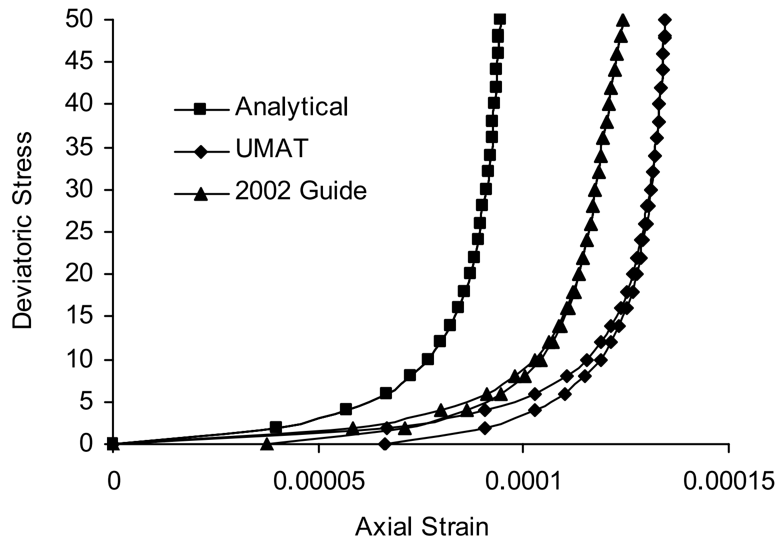

Figure 4.2.1 Single element test for stress hardening loading with 25 load and unload increments

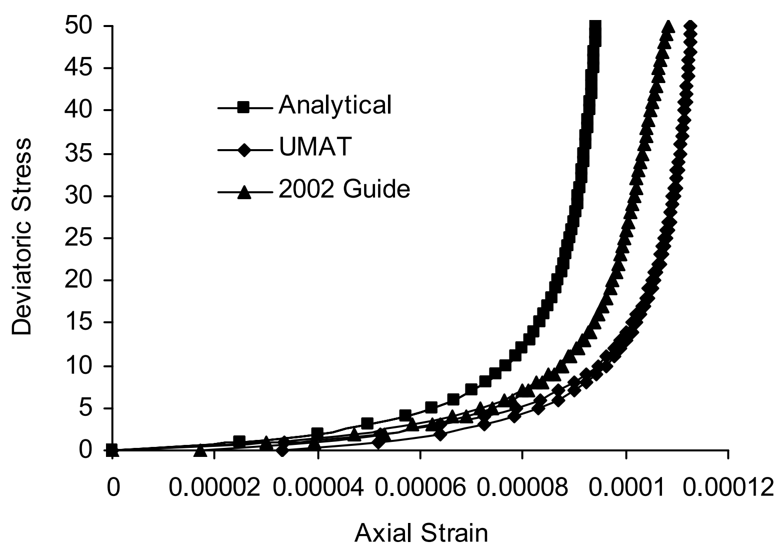

Figure 4.2.2 Single element test for stress hardening loading with 50 load and unload increments

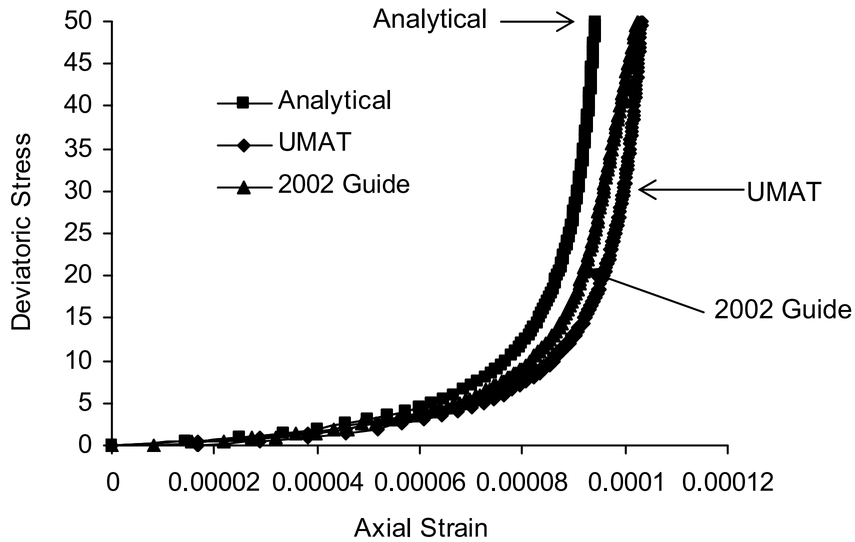

Figure 4.2.3 Single element test for stress hardening loading with 100 load and unload increments

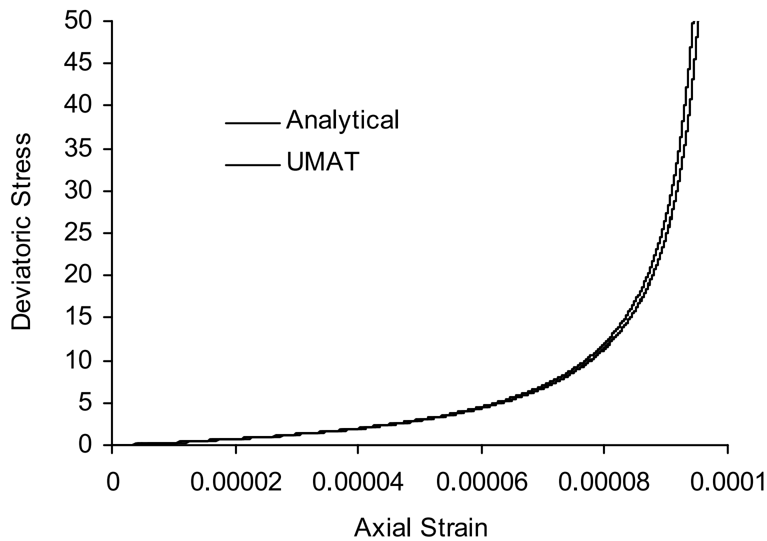

Figure 4.2.4 Single element test for stress hardening loading with 1000 load and unload increments

Figure 4.2.5 shows predictions from the UMAT and NCHRP 1-37A Design Guide as compared to the analytical solution for the stress softening loading where 50 load and unload steps were taken for the numerical solutions. Excellent agreement between the numerical and analytical solutions is seen during loading, however the numerical solutions tend to deviate slightly from the analytical solution during unloading. Figure 4.2.6 shows results from the combined loading set where excellent agreement between numerical and analytical solutions is seen during both loading and unloading.

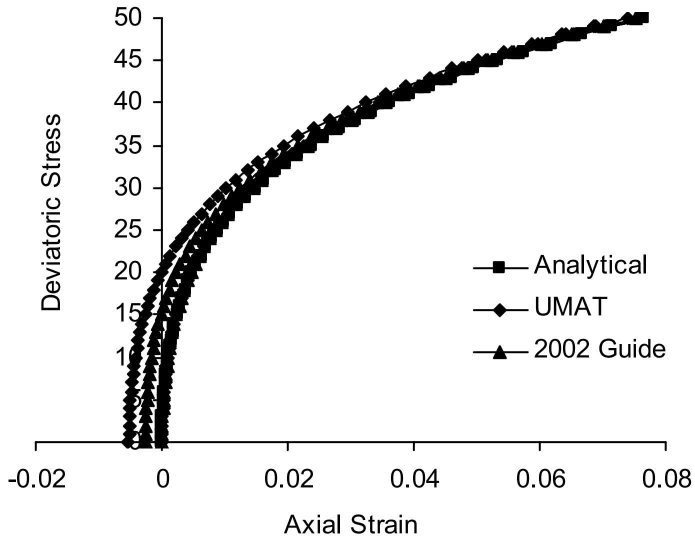

Figure 4.2.5 Single element test for stress softening loading with 50 load and unload increments

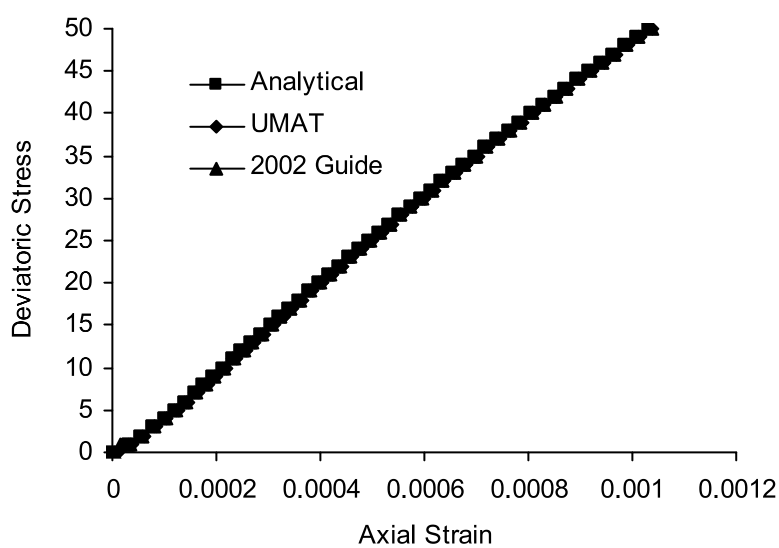

Figure 4.2.6 Single element test for combined loading with 50 load and unload increments

Additional single element tests were performed to evaluate the UMAT for the case of an isotropic linear elastic material ($k_2 = k_3 = 0$) under zero lateral strain loading. The UMAT showed excellent agreement to the analytical prediction for this type of loading.

4.2.2 Tension Cutoff Models

Two models were created to evaluate the tension cutoff feature of the UMAT. The first problem consists of an axisymmetric body having tension cutoff elements sandwiched between non-tension cutoff elements. The model is first subjected to a volumetric compression (no induced tensions) followed by a radial unloading to induce radial tensions. The mesh for the problem is shown in Figure 4.2.7. Element sizes are 1 x 1 (consistent units). All elements are modeled as linearly elastic with E=10000 and ν=0.25. The non-tension cutoff elements (unshaded elements in Figure 4.2.7) are modeled using a conventional linear elastic material model while the tension cutoff elements (shaded elements in Figure 4.2.7) are modeled using the nonlinear M_R model with $k_1 p_a = 10{,}000$ and $k_2 = k_3 = 0$ (i.e., no stress dependence).

Boundary conditions for the mesh are roller boundaries ($u_R = 0$) along the inner boundary of the mesh (left edge, R=0) and roller boundaries ($u_Y = 0$) along the bottom of the mesh (Y=3). The loading consists of an initial volumetric compression of magnitude 1 (i.e., compressive vertical and radial pressures both equal to 1) followed by a radial unloading to a final radial applied pressure of -1. The radial unloading is applied in 20 increments (Step 2 through Step 21).

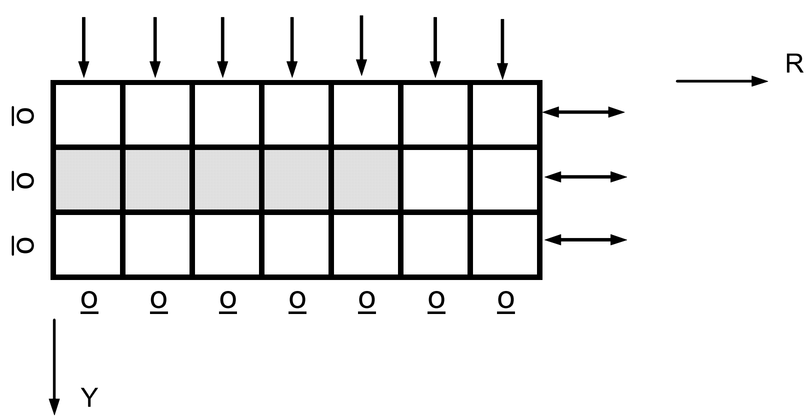

Figure 4.2.7 Mesh for first tension cutoff analysis problem

The results from the two analyses are summarized in Figures 4.2.8 through 4.2.13. The data points in all figures correspond to element centroid locations for stresses and nodal points for displacements. Results are presented for the following load steps:

- Step 1: Immediately after initial volumetric compression
- Step 6: One-quarter of the way through the radial unloading, radial applied pressure equal to 0.5 (compression), no induced radial tension stresses.
- Step 11: One-half of the way through the radial unloading, radial applied pressure equal to zero.
- Step 16: Three-quarters of the way through the radial unloading, radial applied pressure equal to -0.5 (tension), induced radial tension stresses.
- Step 21: Full radial unloading, radial applied pressure equal to -1 (tension), induced radial tension stresses.

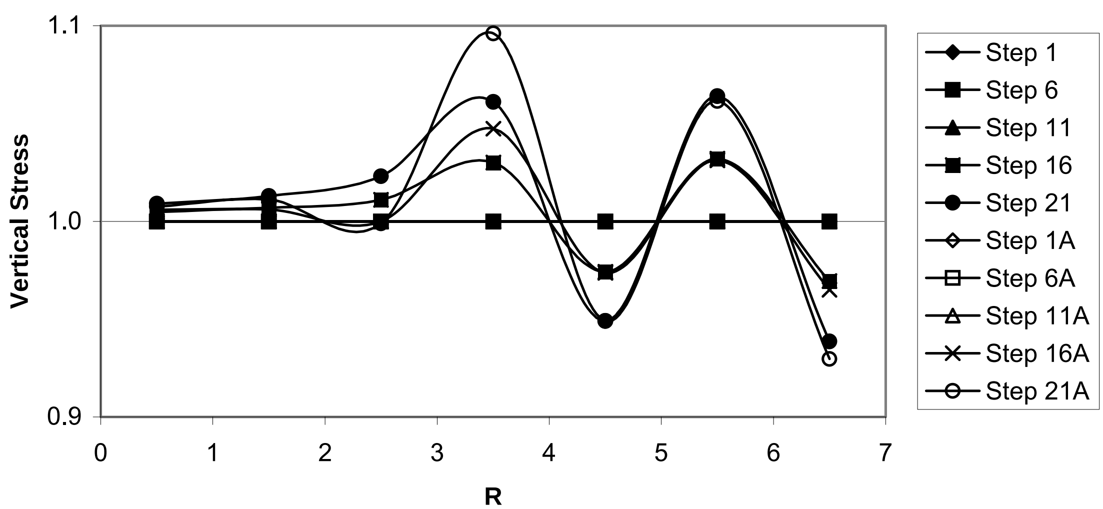

Figure 4.2.8 Vertical stresses at the mid thickness of the middle layer of elements

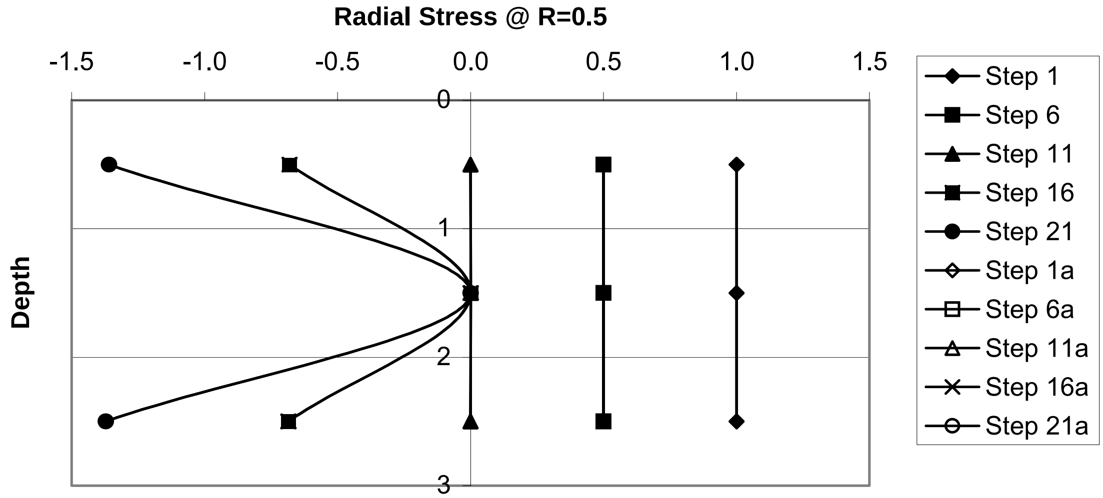

Figure 4.2.9 Radial stresses vs. depth along the inner boundary of the mesh (left edge)

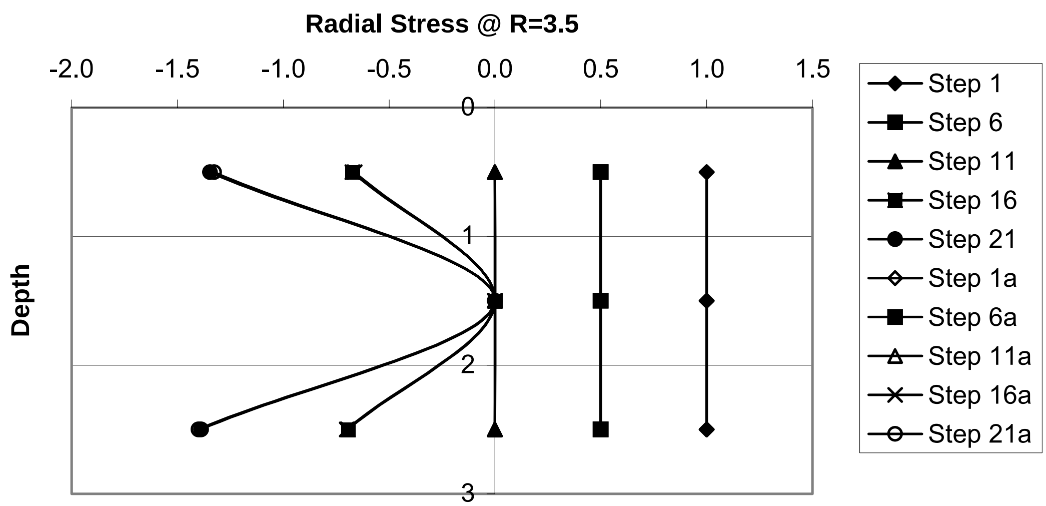

Figure 4.2.10 Radial stresses vs. depth through the center of the mesh

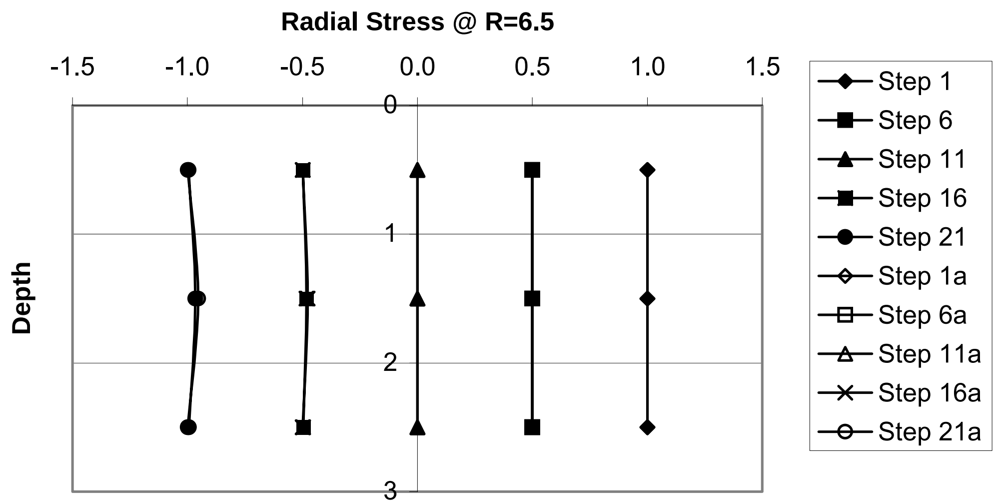

Figure 4.2.11 Radial stresses vs. depth along the outer boundary of the mesh (right edge)

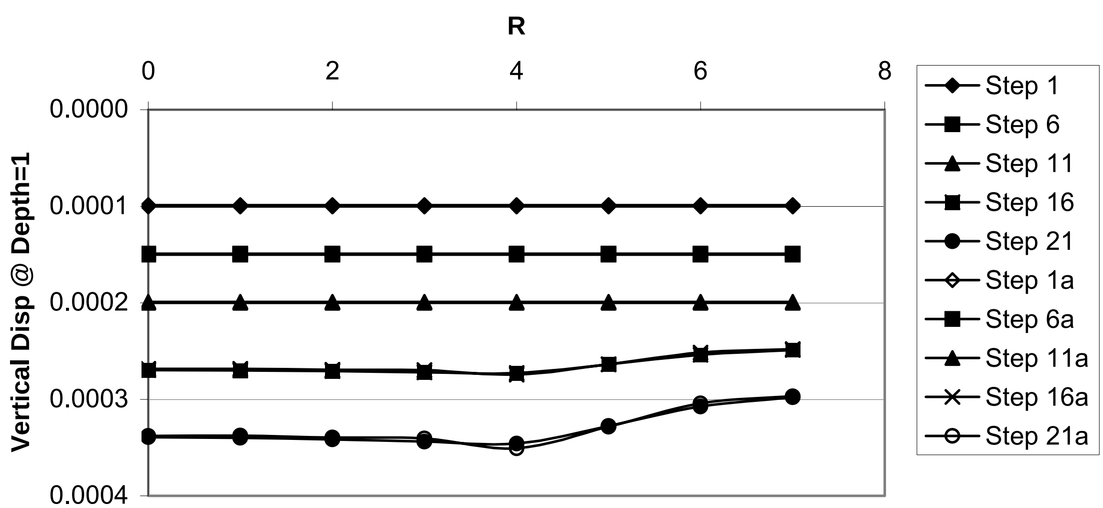

Figure 4.2.12 Vertical displacements along the top of the middle row of elements

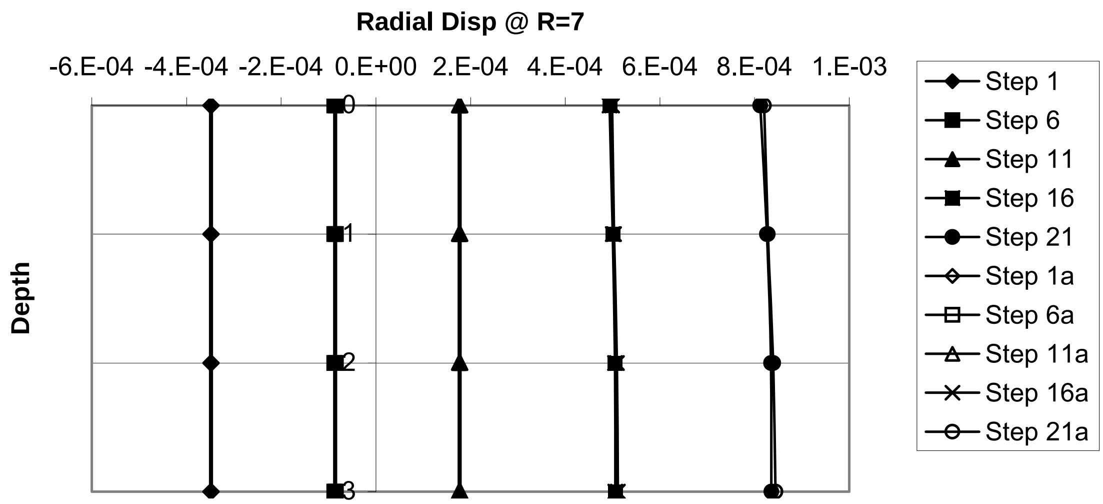

Figure 4.2.13 Radial displacements along the outer boundary of the mesh (right edge)

Figure 4.2.8 shows the vertical stresses at the mid thickness of the mesh (mid thickness of the middle layer of elements) versus radial distance at the 5 load steps. Theoretically, the vertical stresses should be uniformly equal to 1 (compression) at all locations and for all load steps in the analysis. The results in Figure 4.2.8 conform to this theoretical expectation, with just a small amount of numerical noise in Steps 16 and 21 after the tension cutoff behavior has begun. Slight differences are seen between the NCHRP 1-37A Design Guide and UMAT models.

Figures 4.2.9 through 4.2.11 show the radial stresses along various vertical lines at the 5 load steps. Figures 4.2.9 and 4.2.10 correspond to vertical lines passing through the tension cutoff elements. Theoretical expectations are that the radial stresses are uniform with depth and equal the applied radial pressures for load steps 1 through 11; after load step 11, there should be a shedding of load from the "failing" middle layer to the intact elements in the top and bottom layers. At the end of the analysis, all radial load should be carried by the top and bottom layers, with a final radial stress value of 1.5. It is clear that the results in Figures 4.2.9 and 4.2.10 conform to these theoretical expectations, with identical results obtained for the NCHRP 1-37A Design Guide and UMAT models.

The vertical line for Figure 4.2.11 is near the outer radial boundary of the mesh and does not pass through any tension cutoff elements. Theoretically, then, one expects the radial stresses here to equal the applied radial pressures at all load steps. The results in Figure 4.2.11 conform to this expectation for both models.

Vertical displacements along the top of the middle layer of elements are shown in Figure 4.2.12. Theoretically, one expects the vertical displacements to be uniform across the specimen for load steps 1 through 11 before any tension cutoff develops. After tension cutoff develops, the elements "failing" in tension become effectively less stiff and one thus expects to see larger vertical displacements above these elements for load steps 12 through 21. These expected trends are followed by the results in Figure 4.2.12. The NCHRP 1-37A Design Guide and UMAT models produce identical results.

Figure 4.2.13 plots radial displacement along the outer radial boundary of the mesh for the 5 load steps. Theoretically, one would expect to see a radial "bulging" symmetric about the mid thickness of the problem due to the tension failure of the middle sandwich of elements. However, because only one layer of tension cutoff elements is included in the model and because 4 node elements have been employed, the remaining rigidity of the outer "non-failing" elements appears to mask this expected trend in Figure 4.2.13.

The second model developed to evaluate tension cutoff behavior consists of a 3 element axisymmetric model with each element having a size of 1 by 1 (consistent units). The material model parameters are k_1 = 2041, k_2 = 1.05, k_3 = -1.5, p_a = 100 and ν = 0.25. The model is shown in Figure 4.2.14. Elements 1 and 3 have no tension cutoff created by setting the tensile strength to 1000. Element 2 has tension cutoff with a value of 0.01.

Loading for the problem consists of the following steps:

Initial condition:	Uniform and isotropic initial stress of 10 balanced by an external pressure of 10 on all surfaces (Not shown in Figure 4.2.14)
Step A:	Apply vertical stress of 410 in 12 increments with the radial stress of 10 held constant
Step B:	Reduce radial external pressure to zero in 12 increments
Step C:	Force the right hand surface of element 3 to a displacement of 3.0E-3 in 24 increments

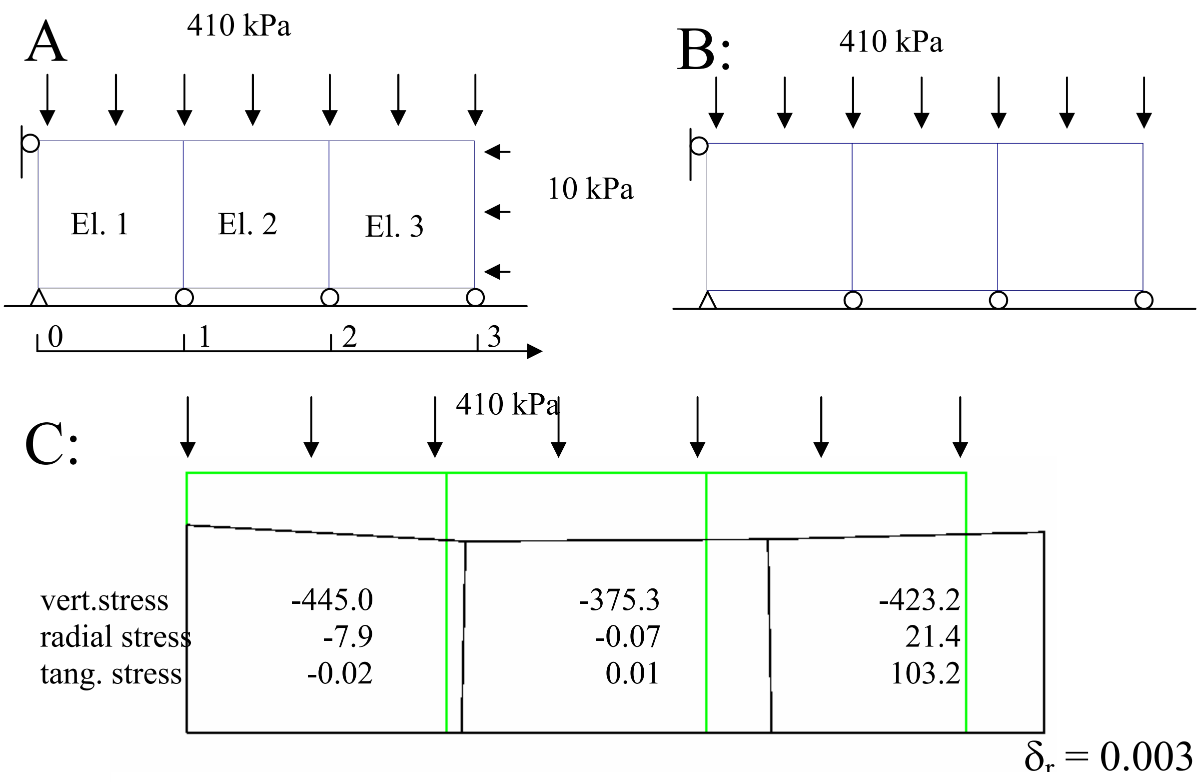

Figure 4.2.14 Mesh and results for second tension cutoff analysis problem

Figure 4.2.14 C shows computed results after step C. From these results it is seen that:

- Element No. 2 becomes elongated due to the no-tension condition. It is near stress-free in radial and tangential directions.
- Element 3 gets a high *tensile* tangential stress: This is consistent with an additional lateral displacement of $\Delta\delta_r$ = 1.25E-3 m from the end of Step B to the end of Step C since element 3 does not have a tension cut-off.
- Vertical stress is shed from element 2 to the stiffer elements 1 and 3, which probably also is why element 1 gets an increased radial stress.

4.2.3 Pavement Models

The third series of benchmark tests were performed to verify the following:

1. Negligible effect of having overlay elements in the model
2. Proper response of the finite element model as compared to predictions from other models
3. Proper numerical implementation of the UMAT for the non linear elastic with tension cutoff model

These three issues were verified by creating response models having the following material models for the base and subgrade layers.

1. Isotropic linear elastic without tension cutoff, with and without overlay elements
2. Isotropic linear elastic with tension cutoff
3. Isotropic non linear elastic with tension cutoff

The response models created had layer thickness and meshing according to the model described in Section 4.1.1. To compare models, response measures (stress, strain, deflection) were extracted from analyses along two paths through the model. The first path corresponds to the vertical centerline axis (axis of symmetry). Stress and strain measures were extrapolated to points along this path. All subsequent plots with an axis of "Depth" correspond to results taken along this path.

The second path is a radial line through the base-subgrade layer interface. Again, stress and strain measures were extrapolated to points along this path. For variables where a jump occurs from the base to the subgrade layer, measures from both the subgrade and base are shown. Subsequent plots with an axis of "Radius" correspond to results taken along this path.

The nomenclature used for response measures are described below, where the 2 direction corresponds to the vertical direction and the 1 direction corresponds to the radial direction.

U2: Displacement in the 2 direction.

E11: Strain in the 1 direction

E22: Strain in the 2 direction

S11: Stress in the 1 direction

S22: Stress in the 2 direction

SP = hydrostatic stress = -3*(S11+S22+S33)

ST = von Mises stress = 3*τ_{oct}/sqrt(2)

Stress and strain is positive in tension, negative in compression, with the exception of SP which is positive in compression. The stress measures shown in the figures to follow include self-weight stresses due to gravity loading.

The first step taken to evaluate the operation of response models created following the material presented in Section 4.2.1 involved analyzing four comparable pavement response models. Each model used or simulated isotropic linear elastic without tension cutoff material behavior for all layers. These analyses were performed to verify that each predicted the same response for the simplest case of material models. Table 4.2.2 lists the properties used in an Abaqus model established following the material presented in Section 4.2.1 and using a conventional (standard) isotropic linear elastic model for base and subgrade layers. Table 4.2.3 gives the properties used in a second identical Abaqus model with the exception that overlay elements were added for the base and subgrade finite element regions. Table 4.2.4 lists the properties used in a third identical Abaqus model using the isotropic non-linear elastic model with tension cutoff (UMAT) model described in Section 4.1.4 but with properties simulating isotropic linear elastic without tension cutoff behavior. Table 4.2.5 gives properties used in a model set up using the NCHRP 1-37A Design Guide to match the Abaqus models described above and using its isotropic non-linear elastic model with tension cutoff model but with properties simulating isotropic linear elastic without tension cutoff behavior.

Figures 4.2.15-4.2.26 show results from the analyses described above. All of the results show excellent correspondence between the Abaqus analyses with and without overlay elements, indicating that the use of overlay elements with the properties denoted above did not provide any additional stiffness to the model. The UMAT with overlay elements also produced excellent correspondence to the Abaqus analyses indicating that the UMAT correctly reproduces linear elastic behavior. The jumpiness in the vertical stresses within the asphalt concrete layer (Figure 4.2.18) is due to the way in which Abaqus extrapolates values to the centerline axis. Examination of centroid values in the 4 elements along the centerline indicate values that fall along the trendline seen in Figure 4.2.18.

Table 4.2.2 Material layer properties for Abaqus model with a standard isotropic linear elastic without tension cutoff for all layers

Layer	Unit Weight (kN/m^3)	Elastic Modulus, E (kPa)	Poisson's Ratio
Asphalt Concrete	23	2,500,000	0.35
Base (finite)	20	41,903	0.25
Base (infinite)	20	41,903	0.25
Subgrade (finite)	18	20,500	0.25
Subgrade (infinite-side)	18	20,500	0.25
Subgrade (infinite-bottom)	18	20,500	0.25

Table 4.2.3 Material layer properties for Abaqus model with a standard isotropic linear elastic without tension cutoff for all layers and with overlay elements

Layer	Unit Weight (kN/m^3)	Elastic Modulus, E (kPa)	Poisson's Ratio	g_1^P	k_1^P	τ_1
Asphalt Concrete	23	2,500,000	0.35	---	---	---
Base (finite)	20	41,903	0.25	---	---	---
Base (infinite)	20	41,903	0.25	---	---	---
Base (overlay)	0	41,903	0.25	1.0	1.0	0.01
Subgrade (finite)	18	20,500	0.25	---	---	---
Subgrade (infinite-side)	18	20,500	0.25	---	---	---
Subgrade (infinite-bottom)	18	20,500	0.25	---	---	---
Subgrade (overlay)	0	20,500	0.25	1.0	1.0	0.01

Table 4.2.4 Material layer properties for Abaqus model with the isotropic non linear elastic with tension cutoff model simulating isotropic linear elastic without tension cutoff behavior and with overlay elements

Layer	Unit Weight (kN/m^3)	Poisson's Ratio, ν	Elastic Modulus (kPa)				
Asphalt Concrete	23	0.35	2,500,000				
Base (infinite)	20	0.25	41,903				
Subgrade (infinite-side)	18	0.25	20,500				
Subgrade (infinite-bottom)	18	0.25	20,500				
				g_1^P	k_1^P	τ_1	
Base (overlay)	0	0.25	41,903	1.0	1.0	0.01	
Subgrade (overlay)	0	0.25	20,500	1.0	1.0	0.01	
			p_a (kPa)	k_1	k_2	k_3	T_c (kPa)
Base (finite)	20	0.25	100	41.903	0	0	10,000
Subgrade(finite)	18	0.25	100	20.5	0	0	10,000

Table 4.2.5 Material layer properties for NCHRP1-37A model with its isotropic non linear elastic with tension cutoff model simulating isotropic linear elastic without tension cutoff behavior

Layer	Density, γ (kN/m^3)	Elastic Modulus, E (kPa)	Poisson's Ratio	p_a (kPa)	k_1	k_2	k_3	T_c
Asphalt Concrete	23	2,500,000	0.35	---	---	---	---	---
Base (finite)	20	---	0.25	100	41.903	0	0	10,000
Base (infinite)	20	41,903	0.25	---	---	---	---	---
Subgrade (finite)	18	---	0.25	100	20.5	0	0	10,000
Subgrade (infinite-side)	18	20,500	0.25	---	---	---	---	---
Subgrade (infinite-bottom)	18	20,500	0.25	---	---	---	---	---

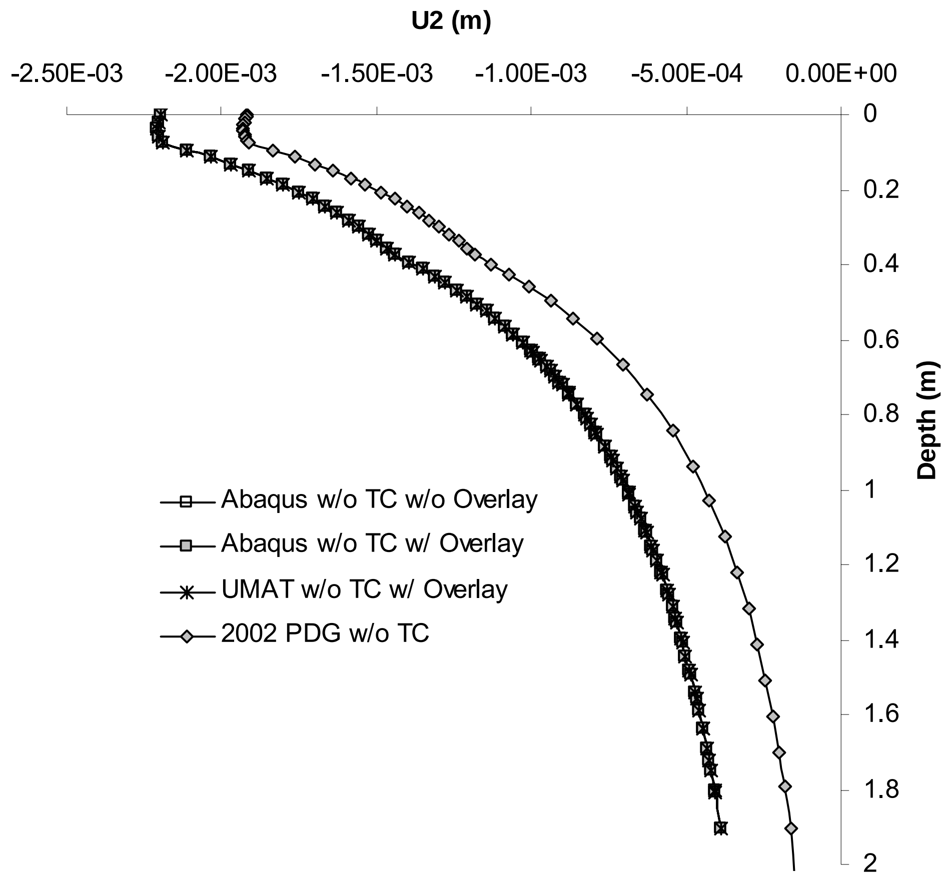

Figure 4.2.15 U2 vs. Depth, isotropic linear elastic without tension cutoff analyses, with and without overlay elements

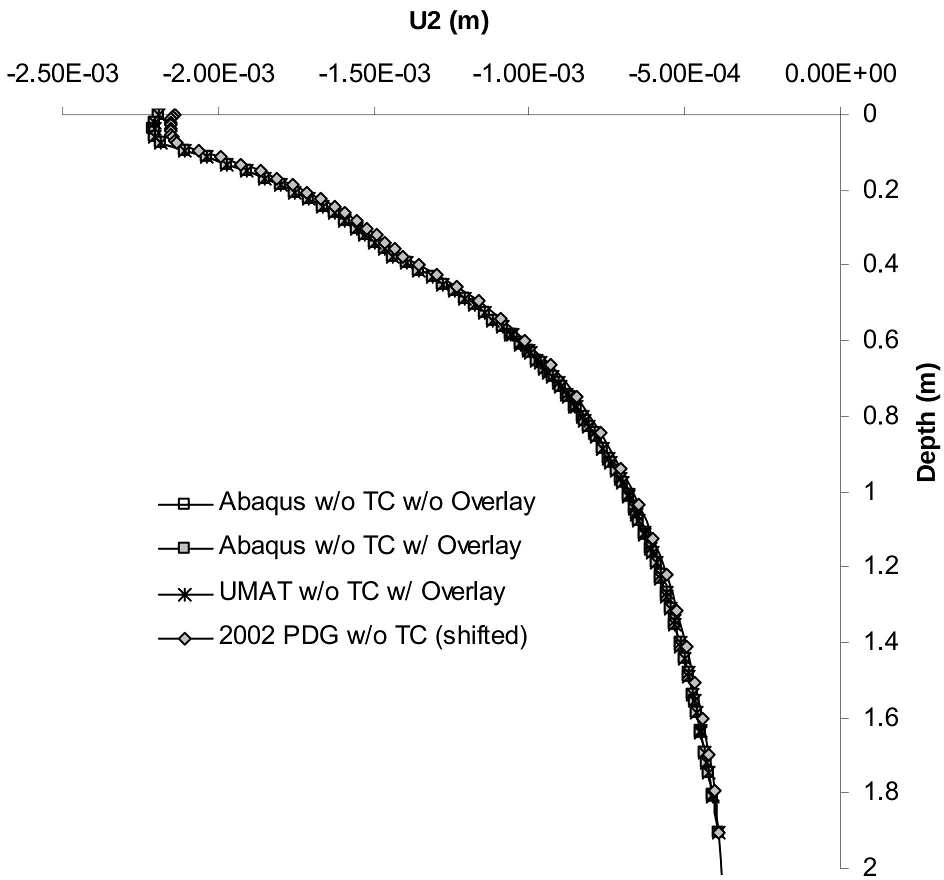

Figure 4.2.16 U2 vs. Depth, isotropic linear elastic without tension cutoff analyses, with and without overlay elements and with shifted data for NCHRP 1-37A analysis

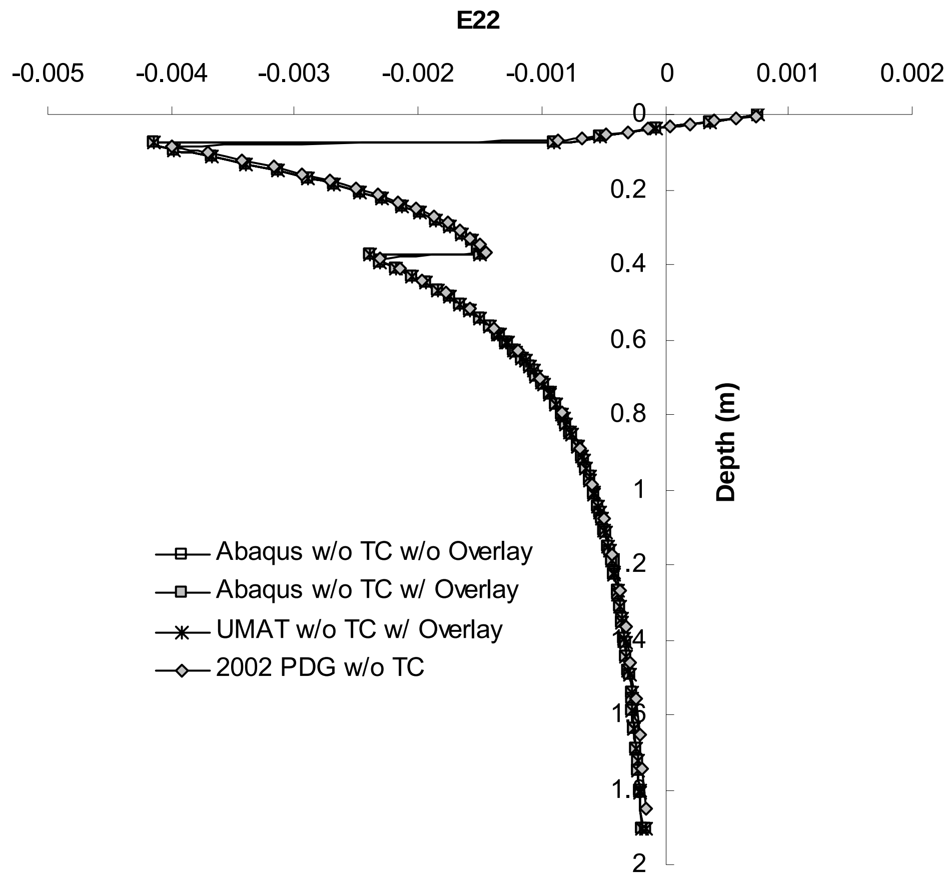

Figure 4.2.17 E22 vs. Depth, isotropic linear elastic without tension cutoff analyses, with and without overlay elements

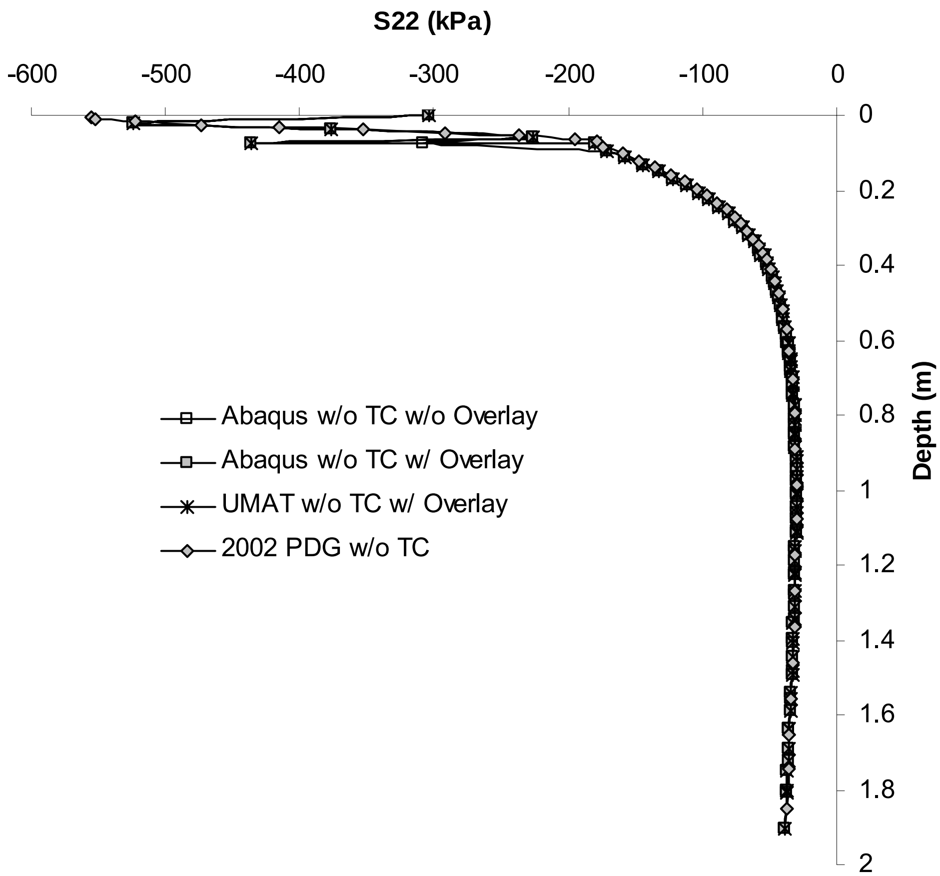

Figure 4.2.18 S22 vs. Depth, isotropic linear elastic without tension cutoff analyses, with and without overlay elements

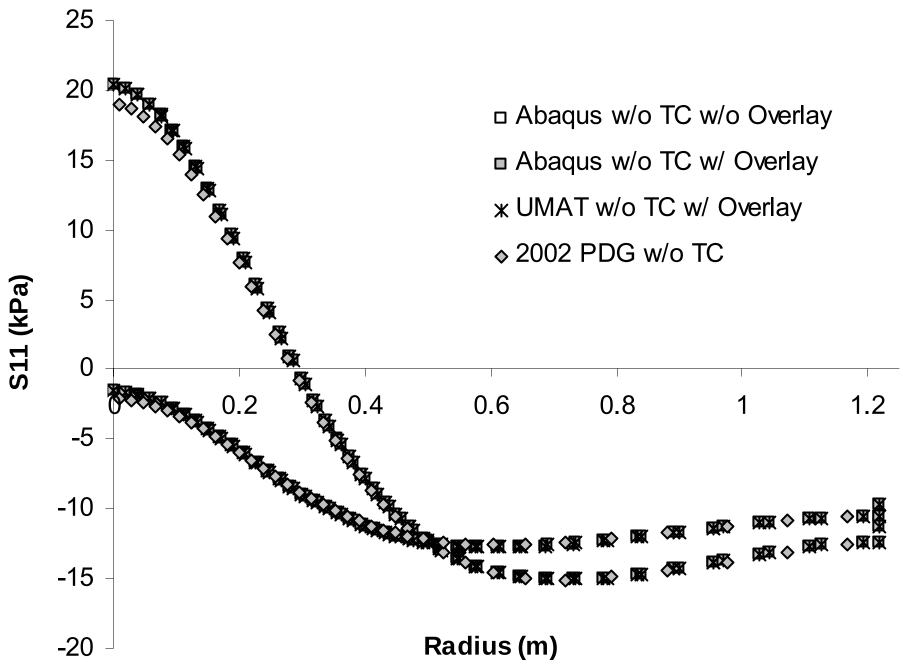

Figure 4.2.19 S11 vs. Radius, isotropic linear elastic without tension cutoff analyses, with and without overlay elements

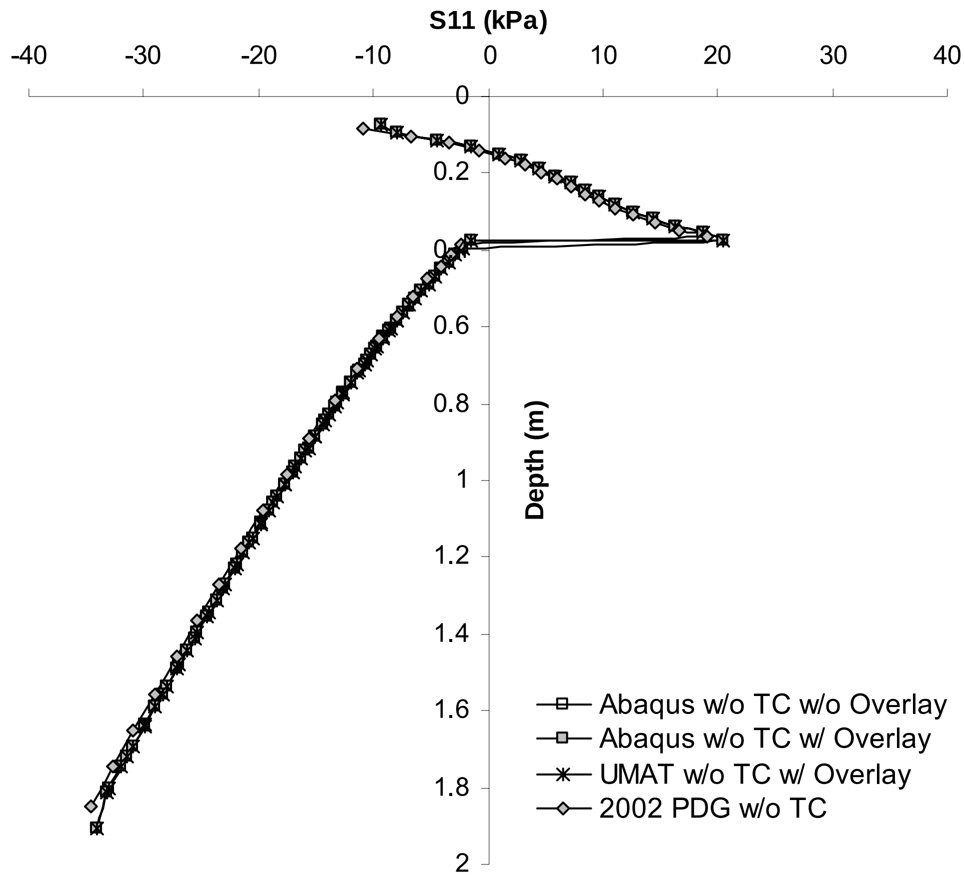

Figure 4.2.20 S11 vs. Depth, isotropic linear elastic without tension cutoff analyses, with and without overlay elements

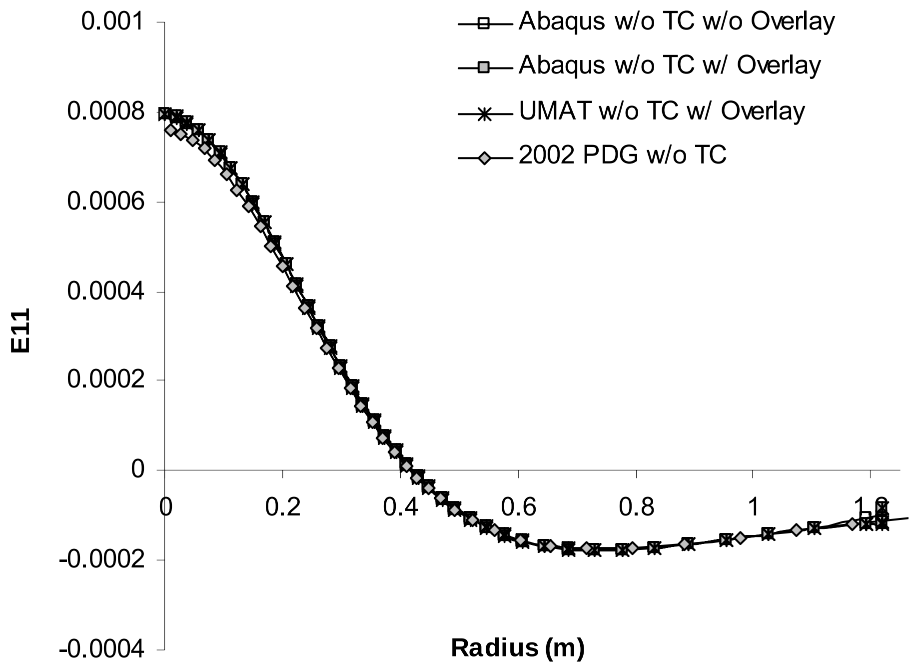

Figure 4.2.21 E11 vs. Radius, isotropic linear elastic without tension cutoff analyses, with and without overlay elements

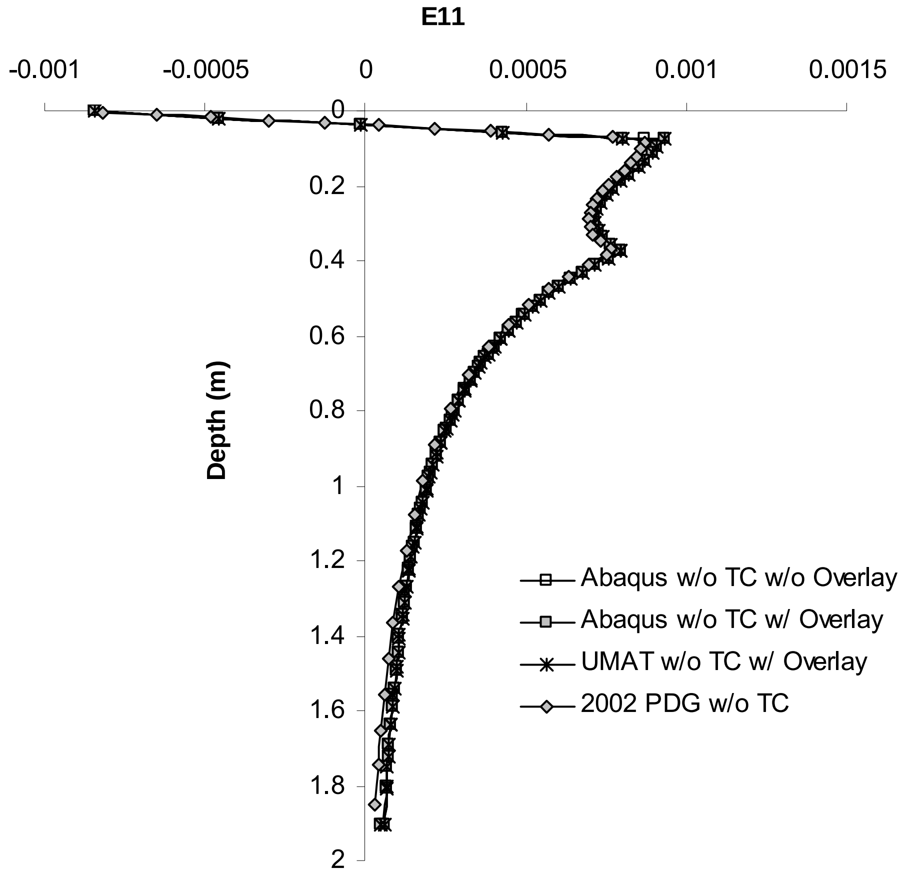

Figure 4.2.22 E11 vs. Depth, isotropic linear elastic without tension cutoff analyses, with and without overlay elements

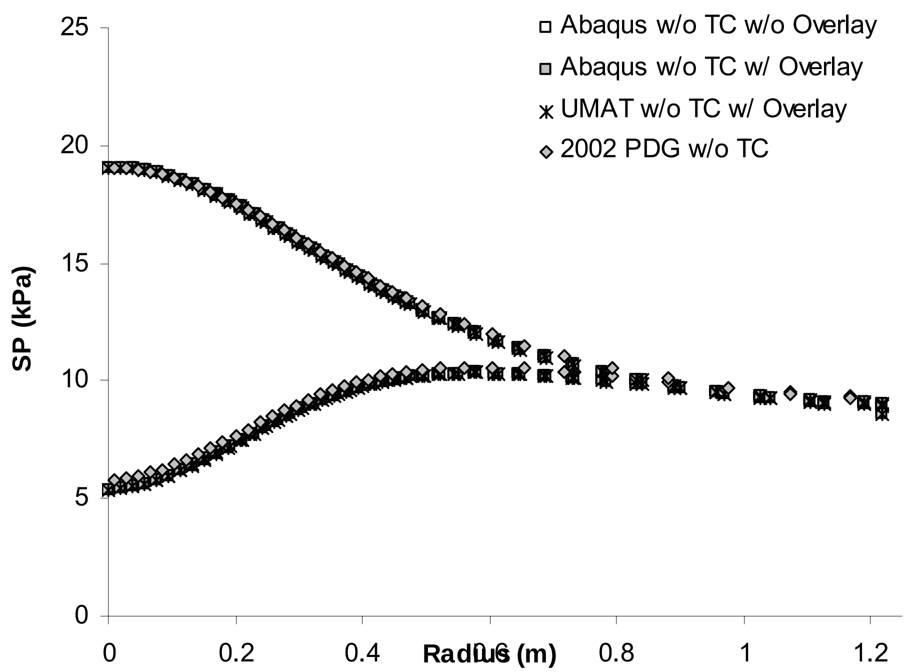

Figure 4.2.23 SP vs. Radius, isotropic linear elastic without tension cutoff analyses, with and without overlay elements

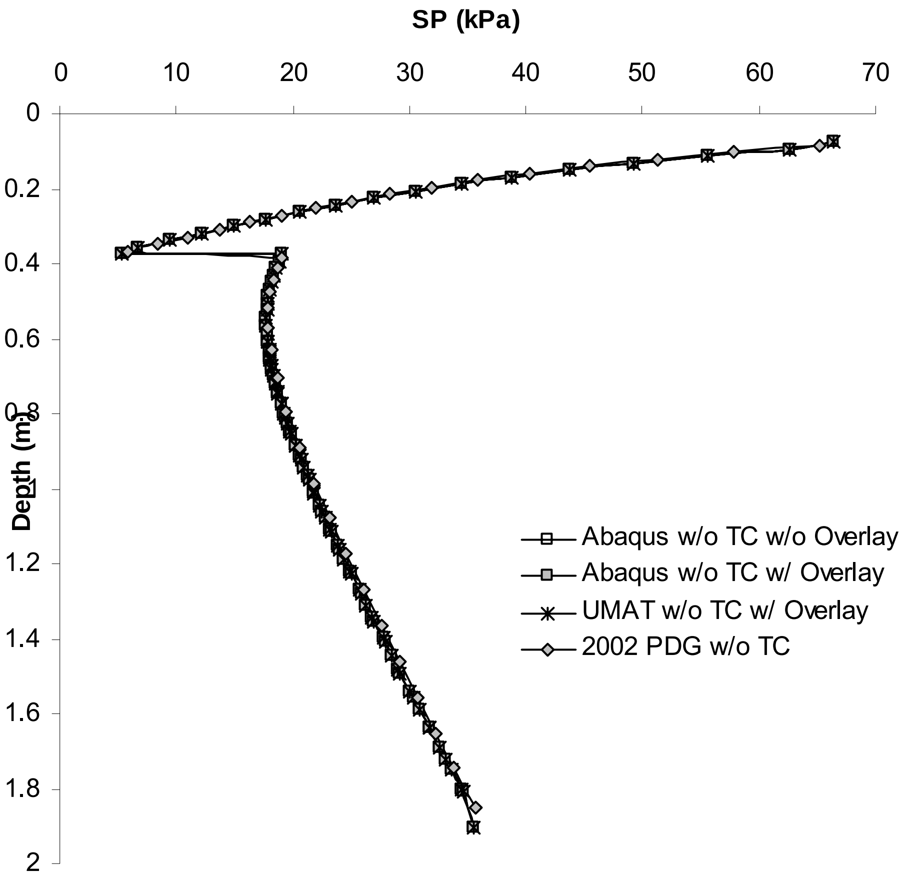

Figure 4.2.24 SP vs. Depth, isotropic linear elastic without tension cutoff analyses, with and without overlay elements

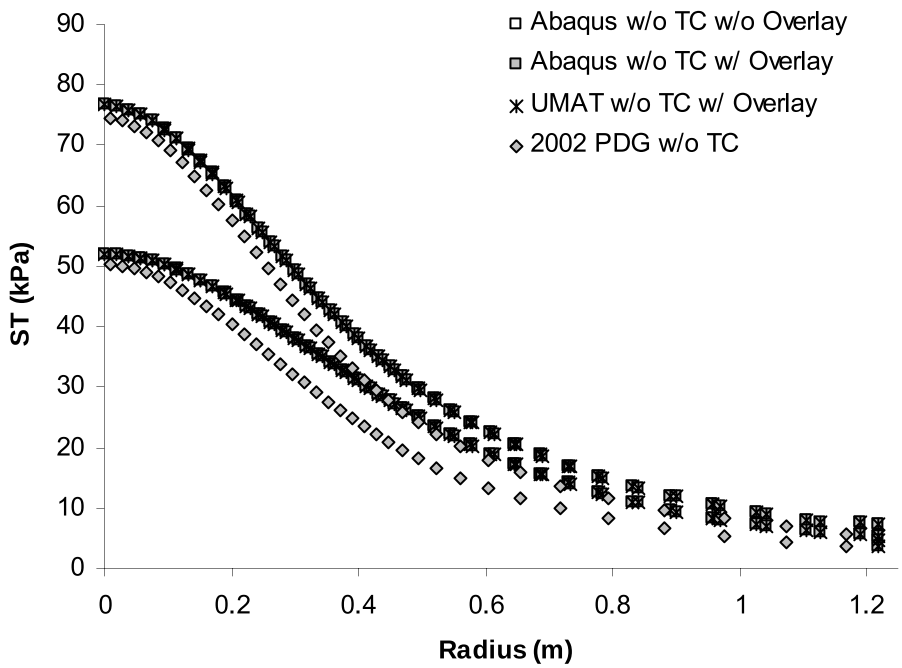

Figure 4.2.25 ST vs. Radius, isotropic linear elastic without tension cutoff analyses, with and without overlay elements

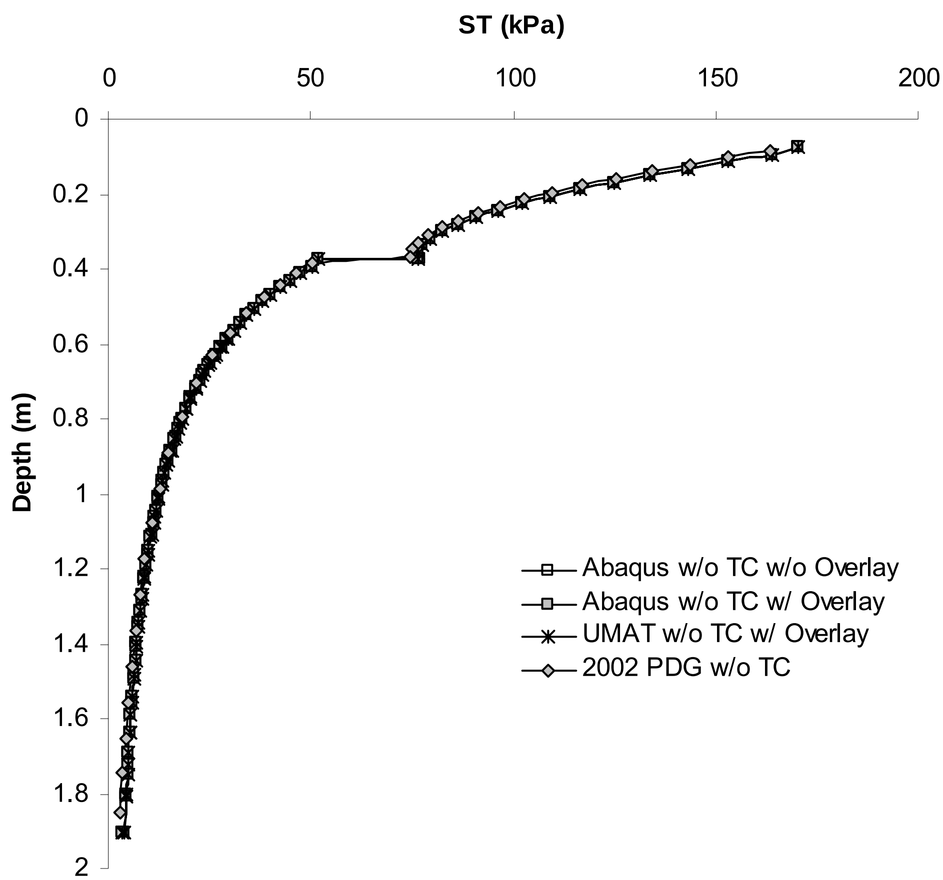

Figure 4.2.26 ST vs. Depth, isotropic linear elastic without tension cutoff analyses, with and without overlay elements

The majority of the results indicate excellent correspondence between the Abaqus analyses and the analysis using the NCHRP 1-37A Design Guide. Several figures indicate discrepancies and will be elaborated on below. Figure 4.2.15 indicates a shift in vertical displacement between the Abaqus and NCHRP 1-37A Design Guide results. Since Figure 4.2.17 indicates close agreement in vertical strain, the disagreement in Figure 4.2.15 may be due to a difference in the way strains are calculated and accumulated in the subgrade bottom infinite elements. Shifting the NCHRP 1-37A Design Guide vertical displacement results by the difference between the Abaqus and NCHRP 1-37A Design Guide results at a level corresponding to the bottom of the finite elements results in much closer, but not perfect, agreement, as shown in Figure 4.2.16.

To verify that the Abaqus models described above produced reasonable solutions, additional sets of models were run and compared to a closed-form solution from the theory of elasticity.

The first set involved assigning all layers a constant elastic modulus of 20,500 kPa and a Poisson's ratio of 0.25. A solution for a homogeneous isotropic linear elastic half-space was used to compare to the results from Abaqus. Figure 4.2.27 shows the vertical displacement versus depth under the centerline of the load for the Abaqus and exact solution where excellent correspondence is seen. A second set of models was created with the properties given in Table 4.2.6. These models corresponded to a 3-layer elastic system where an exact solution was available. The Abaqus model gave a surface displacement of 2.82 mm. Double interpolation of tabular numbers was required for the exact solution, which produced a surface displacement of 2.92 mm. The 3.5 % error between the two solutions is most likely due to the interpolation needed for the exact solution. These results indicate that the Abaqus model properly calculates and accumulates strain in the bottom subgrade infinite element region.

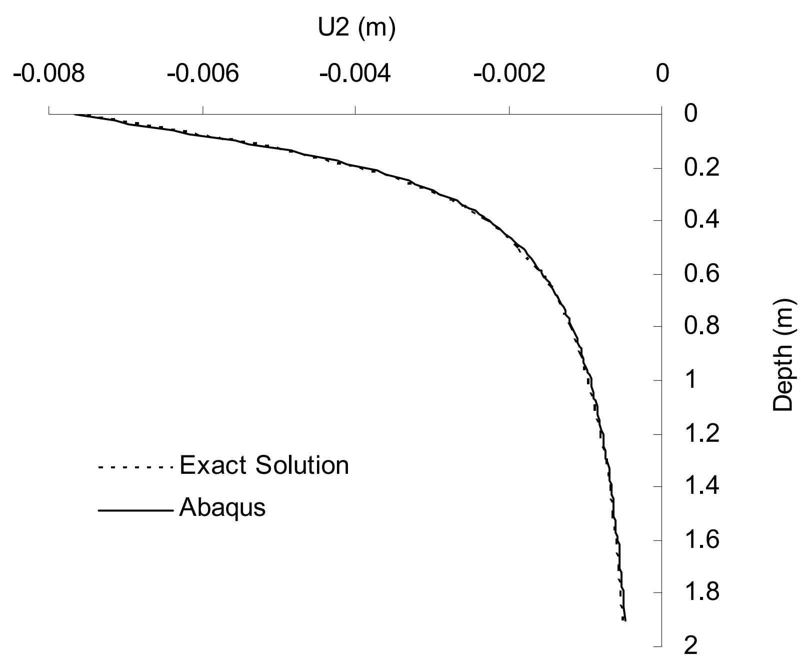

Figure 4.2.27 Comparison of Abaqus and exact solution for a homogeneous isotropic linear elastic half-space

Table 4.2.6 Material layer properties for Abaqus and exact solution for a 3-layer elastic system

Layer	Unit Weight (kN/m^3)	Elastic Modulus (kPa)	Poisson's Ratio
Asphalt Concrete	23	820,000	0.35
Base (finite)	20	41,000	0.35
Base (infinite)	20	41,000	0.35
Subgrade (finite)	18	20,500	0.35
Subgrade (infinite-side)	18	20,500	0.35
Subgrade (infinite-bottom)	18	20,500	0.35

Small and insignificant differences are seen between horizontal stress (S11) in Figure 4.2.18 for values within the base layer (the two curves correspond to values in the base and values in the subgrade). Similarly, small and insignificant differences are seen in values of E11 in the base and subgrade layers (Figures 4.2.21 and 4.2.22). Values of SP correspond well, while values of ST differ slightly. These differences may be due to the use of values from the design guide model that are taken from element centroids closest to the line of interest.

Overall, very good agreement is seen between the Abaqus analyses and those of the NCHRP 1-37A Design Guide indicating that the procedure established in Section 4.2.1 for pavement response models produces nearly identical responses as the NCHRP 1-37A Design Guide and that the inclusion of overlay elements has no effect on response.

The second series of response models was created to evaluate the operation of the tension cutoff feature. Three models were created that used or simulated isotropic linear elastic properties with tension cutoff for the base and subgrade layers. The first model used the standard isotropic linear elastic model in Abaqus but with a *No Tension feature added. This feature operates like the tension cutoff feature in the UMAT described in Section 4.1.4 in that the principal stresses are calculated and those experiencing tension are set equal to zero. Overlay elements were included in this model to provide for numerical stability. The properties for this model are the same as those shown in Table 4.2.3 only with the *No Tension feature added. The second model used the UMAT described in Section 4.1.4 with properties chosen to simulate isotropic linear elastic behavior with tension cutoff. The properties for this model are identical to those shown in Table 4.2.4 with the exception that the tensile strength for the base and subgrade finite layers was set to a value of 0.01 kPa. The third model used the NCHRP 1-37A Design

Guide model with properties chosen to simulate isotropic linear elastic behavior with tension cutoff. The properties for this model are identical to those shown in Table 4.2.5 with the exception that the tensile strength for the base and subgrade finite layers was set to a value of 0.01 kPa.

Figures 4.2.28 – 4.2.38 show a comparison of results for the three models. Good agreement is seen between the Abaqus model with the *No Tension feature and the Abaqus UMAT model. This is to be expected since the tension cutoff is formulated in basically the same way for the two models. The NCHRP 1-37A Design Guide model is seen to yield responses that are different from the Abaqus models. The results given in Section 4.2.2 for relatively simple examples designed to directly evaluate the tension cutoff feature showed a favorable comparison between the UMAT and NCHRP 1-37A Design Guide models, indicating that the tension cutoff feature had been formulated in a similar fashion. The discrepancies seen in Figures 4.2.28 – 4.2.38 are therefore due to the numerical implementation of the solution, which is an integral component of the architecture of the finite element software. While Abaqus offers certain parameters that can be selected to control the numerical implementation of the solution, very little can be done as a user to change this process.

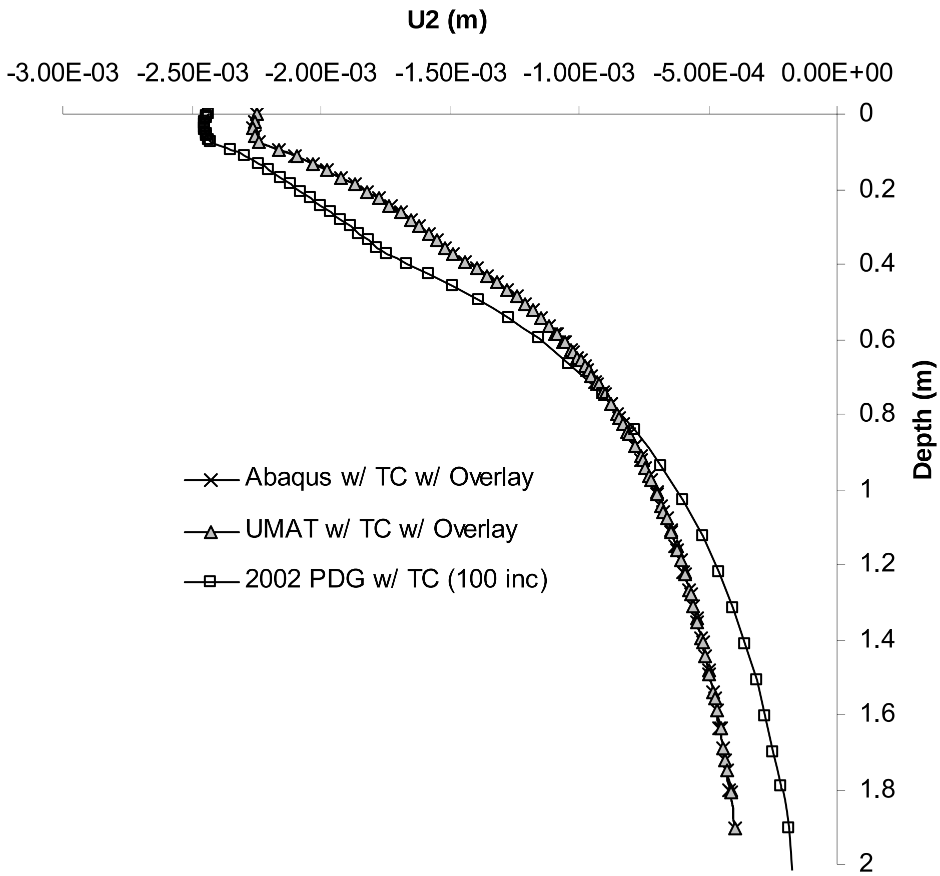

Figure 4.2.28 U2 vs. Depth, isotropic linear elastic with tension cutoff analyses

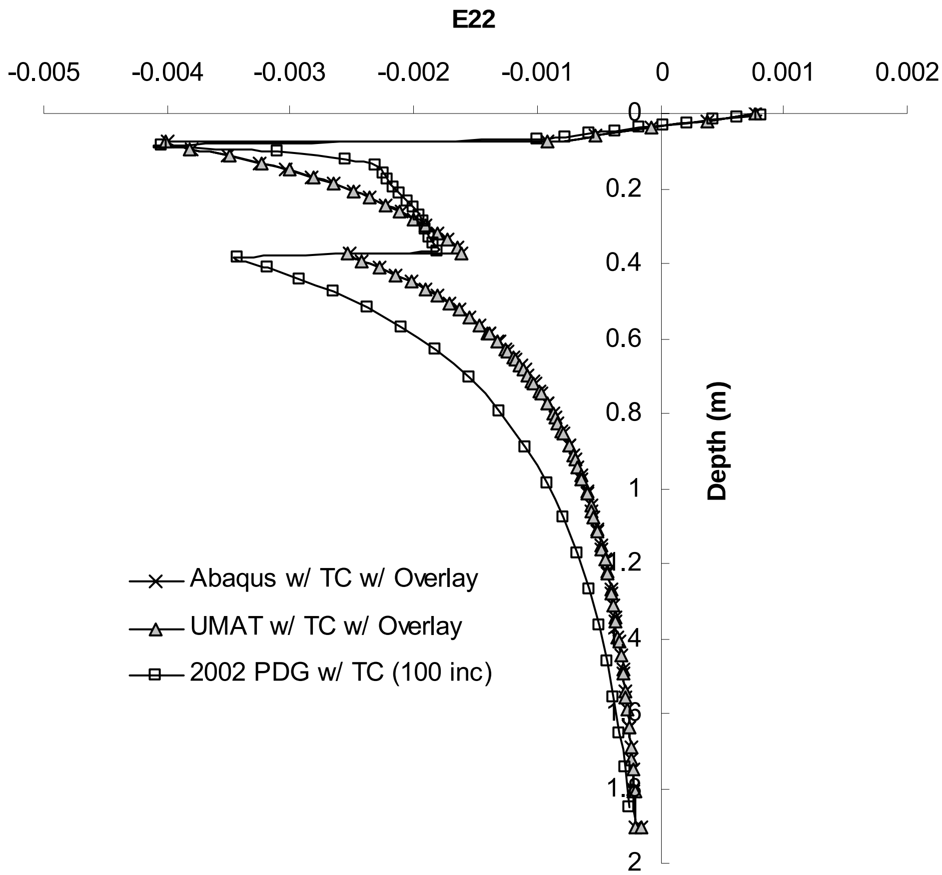

Figure 4.2.29 E22 vs. Depth, isotropic linear elastic with tension cutoff analyses

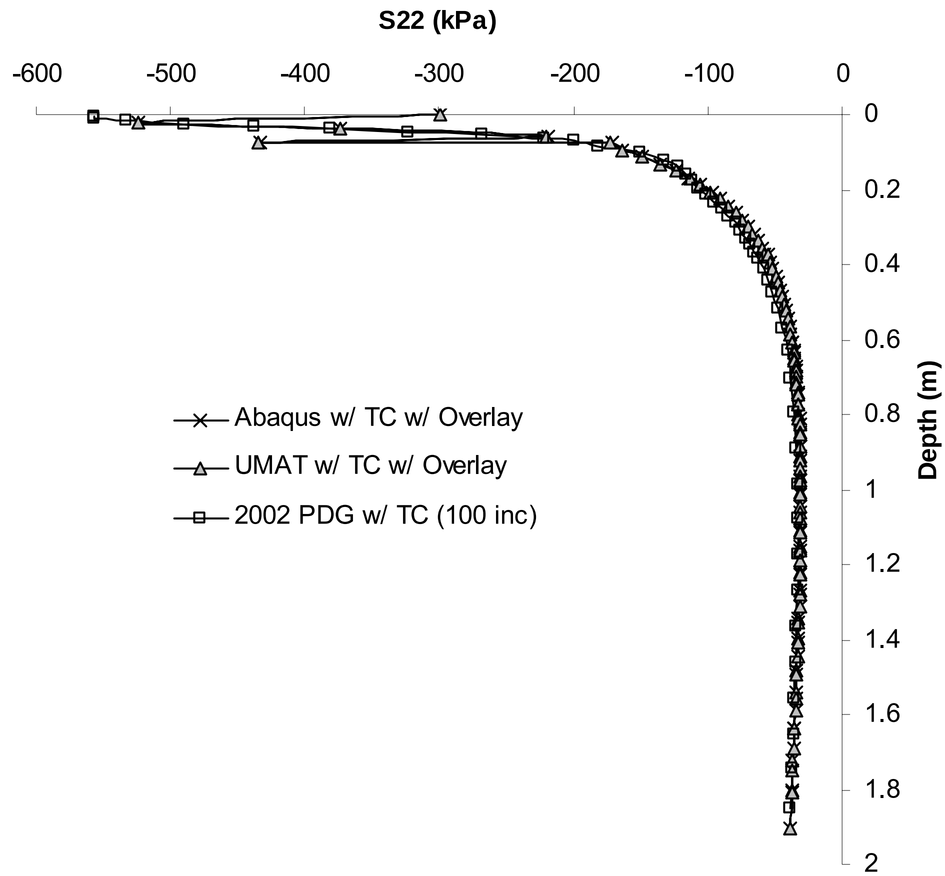

Figure 4.2.30 S22 vs. Depth, isotropic linear elastic with tension cutoff analyses

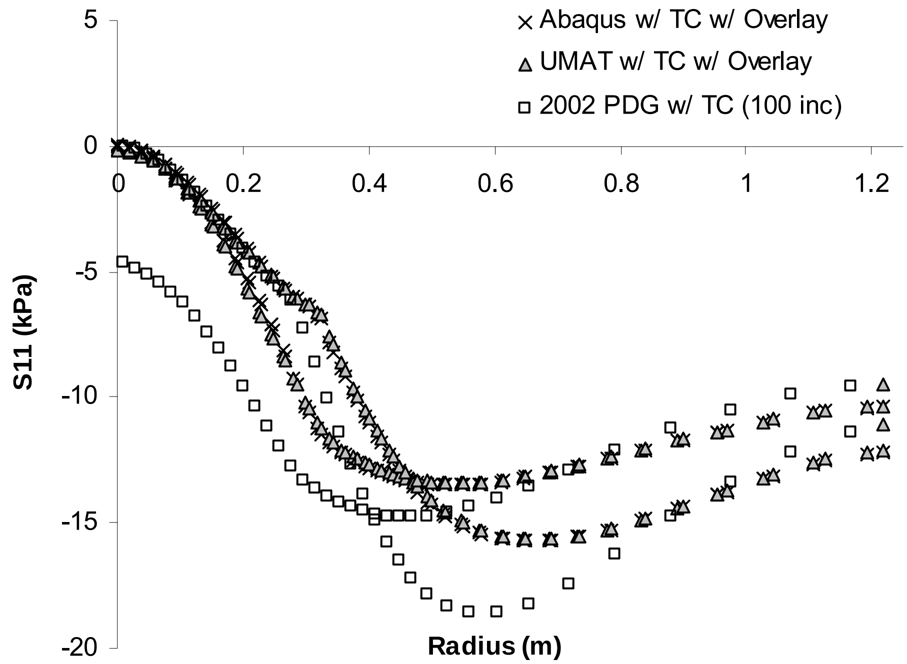

Figure 4.2.31 S11 vs. Radius, isotropic linear elastic with tension cutoff analyses

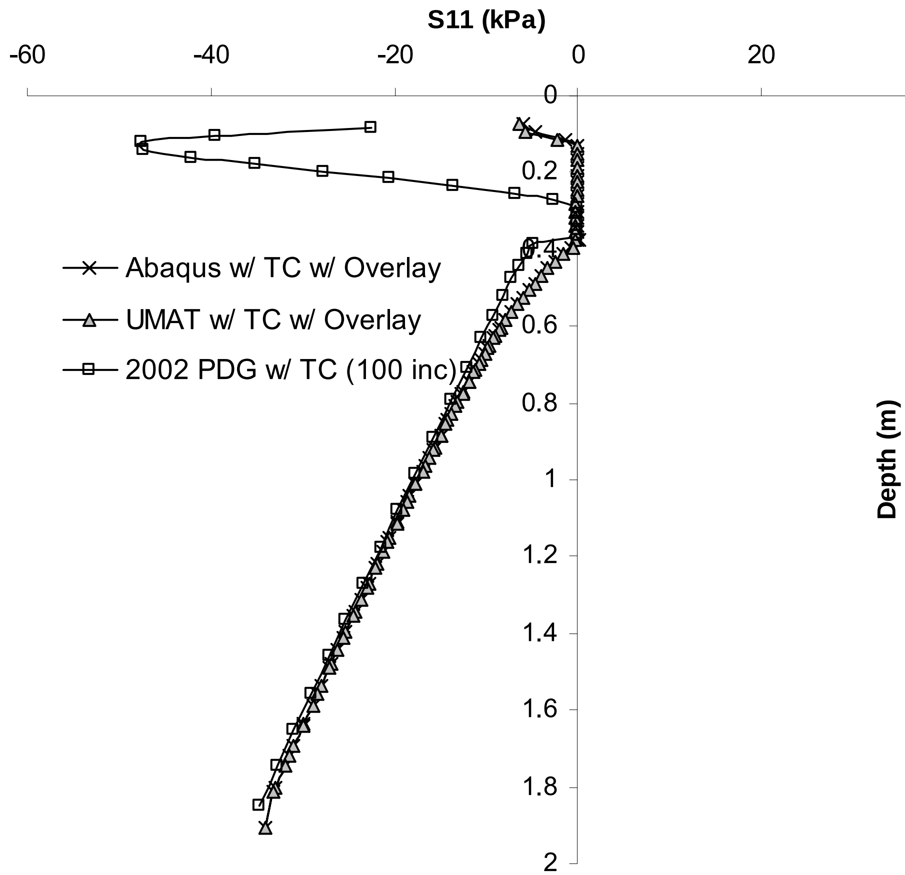

Figure 4.2.32 S11 vs. Depth, isotropic linear elastic with tension cutoff analyses

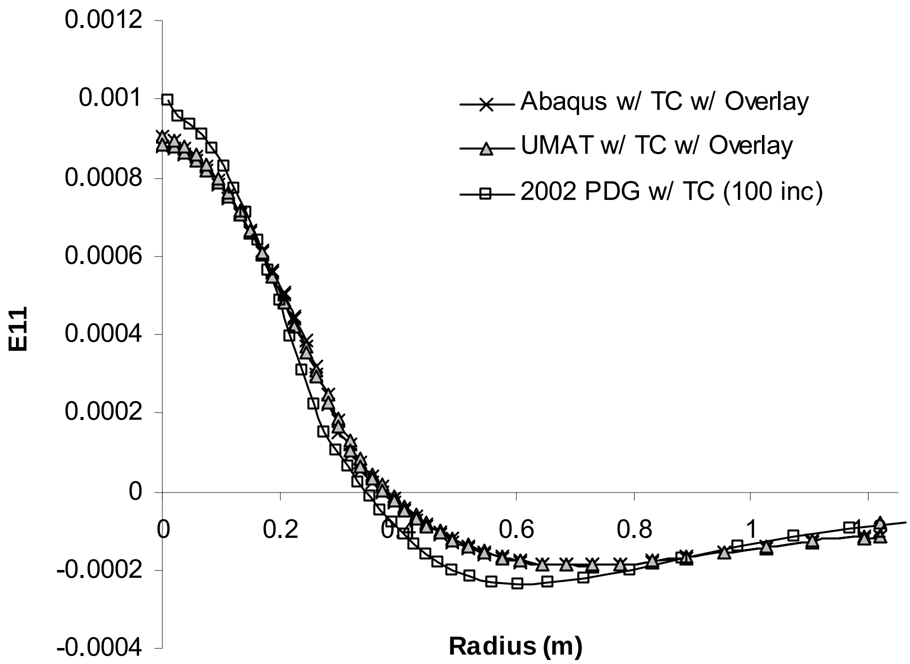

Figure 4.2.33 E11 vs. Radius, isotropic linear elastic with tension cutoff analyses

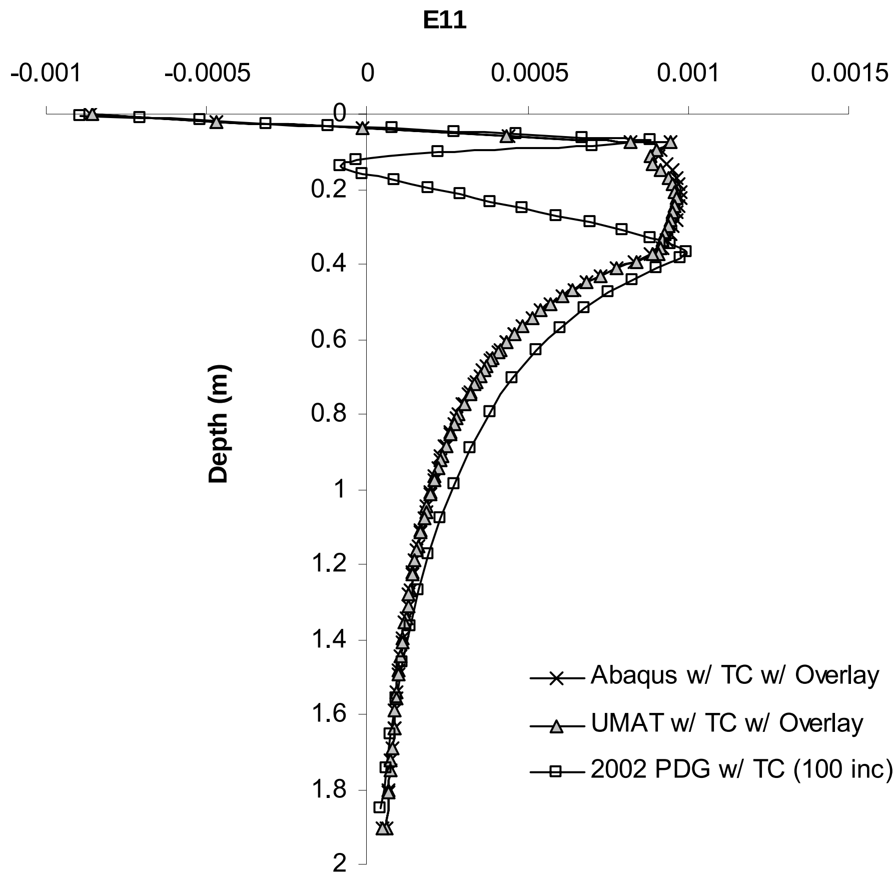

Figure 4.2.34 E11 vs. Depth, isotropic linear elastic with tension cutoff analyses

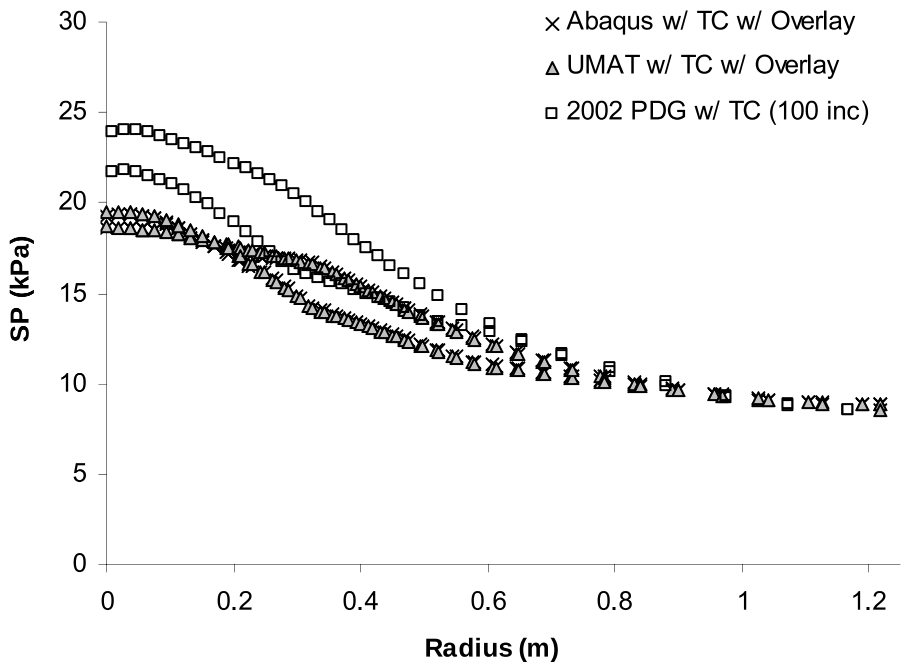

Figure 4.2.35 SP vs. Radius, isotropic linear elastic with tension cutoff analyses

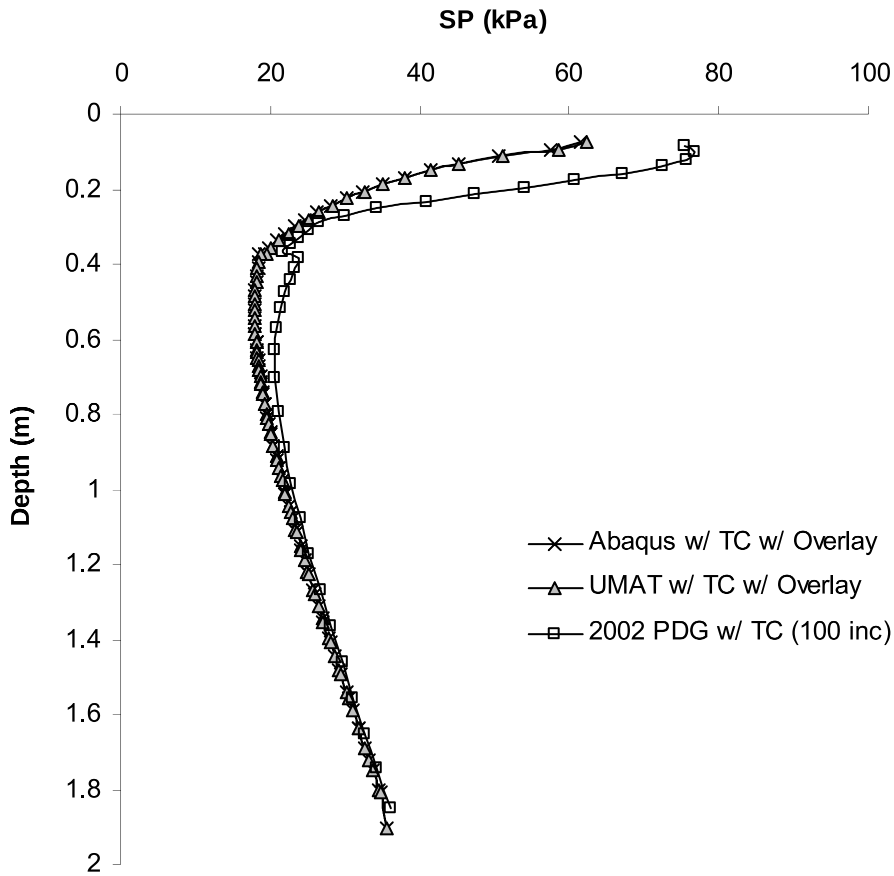

Figure 4.2.36 SP vs. Depth, isotropic linear elastic with tension cutoff analyses

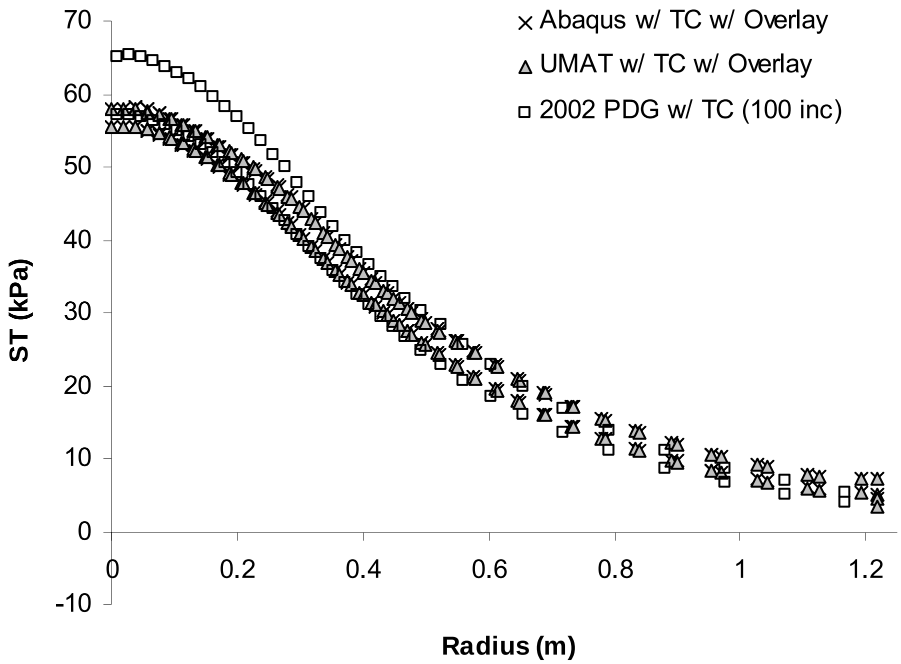

Figure 4.2.37 ST vs. Radius, isotropic linear elastic with tension cutoff analyses

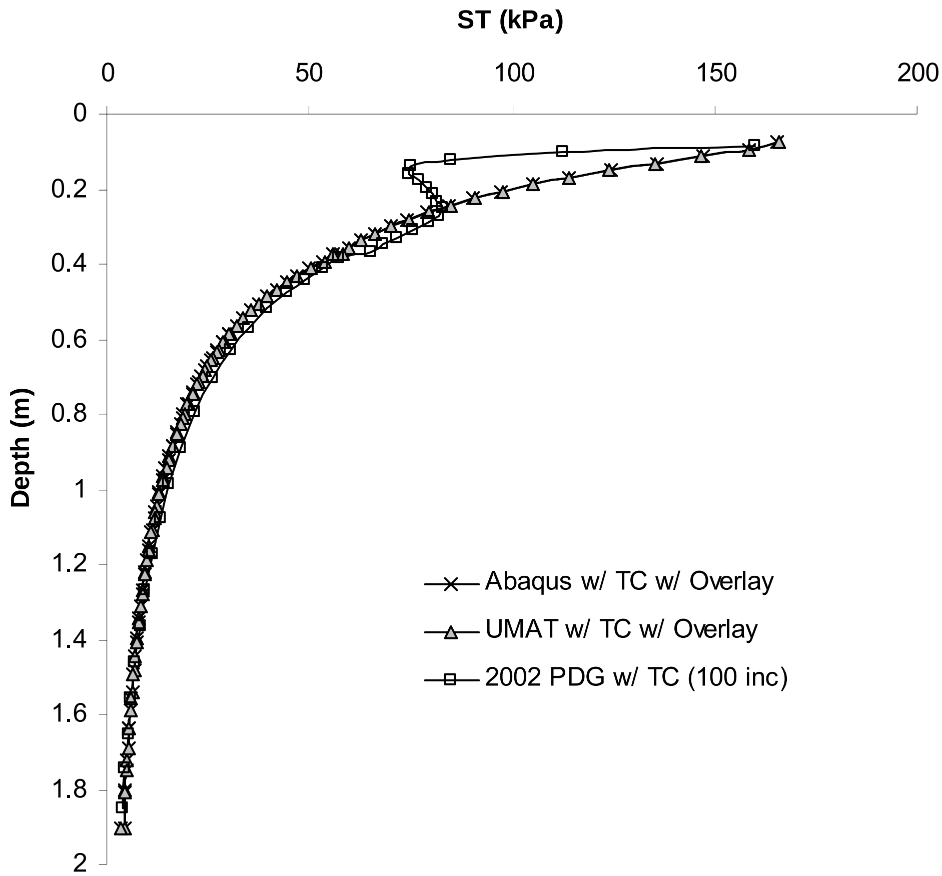

Figure 4.2.38 ST vs. Depth, isotropic linear elastic with tension cutoff analyses

The final analysis performed consisted of an Abaqus model with the UMAT described in Section 4.1.4 having the properties given in Table 4.2.7. Non linear properties were activated for the both the base and subgrade layers and correspond to those properties determined for the MSU aggregate and MSU CS subgrade. Results from this analysis are given in Figures 4.2.39 – 4.2.49 and are provided as a check on the reasonableness of the response parameters.

Table 4.2.7 Material layer properties for Abaqus model with isotropic non linear elastic with tension cutoff model

Layer	Unit Weight (kN/m^3)	Poisson's Ratio, ν	Elastic Modulus (kPa)				
Asphalt Concrete	23	0.35	2,500,000				
Base (infinite)	20	0.25	16,320				
Subgrade (infinite-side)	18	0.25	12,940				
Subgrade (infinite-bottom)	18	0.25	16,118				
				g_1^P	k_1^P	τ_1	
Base (overlay)	0	0.25	16,320	1.0	1.0	0.01	
Subgrade (overlay)	0	0.25	12,940	1.0	1.0	0.01	
			p_a (kPa)	k_1	k_2	k_3	T_c (kPa)
Base (finite)	20	0.25	101.3	957	0.906	-6.140	0.001
Subgrade(finite)	18	0.25	101.3	139	0.187	-3.281	0.001

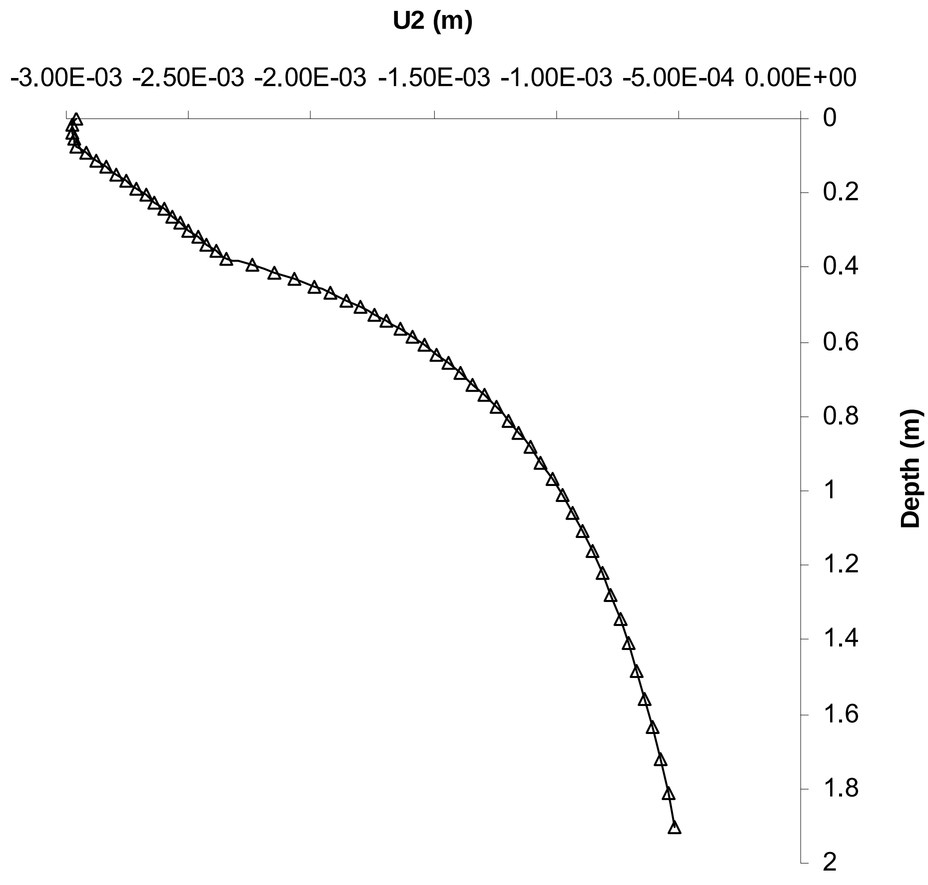

Figure 4.2.39 U2 vs. Depth, isotropic non linear elastic with tension cutoff analyses

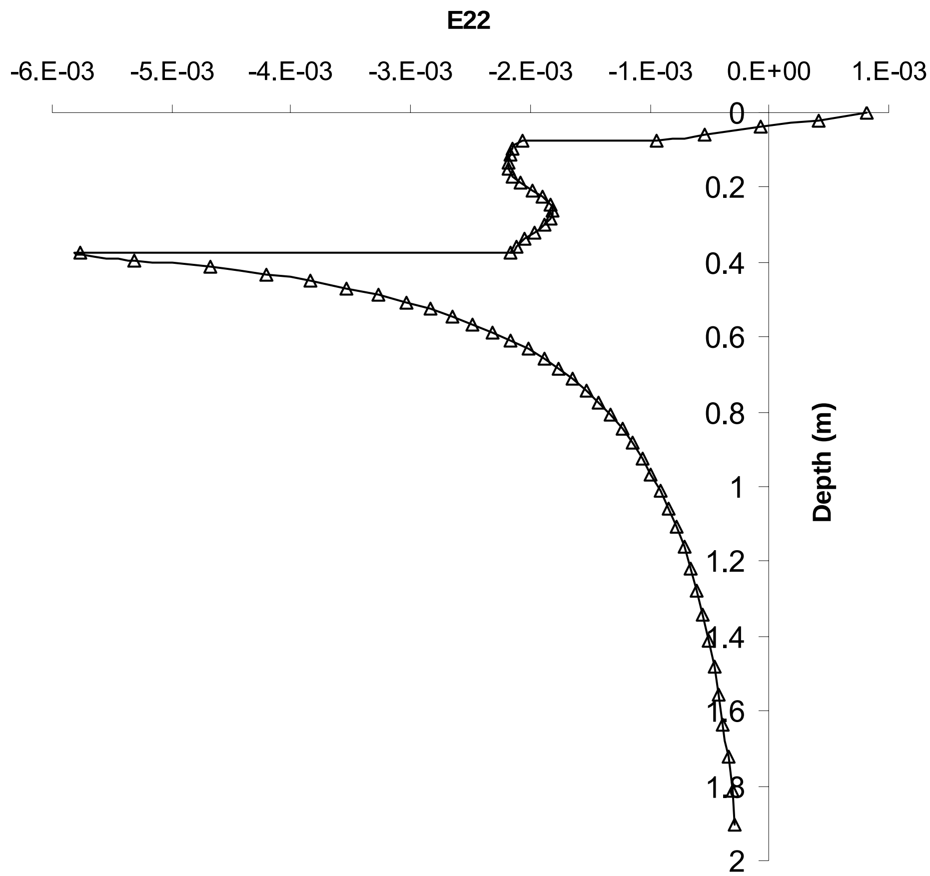

Figure 4.2.40 E22 vs. Depth, isotropic non linear elastic with tension cutoff analyses

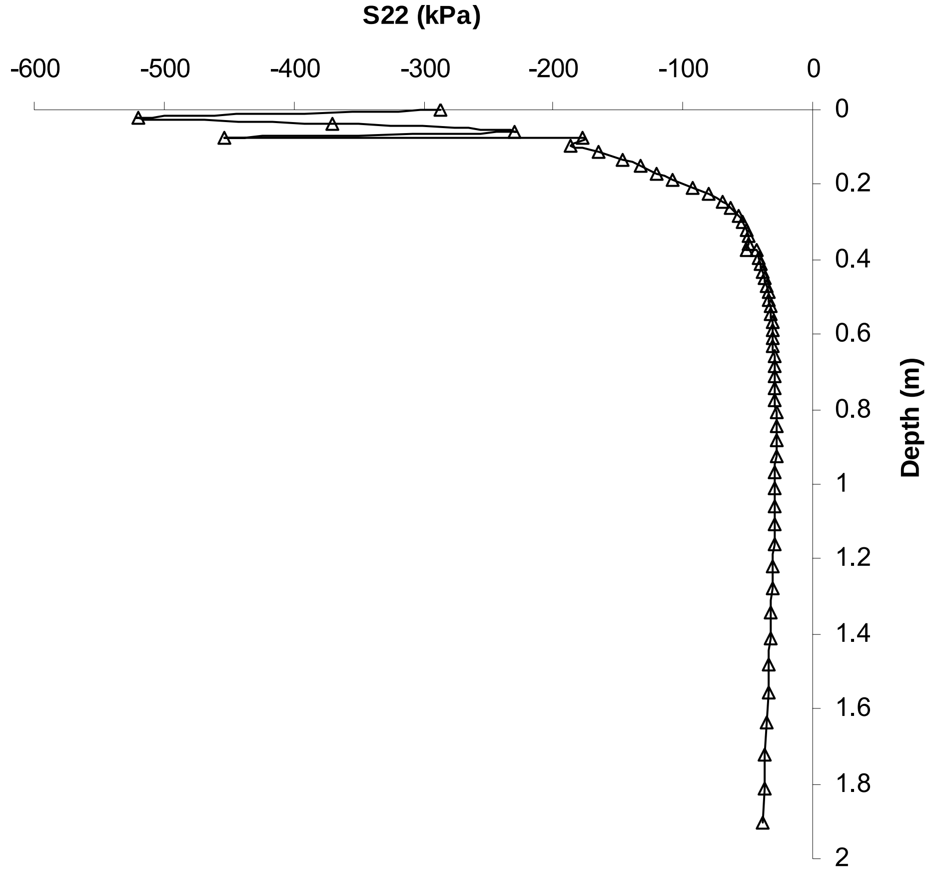

Figure 4.2.41 S22 vs. Depth, isotropic non linear elastic with tension cutoff analyses

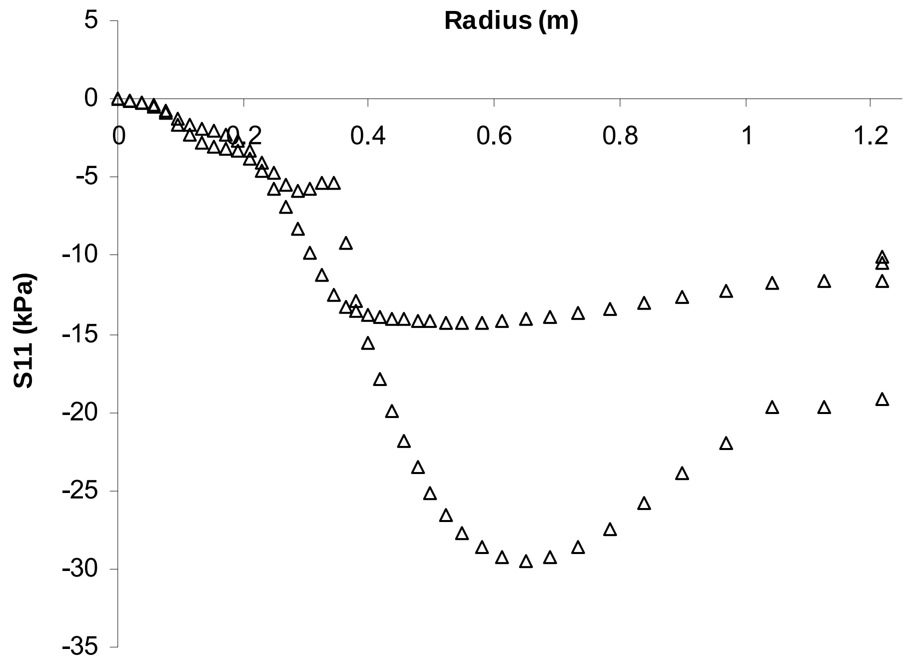

Figure 4.2.42 S11 vs. Radius, isotropic non linear elastic with tension cutoff analyses

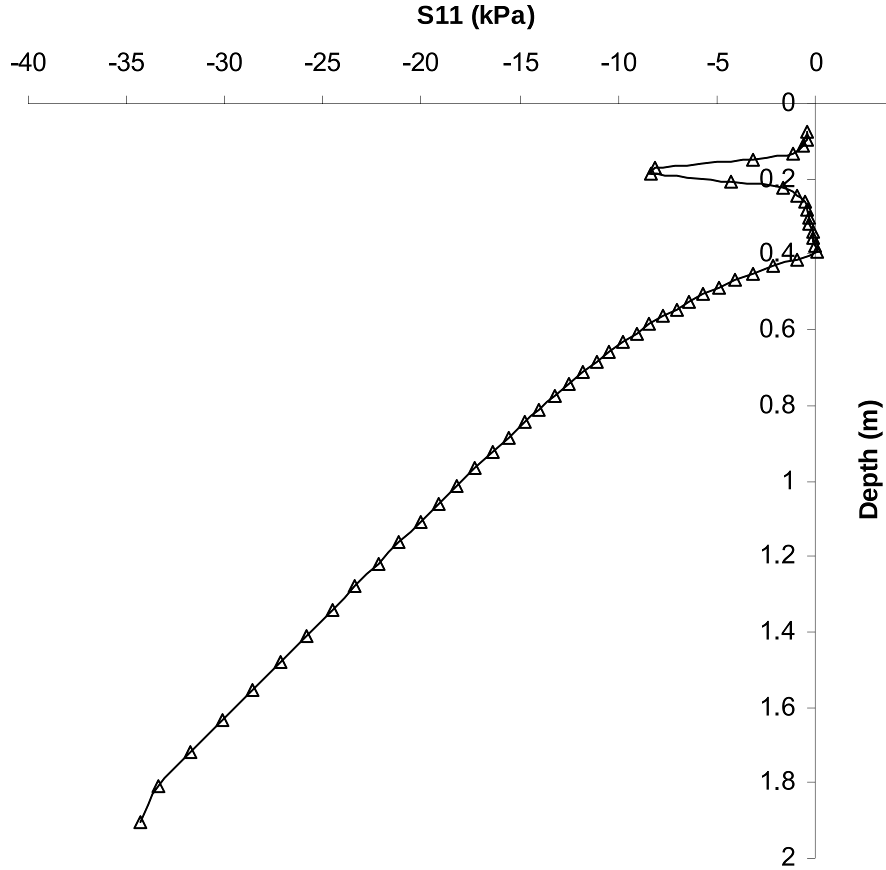

Figure 4.2.43 S11 vs. Depth, isotropic non linear elastic with tension cutoff analyses

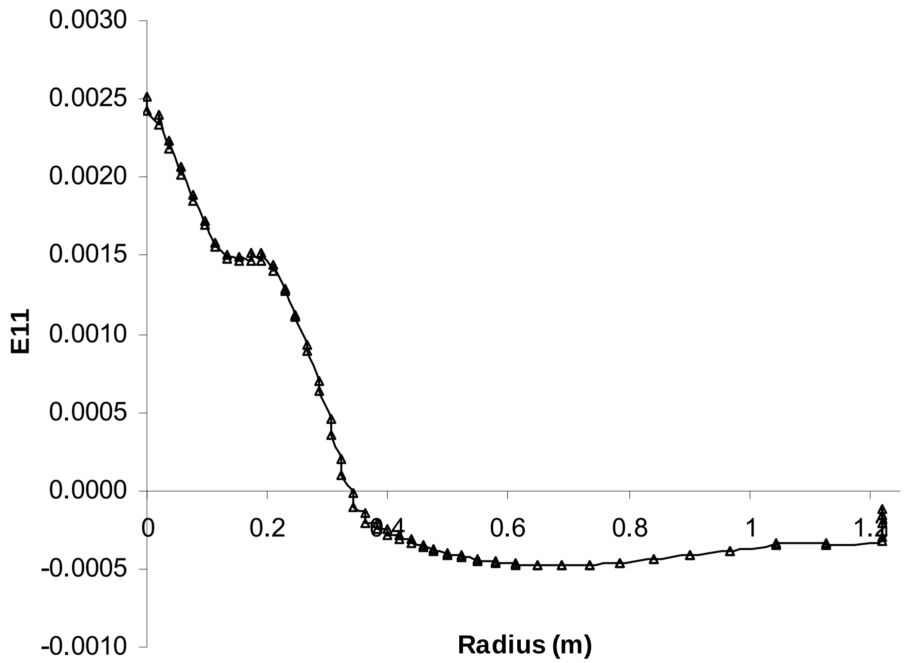

Figure 4.2.44 E11 vs. Radius, isotropic non linear elastic with tension cutoff analyses

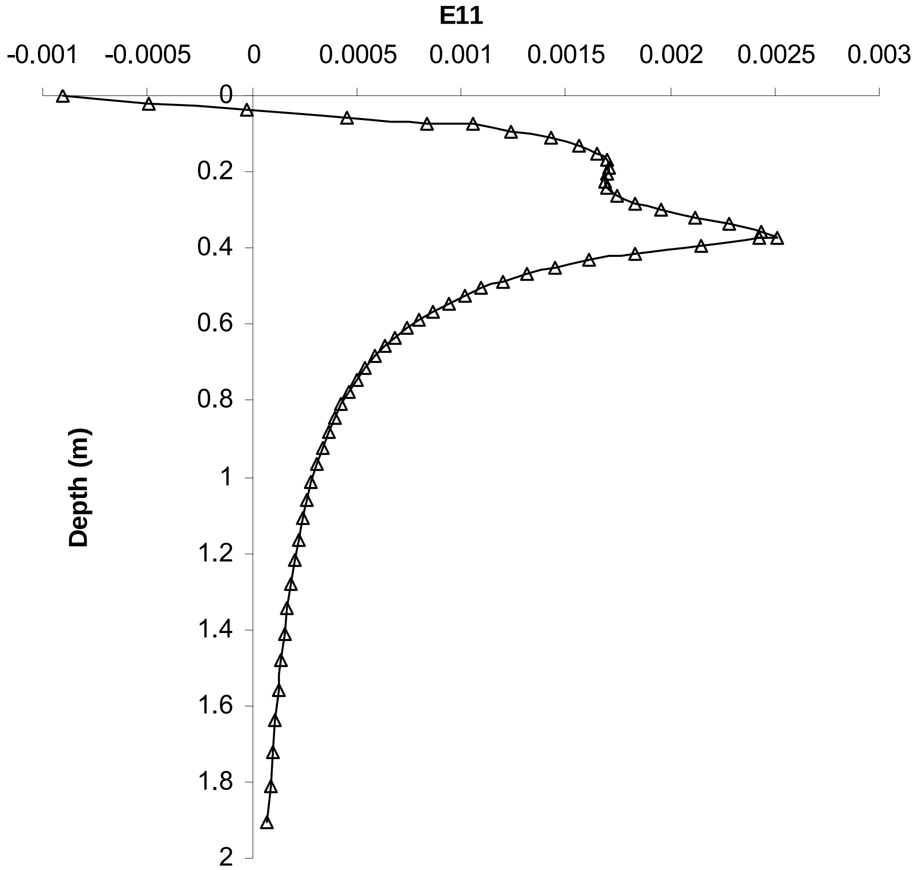

Figure 4.2.45 E11 vs. Depth, isotropic non linear elastic with tension cutoff analyses

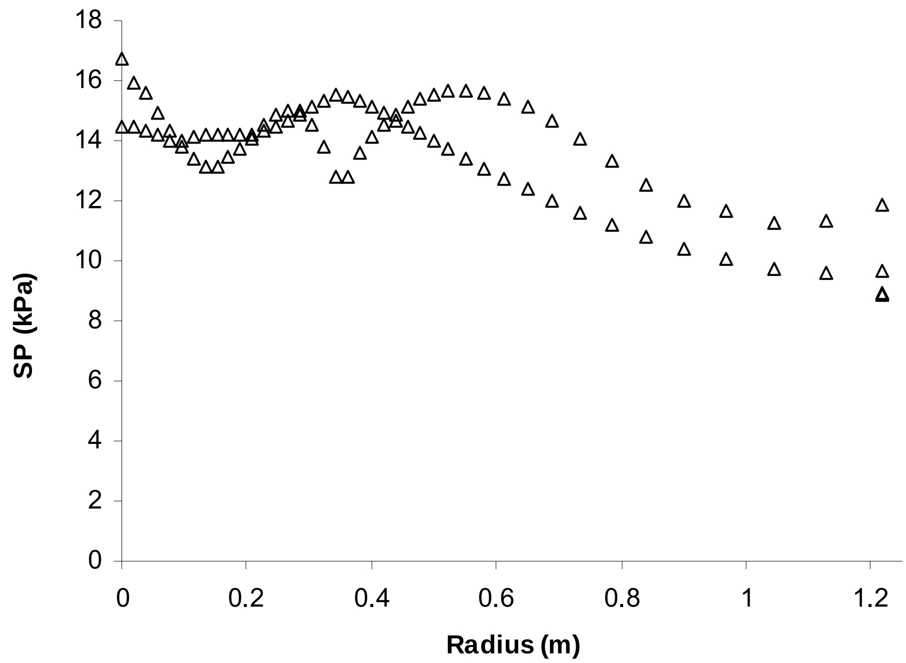

Figure 4.2.46 SP vs. Radius, isotropic non linear elastic with tension cutoff analyses

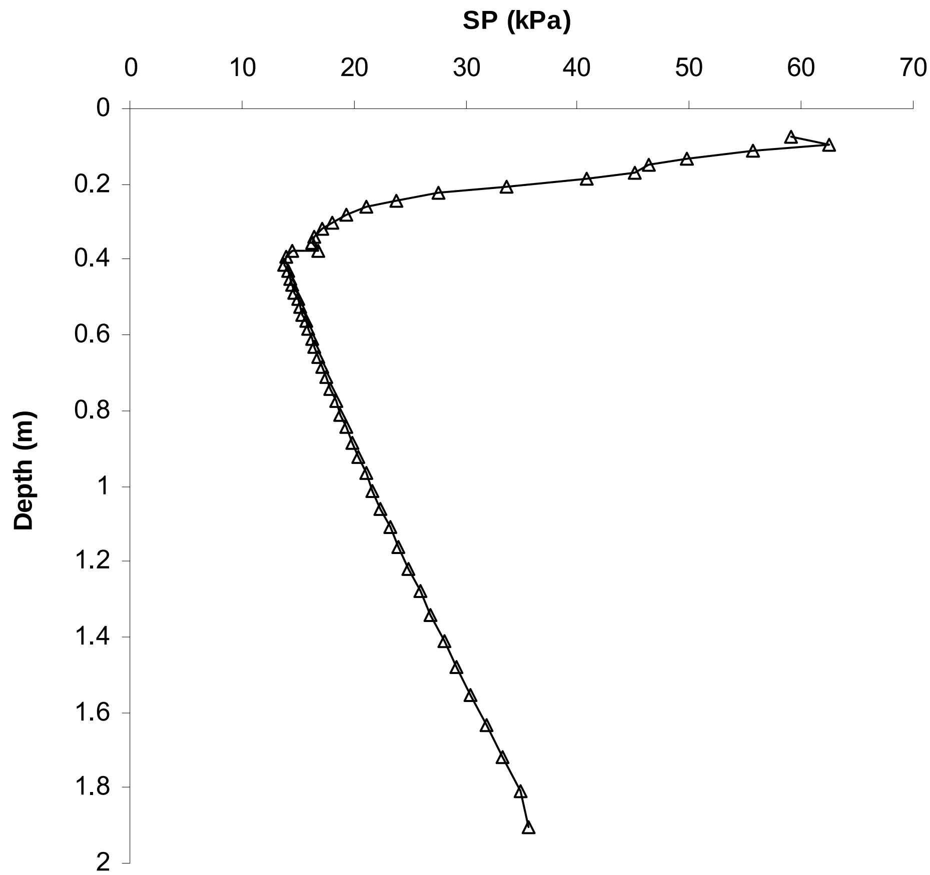

Figure 4.2.47 SP vs. Depth, isotropic non linear elastic with tension cutoff analyses

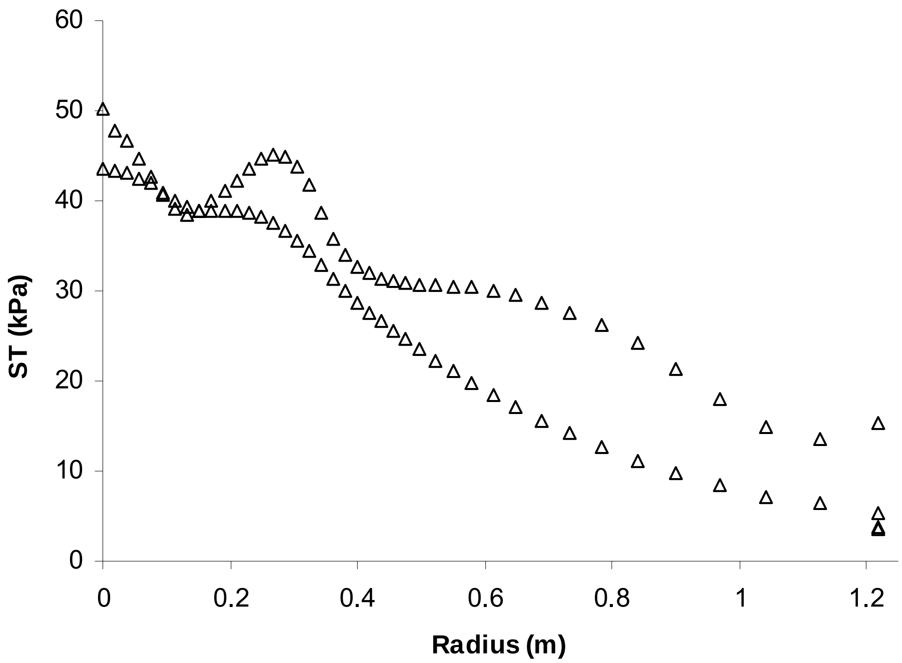

Figure 4.2.48 ST vs. Radius, isotropic non linear elastic with tension cutoff analyses

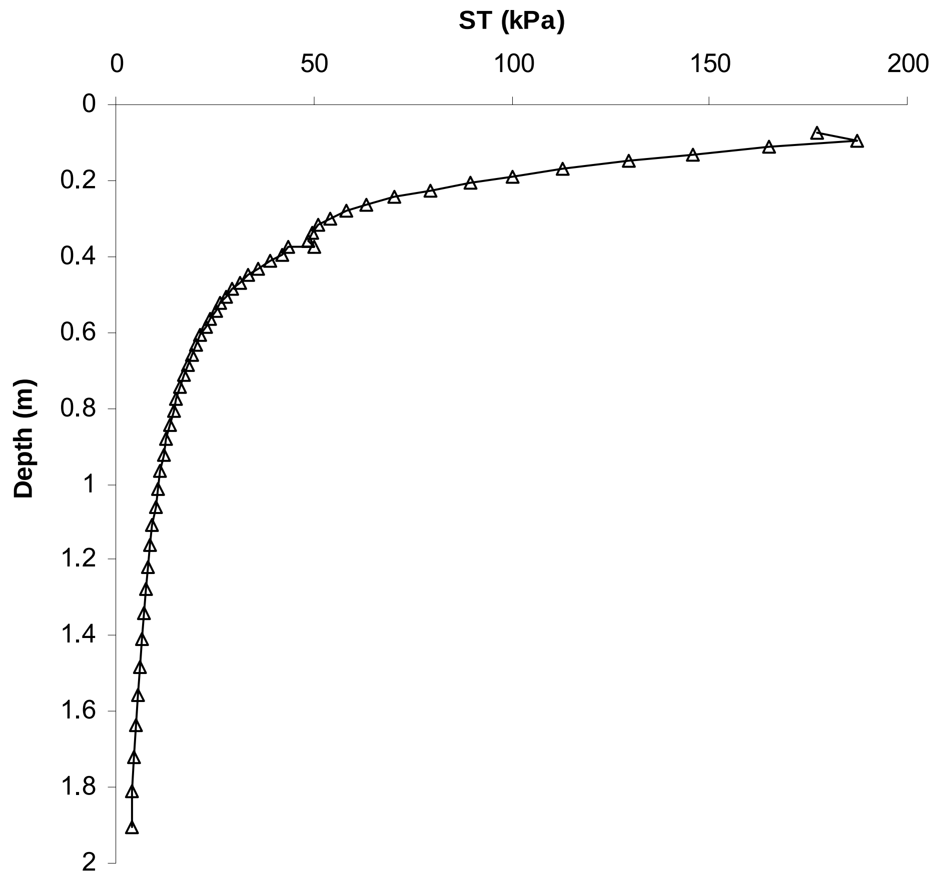

Figure 4.2.49 ST vs. Depth, isotropic non linear elastic with tension cutoff analyses

5.0 REINFORCED PAVEMENT RESPONSE MODELS

The preceding chapters have established material models and basic finite element response model setup procedures necessary to create response models for reinforced pavements. In this chapter, these components are combined together and used with new techniques introduced for modeling reinforced pavements to establish a methodology for mechanistic-empirical modeling of reinforced pavements.

In general, reinforced response models were created by following a conventional approach of directly including elements for the reinforcement sheet and contact surfaces between the reinforcement and surrounding materials. As will be demonstrated in this chapter, set up of models by simply including the reinforcement layer in this manner results in a gross underprediction of benefit from the reinforcement. This indicates that fundamental mechanisms and processes involved in reinforced pavements are missing from a simple static, single load cycle analysis involving only the insertion of the reinforcement sheet in a response model. In particular, processes involving interaction of the reinforcement with surrounding pavement materials during construction and compaction of the base aggregate layer and during repeated loading by vehicular traffic is absent from a simple analysis of the reinforced pavement. These processes tend to lead towards the development of lateral confinement of the base aggregate layer that is otherwise absent or greatly diminished in pavements without reinforcement. This led to the creation of response model modules that simulate certain construction and traffic loading effects that the reinforcement has on the pavement system. The basic reinforced response model set up and modules are described in this section. These modules include a response model describing effects during compaction and three response models used in succession and in an iterative manner to describe the effects of reinforcement during traffic loading. Figure 5.0.1 provides a flow chart of these response models. The Compaction and Traffic I response model modules are analyzed once for a given pavement cross section. The Traffic II and III models are analyzed a number of times to describe pavement response during different periods of the pavement life as permanent strain is developed in the reinforcement.

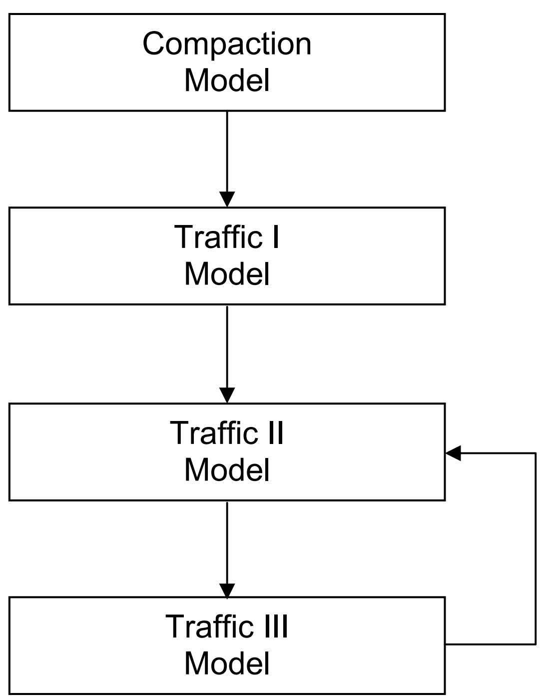

Figure 5.0.1 Flow chart of response model modules

5.1 Reinforced Response Model Setup

Reinforcement was added to the response model described in Section 4.1 by including a layer consisting of a thin sheet composed of 2-node membrane elements. Membrane elements have the ability to carry loads in tension but have no bending stiffness or ability to carry load in compression. An isotropic linear elastic model having input parameters of elastic modulus and Poisson's ratio was used for the reinforcement material, where these parameters were determined in terms of other reinforcement properties as described in Section 3.5. The reinforcement was meshed according to the same meshing rules described in Section 4.1.1 for the lateral or radial direction of the model. The reinforcement sheet ended at the end of the finite element region (see Figure 4.1.1). Degree of freedom constraints were place on the ending node of the reinforcement sheet. The vertical and horizontal displacement degrees of freedom were constrained (tied) to be equivalent to the corresponding nodes in the layer immediately above and below this node.

The upper and lower surfaces of the reinforcement were set up to be contact surfaces where the Coulomb friction model described in Section 3.6.3 was assigned to each surface. For each surface, pertinent material properties consisted of values of coefficient of friction (μ) and elastic slip (E_{slip}) (see Figure 3.6.10). Specific details concerning the assignment of these values to each of the two surfaces is provided in the following sections as specific steps taken to model the reinforced pavement are explained.

An example analysis was performed with a reinforced model set up according to the steps described above and compared to an identical model without reinforcement. The model was set up to match the geometry and properties of materials used in the construction of one of the MSU box test sections (CS11), which is described in Section 6.1.1. This test section consisted of 76.2 mm of asphalt concrete, 300 mm of base aggregate and 1.045 m of a soft clay subgrade. Reinforcement product B (see Table 3.5.1) was used in this test section and placed at the bottom of the base. Infinite elements were not required for this model since the extent of the pavement layers was confined by the box in which they were constructed. The properties used for the models are listed in Table 5.1.1. No relative movement was allowed for the interface between the reinforcement and the subgrade and was specified by "Rough Contact". The field calibration constants for the permanent deformation equations were determined from steps described in Section 6.1.2.

Table 5.1.1 Material layer properties for CS11 Test Section

Layer	Unit Weight (kN/m^3)	Poisson's Ratio, ν	Elastic Modulus (MPa)				
Asphalt Concrete	23.4	0.35	5356				
Reinforcement	---	0.25	426				
				g_1^P	k_1^P	τ_1	
Base (overlay)	0	0.25	17.343	1.0	1.0	0.01	
Subgrade (overlay)	0	0.25	12.377	1.0	1.0	0.01	
			p_a (kPa)	k_1	k_2	k_3	T_c (kPa)
Base (finite)	21.8	0.25	101.3	957	0.906	-0.614	0.001
Subgrade (finite)	16.5	0.25	101.3	139	0.187	-3.281	0.001
Interface Contact Properties							
						μ	E_{slip} (m)
Reinforcement-Aggregate Interface						1.473	0.0001453
Reinforcement-Subgrade Interface						Rough Contact	
Asphalt Concrete Permanent Deformation Properties							
	k_1	k_2	k_3	β_1		β_2	β_3
Asphalt Concrete	-3.3426	1.734	0.4392	0.15		0.892	0.275
Unbound Layer Permanent Deformation Properties							
			$\varepsilon_0/\varepsilon_r$	ρ	β	ξ_1	ξ_2
Base			88.7	7440	0.127	0.4570	2.359
Subgrade			4690	4.13E26	0.0361	0.8552	0.9983

Figure 5.1.1 shows predictions of permanent surface deformation for the unreinforced and reinforced models. These predictions were made using the permanent deformation models for asphalt concrete, unbound aggregate and subgrade described in Sections 3.1.2 and 3.2.2. The reinforced model shows only a modest (8.4 %) increase in the number of traffic passes carried at a surface deformation of 25 mm (53,850 vs. 58,400 traffic passes). For this test section with this particular reinforcement product, the reinforced test section was seen to carry 17 times the number of load passes necessary to reach 25 mm of surface deformation as compared to a similar unreinforced test section. These results indicate that fundamental mechanisms and processes involved in reinforced pavements are missing from a simple static, single load cycle analysis involving only the insertion of the reinforcement sheet in a response model as detailed above. In particular, processes involving interaction of the reinforcement with surrounding pavement materials during construction and compaction of the base aggregate layer and during repeated loading by vehicular traffic is absent from the simple analysis described in this section. The

following sections develop response modeling modules that are used to account for these processes.

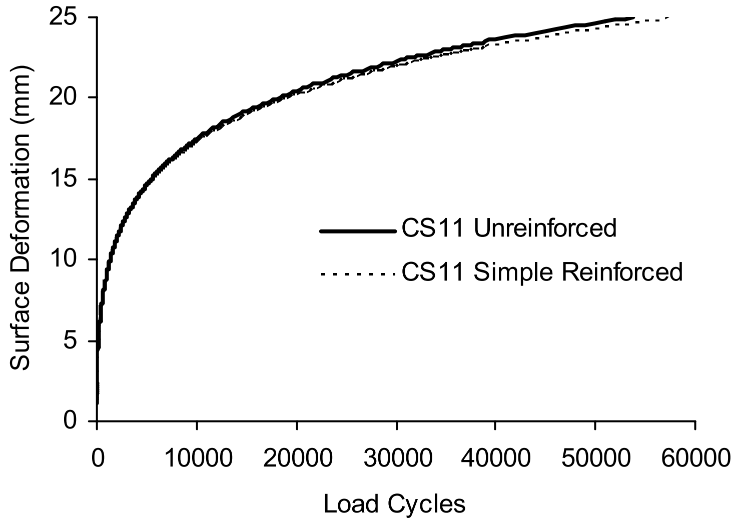

Figure 5.1.1 Surface deformation vs. load cycles for CS11 reinforced model and comparative unreinforced model using simple reinforcement

5.2 Compaction Module

Evidence exists from numerous field studies showing that many geosynthetics offer benefits during the construction of the roadway. While separation and filtration functions of geosynthetics have been widely recognized for roadway construction operations over soft wet soils, reinforcement geosynthetics can provide restraint to aggregate during compaction. A restraining action is most prominent when compacting on subgrades where the yielding occurs in both the vertical and lateral directions. This restraint most likely means that aggregate placement density increases but perhaps more fundamentally means that higher lateral earth pressures can be locked into the compacted aggregate.

From a response modeling perspective, greater lateral stresses at the beginning of an analysis will mean that modulus of the material will be initially higher when non-linear stress-dependent elastic material models are used. In addition, the onset of lateral tensile stress will be delayed, meaning that less deformation will be experienced when using models employing a tension cutoff.

The principal effect of the reinforcement layer during compaction is to limit lateral movement of the aggregate as compaction tends to compress and shove material vertically and laterally. On a local level, restraint is provided by aggregate interacting with and transferring load to the reinforcement. As compaction equipment is worked around on the aggregate layer, aggregate never assumes a predominant direction of motion, meaning that the creation of tensile strains in the reinforcement may be negated and reversed when equipment operates in another location. The effect of this random process is to leave the aggregate with locked in horizontal stresses and the geosynthetic in a relatively strain free state. As such, the process should not be viewed as a reinforcement pretensioning effect, which experimentally has not been shown to be effective. The tensile modulus of the reinforcement is, however, important in this process in that it will contribute to the reduction of lateral movement of the aggregate during each pass of a piece of compaction equipment and will contribute to the build up of locked in horizontal stresses. In addition, the contact properties between the aggregate and the reinforcement are of importance with interfaces showing less shear stiffness leading to lower values of locked in horizontal stresses.

A simple procedure was sought to model this process within the context of a finite element pavement response model. Exact replication of this random and complex process is extremely difficult and unwarranted. The procedure developed involves assigning thermal contractive properties to the reinforcement sheet and creating shrinkage of the material by applying a temperature decrease. These steps provide a means of describing the locked in horizontal stresses in the aggregate due to relative motion between the aggregate and the reinforcement. The procedure developed consists of the following steps:

1. A reinforced response model is developed following the procedures described in Sections 4.1 and 5.1. This response model will have the same geometry and meshing as all subsequently used reinforced response models. If the reinforcement is placed between the base and subgrade layers, the reinforcement-subgrade contact surface is given a large value of E_{slip} (E_{slip} = 1 m) to simulate a nearly frictionless surface. This is done with the expectation that friction developed between the subgrade and reinforcement in the field does little to offer additional resistance against aggregate movement. To minimize the effect of the asphalt concrete layer and to more realistically simulate the construction compaction operation, the modulus of the asphalt concrete is given a small value (1 kPa). This is done to avoid creating an additional model where the asphalt concrete layer is removed.

2. A geostatic initial stress state is established using an earth pressure coefficient of 1 for all layers as was done in models of unreinforced pavements.
3. The reinforcement is assigned a thermal coefficient of expansion (α) equal to 1.0 (ºC)$^{-1}$and an initial temperature of 0.0 ºC.
4. A contractive strain or shrinking is created for a region of the reinforcement extending from the centerline of the model to a radius of 450 mm by applying a decrease in temperature to the reinforcement. The temperature decrease produces a tendency for shrinkage strain in the reinforcement with the maximum value in the unconstrained case being equal to:

$$\varepsilon = \alpha T \tag{5.2.1}$$

5. Horizontal stresses at the element centroid are extracted from the model once the temperature decrease has been applied for a column of elements in the base along the model centerline.
6. These horizontal stresses, along with the geostatic vertical stresses due to material self-weight, are then used as the initial stresses for the entire base layer in a subsequent reinforced response model.

Step 4 creates tensile load in the reinforcement and an increase in lateral stress in the aggregate through shear interaction between the reinforcement and the aggregate. This procedure essentially models in reverse and in a simplified way the complex effect of aggregate being shoved laterally back and forth. The introduction of a tensile strain in the reinforcement through a temperature decrease should be viewed as an artifact of the approach taken to describe the effect of aggregate moving relative to the reinforcement.

To examine the effect of the steps described above on lateral or radial stress in the base aggregate layer, a parametric study was conducted using the model described in Section 4.1. This model had 75 mm of asphalt concrete and 300 mm of base aggregate and used infinite elements at the side and bottom boundaries of the model. The basic properties for the materials used in this model in this parametric study are listed in Table 5.2.1. In the parametric study, the following properties and parameters were varied individually as the other basic properties were held constant. These properties are believed to be the most important in terms of controlling the radial stress developed in the compaction model. The basic properties are underlined in the listing below.

1. Reinforcement Modulus, E (kPa): 5×10^3, 5×10^4, $\underline{5\times10^5}$, 5×10^6, 5×10^{25}
2. Reinforcement-Aggregate Elastic Slip, E_{slip} (m): 1, 0.1, 0.01, 0.001, $\underline{0.0001}$, 1×10^{-10}
3. Base Aggregate Modulus, k_1: $\underline{957}$, 500
4. Temperature Decrease, ΔT: 0.005, $\underline{0.01}$, 0.05 ºC

Table 5.2.1 Material layer properties for parametric study using the Compaction model

Layer	Unit Weight (kN/m^3)	Poisson's Ratio, ν	Elastic Modulus (kPa)				
Asphalt Concrete	23	0.35	1.0				
Base (infinite)	20	0.25	16,320				
Reinforcement	---	0.25	500,000				
Subgrade (infinite-side)	18	0.25	12,940				
Subgrade (infinite-bottom)	18	0.25	16,118				
				g_1^P	k_1^P	τ_1	
Base (overlay)	0	0.25	16,320	1.0	1.0	0.01	
Subgrade (overlay)	0	0.25	12,940	1.0	1.0	0.01	
			p_a (kPa)	k_1	k_2	k_3	T_c (kPa)
Base (finite)	20	0.25	101.3	957	0.906	-0.614	0.001
Subgrade(finite)	18	0.25	101.3	139	0.187	-3.281	0.001
Interface Contact Properties							
						μ	E_{slip} (m)
Reinforcement-Aggregate Interface						1.0	0.0001
Reinforcement-Subgrade Interface						1.0	1.0

Results of radial stress resulting from the compaction model are shown in Figures 5.2.1 – 5.2.4 in terms of a lateral earth pressure coefficient, which is computed as the value of the radial stress divided by the geostatic vertical stress due to material self weight. The earth pressure coefficient can be viewed as a multiplier that would be applied to the geostatic horizontal stress in an unreinforced model with an initial earth pressure coefficient of 1 to arrive at the horizontal stresses in the base resulting from the compaction process with reinforcement present. Figure 5.2.1 shows the influence of the elastic modulus of the reinforcement where it is seen that the earth pressure coefficient with depth increases as reinforcement modulus increases but appears to reach a limit for very high values of reinforcement modulus. The results also show the earth pressure coefficient to increase with depth due to the influence of the reinforcement, which would be expected since interaction of aggregate with the reinforcement during compaction would be most strong for material closest to the reinforcement. The curve for the basic set of properties, shown as a dark line in Figure 5.2.1, appears to yield a reasonable variation of earth pressure coefficient with depth, ranging from just over 1 at the top of the base to approximately 6 at the bottom of the base. Aggregate materials most likely approach a passive earth pressure state during compaction where an earth pressure coefficient ranging from 5 to 10 could be expected for materials having a friction angle ranging from 40 to 55 degrees.

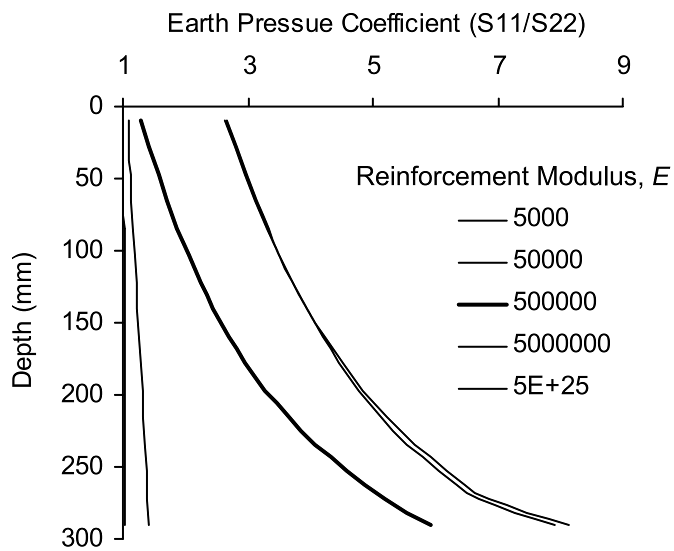

Figure 5.2.1 Lateral earth pressure coefficient vs. depth for variation of reinforcement elastic modulus

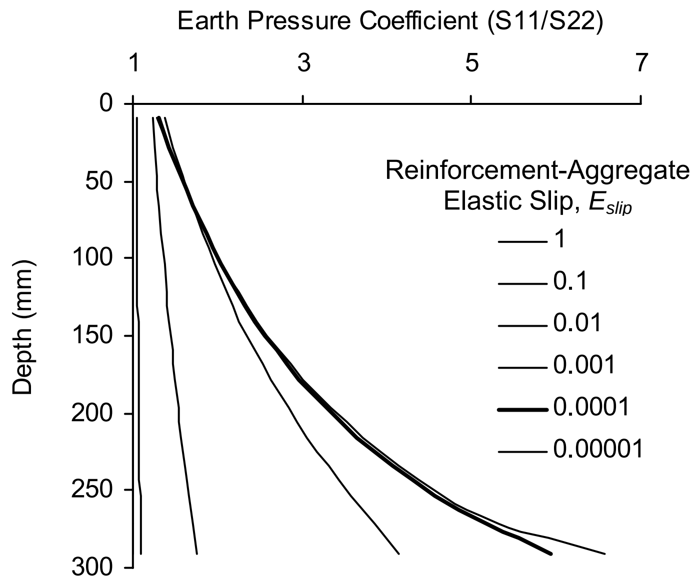

Figure 5.2.2 Lateral earth pressure coefficient vs. depth for variation of reinforcement-base interaction elastic slip

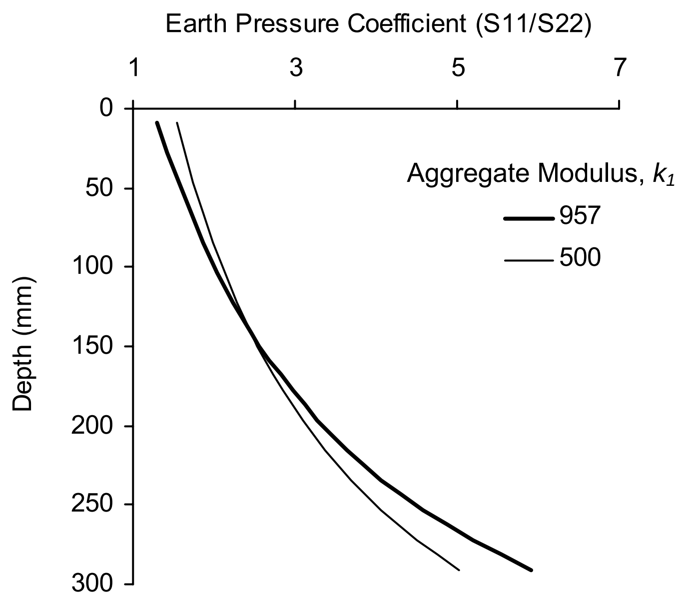

Figure 5.2.3 Lateral earth pressure coefficient vs. depth for variation of base aggregate modulus

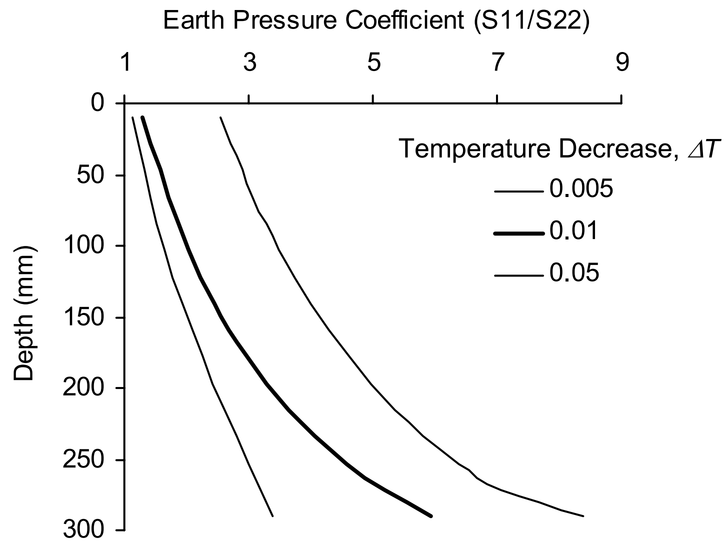

Figure 5.2.4 Lateral earth pressure coefficient vs. depth for variation of temperature decrease

Figure 5.2.2 shows the effect of the elastic slip parameter for the reinforcement-aggregate interface. The results show an increase in earth pressure coefficient as E_{slip} decreases, indicating that as interface shear modulus increases, radial stress from the compaction model increases. Figure 5.2.3 shows that the modulus of the base, given by a variation in the resilient modulus parameter k_1, influences radial stress during compaction with higher modulus base materials being able to interact better with the reinforcement and develop higher lateral earth pressures during compaction. The effect of the temperature decrease imposed on the reinforcement (Figure 5.2.4) is also significant. No experimental work has been conducted to provide data to which radial stress predictions from the compaction model could be compared, which would in turn allow for a calibration of the temperature decrease to impose. The temperature decrease of 0.01 appears to provide reasonable values of radial stress increase due to compaction and is therefore used as the temperature decrease for compaction models used subsequently in this study.

The compaction model described above does not explicitly account for the effect of variations in subgrade resilient modulus properties. Intuitively, it would be expected that less effect would be seen on stiffer subgrade materials. The sensitivity study given in Section 7 will further examine this issue by examining the combined effect of the compaction model and the other response model modules described in Sections 5.3 – 5.4 for various pavement structures with different subgrade materials.

To illustrate the effect of the compaction model on pavement performance, the compaction model was run for the response model described in Section 5.1 for the MSU test section CS11. The material properties for this model are listed in Table 5.2.2. The value of μ for the reinforcement-aggregate interface was determined from monotonic pullout tests (Perkins and Cuelho, 1999). The value of E_{slip} for the reinforcement-aggregate interface was determined from the 5 steps described in Section 3.6.3. The normal stress used in Equations 3.6.6 and 3.6.7 corresponds to the vertical stress on the interface due to self-weight stresses and was equal to 8.32 kPa. The shear stress used in Equation 3.6.6 was determined by multiplying the coefficient of friction by the normal stress, yielding a value of 12.3 kPa. This implies that the shear stress reaches its maximum value under a normal stress due to material self-weight during compaction. Figure 5.2.5 shows the calculated earth pressure coefficient in the base aggregate layer for this analysis due to the compaction model.

Table 5.2.2 Material layer properties for CS11 Test Section used in compaction model

Layer	Unit Weight (kN/m^3)	Poisson's Ratio, ν	Elastic Modulus (MPa)				
Asphalt Concrete	23.4	0.35	1.0				
Reinforcement	---	0.25	426				
				g_1^P	k_1^P	τ_1	
Base (overlay)	0	0.25	17.343	1.0	1.0	0.01	
Subgrade (overlay)	0	0.25	12.377	1.0	1.0	0.01	
			p_a (kPa)	k_1	k_2	k_3	T_c (kPa)
Base (finite)	21.8	0.25	101.3	957	0.906	-0.614	0.001
Subgrade (finite)	16.5	0.25	101.3	139	0.187	-3.281	0.001
Interface Contact Properties							
						μ	E_{slip} (m)
Reinforcement-Aggregate Interface						1.473	0.0000657
Reinforcement-Subgrade Interface						1.0	1.0

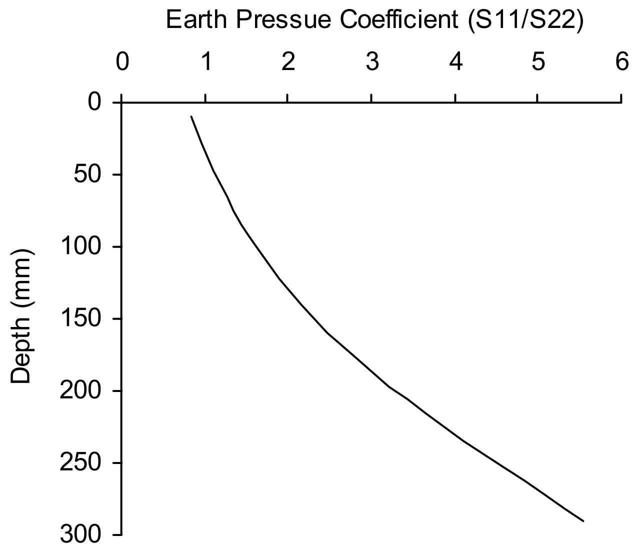

Figure 5.2.5 Lateral earth pressure coefficient vs. depth for CS11 compaction model

The radial stresses in the column of elements in the base layer along the model centerline were then used along with the geostatic vertical stresses as initial stresses in a subsequent reinforced pavement response model where pavement load was applied. This model has the same material properties given in Table 5.1.1. The value of E_{slip} for the reinforcement-aggregate interface was determined in this case by assuming a normal stress of 35 kPa and a shear stress of 5 kPa. These values were determined by examining several reinforced models and noting typical values of normal stress and shear stress under the area of influence. This feature could be improved by having an interface shear model that directly incorporated Equation 3.6.6 and was thereby a non linear stress dependent model.

Figure 5.2.6 shows the predicted surface deformation versus load cycles from this model as compared to an unreinforced model and the simple reinforced model described in Section 5.1. From this figure it is seen that the effect of the compaction model is to reduce permanent deformation due to the stiffening effect in the base. The reinforced model with the compaction induced stresses results in 23 % more traffic passes necessary to reach 25 mm of surface deformation. While this is an improvement over the simple reinforced model, the result is still far below the benefit seen in this test section. The subsequent sections develop response model modules that account for additional reinforcement effects due to processes that occur during vehicular traffic loading.

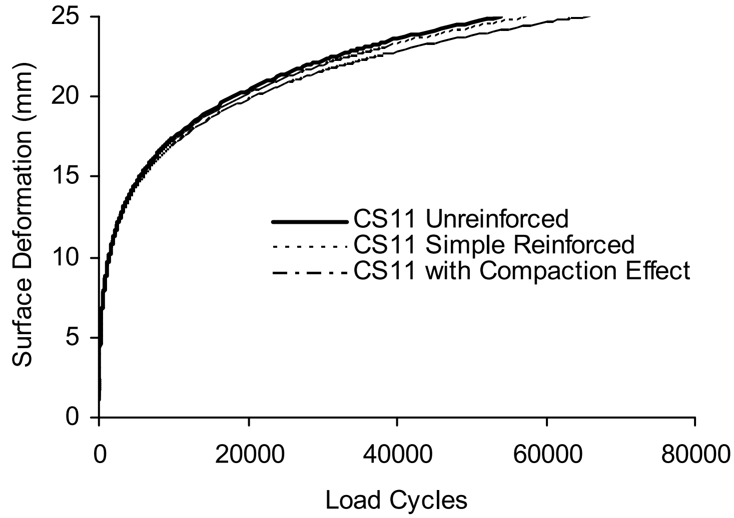

Figure 5.2.6 Surface deformation vs. load cycles for CS11 reinforced model with compaction model induced initial stresses

For situations where the reinforcement is elevated in the base aggregate layer, compaction induced stresses are evaluated only for elements above the reinforcement since this would correspond to the material influenced by compaction on top of the reinforcement layer.

5.3 Traffic I Module

In addition to an increased horizontal stress due to compaction of aggregate on top of a layer of reinforcement, lateral confinement of the aggregate base layer also develops during vehicular loading of the roadway. Additional lateral confinement is due to the development of interface shear stresses between the aggregate and the reinforcement, which in turn transfers load to the reinforcement. As a cycle of traffic load is applied, there is both a resilient or recoverable shear stress and a permanent shear stress that exists when the traffic load is removed. The permanent interface shear stress continues to grow as repeated traffic loads are applied, meaning that the lateral confinement of the aggregate base layer becomes greater with increasing traffic load repetitions. The Traffic I response model module is used to provide data for the resilient interface shear stress distribution between the reinforcement and the surrounding materials.

Experimental data presented in Section 3.7 showed the development of permanent radial strain in the reinforcement with traffic load applications. Experimental data and theoretical considerations were made to show the equality between the ratio of permanent to resilient strain in the reinforcement to the ratio of permanent to resilient shear stress on the reinforcement-aggregate interface. This led to equations describing the permanent shear stress on the interface as a function of traffic passes (Equations 3.7.8 and 3.71, repeated below)

$$\tau_{\mathrm{p}} = \tau_r \frac{\varepsilon_p}{\varepsilon_r} \tag{5.3.1}$$

$$\log\left(\frac{\varepsilon_p}{\varepsilon_r}\right) = \log(A) + B\log\left(\frac{N}{N_{25\,mm}}\right) \tag{5.3.2}$$

where:

τ_p: permanent shear stress on interface

τ_r: resilient shear stress on interface

ε_p: permanent strain in the reinforcement

ε_r: resilient strain in the reinforcement

$N/N_{25\,mm}$: ratio of actual traffic passes to passes necessary for 25 mm permanent deformation

A, B: Interface shear stress growth parameters

Parameters A and B were determined for particular geosynthetic products from test section response measurements and were listed in Table 3.7.2. These values were seen to vary between the two material directions of a particular product. Since an axisymmetric response model is used, the values of A and B for each material direction for a given reinforcement product are averaged and are used for the interface shear stress growth equations. These average values are listed in Table 5.3.1 for products A, B and C.

Table 5.3.1 Average values of interface shear stress growth parameters A and B

Geosynthetic	A	B
A	3.65	0.18
B	24.1	0.46
C	40.5	0.41

The Traffic I module provides a means of determining the resilient interface shear stress (τ_r) for use in Equation 5.3.1. The Traffic I response model module is a reinforced model having an identical cross-section and material properties as the compaction model with the following exceptions:

a. The asphalt concrete layer is given appropriate elastic properties for the problem.
b. The reinforcement-aggregate interface property E_{slip} is set to a value calculated from the 5 steps described in Section 3.6.3 and using values for normal stress of 35 kPa and shear stress of 5 kPa.
c. The reinforcement-subgrade interface is given Rough contact properties.
d. Pavement load is applied as a load step.
e. Initial stresses for the aggregate base layer are set equal to those determined from the compaction model.

The response model resulting from the steps described above corresponds to the model giving the data labeled "CS11 with Compaction Effects" in Figure 5.2.6. From this model, the interface shear stresses for both interface surfaces are extracted when full pavement load is applied. These interface shear stresses distributions are summed and taken as the values for τ_r as a function of model radius. Figure 5.3.1 shows this data from the Traffic I model for the CS11 pavement cross section. The jumpiness in this data reflects some of the numerical convergence difficulties in these models. The shear stresses for both interfaces are summed and used for τ_r in Equation 5.3.2 since both sets of shear stresses lead to the development of strain in the reinforcement.

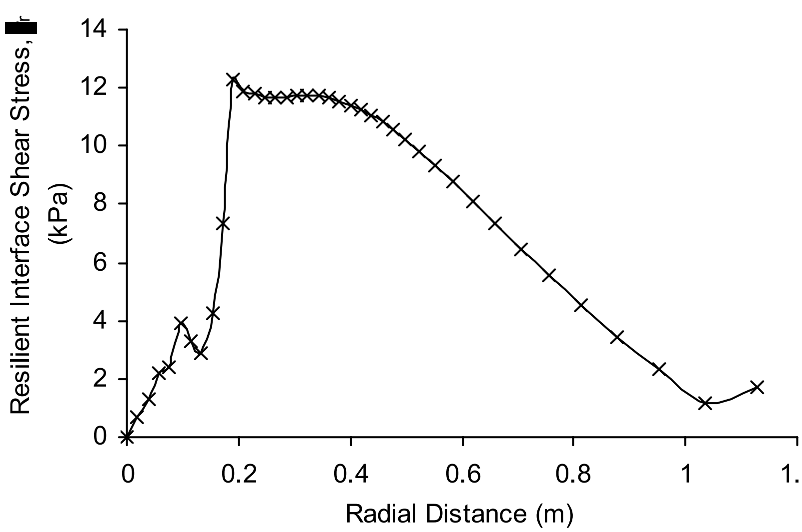

Figure 5.3.1 Resilient interface shear stress vs. model radius for CS11 Traffic I model

The shear stress distribution shown in Figure 5.3.1 is then scaled by selected values of $\varepsilon_p/\varepsilon_r$ leading to new shear stress distribution curves representing different periods in the life of the pavement. For the analysis of test section CS11 using geosynthetic B, values of $\varepsilon_p/\varepsilon_r$ of 0.25, 0.5, 1.0, 2.5, 5.0, 10.0, 15.0 and 24.1 were selected, where the final value of 24.1 corresponds to the end of pavement life when $N/N_{25\ mm}$ = 1. The equivalent nodal forces are then calculated by distributing the shear stresses over the contributory area of each node.

5.4 Traffic II Module

The Traffic II response model module gives the elevated horizontal stresses in the base due to compaction effects and for the additional locked in stresses due to the increasing tensile strains in the reinforcement with increasing traffic. This is accomplished by applying the nodal forces due to the permanent interface shear stresses for a particular pavement life period from the Traffic I model to an unreinforced model having an identical cross-section and pavement layer properties. The Traffic II model starts with an initial state of stress that comes from that determined in the Compaction model. If the unreinforced Traffic II model is meshed identical to the reinforced Traffic I model, the nodal forces can be applied to nodes at the same location for the nodes in the reinforced model. In the unreinforced Traffic II model, the nodes at the same locations as those in the reinforced model are common nodes for material above and below this horizontal line. The full value of the nodal forces is therefore used since it is resisted by material above and below the level of the nodes. Once these nodal forces have been applied, the horizontal stresses at element centroids for the column of base aggregate elements along the model centerline are extracted. These horizontal stresses along with the geostatic vertical stresses are then taken as initial stresses in a subsequent and final response model (i.e. Traffic III module). The analysis using the Traffic II model is repeated for the number of $\varepsilon_p/\varepsilon_r$ ratios selected to determine equivalent nodal forces. Thus the Traffic II analysis provides a means of assessing the effect of permanent interface shear stresses on lateral stresses developed in the base aggregate layer for different periods in the life of the pavement within the context of a finite element response model.

For situations where the reinforcement is elevated in the base aggregate layer, the horizontal stresses are evaluated and used in the subsequent model for elements above and below the reinforcement.

5.5 Traffic III Module

The Traffic III model uses the same pavement response model as the Traffic I model but uses the horizontal stresses determined from the Traffic II model along with the geostatic vertical stresses as initial stresses. This model is run for the same number of Traffic II models evaluated. From each model, the distribution of vertical strain versus depth along the model centerline is extracted and used in conjunction with the damage models for permanent deformation to determine permanent surface deformation for the load cycles that apply to the period for which the $\varepsilon_p/\varepsilon_r$ ratios apply. In addition, the maximum tensile strain in the asphalt concrete layer is extracted for each analysis.

For each data set of vertical resilient strain versus depth, the damage models for permanent deformation (Sections 3.1.2 and 3.2.2) are used to determine a curve of permanent surface deformation versus traffic load applications. This curve is taken to apply to the load cycles ranging from the previous $\varepsilon_p/\varepsilon_r$ ratio to the current $\varepsilon_p/\varepsilon_r$ ratio. In order to initiate this process, a value of $N_{25\ mm}$ must be assumed for use in Equation 5.3.2. As an example, Table 5.5.1 shows the $\varepsilon_p/\varepsilon_r$ ratios and corresponding values of actual load cycles for an assumed value of $N_{25\ mm}$ = 410,000. Figure 5.5.1 shows the permanent surface deformation versus load cycles for each $\varepsilon_p/\varepsilon_r$ ratio where the curves corresponding to larger $\varepsilon_p/\varepsilon_r$ ratios lie successively to the right.

Table 5.5.1 N_{actual} vs. $\varepsilon_p/\varepsilon_r$ for an assumed $N_{25\ mm}$ = 410,000

$\varepsilon_p/\varepsilon_r$	N_{actual}
0.25	20
0.5	90
1.0	406
2.5	2957
5.0	13,425
10.0	60,578
15.0	146,258
24.1	410,000

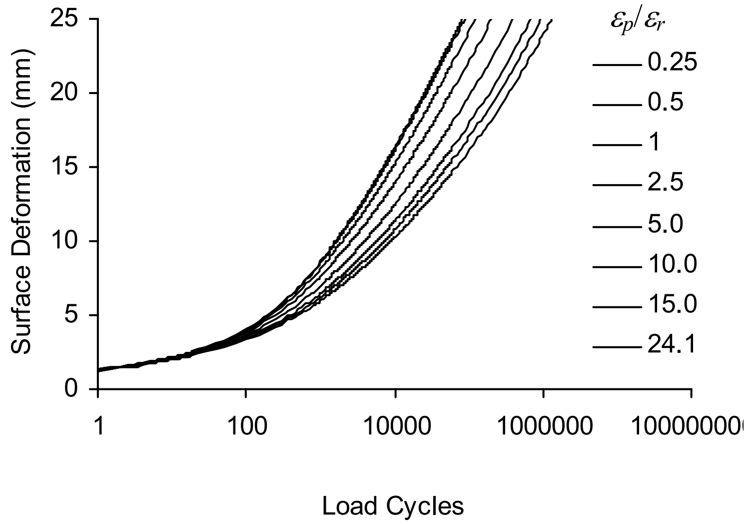

Figure 5.5.1 Permanent surface deformation vs load cycles for individual $\varepsilon_p/\varepsilon_r$ ratios

A cumulative surface deformation curve is then computed by taking deformation that occurs for each period and accumulating it over the number of analysis periods. The assumed value of $N_{25\ mm}$ is then adjusted until the cumulative curve produces a deformation of 25 mm at a value of load cycles equal to $N_{25\ mm}$. Figure 5.5.2 shows each of the curves seen in Figure 5.5.1 along with the cumulative curve. Figure 5.5.2 also shows the curve from the corresponding unreinforced model. Using this procedure, the cumulative curve yields 7.6 times then number of load cycles to reach 25 mm permanent surface deformation as compared to the unreinforced section.

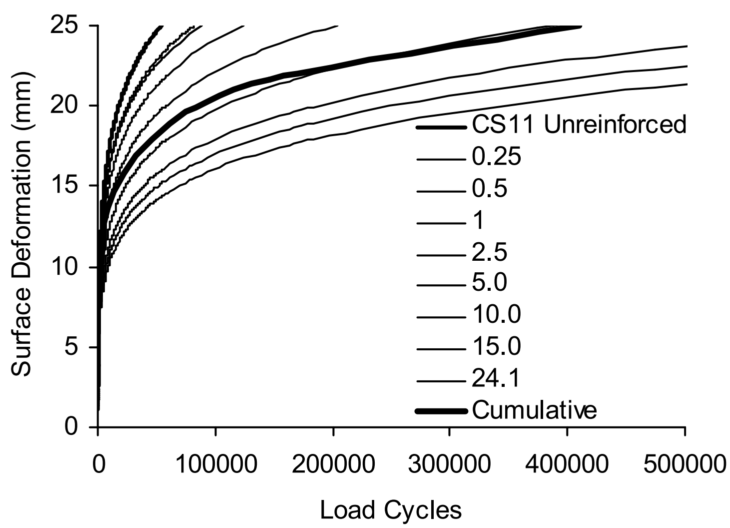

Figure 5.5.2 Permanent surface deformation vs load cycles for all $\varepsilon_p/\varepsilon_r$ ratios

The procedure described above requires special consideration when applying the damage law for asphalt concrete fatigue described in Section 3.1.3. A performance period is defined for the pavement as the number of load cycles necessary to reach 25 mm permanent surface deformation from the cumulative curve described above. The performance period is broken into a series of analysis periods corresponding to each period of load cycles for the $\varepsilon_p/\varepsilon_r$ ratios used. The response model is used to calculate maximum tensile strain in the asphalt, ε_t, for each analysis period i. The damage model for fatigue (Equation 3.1.6) is used to calculate the number of cycles to fatigue failure, N_f, under the tensile strain pertaining to the analysis period i. Fatigue life for an analysis period i is denoted as $N_{f\text{-}i}$.

Each analysis period experiences a certain number of load applications, n_i. The partial damage or damage ratio for any analysis period is given as:

$$d_i = \frac{n_i}{N_{f-i}} \tag{5.5.1}$$

The accumulated damage over the performance period is given as:

$$D = \sum d_i \tag{5.5.2}$$

If $D < 1$, then fatigue failure has not occurred over the performance period. Accumulated damage, D, represents the ratio of the actual number of applied (or accumulated) cycles to the fatigue life pertaining to the performance period ($N_{f\text{-}p}$), or

$$D = \frac{\sum n_i}{N_{f-p}} \tag{5.5.3}$$

The fatigue life pertaining to the performance period, $N_{f\text{-}p}$, is then:

$$N_{f-p} = \frac{\sum n_i}{D} = \frac{\sum n_i}{\sum d_i} = \frac{\sum n_i}{\sum \left(\frac{n_i}{N_{f-i}} \right)} \tag{5.5.4}$$

5.6 Reinforced Aggregate

The results shown in Figure 5.5.2 do not include a reduction in permanent strain in the base aggregate layer through the use of reinforcement ratios (see Table 3.4.8) for aggregate within the zone of reinforcement. The large scale reinforced triaxial tests showed that aggregate within a zone of 150 mm above and below the reinforcement experienced a reduction in permanent strain, where this reduction was expressed in terms of reinforcement ratios applied to the parameters in the damage model for permanent strain in the unbound aggregate layer. Application of these reinforcement ratios to the results shown in Figure 5.5.2 is shown in Figure 5.6.1, where the cumulative deformation curve is compared to results from this test section. Comparison of the cumulative deformation curves from Figures 5.5.2 and 5.6.1 shows that the reduction of permanent strain through the use of reinforcement ratios results in an additional 244,000 load cycles that can be applied before 25 mm of permanent surface deformation occurs. With the use of reduced permanent strain in the aggregate layer, the reinforced section is seen to carry 12.1 times the traffic passes as compared to an equivalent unreinforced section. The use of the response model modules described above with the use of reduced permanent strain parameters is seen to yield a reasonable prediction of the experimental data seen from the test section. Predictions from other sections are presented in Section 6.

6.0 FIELD CALIBRATION AND REINFORCED MODEL EVALUATION

The damage model for permanent deformation in the asphalt concrete and unbound pavement layers contains field calibration parameters (β_1, β_2 and β_3 for the asphalt concrete material and ξ_1, ξ_2 for each unbound layer). These parameters were calibrated separately for the unreinforced test sections from the MSU and CRREL test facilities. These parameters were then used for the reinforced test sections to evaluate the suitability of the methods described in Section 5.

6.1 MSU Test Sections

6.1.1 Response Model Setup

Test sections were previously constructed in a large-scale laboratory facility and reported by Perkins (1999). These sections were constructed in a reinforced concrete box measuring 2 m by 2 m and 1.5 m in height. Pavement cross sections consisting of subgrade, base aggregate and asphalt concrete were constructed within the box. A repetitive load of 40 kN was applied to a circular plate measuring 305 mm in diameter. Instrumentation was included in these sections to measure pavement surface deformation, stress and strain in the aggregate and subgrade layers and strain in the reinforcement.

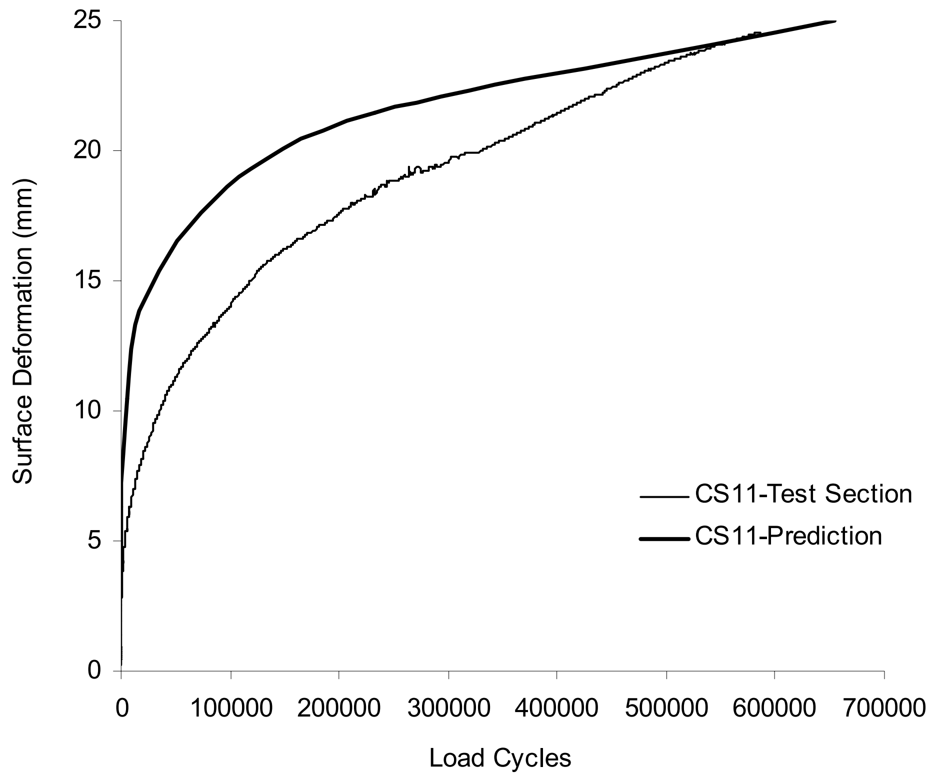

Figure 5.6.1 Permanent surface deformation vs. load cycles for test section CS11

The response model used in Section 5 for the MSU test section CS11 was set up to match the geometry and materials associated with that test section. Individual models were set up for 8 MSU test sections reported in Perkins (1999). Of these 8 sections, three were unreinforced (CS2, CS8 and CS9) and were used to field calibrate the parameters ξ_1 and ξ_2 for the damage model for permanent deformation for unbound materials (aggregate and subgrade) and parameters β_1, β_2 and β_3 for permanent deformation of asphalt concrete materials. This field calibration process is described in Section 6.1.2.

The response models for the test sections were created to match the inside dimensions of the concrete box in which the sections were constructed. Since the box was square and an axisymmetric finite element model was used, the radius of the model (1.13 m) was set to provide an equivalent horizontal area as the box having equal sides of 2 m. The thickness of each material layer (asphalt concrete, base aggregate, subgrade) was set equal to the actual values measured in the test sections. Table 6.6.1 lists the layer thickness for the 8 test sections. Material density was also assigned individual values as measured from test sections and are also contained in Table 6.6.1.

Table 6.1.1 Layer thickness of MSU test sections

	Layer Thickness (mm)			Layer Density (kN/m^3)		
Section	Asphalt Concrete	Base Aggregate	Subgrade	Asphalt Concrete	Base Aggregate	Subgrade
CS2	78.4	300	1045	23.1	21.9	16.4
CS5	76.2	300	1045	22.6	21.9	16.5
CS6	75.3	300	1045	23.3	22.2	16.0
CS7	75.3	300	1045	22.9	21.7	16.4
CS8	76.3	300	1045	23.1	22.0	16.7
CS9	79.0	375	970	22.7	22.2	16.5
CS10	75.1	375	970	22.9	21.9	16.4
CS11	77.4	300	1045	23.4	21.8	16.5

Meshing of the models followed the same basic rules described in Section 4.1 in terms of zones of uniform elements, size of elements and meshing in biased areas. Since the box provided rigid confinement to the materials, infinite elements along the bottom and side of the model were not used. The boundary condition for the side of the model prevented movement normal to the vertical face but allowed movement parallel to the face. The boundary condition for the bottom of the box prevented movement in both the vertical and horizontal directions.

A uniform pressure was applied over a radius of 152.4 mm on top of the asphalt surface for pavement load. The magnitude of the pressure was set equal to the average value seen in each test section (Table 6.1.2).

Average temperature in the asphalt concrete during testing was used along with Equations 3.1.2 – 3.1.4 and the parameters listed in Table 3.1.3 to determine elastic modulus and Poisson's ratio for the test sections (Table 6.1.2). Properties used for the base aggregate and subgrade materials are listed in Table 6.1.3 and were the same for each test section. Determination of the field calibration parameters (ξ_1, ξ_2 for the damage model for permanent deformation for unbound materials and β_1, β_2 and β_3 for permanent deformation of asphalt concrete materials) is discussed in Section 6.1.2.

Table 6.1.2 Load pressure and asphalt concrete elastic properties for MSU test sections

Section	Load Pressure[1] (kPa)	Temperture (ºC)	Asphalt Concrete Elastic Properties E (MPa)	Asphalt Concrete Elastic Properties ν
CS2	549	17.0	5.356	0.241
CS5	550	19.0	4.327	0.256
CS6	548	20.8	3.584	0.270
CS7	548	21.7	3.270	0.278
CS8	549	20.0	3.895	0.264
CS9	547	16.0	5.961	0.234
CS10	549	17.0	5.356	0.241
CS11	549	17.0	5.356	0.241

[1]Load plate diameter = 305 mm

Table 6.1.3 Material layer properties for MSU CS test sections

Layer	Poisson's Ratio, ν	Elastic Modulus (MPa)				
			g_1^P	k_1^P	τ_1	
Base (overlay)	0.25	variable	1.0	1.0	0.01	
Subgrade (overlay)	0.25	variable	1.0	1.0	0.01	
		p_a (kPa)	k_1	k_2	k_3	T_c (kPa)
Base (finite)	0.25	101.3	957	0.906	-0.614	0.001
Subgrade (finite)	0.25	101.3	139	0.187	-3.281	0.001
Asphalt Concrete Permanent Deformation Properties						
	k_1	k_2	k_3	β_1	β_2	β_3
Asphalt Concrete	-3.3426	1.734	0.4392	0.15	0.892	0.275
Unbound Layer Permanent Deformation Properties						
		$\varepsilon_o/\varepsilon_r$	ρ	β	ξ_1	ξ_2
Base (unreinforced)		88.7	7440	0.127	0.4570	2.359
Base (within reinforced zone)		102	1.38E7	0.127	0.4570	2.359
Subgrade		4690	4.13E26	0.0361	0.8552	0.9983

For the reinforced sections, Table 6.1.4 shows the parameters pertaining to the reinforcement and for the reinforcement interface. The value of μ for the reinforcement-aggregate interface was determined from monotonic pullout tests (Perkins and Cuelho, 1999). The value of E_{slip} for the reinforcement-aggregate interface was determined from the 5 steps described in Section 3.6.3. For the compaction model, the normal stress used in Equations 3.6.6 and 3.6.7 corresponds to the vertical stress on the interface due to self-weight stresses. The shear stress used in Equation 3.6.6 was determined by multiplying the coefficient of friction by the normal stress. For the Traffic I and III models, E_{slip} is calculated using values for normal stress of 35 kPa and shear stress of 5 kPa. The interface shear stress growth equation (Equation 5.3.2) used parameters *A* and *B* listed in Table 5.3.1 for each geosynthetic product. The reinforcement elastic modulus used for reinforcement A was used for all analysis periods.

Table 6.1.4 Reinforcement and interface properties for MSU CS test sections

Test Section	Reinforcement	Reinforcement Elastic Modulus (MPa)	Compaction Model		Traffic I and III Models	
			μ	E_{slip}	μ	E_{slip}
CS5	C	928	1.473	0.1973	1.473	0.3496
CS6	A	234	0.888	0.2094	1.221	0.6514
CS7	B	426	1.473	0.0432	1.473	0.1453
CS10	B	426	1.473	0.0843	1.473	0.1453
CS11	B	426	1.473	0.0657	1.473	0.1453

6.1.2 Unreinforced Test Sections

Three unreinforced sections (CS2, CS8 and CS9, Table 6.1.1) were constructed in the MSU test facility. Test sections CS2 and CS8 were replicate sections while Section CS9 contained a thicker base layer. These sections were used to determine field calibration parameters for the asphalt concrete, base aggregate and subgrade layers. Finite element response models were created for each section according to the procedures described in Section 4.1 and according to the parameters given in Tables 6.1.1 – 6.1.4. Determination of the field calibration parameters was carried out under the following constraints:

1. Values of β_1, β_2 and β_3 were initially set to the default values given in the NCHRP 1-37A Design Guide (as of May 2003), which were 0.6, 1.0 and 1.1. These values were allowed to vary between 0.25 to 2 times these values.
2. The permanent deformation of the asphalt concrete layer was constrained to be within 5 to 10 % of the total surface deformation at the end of the performance period (i.e. when 25 mm of surface deformation was reached), which was observed in test sections.

3. The permanent deformation of the aggregate and subgrade layers were constrained to be within 40 to 50% of the total surface deformation at the end of the performance period (i.e. when 25 mm of surface deformation was reached), which was observed in test sections.
4. Values of ξ_1 and ξ_2 were constrained to vary between limits of 0.25 and 4.

The square of the differences between predictions and test section values of permanent surface deformation for all levels of traffic passes were summed for all three sections. The values of β_1, β_2 and β_3 and ξ_1 and ξ_2 for each unbound layer were then optimized with the constraints noted above. The values of these field calibration parameters were listed in Table 6.1.3. Figures 6.1.1 – 6.1.3 show a comparison of predictions to test section results. These figures show the unreinforced response and damage models to give a reasonable prediction of test section data.

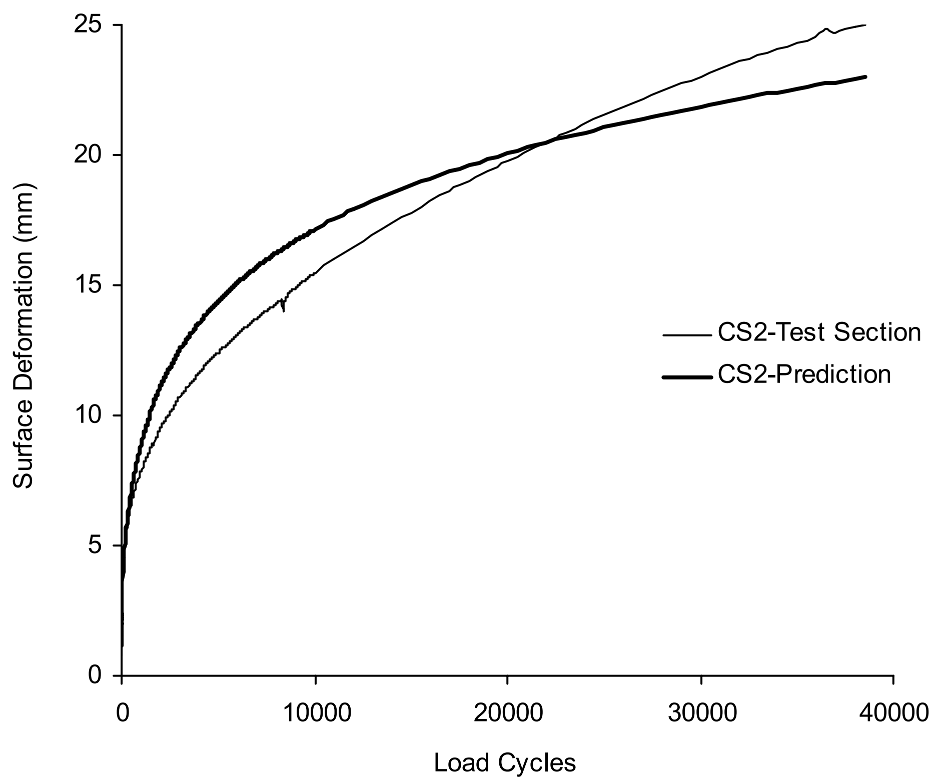

Figure 6.1.1 Predicted and measured permanent surface deformation vs. load cycles for test section CS2

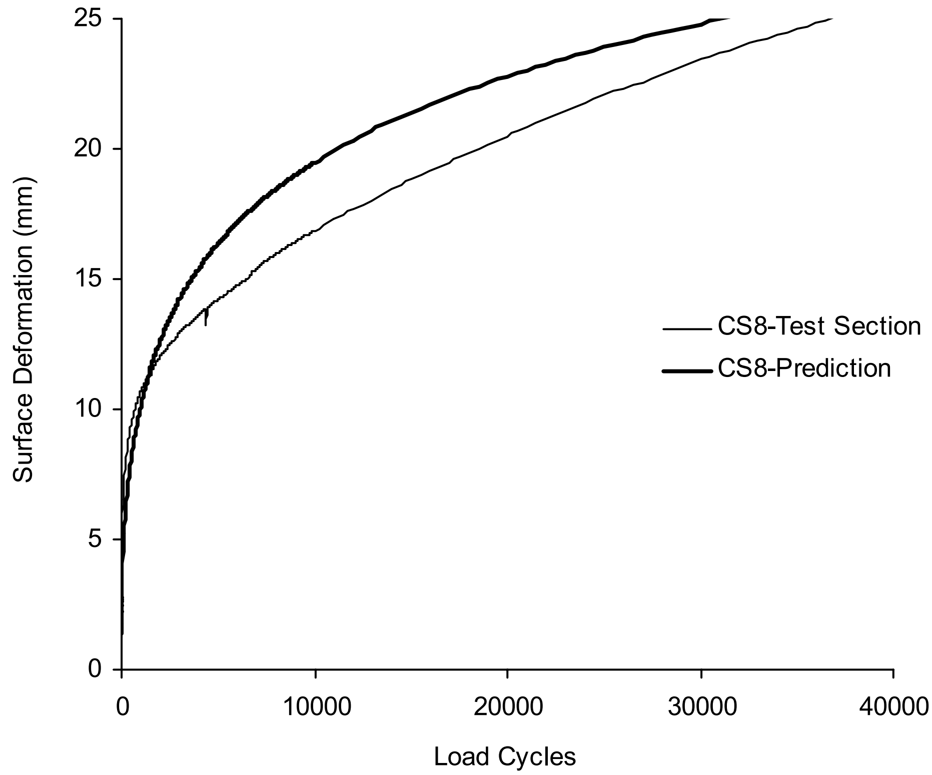

Figure 6.1.2 Predicted and measured permanent surface deformation vs. load cycles for test section CS8

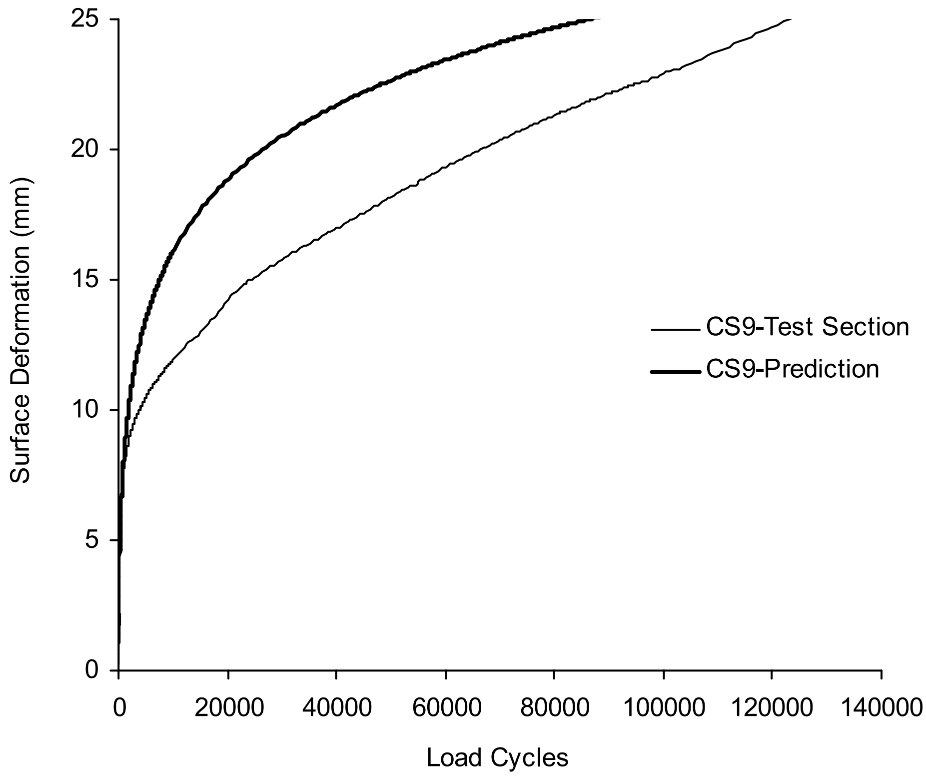

Figure 6.1.3 Predicted and measured permanent surface deformation vs. load cycles for test section CS9

Maximum tensile strain in the asphalt concrete layer was used to determine the fatigue life of the asphalt concrete according to Equation 3.1.6 with values listed in Table 6.1.5. The predicted fatigue life of the asphalt concrete was less than the number of load cycles necessary to reach 25 mm of permanent surface deformation. In the test sections, permanent surface deformation was readily measured such that the number of traffic passes to a failure condition corresponding to 25 mm of rutting could easily be identified. Identification of asphalt fatigue in these sections was difficult and complicated by several factors. The stationary location of the load plate tended to create a strain condition in the asphalt concrete that led to the development of tensile cracks at the bottom of the asphalt concrete layer below the perimeter of the load plate. These cracks could be observed during excavation of the test sections, however the initiation of these cracks were physically impossible to observe during testing. When these cracks did propagate to the surface, they were often difficult to clearly identify due to their close proximity to the edge of the load plate. The relatively rapid loading of these sections meant that very little time-dependent embrittlement of the asphalt concrete developed, which would tend to promote asphalt cracking and retard rutting due to a stiffening effect of the layer. In general, it would not be expected that asphalt concrete fatigue would be observed in these tests sections as it would be in field applications. Thus, predictions of asphalt fatigue life cannot be validated from these test sections.

Table 6.1.5 Asphalt concrete fatigue life predictions for unreinforced MSU test sections

Test Section	Fatigue Life
CS2	18,100
CS8	12,800
CS9	40,000

6.1.3 Reinforced Test Sections

The procedures described in Section 5 were applied to the reinforced MSU test sections where the properties given in Section 6.1.1 were used for these sections. Figures 6.1.4 – 6.1.8 show the resulting predictions of permanent surface deformation versus load cycles for each section. These figures also show the measured surface deformation from the test sections.

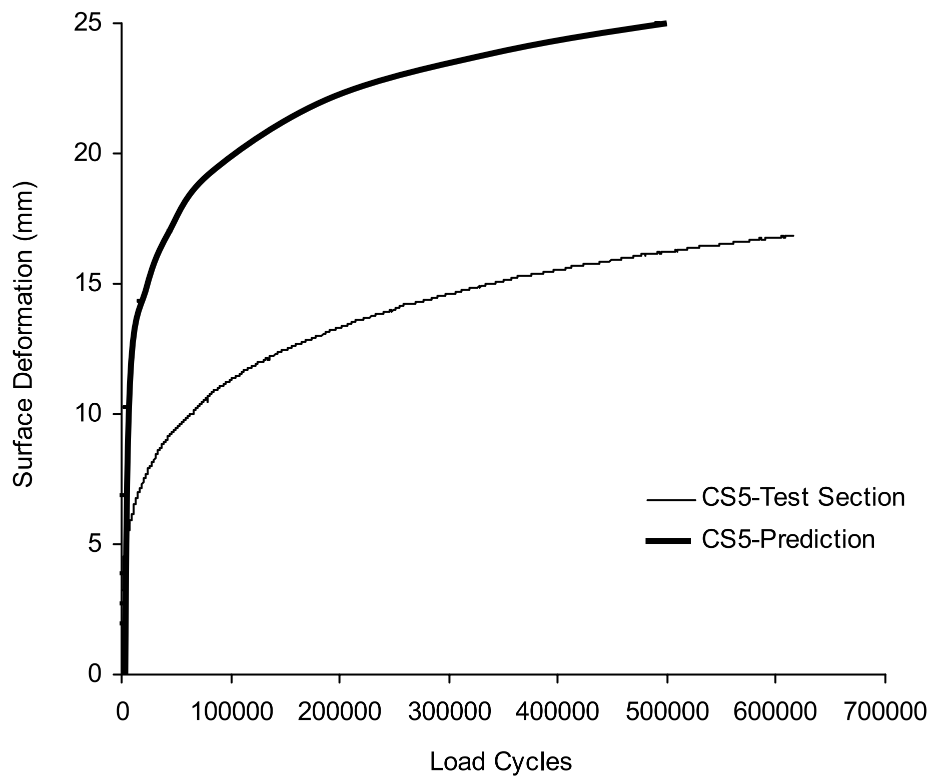

Figure 6.1.4 Predicted and measured permanent surface deformation vs. load cycles for test section CS5

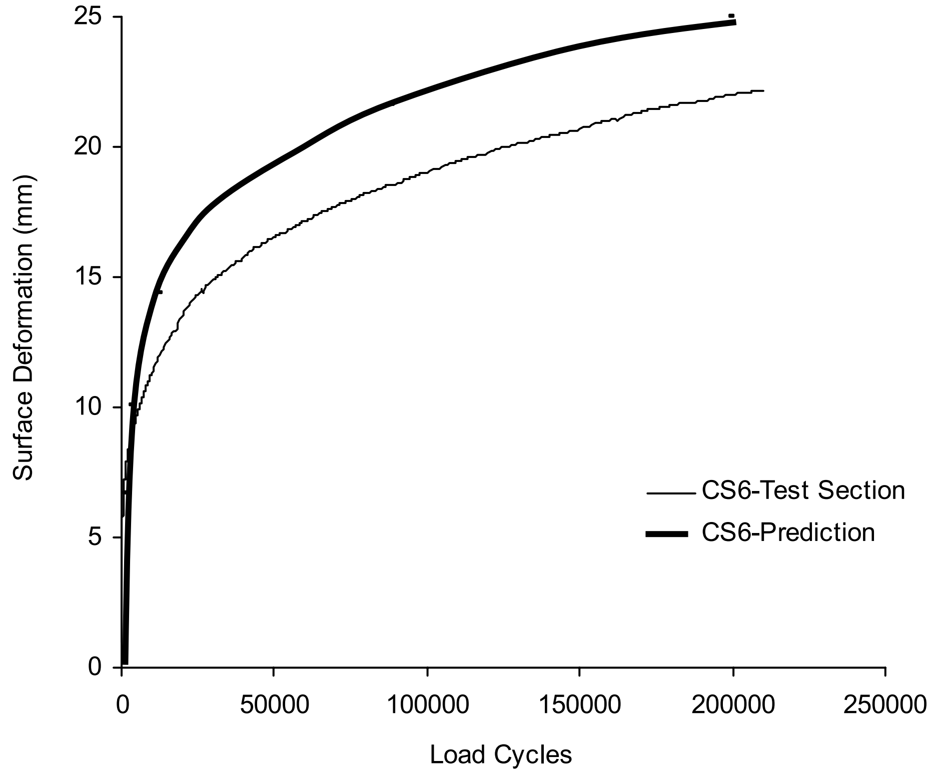

Figure 6.1.5 Predicted and measured permanent surface deformation vs. load cycles for test section CS6

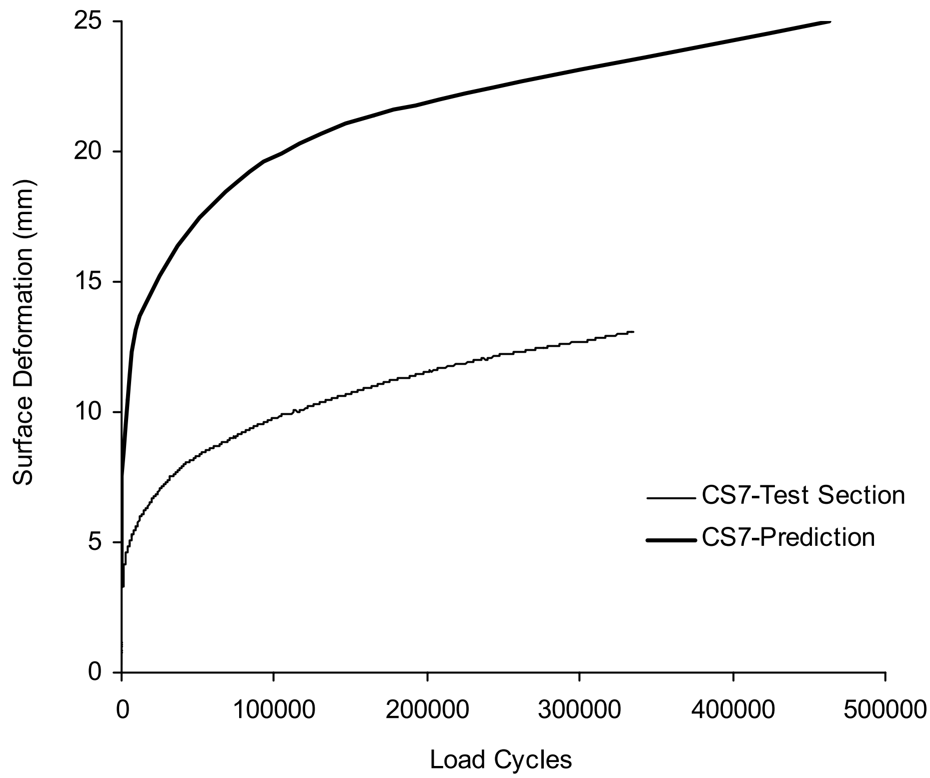

Figure 6.1.6 Predicted and measured permanent surface deformation vs. load cycles for test section CS7

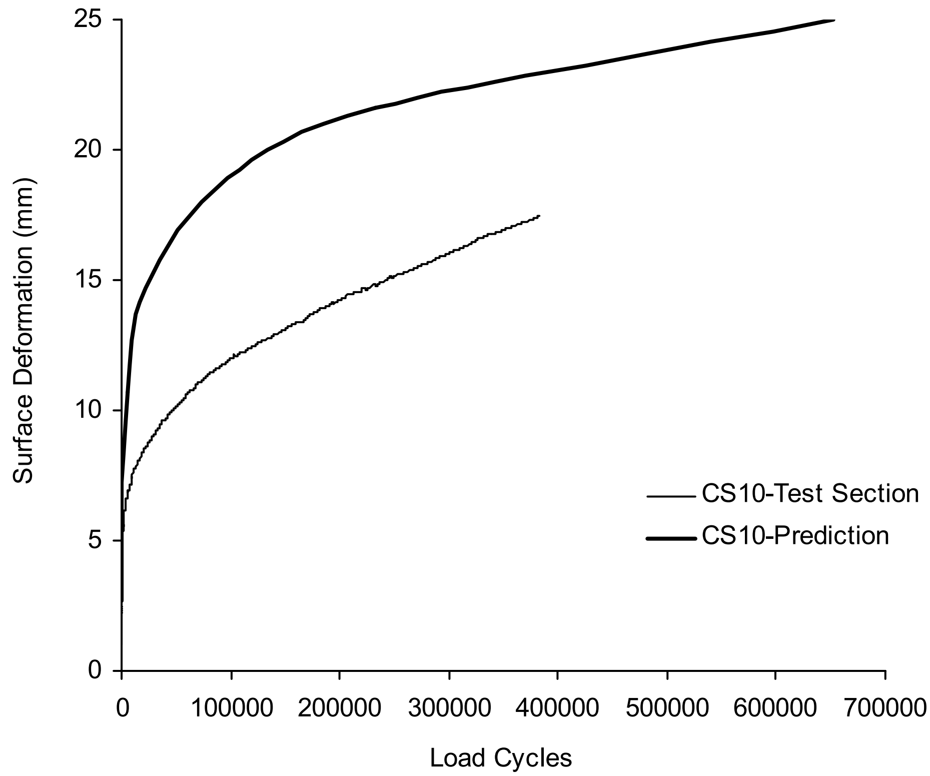

Figure 6.1.7 Predicted and measured permanent surface deformation vs. load cycles for test section CS10

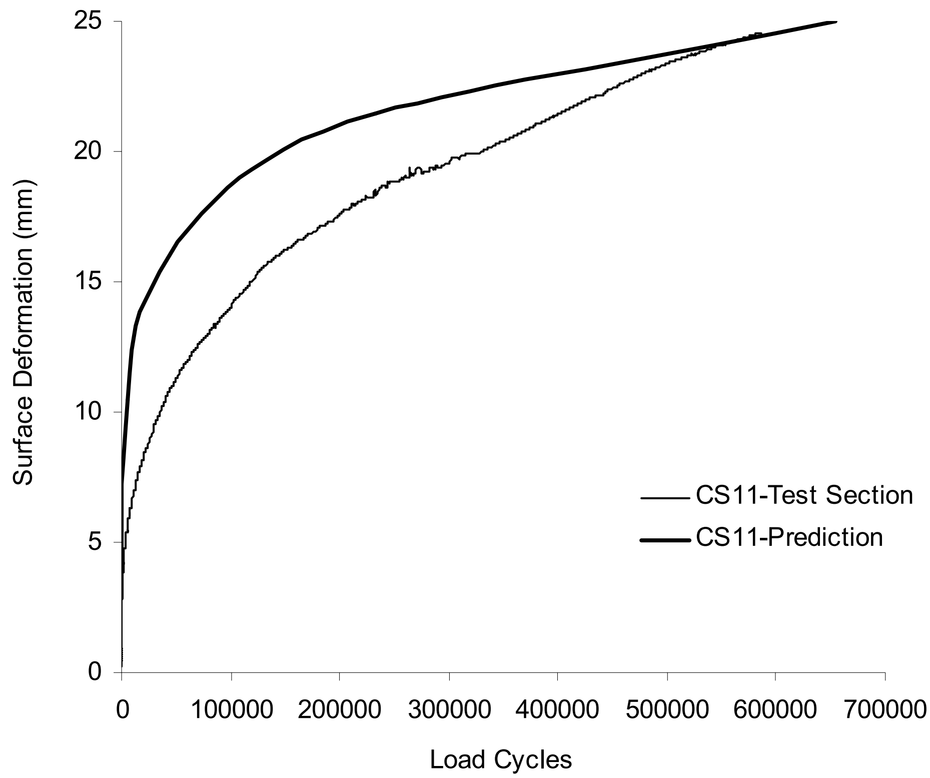

Figure 6.1.8 Predicted and measured permanent surface deformation vs. load cycles for test section CS11

Table 6.1.6 lists the asphalt concrete fatigue life predicted for each section following the procedures described in Section 5.5. Discussion of these results is provided in Section 6.3.

Table 6.1.6 Asphalt concrete fatigue life predictions for reinforced MSU test sections

Test Section	Fatigue Life
CS5	676,000
CS6	152,000
CS7	210,000
CS10	687,000
CS11	843,000

6.2 CRREL Test Sections

6.2.1 Response Model Setup

Response models for the CRREL test sections were set up following similar procedures as those used for the MSU test sections. The CRREL sections were constructed in a long concrete channel to which a dual wheel moving load was applied (Perkins, 2002). The lateral distance from the center of the outside wheel to the concrete wall was 1.4225 m and was used as the radius in the response model. The CRREL test sections contained an additional layer of subgrade that was left in place from previous sections. This layer was 1.35 m thick and was approximately 1.75 m below the pavement surface and was included in the response model. The material was given an elastic modulus of 83 MPa and a Poisson's ratio of 0.25. The elastic modulus was based on a correlation to the materials CBR strength. Table 6.2.1 lists the layer thickness for the four CRREL sections. Table 6.2.2 lists the temperature and elastic properties used for the asphalt concrete material. Table 6.2.3 lists the material layer properties for these sections. Table 6.2.4 lists the properties used for the reinforcement materials and interface properties.

Table 6.2.1 Layer thickness of CRREL test sections

	Layer Thickness (mm)			Layer Density (kN/m^3)		
Section	Asphalt Concrete	Base Aggregate	Subgrade	Asphalt Concrete	Base Aggregate	Subgrade
CRREL1	78.6	331	1335	20.9	21.7	18.8
CRREL2	82.9	325	1337	21.8	21.6	18.8
CRREL3	82.9	325	1337	21.8	21.8	18.8
CRREL4	82.9	325	1337	21.8	21.8	18.8

Table 6.2.2 Asphalt concrete elastic properties for CRREL test sections

	Temperture (ºC)	Asphalt Concrete Elastic Properties	
Section		E (MPa)	ν
CRREL1	20.0	4.664	0.251
CRREL2	19.8	4.664	0.251
CRREL3	19.8	4.664	0.251
CRREL4	19.8	4.664	0.251

Table 6.2.3 Material layer properties for CRREL test sections

Layer	Poisson's Ratio, ν	Elastic Modulus (MPa)				
			g_1^P	k_1^P	τ_1	
Base (overlay)	0.25	variable	1.0	1.0	0.01	
Subgrade (overlay)	0.25	variable	1.0	1.0	0.01	
		p_a (kPa)	k_1	k_2	k_3	T_c (kPa)
Base (finite)	0.25	101.3	662	1.01	-0.585	0.001
Subgrade (finite)	0.25	101.3	170	0.45	-16.39	0.001
Asphalt Concrete Permanent Deformation Properties						
	k_1	k_2	k_3	β_1	β_2	β_3
Asphalt Concrete	-3.3426	1.734	0.4392	0.19	0.85	0.38
Unbound Layer Permanent Deformation Properties						
		$\varepsilon_o/\varepsilon_r$	ρ	β	ξ_1	ξ_2
Base (unreinforced)		82.6	789	0.165	0.25	3.3
Base (within reinforced zone)		102	1.38E7	0.127	0.4570	2.359
Subgrade		839	4.75E15	0.0455	2.9	1.48

Table 6.2.4 Reinforcement and interface properties for CRREL test sections

Test Section	Reinforcement	Reinforcement Elastic Modulus (MPa)	Compaction Model		Traffic I and III Models	
			μ	E_{slip}	μ	E_{slip}
CRREL2	B	426	1.473	0.0696	1.473	0.1453
CRREL3	A	234	0.900	0.2207	1.221	0.6514
CRREL4	C	928	1.473	0.2087	1.473	0.3496

The use of a dual wheel load in the CRREL test sections required several special considerations in the set up and extraction of results from the pavement response model. The dual wheels used in the CRREL test sections had a tire width of 223 mm with 111.6 mm of clear distance between the wheels. A total load of 40 kN was applied to the wheels. Since a 2-D axisymmetric response model was used, a superposition technique was used to evaluate the effect of dual wheel loads. This technique is similar to that used in the NCHRP 1-37A Design Guide and is based on Schwartz (2002). In order to have a convenient means of extracting results for superposition, an even number of uniform elements were created in the horizontal direction from the model centerline axis out to a distance equal to the center to center distance between the wheels (i.e. 335 mm). The number of elements was chosen to maintain an aspect ratio close to 1 through the thickness of the asphalt concrete layer. This resulted in 18 elements of a width of 18.6 mm. The radius of the tire load was then set equal to the closest number of elements approximating the true half-width of the tire, which was 111.5 mm). This resulted in 6 elements over which the tire pressure was applied in the model corresponding to a radius of 111.7 mm, which closely approximates the true tire half-width. The tire pressure applied in the model was then computed by dividing 20 kN by the area corresponding to a circular load of radius = 111.7 mm and resulted in a pressure of 510.5 kPa.

The response model then imposed a pressure of 510.5 kPa acting over 6 elements on the pavement surface corresponding to a load radius of 111.7 mm. Vertical strain was then extracted from the response model for 19 vertical lines of nodes through the asphalt concrete, base aggregate and subgrade layers. Similarly, asphalt concrete tensile strain was extracted along these same 19 lines for nodes through the asphalt concrete layer. Superposition of two tire loads was then calculated by summing strains at corresponding depths for lines 1 and 19, 2 and 18, 3 and 17, … 9 and 11, and 10 and 10. The maximum superimposed tensile strain in the asphalt concrete layer was then used in the damage model for asphalt concrete fatigue. The superimposed vertical strains for each of the 10 vertical locations were then used in the damage model for permanent deformation with the line yielding the maximum deformation used to define rutting of the pavement surface.

For the reinforced models the Compaction, Traffic I, II and III modules were used as described in Section 5 with the exception of the Traffic I module where interface shear stress was extracted for use in the Traffic II module. The shear stress due to the single wheel load in the response model was superimposed as described above to account for the presence of a dual wheel load. The interface shear stress growth equation (Equation 5.3.2) used parameters *A* and *B* listed in Table 5.3.1 for each geosynthetic product.

6.2.2 Unreinforced Test Sections

A single unreinforced test section was available from the series of test sections evaluated in the CRREL facility. A response model was created for this section according to the procedures described in Section 4.1 and according to the parameters given in Tables 6.2.1 – 6.2.4. Determination of the field calibration parameters was carried out under the constraints described for the MSU unreinforced sections (Section 6.1.2). Figure 6.2.1 shows the predicted permanent surface deformation response versus traffic passes as compared to the measured values from the test section. Fatigue life of the asphalt concrete layer was predicted as 71,800 traffic passes. As with the MSU test sections, measured fatigue life of the asphalt concrete was difficult to determine from these test sections due to the use of a channelized wheel path.

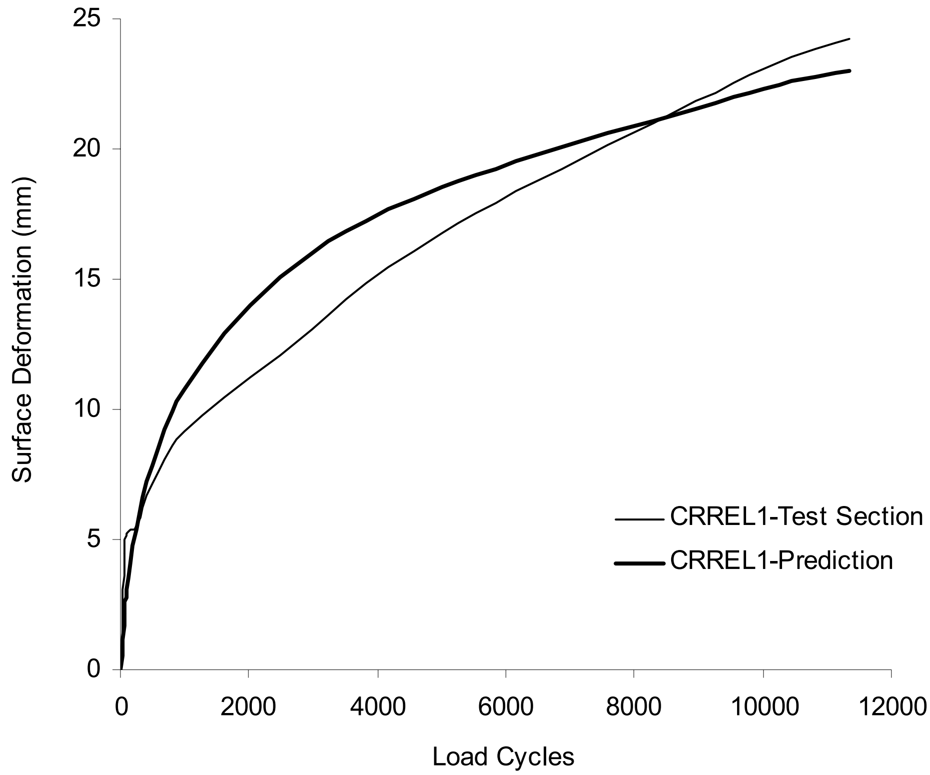

Figure 6.2.1 Predicted and measured permanent surface deformation vs load cycles for test section CRREL1

6.2.3 Reinforced Test Sections

The procedures described in Section 5 were applied to the reinforced CRREL test sections where the properties given in Section 6.2.1 were used for these sections. Figures 6.2.2 – 6.2.4 show the resulting predictions of permanent surface deformation versus load cycles for each section. These figures also show the measured surface deformation from the test sections. These figures show a reasonable comparison between predictions and measured deformation performance.

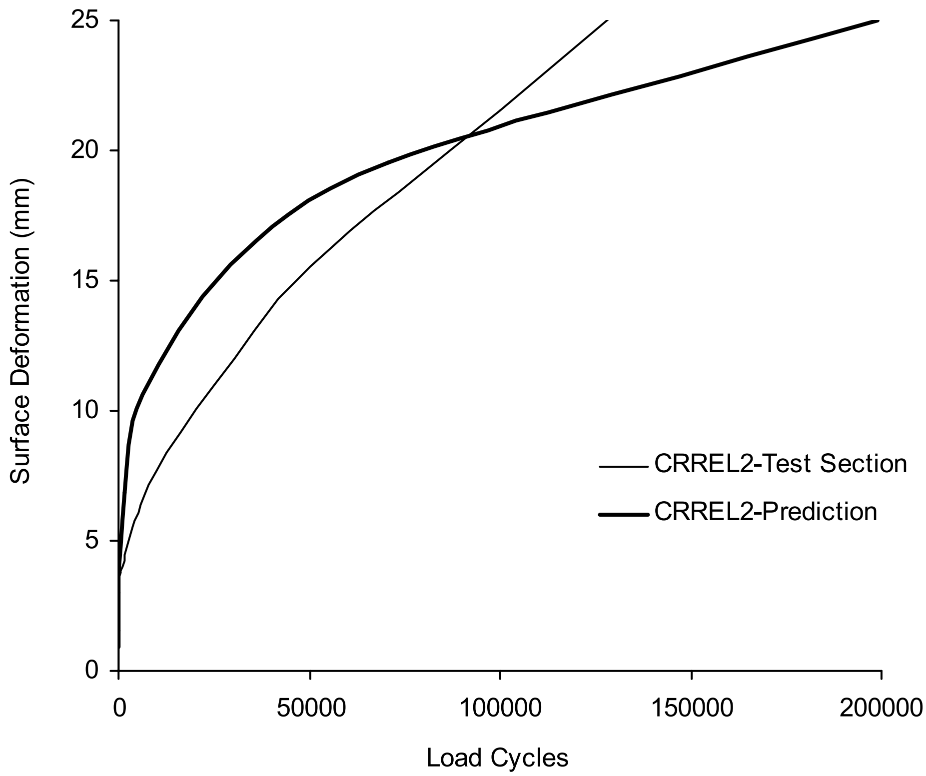

Figure 6.2.2 Predicted and measured permanent surface deformation vs. load cycles for test section CRREL2

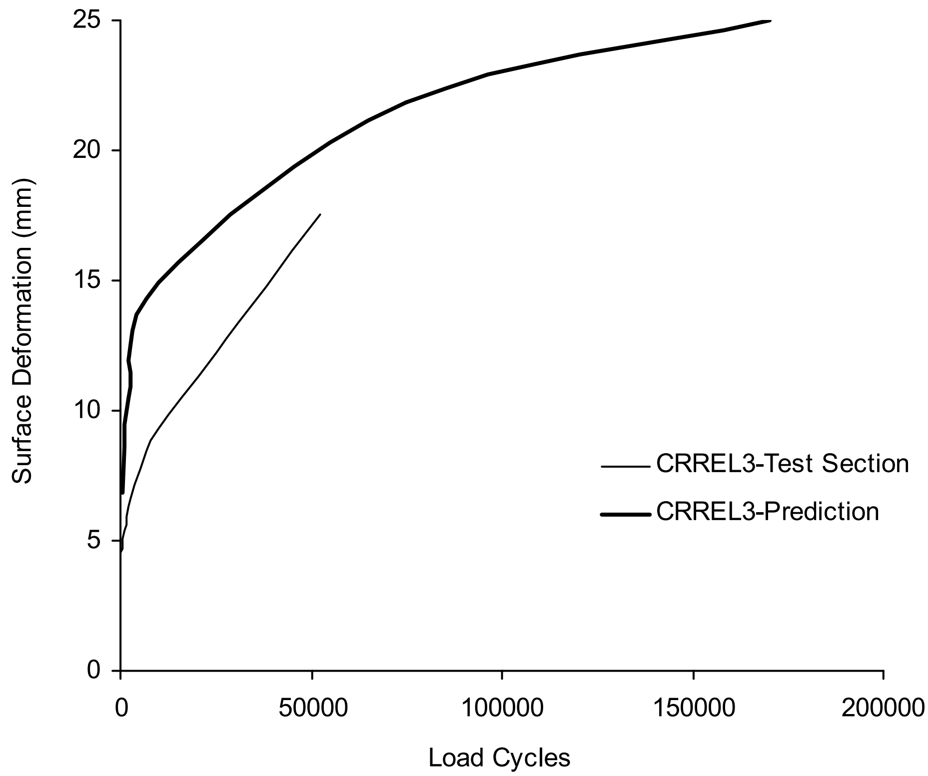

Figure 6.2.3 Predicted and measured permanent surface deformation vs. load cycles for test section CRREL3

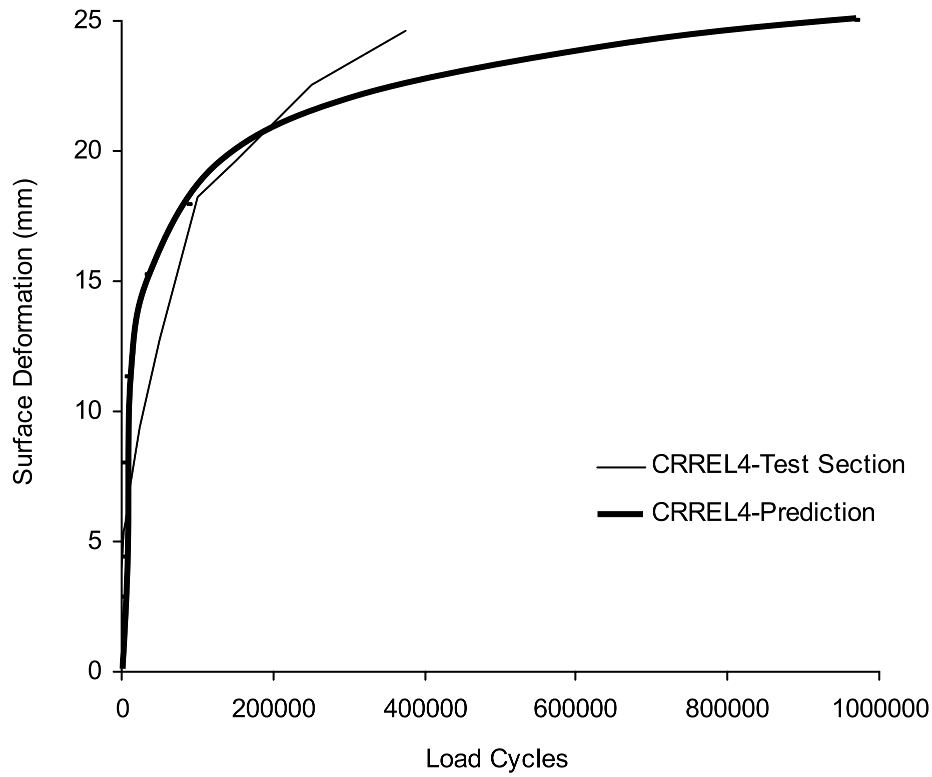

Figure 6.2.4 Predicted and measured permanent surface deformation vs. load cycles for test section CRREL4

Table 6.2.5 lists the asphalt concrete fatigue life predicted for each section following the procedures described in Section 5.5. In these sections, the predicted fatigue life exceeded the number of traffic passes necessary to reach 25 mm of permanent surface deformation. As with the MSU box test sections, identification of asphalt concrete fatigue life in the CRREL test sections was difficult to determine.

Table 6.2.5 Asphalt concrete fatigue life predictions for reinforced CRREL test sections

Test Section	Fatigue Life
CRREL2	3,087,000
CRREL3	458,000
CRREL4	7,481,000

6.3 Discussion of Results

The purpose of this discussion is to examine the general trends in predictions of pavement performance for reinforced and unreinforced pavements based on the results from the models created for the MSU and CRREL test sections. Since the failure mode of asphalt fatigue was difficult to identify in these two test facilities, the discussion of the predictions shown in this section is not necessarily intended to relate directly to observed failure modes in these test sections.

Table 6.3.1 shows predictions of number of traffic passes to 25 mm permanent surface deformation and fatigue life for each of the MSU and CRREL test sections. The predictions show that the MSU unreinforced sections were controlled by asphalt concrete fatigue. Reinforced test sections CS6 and CS7 were also controlled by fatigue. In the reinforced sections CS5, CS10 and CS11, the failure mode switched from fatigue to permanent surface deformation. For the CRREL sections where a dual wheel was modeled, failure was controlled by permanent deformation in all test sections. These results show the ability of the modeling techniques to differentiate between failure modes and to show the effects of the reinforcement on the control of these failure modes. Results of this type are further illustrated in Section 7 for a range of pavement cross sections.

Table 6.3.1 Predicted traffic passes to 25 mm surface deformation and fatigue life for MSU and CRREL test sections

Test Section	Traffic Passes to 25 mm Surface Deformation	Fatigue Life
CS2	59,600	18,100
CS8	31,200	12,800
CS9	86,200	40,000
CS5	492,000	676,000
CS6	199,000	152,000
CS7	464,000	210,000
CS10	652,000	687,000
CS11	654,000	843,000
CRREL1	15,950	71,800
CRREL2	198,700	3,087,000
CRREL3	170,000	458,000
CRREL4	968,000	7,481,000

7.0 SENSITIVITY STUDY

7.1 Study Matrix

A sensitivity study was performed to evaluate reinforced models for bracketing combinations of pavement traffic level, subgrade stiffness, reinforcement type and reinforcement position. The majority of the models were set up to evaluate the increased number of traffic passes that could be applied when reinforcement was added to the cross section. Several models were created to evaluate the reduction in base course thickness for an equal number of traffic passes for reinforced and unreinforced sections.

Three levels of traffic passes relative to those anticipated for reinforced pavements were used to create models, corresponding to:

1. High Traffic Passes (10 million)
2. Medium Traffic Passes (1 million)
3. Low Traffic Passes (100,000)

Two subgrade material types were used, corresponding to:

1. Weak (A-7-6), assumed M_R = 4000 psi (for purposes of pavement cross-section design)
2. Firm (A-4), assumed M_R = 14,000 psi (for purposes of pavement cross-section design)

The six combinations given by the traffic pass levels and subgrade stiffnesses above were used to design pavement cross sections using the AASHTO ’93 method. The pertinent inputs and resulting layer thicknesses for these six pavement cross sections are listed in Table 7.1.1. Certain inputs (standard normal deviate, terminal serviceability) were changed between sections to reflect an appropriate design standard for the design traffic level. Unreinforced and reinforced pavement response models were then created for each of the six pavement cross sections. Two reinforced sections were created for each cross section using properties pertinent to geosynthetics A and C. The same permanent deformation properties were used for both the weak and firm subgrade due to the lack of data showing clear and sensible differences between subgrade materials. The resilient modulus properties used for the firm subgrade were taken from the A-4 subgrade (MSU-SSS subgrade) material (Table 3.2.6). Resilient modulus properties for the base aggregate and weak subgrade were the same as that used for the MSU aggregate and the MSU CS subgrade (see Table 3.2.6). Table 7.1.2 gives material layer properties used in the cross sections. Table 7.1.3 gives the interface properties used for each response model module for each reinforced cross section.

Table 7.1.1 AASHTO '93 inputs and pavement cross sections for sensitivity study

	Pavement Sections					
	High-Weak	High-Firm	Medium-Weak	Medium-Firm	Low-Weak	Low-Firm
ESAL	10,000,000	10,000,000	1,000,000	1,000,000	100,000	100,000
Reliability (%)	90	90	85	85	80	80
Standard Normal Deviate	-1.282	-1.282	-1.037	-1.037	-0.841	-0.841
Overall Standard Deviation	0.35	0.35	0.35	0.35	0.35	0.35
Initial Serviceability	4.2	4.2	4.2	4.2	4.2	4.2
Terminal Serviceability	2.5	2.5	2.25	2.25	2.0	2.0
AC Layer Coefficient	0.4	0.4	0.4	0.4	0.4	0.4
Base Layer Coefficient	0.14	0.14	0.14	0.14	0.14	0.14
Base Layer M_R (psi)	30,616	30,616	30,616	30,616	30,616	30,616
Subgrade M_R (psi)	4000	14,000	4000	14,000	4000	14,000
AC Thickness (mm)	180	180	117	117	75	75
Base Thickness (mm)	544	178	397	118	267	85

Table 7.1.2 Material layer properties for sensitivity models

Layer	Unit Weight (kN/m^3)	Poisson's Ratio, ν	Elastic Modulus (MPa)				
Asphalt Concrete	23	0.25	5000				
Reinforcement A	---	0.25	234				
Reinforcement C	---	0.25	928				
				g_1^P	k_1^P	τ_1	
Base (overlay)	0	0.25	variable	1.0	1.0	0.01	
Subgrade (overlay)	0	0.25	variable	1.0	1.0	0.01	
			p_a (kPa)	k_1	k_2	k_3	T_c (kPa)
Base (finite)	21	0.25	101.3	957	0.906	-0.614	0.001
Subgrade-Weak	18	0.25	101.3	139	0.187	-3.281	0.001
Subgrade-Firm	18	0.25	101.3	449	1.03	-1.856	0.001
Asphalt Concrete Permanent Deformation Properties							
	T (ºF)	k_1	k_2	k_3	β_1	β_2	β_3
Asphalt Concrete	70	-3.3426	1.734	0.4392	0.15	0.892	0.275
Unbound Layer Permanent Deformation Properties							
			$\varepsilon_0/\varepsilon_r$	ρ	β	ξ_1	ξ_2
Base			88.7	20,000	0.127	0.14	3.5
Reinforced Base			102	37E06	0.127	0.14	3.5
Subgrade			4690	4.13E26	0.0361	0.8552	0.9983
Interface Shear Stress Growth							
			A	B			
Reinforcement A			3.65	0.18			
Reinforcement C			40.5	0.41			

Table 7.1.3 Interface properties for sensitivity models

	μ	σ_I (kPa)	τ_I (kPa)	G_I (kPa)	E_{slip} (m)
HW-R1 Compaction	1.473	15.564	22.926	73,377	0.000312
HW-R1 TrafficI&III	1.473	35	5	147,486	0.0003496
HW-R2 Compaction	0.888	15.564	13.821	42,133	0.000328
HW-R2 TrafficI&III	1.221	35	5	65,622	0.0006514
HF-R1 Compaction	1.473	7.878	11.604	60,818	0.000191
HF-R1 TrafficI&III	1.473	35	5	147,486	0.0003496
HF-R2 Compaction	0.888	7.878	6.996	34,831	0.000201
HF-R2 TrafficI&III	1.221	35	5	65,622	0.0006514
MW-R1 Compaction	1.473	10.65	15.69	66,528	0.000236
MW-R1 TrafficI&III	1.473	35	5	147,486	0.0003496
MW-R2 Compaction	0.888	10.65	9.457	38,141	0.000248
MW-R2 TrafficI&III	1.221	35	5	65,622	0.0006514
MF-R1 Compaction	1.473	5.169	7.614	52,295	0.000146
MF-R1 TrafficI&III	1.473	35	5	147,486	0.0003496
MF-R2 Compaction	0.888	5.169	4.59	30,292	0.000152
MF-R2 TrafficI&III	1.221	35	5	65,622	0.0006514
LW-R1 Compaction	1.473	7.33	10.80	59,386	0.000182
LW-R1 TrafficI&III	1.473	35	5	147,486	0.0003496
LW-R2 Compaction	0.888	7.33	6.51	34,044	0.000191
LW-R2 TrafficI&III	1.221	35	5	65,622	0.0006514
LF-R1 Compaction	1.473	3.51	5.17	54,567	0.000140
LF-R1 TrafficI&III	1.473	35	5	147,486	0.0003496
LF-R2 Compaction	0.888	3.51	3.12	26,400	0.000118
LF-R2 TrafficI&III	1.221	35	5	65,622	0.0006514

H, M, L = High, Medium, Low Traffic
W, F = Weak, Firm Subgrade
R1, R2 = Reinforcement 1, Reinforcement 2

7.2 Study Results

Table 7.2.1 shows predictions of number of traffic passes to 25 mm of permanent surface deformation and fatigue life for each of the 18 pavement cross sections. Values of N_R/N_U correspond to the ratio of traffic passes for reinforced sections to unreinforced sections for each reinforcement product. The results show a clear and marked difference between the two reinforcement products. The results show negligible to modest reinforcement effects on rutting in the sections having a firm subgrade and for the high traffic section on a weak subgrade. The results showing negligible reinforcement effect are consistent with results reported by Berg et al. (2000). The modest values of reinforcement effect seen in these sections have not been validated by test sections constructed with these conditions. However, this is consistent with conventional wisdom that reinforcement will be less beneficial for these types of sections having a firm subgrade or a thick section. The sections on a weak subgrade with medium to low traffic show the most effect on rutting from reinforcement with the low traffic section showing greater values of improvement. These improvement levels are consistent with those observed in test sections. The modest to high values of improvement on fatigue life have not been validated in test sections, which is due mainly to the fact that most constructed test sections reported in the literature have failed by rutting.

All of the unreinforced test sections for the 6 pavement cross sections were controlled by asphalt concrete fatigue. The predictions for the MSU test sections also were controlled by fatigue, however the unreinforced CRREL section was controlled by rutting. Had a dual wheel load been used in the sensitivity study, the failure mode of the pavement may have switched to permanent deformation for some of the sections. All the reinforced sections, with the exception of the High-Weak and High-Firm cross sections with reinforcement C, were also controlled by fatigue. Again, this conclusion may have changed if dual wheel loading had been used in the model.

Two additional reinforced models corresponding to the medium traffic / weak subgrade cross section were evaluated with reinforcement C placed at the midpoint of the base and at a position 1/3 above the bottom of the base. Table 7.2.2 lists the results of traffic passes to 25 mm surface deformation and fatigue life for these sections. The results show that in terms of rutting, maximum benefit is seen when the reinforcement is at the bottom of the base. For fatigue, elevating the reinforcement provides more benefit. In terms of overall design, placement of the reinforcement at the 1/3 base position is optimal since it gives the greatest number of traffic passes for the controlling mode of failure (rutting) for each of the three cross sections. It is also interesting to note that the number of traffic passes for the failure modes of rutting and fatigue are approximately equal for the 1/3 reinforcement position. Reinforcement placement at the 1/3 position has been seen to be optimal in test sections summarized by Berg et al. (2000).

Table 7.2.1 Sensitivity study results

	Pavement Sections					
	High-Weak	High-Firm	Medium-Weak	Medium-Firm	Low-Weak	Low-Firm
AC Thickness (mm)	180	180	117	117	75	75
Base Thickness (mm)	544	178	397	118	267	85
Cycles to 25 mm rut, U	3,850,000	3,356,000	1,186,000	1,056,000	118,706	244,000
Cycles to 25 mm rut, R (C)	7,900,000	4,920,000	6,690,000	2,930,000	1,330,000	477,000
Cycles to 25 mm rut, R (A)	4,750,000	3,580,000	1,905,000	1,775,000	435,000	287,000
N_{R-C}/N_U	2.05	1.47	5.64	2.77	11.2	1.95
N_{R-A}/N_U	1.23	1.07	1.61	1.68	3.66	1.18
Cycles to fatigue, U	1,875,000	1,875,000	126,000	107,000	8530	11,200
Cycles to fatigue, R (C)	11,034,000	7,848,000	3,646,000	368,000	780,000	31,600
Cycles to fatigue, R (A)	2,459,000	2,444,000	348,000	160,000	103,000	13,300
N_{R-C}/N_U	5.88	4.19	28.9	3.44	91.4	2.82
N_{R-A}/N_U	1.31	1.30	2.76	1.50	12.1	1.19

Table 7.2.2 Effect of reinforcement position

	Reinforcement at bottom	Reinforcement 1/3 up from bottom	Reinforcement in middle of base
AC Thickness (mm)	117	117	117
Base Thickness (mm)	397	397	397
Cycles to 25 mm rut, U	1,186,000	1,186,000	1,186,000
Cycles to 25 mm rut, R	6,690,000	5,400,000	4,420,000
N_R/N_U	5.64	4.55	3.73
Cycles to fatigue, U	126,000	126,000	126,000
Cycles to fatigue, R	3,646,000	5,437,000	5,557,000
N_R/N_U	28.9	43.1	44.1

Three additional unreinforced sections using the same properties and geometry as the low traffic / weak subgrade cross sections were created with a base thickness that was equal to 763, 534 and 411 mm. Results from these and the other unreinforced and reinforced sections for this case are shown in Figures 7.2.1 and 7.2.2. In these figures, the traffic passes to 25 mm permanent surface deformation and to fatigue life are plotted against the base thickness for the four unreinforced models. The dashed lines shown in each figure correspond to the traffic passes for this same case for reinforcement products A and C for a base thickness of 267 mm. From Figure 7.0.1, it is seen that the reinforced sections with products A and C would yield the same performance as an unreinforced section with a base thickness of 431 and 600 mm, respectively. This implies that a section with an unreinforced base of 600 mm could be reduced to 267 mm with reinforcement C added at the bottom of the base (a 56 % reduction). Similarly, for reinforcement A, a 38 % reduction from 431 mm to 267 mm is seen.

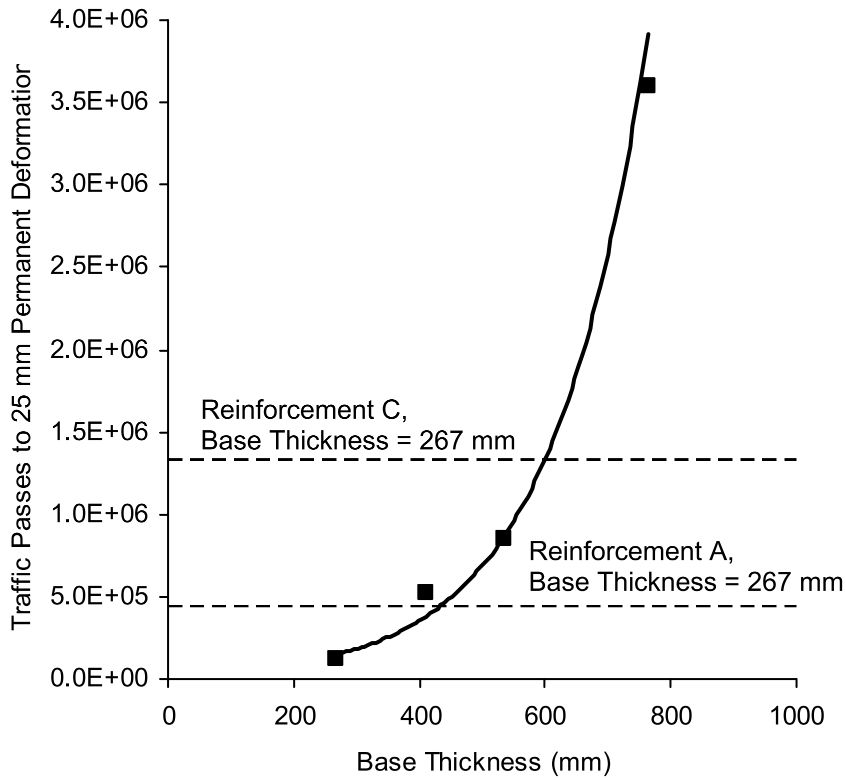

Figure 7.2.1 Traffic passes to 25 mm permanent surface deformation vs. base thickness for Low-Weak case

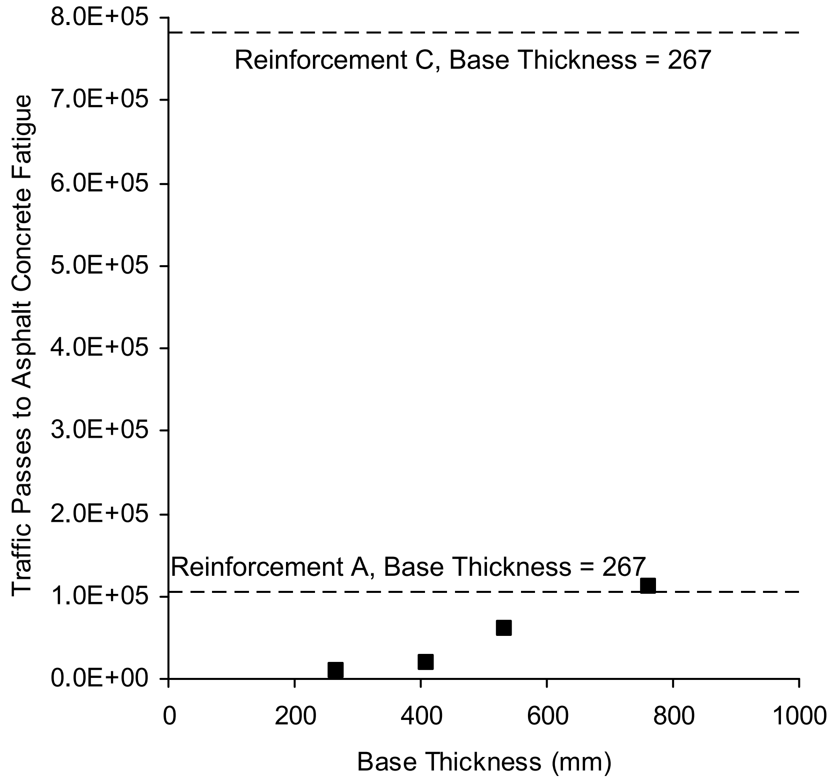

Figure 7.2.2 Fatigue life vs. base thickness for Low-Weak case

In terms of fatigue life, Figure 7.2.2 shows large potential reductions in base course thickness. As an example, consider the results for reinforcement A. Figures 7.2.1 and 7.2.2 can be used to estimate the number of traffic passes for 25 mm of rut and fatigue life for an unreinforced base course thickness of 725 mm, yielding 3,022,000 traffic passes for 25 mm rut and 103,000 passes for fatigue life. This base course thickness was chosen since it produced the same passes to fatigue life as the reinforced section with geosynthetic A. This results in a base reduction of 63 % from 725 mm to 276 mm for an equivalent fatigue life. Since fatigue life controls both the unreinforced and reinforced designs, this is also the base thickness reduction that would control the overall design of the section. For geosynthetic C, an even greater base reduction would be seen for the controlling case of fatigue.

An additional section within the high traffic / firm subgrade case was examined to evaluate base course thickness reduction. An unreinforced section of 544 mm thickness was created having otherwise the same properties as the unreinforced High-Firm section. Figures 7.2.3 and

7.2.4 show base thickness versus traffic passes to 25 mm rut and fatigue life for the two base thicknesses examined. Also shown on these figures are the traffic passes carried by each reinforced section having a base thickness of 178 mm. Recognizing that the curve between these two points is only an approximation, the procedure used above indicates base thickness reductions of 26 and 4 % for geosynthetics C and A based on rutting. As with the Low-Weak case, high base thickness reductions are seen for the failure mode of fatigue.

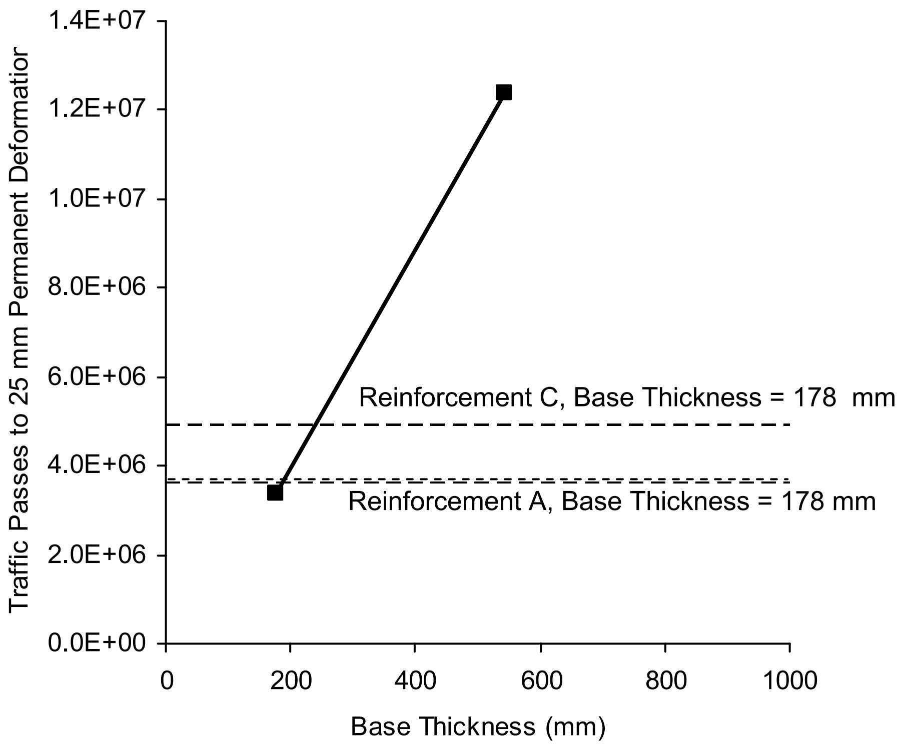

Figure 7.2.3 Traffic passes to 25 mm permanent surface deformation vs. base thickness for High-Firm case

Intuitively, the base course reductions associated with the failure mode of asphalt fatigue appear high. It should be noted, however, that documented results from test sections, field trials or long term field installations where both unreinforced and reinforced test sections failed by asphalt fatigue are unavailable. The base thickness reductions for the case of low traffic / weak subgrade based on rutting appear to be in line with results from test sections. The base thickness reduction based on rutting for the high traffic / firm subgrade case has not been confirmed by documented results from test sections or field trials.

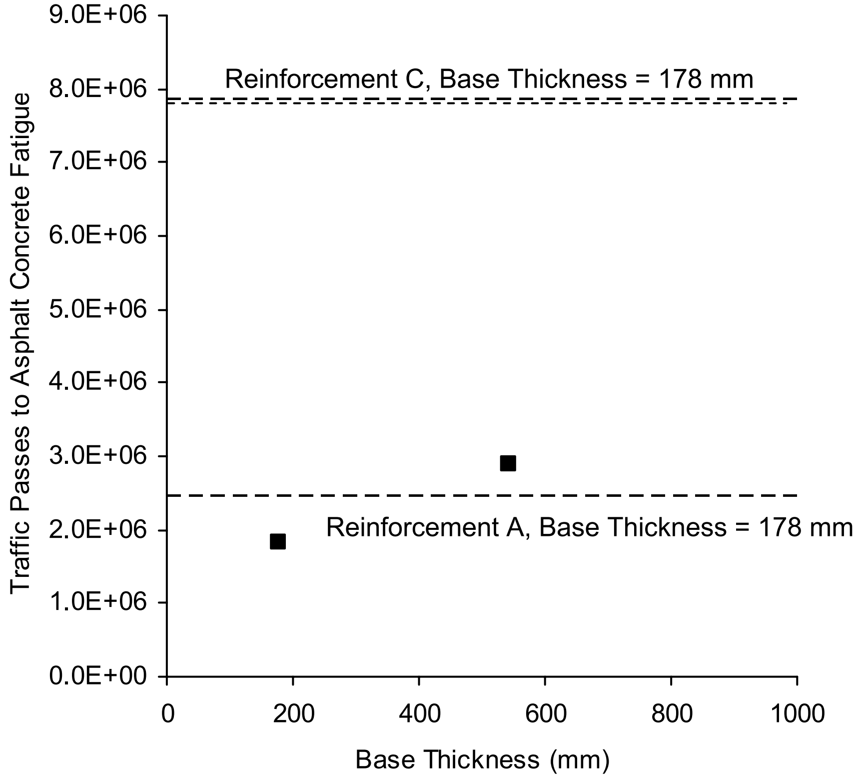

Figure 7.2.4 Fatigue life vs. base thickness for High-Firm case

8.0 MATERIAL MODEL STUDY

Unreinforced response models were set up following the procedures described in Section 4.1. The models were given the material properties listed in Table 8.0.1. Different models were created where the following material models were used for the base aggregate layer and where the properties used for these material models were listed in Tables 3.3.1 – 3.3.5. For the isotropic non linear elastic with tension cutoff model, the properties for the MSU aggregate listed in Table 3.2.6 were used.

1. Isotropic Linear Elastic (ILE)
2. Anisotropic Linear Elastic (ALE)
3. Isotropic Linear Elastic with Tension Cutoff (ILE-TC)
4. Anisotropic Linear Elastic with Tension Cutoff (ALE-TC)
5. Isotropic Non Linear Elastic with Tension Cutoff (INLE)
6. Anisotropic Non Linear Elastic with Tension Cutoff (ANLE)

Table 8.0.1 Material layer properties for material model study

Layer	Unit Weight (kN/m^3)	Poisson's Ratio, ν	Elastic Modulus (MPa)				
Asphalt Concrete	23	0.264	3895				
Reinforcement C	---	0.25	928				
				g_1^P	k_1^P	τ_1	
Base (overlay)	0	0.25	16.32	1.0	1.0	0.01	
Subgrade (overlay)	0	0.25	12.94	1.0	1.0	0.01	
			p_a (kPa)	k_1	k_2	k_3	T_c (kPa)
Subgrade (finite)	18	0.25	101.3	139	0.187	-3.281	0.001
Asphalt Concrete Permanent Deformation Properties							
	T (ºF)	k_1	k_2	k_3	β_1	β_2	β_3
Asphalt Concrete	68	-3.3426	1.734	0.4392	0.15	0.892	0.275
Unbound Layer Permanent Deformation Properties							
			$\varepsilon_o/\varepsilon_r$	ρ	β	ξ_1	ξ_2
Base			88.7	7440	0.127	0.457	2.36
Reinforced Base			102	13.7E06	0.127	0.457	2.36
Subgrade			4690	4.13E26	0.0361	0.8552	0.9983
Interface Contact Properties							
			μ	E_{slip} (m)			
Reinforcement-Aggregate Interface: Compaction Module			1.473	0.0001973			
Reinforcement-Aggregate Interface: Traffic I & III Modules			1.473	0.0003496			
Interface Shear Stress Growth							
			A	B			
Reinforcement C			40.5	0.41			

The properties of these models were adjusted to the values given in Tables 3.3.1 – 3.3.5 to produce a similar permanent surface deformation versus traffic pass response. Figure 8.0.1 shows this response for the 6 unreinforced response models showing the similarity obtained between the six unreinforced sections. Table 8.0.2 lists the predicted fatigue life of each unreinforced section.

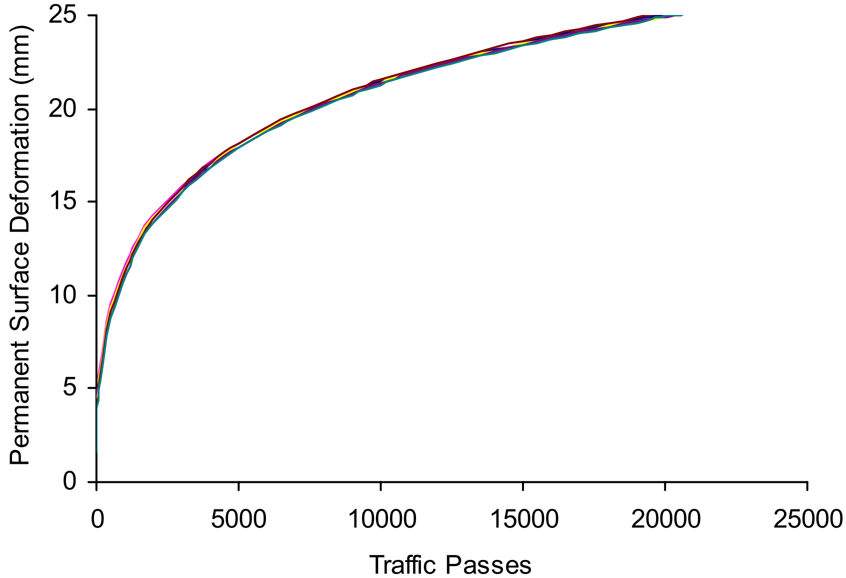

Figure 8.0.1 Permanent surface deformation vs. traffic passes for unreinforced material model study cases

Table 8.0.2 Asphalt concrete fatigue life for unreinforced material model study cases

Case	Fatigue Life
ILE	8,909
ALE	6,087
ILE-TC	6,547
ALE-TC	5,319
INLE	8,400
ANLE	7,622

Reinforced response models were created for each of the 6 cases described above using the reinforcement properties listed in Table 8.0.1 and following the procedures established in Section 5. Figure 8.0.2 shows the predicted permanent surface deformation versus traffic passes for each of the reinforced models. The curve for the unreinforced section using the ILE model is also shown on Figure 8.0.2 for purposes of comparison. Figure 8.0.3 shows the predicted fatigue life for each reinforced section compared to the average of the fatigue life for the unreinforced sections. Figures 8.0.2 and 8.0.3 show that the ability of the reinforced response model to illustrate significant effects from the reinforcement improves as tension cutoff is added to the material model for the base aggregate but improves considerably more when a non linear material model is used. Given that the reinforced response models have been formulated to show effects from increases in confinement in the base aggregate layer, a non linear stress dependent model is expected to show the greatest effects from reinforcement. The addition of anisotropy to the base aggregate material model does not appear to offer any advantages to the ability to show reinforcement effects.

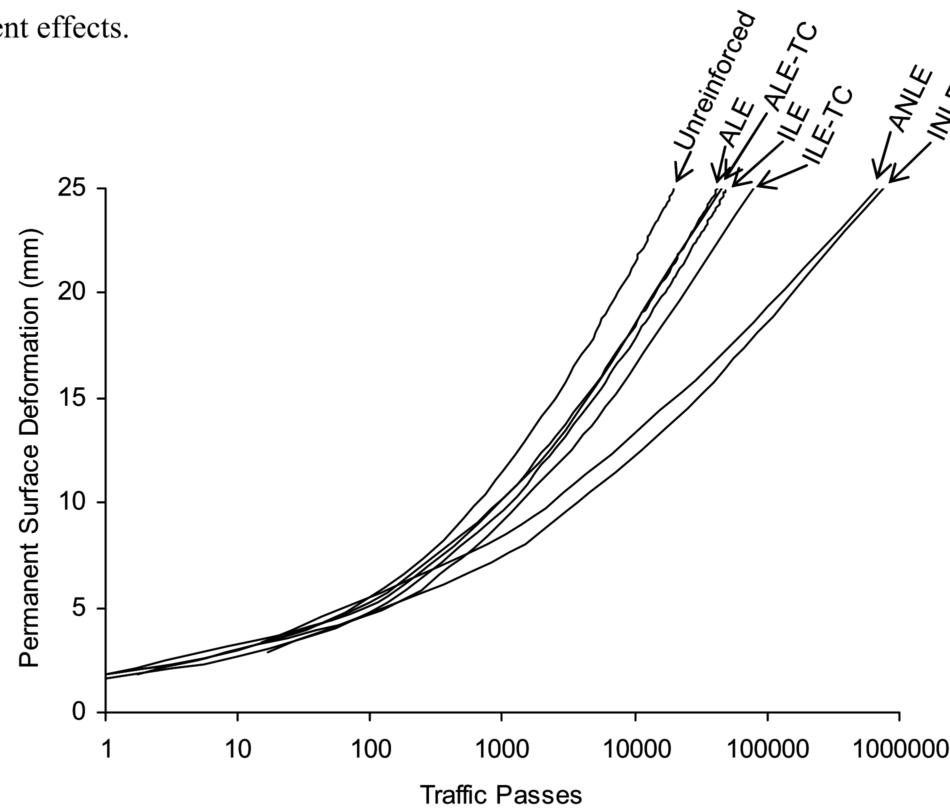

Figure 8.0.2 Permanent surface deformation vs. traffic passes for reinforced material model study cases

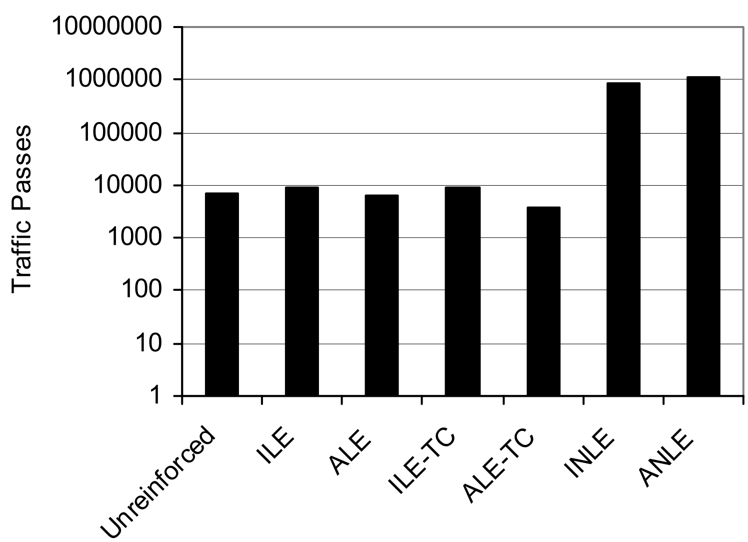

Figure 8.0.3 Fatigue life for reinforced material model study cases

9.0 SUMMARY AND DISCUSSION OF PROPOSED METHOD

The purpose of this section is to provide a summary of the methods developed in this project for reinforced pavements and a discussion of some of the key features associated with these methods. Reference is given to the appropriate sections where these methods have been developed in detail. This section also provides a flow chart and discussion of implementation steps that are needed in the NCHRP 1-37A Design Guide software to include results from this project. It should be noted that many of the steps summarized in this section are needed to implement the proposed methods in existing NCHRP 1-37A Design Guide software but will be transparent to the end user. In Section 10.5, the additional steps required of the end user beyond those contained in the NCHRP 1-37A Design Guide are summarized.

Reinforced pavements are designed and evaluated by first establishing the material properties for material and damage models for the layers and components of the system. Table 9.0.1 summarizes these models proposed for reinforced pavements and describes which models are part of the existing NCHRP 1-37A Design Guide and which are new models proposed in this study. These models and parameters consist of:

Table 9.0.1 Material and damage models proposed in this study for reinforced pavements

	Mechanistic Models		Empirical Models	
	NCHRP 1-37A Material Models	New Material Models	NCHRP 1-37A Damage Models	New Models
Asphalt Concrete	• Dynamic Modulus		• Permanent Deformation • Fatigue	
Unbound Aggregate	• Non-Linear Elastic with Tension Cutoff		• Permanent Deformation of Unreinforced Aggregate	• Permanent Deformation of Reinforced Aggegate
Reinforcement-Aggregate Interaction		• Coulomb Friction		• Interface Shear Stress Growth
Reinforcement		• Isotropic Linear Elastic		
Subgrade Soil	• Non-Linear Elastic with Tension Cutoff		• Permanent Deformation	

1. Asphalt Concrete
   a. Material Model and Parameters: The material model used in the finite element response model is a linear elastic model. The elastic modulus is taken as the dynamic modulus determined from tests and equations contained in Section 3.1.1. Poisson's ratio is computed from equations given in Section 3.1.1.
   b. Damage Model for Permanent Deformation: The parameters for permanent deformation are determined from equations and parameters given in Section 3.1.2.
   c. Damage Model for Fatigue: The parameters for fatigue are determined from equations and parameters given in Section 3.1.3.
   d. All material and damage models for the asphalt concrete are from the NCHRP 1-37A Design Guide.
2. Unbound Base Aggregate
   a. Material Model and Parameters: The material model used is an isotropic non linear elastic with tension cutoff model corresponding to that used in the NCHRP 1-37A Design Guide. Parameters for the model are determined from resilient modulus tests described in Section 3.2.1. Work performed in this project has shown that the material parameters for this model do not change when reinforcement is present. The stress state in the aggregate changes which in turn changes the modulus of the aggregate when reinforcement is present.
   b. Damage model for Permanent Deformation of Reinforced Aggregate
      i. The modified Tseng and Lytton model is used as the basis for describing permanent deformation in the reinforced aggregate. This model was described in Section 3.2.2. Basic parameters for the model are determined from tests on unreinforced aggregate according to the procedures described in Section 3.2.2 and corresponds to the model used in the NCHRP 1-37A Design Guide. Work performed in this project has shown that for aggregate in the pavement cross section within a zone of reinforcement and within a zone of stress states above a threshold degree of mobilization, reinforcement has the effect of changing two of the parameters contained in the permanent deformation model. These changes are expressed as reinforcement ratios defined as the ratio of this parameter for reinforced aggregate to that of the unreinforced aggregate. These reinforcement ratios are used to modify the unreinforced values for

any set of aggregate parameters and for any reinforcement material. This approach is consistent with the NCHRP 1-37A Design Guide where default values are used for the permanent deformation parameters for unreinforced aggregate. Table 3.4.8 lists the reinforcement ratios used.

ii. The zone of reinforcement where the reinforcement ratios described above apply is equal to distance of 150 mm. For cases where the reinforcement is placed within the base layer, the zone of reinforcement described above is taken above and below the layer of reinforcement.

iii. Within the zone of reinforcement, only the elements having a stress state above a degree of friction mobilization equal to 30 degrees are assigned reinforced permanent deformation properties. This provision is what allows thick pavement sections where the reinforcement is deep in the section to not have predicted improvements from the reinforcement.

iv. While the work performed in this project showed the difficulty of distinguishing reinforcement ratios between different products and the need to develop average reinforcement ratios for reinforcement products as a whole, there may still be a need to have a limiting material specification for this application such that these reinforcement ratios are not applied to an inappropriate reinforcement product. It may also be expected, however, that the use of actual material properties for the reinforcement and reinforcement-aggregate interface for such inappropriate products would result in negligible improvement in spite of the use of the reinforcement ratios described above.

v. It should be noted that even though the same reinforcement ratios are used for all reinforcement products, differentiation between products is still made through the material and interface properties used for a particular product.

c. Damage Model for Permanent Deformation of Unreinforced Aggregate: Any aggregate not falling within the reinforced zone described above uses the model and parameters described in Section 3.2.2. This model corresponds to that used in the NCHRP 1-37A Design Guide.

3. Unbound Subgrade
   a. Material Model and Parameters: The material model used is an isotropic non linear elastic with tension cutoff model corresponding to that used in the NCHRP 1-37A Design Guide. Parameters for the model are determined from resilient modulus tests described in Section 3.2.1.
   b. Damage Model for Permanent Deformation: The model and parameters described in Section 3.2.2 are used. This model corresponds to that used in the NCHRP 1-37A Design Guide.
4. Reinforcement Materials: An isotropic linear elastic material model was used in the finite element response model in this project. The elastic modulus used in this model was computed as an equivalent modulus from 4 elastic constants describing the true orthotropic properties of the material. Equivalent Poisson's ratio was taken as 0.25 when computing the equivalent isotropic elastic modulus. The equation used to determine the equivalent isotropic elastic modulus is given in Section 3.5.5. The tests used to establish the four orthotropic elastic constants used to calculate the equivalent isotropic elastic modulus are:
   a. Cyclic strain-controlled tests were used to determine an elastic modulus in the machine and cross machine directions. This modulus was computed as a resilient modulus after a large number of load cycles were applied at a given permanent strain value. Certain materials showed the modulus to change with permanent strain, while others showed a constant value of modulus with permanent strain. In this project, no attempt was made to account for the non linear nature of modulus with permanent strain. Improvements in this model would be to include a means of calculating an equivalent isotropic modulus from orthotropic values that were a function of permanent strain in the reinforcement.
   b. Limited biaxial loading tests were examined for use in determining the in-plane Poisson's ratio (being the 3rd orthotropic property needed to calculate the equivalent isotropic modulus). This test shows promise in providing this material property but needs to be examined in more detail.
   c. Aperture stability modulus tests were proposed to determine the in-plane shear modulus (being the 4th orthotropic property needed to calculate the equivalent isotropic modulus). The test appears to yield reasonable values for geogrid materials but artificially high

values for woven geotextiles. Work is needed to establish reasonable values for use with non geogrid reinforcement materials.

5. Reinforcement-Aggregate Interaction: Cyclic pullout tests were performed following a protocol similar to a resilient modulus test. From these tests, an interface shear modulus was determined and was shown to be a function of normal stress and shear stress on the interface. An equation similar to that used for resilient modulus of unbound aggregate was used to describe the dependency of interface shear modulus on normal and shear stress. In the models used in this project, this shear modulus was related to the Coulomb friction parameter E_{slip} along with an appropriate value of coefficient of friction. An appropriate shear and normal stress state was used in calculating these values. An improvement to the model would be to directly express the interface shear modulus by the stress-dependent equation developed. Since slip is rarely seen in these models, specification of a coefficient of friction should not be necessary.
6. Interface Shear Stress Growth: Experimental results of permanent and resilient strain in the geosynthetic as a function of traffic load applications is used along with theoretical considerations to express the permanent shear stress acting between the base aggregate and the geosynthetic in terms of the resilient interface shear stress and the number of applied traffic loads (Section 3.7). The empirical expression of the ratio of permanent to resilient reinforcement strain has currently been obtained from test section data for three reinforcement products. Data from existing and new test sections will need to be evaluated to develop this expression for other reinforcement products and to see if this expression can be related to more fundamental reinforcement material and interface properties.

With these material models and parameters, the following steps are taken to establish reinforced pavement response models:

1. A reinforced response model mesh is established by following the guidelines described in Section 5.1 and assigning the material properties described above.
2. A Compaction response model module is created by the following steps:
   a. The reinforced response model developed in step 1 is used.

b. If the reinforcement is placed between the base and subgrade layers, the reinforcement-subgrade contact surface is given a large value of E_{slip} (E_{slip} = 1 m) to simulate a nearly frictionless surface. If a model is used where the interface shear modulus is directly specified, this value should be set to a low value (1 kPa).

c. For the reinforcement surfaces in contact with base aggregate, values of E_{slip} and μ are established by:

   i. The coefficient of friction, μ, is set equal to a value determined from standard pullout or direct shear tests.

   ii. The normal stress on the interface is taken as the overburden pressure due to the self-weight of the materials above the interface.

   iii. The shear stress on the interface is calculated as the product of the normal stress and coefficient of friction.

   iv. The interface shear modulus is calculated from Equation 3.6.6.

   v. E_{slip} is calculated from the normal stress, coefficient of friciton and interface shear modulus from Equation 3.6.7.

   If a non linear model for interface shear modulus according to Equation 3.6.6 is used directly in the model, then steps i-v would not be necessary.

d. The asphalt concrete is given a small value (1 kPa) for elastic modulus.

e. A geostatic initial stress state is established using an earth pressure coefficient of 1 for all layers.

f. The reinforcement is assigned a thermal coefficient of expansion (α) equal to 1.0 $(°C)^{-1}$ and an initial temperature of 0.0 °C.

g. A temperature decrease of 0.01 °C is applied to a region of the reinforcement extending from the centerline of the model to a radius of 450 mm.

h. Horizontal stresses at the element centroid are extracted from the model once the temperature decrease has been applied for a column of elements above the base along the model centerline.

i. These horizontal stresses, along with the geostatic vertical stresses due to material self-weight, are used as the initial stresses for the entire base layer in the Traffic I and Traffic II response model modules.

3. A Traffic I response model module is created by the following steps:
   a. The response model created in step 1 is used.
   b. The asphalt concrete layer is given appropriate elastic properties for the problem.
   c. For interfaces between the reinforcement and the aggregate, the interface property E_{slip} is set to a value calculated from the 5 steps described in step 2 c and using values for normal stress of 35 kPa and shear stress of 5 kPa. If a non linear model for interface shear modulus according to Equation 3.6.6 is used directly in the model, then this step would not be necessary.
   d. If the reinforcement is placed on the subgrade, the reinforcement-subgrade interface is given Rough contact properties.
   e. Initial horizontal stresses for the aggregate base layer are set equal to those determined for the compaction model. Vertical initial stresses in the base layer are set equal to geostatic values. Vertical and horizontal initial stresses in all other layers are set equal to geostatic values with and earth pressure coefficient of 1.
   f. Pavement load is applied as a load step.
   g. The interface shear stress distribution for both interfaces is extracted from the model for all node positions along the interface and summed to yield values of shear stress versus model radius.
   h. The values of interface shear stress from step g are used as the resilient shear stress in Equation 5.3.1 and along with Equation 5.3.2 the permanent interface shear stress distribution is calculated for a series of permanent to resilient reinforcement strain ratios corresponding to different points in the life of the pavement.
   i. Equivalent nodal forces are determined from the interface shear stress distributions determined in step h.
4. Traffic II response model modules are created for each of the equivalent nodal force distributions from step 3 i. This is accomplished by:
   a. An unreinforced model having the same geometry and layer properties as the reinforced model is created.
   b. Initial horizontal stresses for the aggregate base layer are set equal to those determined from the compaction model. Vertical initial stresses in the base layer are set equal to

geostatic values. Vertical and horizontal initial stresses in all other layers are set equal to geostatic values with an earth pressure coefficient of 1.

c. Nodal forces from step 3 i are applied as a load step in a series of models for each nodal force distribution.
d. Horizontal stresses at the element centroid are extracted from the model once the nodal forces have been applied for a column of elements in the base along the model centerline.
e. These horizontal stresses, along with the geostatic vertical stresses due to material self-weight, are used as the initial stresses for the entire base layer in the series of Traffic II response model modules.

5. Traffic III response model modules are created by:
   a. The reinforced response model corresponding to the Traffic I model is used.
   b. A series of models are created by inserting the stresses from step 4 e as initial stresses into the model from step 5 a.
   c. Pavement load is applied to each response model.
   d. Maximum tensile strain in the asphalt concrete layer and vertical strain in the pavement layers is extracted for each response model.
   e. Principal stresses or measures of the first and second invariants of stress are extracted for elements along the model centerline in the base aggregate and used to calculate a mobilized friction angle.
   f. Superposition of the strain and stress measures from steps 5 d and e for cases of dual or multiple wheel loads is used to calculate worse case superimposed strain values.

Response measures from step 5 d for the series of response models created and analyzed in step 5 are used to determine asphalt concrete fatigue life and permanent surface deformation by the following steps:

1. Each data set of vertical strain versus depth in the pavement layers is used to determine permanent surface deformation versus traffic passes using permanent deformation models for the asphalt concrete, unreinforced and reinforced aggregate, and subgrade materials.
2. The permanent deformation properties for the reinforced aggregate are calculated by applying reinforcement ratios given in Table 3.4.8 to unreinforced aggregate properties.

3. The zone in which the reinforced permanent deformation properties apply is equal to the minimum of 150 mm or the zone in which the mobilized friction angle (calculated from step 5 e) exceeds 30 degrees. For cases where the reinforcement rests on the subgrade, this zone extends above the reinforcement. For cases where the reinforcement is placed in the base aggregate layer, this zone extends both above and below the reinforcement.
4. The cumulative permanent surface deformation curve is generated by:
   a. Assume the number of traffic passes to reach 25 mm of permanent surface deformation.
   b. Calculate the number of traffic passes corresponding to the permanent to resilient reinforcement strain ratios used to generate each data set of vertical strain versus depth by Equation 3.7.1.
   c. Sum the permanent surface deformation accumulated over each analysis period to determine the cumulative permanent surface deformation.
   d. Adjust the number of traffic passes to reach 25 mm of permanent surface deformation in Equation 3.7.1 until the cumulative curve produces 25 mm of permanent surface deformation in this number of traffic passes. This is a trial and error procedure that is generally accomplished within 5 trials.
5. Asphalt fatigue life is determined by using Equation 5.5.4 along with the asphalt tensile strain data from step 5 d and traffic passes for each analysis period from step 4.

10.0 RESEARCH NEEDED

In order to reduce the time needed for implementation of the results of this project, the approach taken in this research project was to use, whenever possible, established methods for material modeling and testing, response modeling and damage modeling. In the course of this research effort, several areas were identified where existing techniques and methods were insufficient for providing tools needed for describing reinforced pavement response. These areas broadly fall under the categories of material modeling, material testing, response model development, and validation of predictions. Work was performed both within and outside this project to provide methods for the new areas identified. In some cases, promise was shown with the methods developed, yet further development is needed. In this section, a description of the areas where additional research is needed is provided.

10.1 Material Modeling

New models were introduced in this project for components associated with the reinforcement materials. In particular, a material model for the reinforcement, a shear interaction model for the reinforcement-aggregate interface and a permanent interface shear stress growth model was introduced. The model used for the reinforcement was an isotropic linear elastic model where the elastic modulus was computed as an equivalent modulus from 4 in-plane elastic properties corresponding to an orthotropic material. Testing work described in the next section showed that the two elastic moduli corresponding to the two principal directions of the material varied with the permanent strain. Therefore, an isotropic non linear elastic material model should be used for the reinforcement where the equivalent elastic modulus is calculated from the techniques developed in this project for the values of the two elastic moduli as functions of permanent strain in the reinforcement. Information on permanent strain in the reinforcement will be obtained from the permanent to resilient strain equation used in the interface shear stress growth equations (i.e. Equation 3.7.1).

Cyclic pullout testing showed that the interface shear modulus was dependent on the normal and shear stress on the interface. A non linear stress dependent model for interface shear modulus corresponding to Equation 3.6.6 should be developed and implemented in the pavement response model.

10.2 Material Testing

Testing methods for components associated with the reinforcement were examined to provide parameters pertinent to pavement applications where dynamic strains and displacements are relatively small and repeated. Provided below is a list of testing methods where additional work is needed to establish testing protocols.

1. The cyclic wide-width tension tests showed great promise for providing values of elastic modulus for the two principal directions of the material. These tests are modeled after the existing ASTM standard wide-width tension tests (ASTM D4595 for geotextiles and ASTM D6637 for geogrids) with the exception of the cyclic loading protocol. Additional work is needed to establish the most efficient loading protocol for this test and to evaluate this test for other reinforcement products. In particular, it may be seen that loading to a particular

permanent strain followed by stress relaxation or creep and subsequent reloading provides the same information without the need to provide load cycles. Additional testing should also be performed to establish the influence of strain rate, temperature and confinement on measured elastic modulus for conditions pertinent in pavements. Once the loading protocol is established, it could be added to the ASTM standard through the ASTM reinforcement in pavements task group that was set up as part of the implementation effort in this project.

2. The biaxial loading test for determining Poisson's ratio should be further evaluated. Issues pertinent to this test include whether a loading protocol similar to that used for the tension tests described in item 1 are necessary for this test. This test should also be evaluated for a range of geosynthetic materials to see if reasonable values are obtained.
3. The torsional rigidity test method used for evaluating the in-plane shear modulus is currently being reviewed by ASTM for standardization. Additional work is needed to establish values for in-plane shear modulus for non geogrid materials.
4. The cyclic pullout testing described in this report showed great promise for describing a stress dependent interface shear modulus. The test is based on the existing ASTM standard for pullout (ASTM D6706) with the exception of the specimen length and cyclic loading protocol. Further development work is needed for this test to establish appropriate specimen dimensions, instrumentation and loading conditions needed for meaningful and repeatable results. The existing standard could be readily modified by the ASTM reinforcement in pavements task group.
5. The interface shear stress growth model was developed from test section data for three geosynthetics. Data from other test sections should be examined to see if similar data is obtained. Additional test section work may be needed to produce this data for other reinforcement products. Work should be performed to see if the shear stress growth parameters can be related to other reinforcement and interaction material properties.

10.3 Response Modeling

For the response models developed for reinforced pavements, several steps should be taken to determine if streamlining of the methods developed is possible. These steps include:

1. Examine if simpler (i.e. isotropic linear elastic) models can be used for the compaction, traffic I and traffic II response model modules for the unbound aggregate and subgrade layers while still providing similar confinement (lateral stress) values seen when using the isotropic non linear elastic models for the base and subgrade layers. This would reduce computational time associated with these modeling steps.
2. Examine whether interface slip occurs in any of the reinforced response model modules, thereby indicating whether a coefficient of friction is needed for the interface model.
3. The procedure developed in this project requires the traffic II and III models to be run multiple times for different pavement life periods corresponding to different values of permanent to resilient reinforcement strain ratio within the shear stress growth equation. The cumulative permanent surface deformation curve and the fatigue life resulting from the combination of these analyses may be approximated from a single analysis at an appropriately selected value of permanent to resilient reinforcement strain ratio. This would eliminate the need to run multiple traffic II and III models for different permanent to resilient reinforcement strain ratios.
4. Verify that the use of aggregate permanent deformation reinforcement ratios in pavement sections using weak reinforcement products results in negligible improvement from the reinforcement.
5. A larger number of cases involving placement position of the reinforcement within the base course layer should be examined to arrive at general recommendations for reinforcement placement position.

10.4 Validation

Results from the sensitivity study showed effects from the reinforcement for pavement cross sections that have not been examined by the construction of test sections. Additional test sections should be constructed to validate results for the following cases:

1. Test sections with thicker pavement layers and stronger subgrades should be constructed to validate the rutting benefits seen in the sensitivity study. If results from these test sections show negligible benefit in comparison to the model predictions, means of reducing the contribution from the compaction model by using a temperature drop whose magnitude

decreases with increasing subgrade stiffness could be examined and calibrated from the test sections. This work may also point to the need to use temperature drops of greater magnitudes than those used in this project for situations where soft yielding subgrades are present.

2. The benefit of reinforcement on asphalt concrete fatigue should be established and experimentally verified to validate the large benefit values seen in this project.

11.0 IMPLEMENTATION

11.1 Completed Activities

Implementation through technology transfer and outreach were key components of this study. Technology transfer and outreach activities have included project team member participation, including presentations on the progress of this research in national and international committees, societies and conferences, and liaison with the GMA. National and international committees include the TRB committee A2K07 and A2K07(2), the AASHTO Subcommittee on Materials Section 4E task group on geosynthetics, and European COST committees. Presentations on the progress of the work have also been given at technical society conferences including the North American Geosynthetics Society (NAGS) biannual Conference and the International Geosynthetics Society (IGS) Conference. The complete implementation program is included in Appendix B.

Pending approval of the final report by FHWA, a section on base reinforcement in pavement sections outlining the design method developed in this study will be included in the FHWA/NHI course on Geotechnical Aspects of Pavements (NHI Course No.132040), which is under development at this time. A summary of the procedure will also be submitted to FHWA for inclusion in the FHWA/NHI document "Geosynthetic Design and Construction Guidelines Participant Notebook (Publication No. FHWA HI-95-038) and associated National Highway Institute Course No. 13213.

In order for this work to move forward and be available to end users, a project will need to be initiated involving incorporation of these methods in the existing NCHRP 1-37A Design Guide software with an addendum to this guide issued. Once this is completed, the end user will see the following requirements in addition to those contained in the NCHRP 1-37A Design Guide needed to design reinforced pavements.

1. Identification of material properties for the reinforcement.
2. Identification of interface properties between the reinforcement and the base aggregate layer.
3. Identification of the shear stress growth function for the reinforcement-aggregate interface.

As can be seen from this list, the additional requirements fall exclusively within the category of material property identification; all other details of the method should be handled internal to the software. As described in Section 10.3, several research areas have been identified to establish material testing methods for defining properties listed in item 1-3 above. This work should start immediately such that these methods are firmly established prior to the execution of an implementation project for this work.

11.2 Implementation in the NCHRP 1-37A Design Guide Software

A conceptual flow chart for the NCHRP 1-37A analysis procedure is given in Figure 11.2.1. The major components are: (a) data input and analysis preparation; (b) pavement response analysis using either using multilayer elastic theory or nonlinear finite element analysis, depending upon whether nonlinear unbound material behavior is to be considered in the analysis; and (c) distress prediction and accumulation. It is important to remember that the NCHRP 1-37A procedure tracks seasonal variations in pavement properties and response. Consequently, a separate set of analyses is required for each analysis subseason (typically two to four weeks duration). Pavement distresses are accumulated over all subseasons in the analysis period (i.e., pavement design life).

Material properties (e.g., temperature-dependent asphalt stiffness) and pavement sublayering (e.g., to reflect changing freeze/thaw conditions) will in general vary from one analysis subseason to the next. These seasonal variations affect all stresses and strains within the pavement structure, including those in the reinforced base layer. Within each analysis subseason, a suite of analyses must be performed corresponding to the different traffic load levels defined by the traffic spectra. The material properties and pavement sublayering are held constant while the analysis marches in increasing magnitude through the various traffic load levels of interest.

The implementation of the reinforced pavement analysis methodology developed in this project into the NCHRP 1-37A software should be relatively straightforward. Most of the required changes affect the nonlinear finite element analysis module in the NCHRP 1-37A software; by definition, the influence of geosynthetic reinforcement cannot be modeled using the linear multilayer elastic analysis option. The major changes to the existing software can be grouped into three categories: (a) analysis setup (preprocessing); (b) finite element analysis; and (c) distress prediction (post-processing). The required modifications to the NCHRP 1-37A software are detailed below for each category.

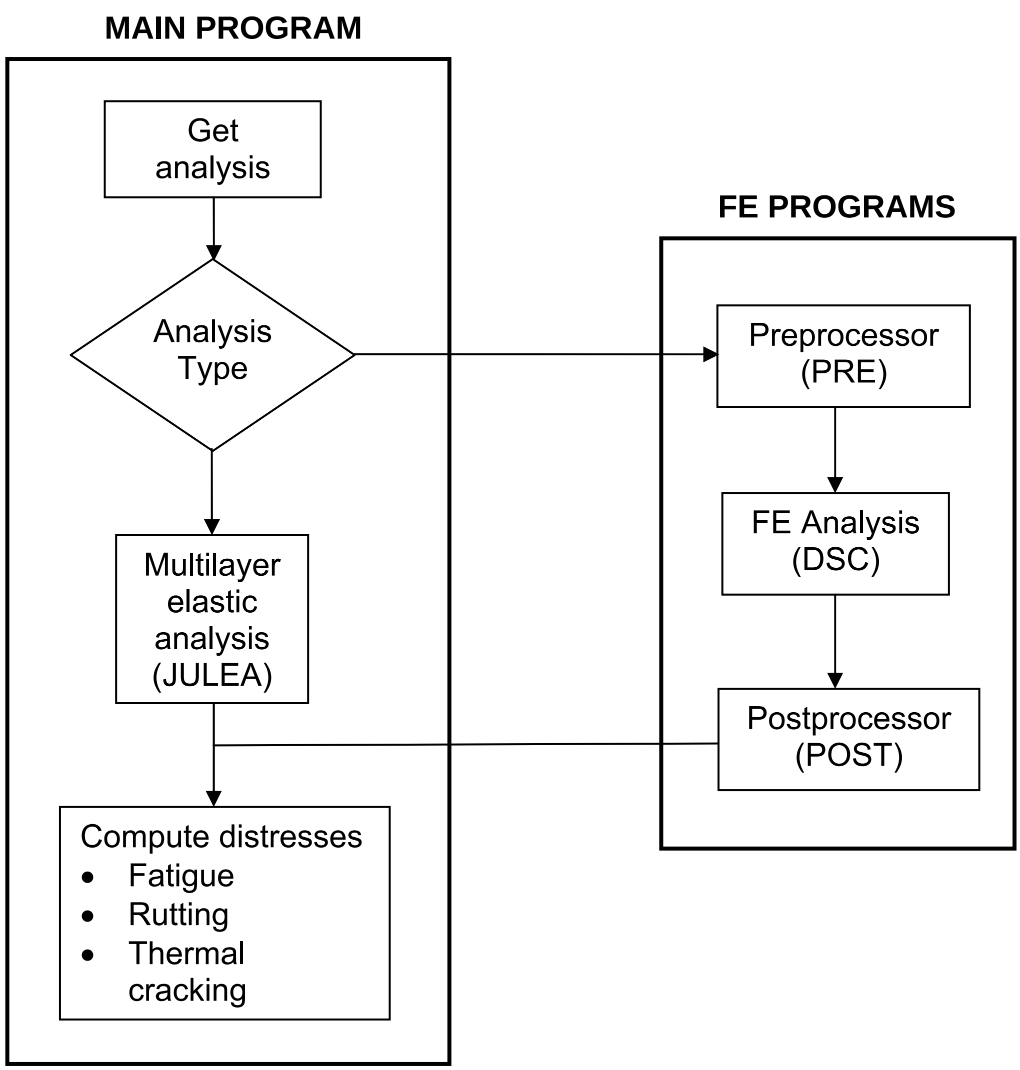

Figure 11.1.1 Conceptual flow chart for NCHRP 1-37A flexible pavement design analyses

11.2.1 Analysis Setup

1. The input screens must be modified to permit entry of the relevant material properties for the geosynthetic reinforcement layer (geosynthetic properties, interface properties, internal model parameters, etc.). Consistent with the other data entry for the NCHRP 1-37A, provision should be made for the entry of Level 1 (measured), Level 2 (determined from correlations), and Level 3 (default) input values.
2. The routines for generating the sublayers in the pavement structure must be modified to create a separate sublayer for the portion of the base layer within the zone of influence of the reinforcement (see Section 3.4.6). This generation of sublayers is done by the main program in the NCHRP 1-37A software, upstream from the actual finite element analysis.
3. The finite element mesh generator module (PRE program) must be modified to create the membrane elements and associated layer interface elements for the geosynthetic reinforcement.

11.2.2 Finite Element Analysis (DSC Module)

1. Membrane elements must be added. The NCHRP 1-37A analysis program currently does not include membrane elements within its element library. However, the formulation for these elements is quite standard and can be easily implemented.
2. The elastic-frictional slip interface material model (see Sections 3.6.2 and 3.6.3) must be added. Although the NCHRP 1-37A finite element analysis software already includes layer interface elements, the only material model implemented for these elements is a linearly-elastic response in terms of normal and shear stiffnesses. An elastic-frictional slip material model is required for the interfaces at the geosynthetic reinforcement. Since the finite element code is already set up to do nonlinear analyses, incorporation of this nonlinear interface slip response should not require major effort.
3. The execution logic in the finite element analysis program must be modified to incorporate the Compaction, Traffic I, Traffic II, and Traffic III models. This will undoubtedly be the most significant of the modifications to the NCHRP 1-37A software. In the NCHRP 1-37A approach, a finite element solution must be calculated for each traffic load level within each subseason. A separate set of analyses is required for each subseason. Figure 2 shows a pseudo-code outline of the finite element analysis procedure implemented in the NCHRP 1-

37A software. The additional steps required to incorporate the reinforced base analysis methodology developed in this project are shown in bold in the figure. Additional considerations related to each of the reinforced base analysis submodels are as follows:

- *Compaction Model*: As described in Section 4.3.2, compaction effects on the initial horizontal stresses in the layer are simulated via an artificial thermal contraction of the geosynthetic membrane in the reinforced pavement analysis methodology. The NCHRP 1-37A finite element program is not currently set up to analyze thermal stresses and strains. However, this analysis capability is quite standard and can be easily incorporated. Note that the compaction model need only be executed once for each analysis subseason; the results can then be used for all traffic load levels within that analysis subseason.
- *Traffic I Model*: The Traffic I model (Section 4.3.3) computes the interface shear stresses in the reinforced pavement under each traffic load level. The initial horizontal stresses for the analysis are the results from the Compaction model; the initial vertical stresses are the usual geostatic *in situ* values. Note that the accumulated permanent strain is required to scale the computed resilient interface shear stress (see discussion in Section 4.3.3); this accumulated permanent strain must either be tracked within the finite element program or, preferably, passed to it as input from the distress accumulation routines in the main program. No additional modifications other than bookkeeping (e.g., extraction of the interface shear stresses and resilient strains) are required to execute the Traffic I model in the NCHRP 1-37A analysis software.
- *Traffic II Model*: The Traffic II model (Section 4.3.4) determines the additional horizontal stresses in the stress-dependent base layer material due to the interface shear stresses at each traffic load level as determined from the Traffic I model. The interface shear stresses are converted to equivalent nodal loads and applied to the mesh along the plane of the interface. The induced horizontal stresses at each element are computed and added to those determined in the Compaction model. No additional modifications other than bookkeeping (e.g., conversion of the interface shear stresses to equivalent nodal loads) are required to execute the Traffic II model in the NCHRP 1-37A analysis software.

- *Traffic III Model*: The Traffic III model (Section 4.3.5) computes the final critical pavement response parameters for the reinforced pavement structure at a given traffic load level. The initial horizontal stresses for the analysis are the combined values from the Compaction and Traffic II models; the initial vertical stresses are the usual geostatic *in situ* values. No additional modifications are required to execute the Traffic III model in the NCHRP 1-37A analysis software.

It should be noted that the NCHRP 1-37A finite element analysis routines in their present form already require substantial execution time.[1] Incorporating the reinforced pavement analysis models will increase this execution time significantly. The Compaction model adds one finite element solution per analysis subseason, which is insignificant in terms of the overall execution time. However, the Traffic I, Traffic II, and Traffic III computations must be performed for each traffic level within the analysis subseason. This will roughly triple the total execution time required to perform the finite element calculations within a single analysis subseason. Careful implementation and optimization of the algorithms will be required to minimize the time required for a solution.

[1] This is expected to improve in the future. At the time of this report, very little effort has been devoted by the NCHRP 1-37A software development team on optimization of the computational efficiency of the flexible pavement analysis routines. Significant effort and progress on increased computational efficiency is expected during the Design Guide implementation phase, however.

Get analysis input information (Main program)

Loop over analysis subseasons

    Begin finite element preprocessing (PRE module)
        Get input data for pavement structure, material properties, load levels
        Generate finite element mesh
        Write input file for finite element analysis
    End finite element preprocessing

    Begin finite element analysis (DSC module)
        Read input file created by PRE module
        Apply geostatic *in situ* vertical and horizontal stresses
        Begin Compaction model
            Set HMA modulus to low value
            Apply artificial thermal contraction to geosynthetic membrane elements
            Determine horizontal stresses in elements
            Reset HMA modulus to original value
        End compaction model
        Loop over traffic load levels (increasing magnitude)
            Begin Traffic I model
                Apply initial stresses from Compaction model
                Apply traffic wheel load (incremental analysis)
                Determine interface shear stresses
                Scale interface shear stresses via $\varepsilon_p/\varepsilon_r$ ratio
                Determine equivalent nodal loads for scaled interface shear stresses
            End Traffic I model
            Begin Traffic II model
                Deactivate geosynthetic membrane and interface elements
                Apply initial stresses from Compaction model
                Apply equivalent nodal loads for interface shear from Traffic I model
                Determine horizontal stresses in elements
                Reactivate geosynthetic membrane and interface elements
            End Traffic II model
            Apply wheel load (incremental analysis) to reinforced pavement mesh (**same as Traffic III model**)
            Write element stresses and strains to output file
        End loop over traffic levels
    End finite element analysis

    Begin finite element postprocessing (POST module)
        Read element stresses and strains from file created by DSC module
        Loop over axle types (tandem, tridem, etc.)
            Loop over wheels
                Superimpose critical pavement response parameters at critical pavement
                    locations for permanent deformation distress
                Write results to output file
                Superimpose critical pavement response parameters at critical pavement
                    locations for fatigue distress
                Write results to output file
            End loop over wheels
        End loop over axle types
    End finite element postprocessing

    Compute incremental and accumulated distresss (Main program)
        Fatigue distresses
        Permanent deformation distresses (**use modified permanent deformation properties**
            for base material within reinforcement zone of influence)

End loop over analysis seasons

Figure 11.1.2 Pseudocode outline of finite element calculations in the NCHRP 1-37A analysis software. Items in bold font are additions required for reinforced flexible pavement analysis.

11.2.3 Distress Prediction

The determination of critical response parameters due to multiple axle and wheel configurations is not changed by any of the reinforced pavement models; consequently, no modifications are required to the POST finite element post-processing module in the NCHRP 1-37A analysis software.

However, some changes will be required in the main program routines that compute and accumulate the incremental contributions to rutting. Within the zone of influence of the reinforcement, the modified Tseng and Lytton rutting model described in Section 3.4.7 must be used to determine the contribution of the reinforced zone to the overall rutting.

No changes are required to the main program routines that compute and accumulate the incremental fatigue damage in the asphalt layers. The critical tensile strains in the asphalt as output by the POST finite element post-processing program

12.0 CONCLUSIONS

Methods have been developed in this project for the design of flexible pavements whose base layer is reinforced with a geosynthetic layer. The methods fall within the framework of mechanistic-empirical methods and have been developed to be compatible with the NCHRP Project 1-37A Pavement Design Guide. The success of this approach in describing fundamental reinforcement mechanisms and pavement performance benefits shows the importance of mechanistic-empirical methods for treating new and complex pavement modeling problems that otherwise have had limited success with purely empirical approaches.

Material models and testing methods were developed for the pavement cross section components associated with the reinforcement. Models and testing methods were developed specifically for pavement applications where small strains and displacements are seen and where loads are repeated. The testing methods, which in all cases were based on extensions of existing test methods, showed promise in providing meaningful mechanistic based material properties that describe differences in performance seen between different geosynthetics. Additional work is needed to optimize these methods and to examine values for a wider range of geosynthetics, perhaps leading to the use of default values for preliminary design and other lower-level design solutions.

Large-scale reinforced resilient modulus and repeated load triaxial tests showed no difference between resilient modulus properties of reinforced and unreinforced aggregate but a significant difference in permanent deformation properties. Variability inherent in permanent deformation tests made it difficult to distinguish differences between reinforcement products. These tests were used to identify permanent deformation properties associated with the zone of reinforcement, the height of the zone of reinforcement above and below the reinforcement layer and the stress state needing to be mobilized prior to seeing a reduction in permanent deformation. These properties were expressed as general values for use with any reinforcement product.

Work in this project showed the need to include response modeling steps that account for fundamental mechanisms of reinforcement and the effect of these mechanisms on confinement of the base aggregate layer. In the absence of these additional response modeling steps, reinforced response models grossly underpredict the performance of reinforced pavements. Response model modules were created to account for reinforcement effects during construction and during vehicular loading of the pavement. These additional models provided a means of describing the increase in lateral confinement of the base aggregate layer seen during compaction of the aggregate layer and during vehicular loading. Results from large-scale reinforced repeated load triaxial tests provided a means of describing a zone of base aggregate over which permanent vertical strain was influenced by the reinforcement. Reasonable comparison of reinforced models to results from test sections using different reinforcement products was obtained with respect to permanent pavement surface deformation. This comparison also showed the ability of the methods developed for distinguishing between reinforcement products. This was accomplished in spite of the use of reinforced permanent deformation properties generic to all reinforcement products by the use of product specific material models for the reinforcement material and the reinforcement-aggregate shear interface, and interface shear stress growth models.

The sensitivity study performed in this project further showed the ability of the methods developed for distinguishing between reinforcement products. This study showed reasonable benefits from the reinforcement in terms of permanent surface deformation for pavement cross sections that agreed well with test sections. Modest rutting benefits were also seen for thick pavement sections and sections with a firm subgrade. Test sections have not been constructed under these conditions to verify these results. Results from the sensitivity study showed appreciable benefits in terms of asphalt concrete fatigue. Since most test sections have failed by rutting, these results have not been evaluated by test sections designed to fail by asphalt fatigue.

It should be noted that while the focus of this work has been on geosynthetic reinforcement products, the procedures developed are also equally applicable for other reinforcement sheets such as steel mesh grids.

13.0 REFERENCES

Adu-Osei, A., Little, D.N. and Lytton, R.L. (2001), *Transportation Research Record 1757*, Washington DC, USA, pp. 82 - 91.

Allen, T., Bell, J.R. and Vinson, T.S. (1983), "Properties of Geotextiles in Cold Regions Applications", *Transportation Research Record,* Report No. 83-6, Transportation Research Institute, Oregon State University, Corvallis, OR.

Andrei, D. (1999) "Development of a Harmonized Test Protocol for the Resilient Modulus of Unbound Materials Used in Pavement Design," unpublished Master of Science thesis, Department of Civil and Environmental Engineering, University of Maryland, College Park, MD.

ASTM (2003), *Annual Book of ASTM Standards*, Vol. 04.13, West Conshohocken, PA, USA.

Austin, D.N., Wu, K.J. and White, D.F. (1993), "The Influence of Test Parameters and Procedures on the Tensile modulus of Stiff Geogrids", *Geosynthetic Soil Reinforcement Testing Procedures,* STP 1190, S.C. Jonathan Cheng, Ed., ASTM, Philadelphia, PA, pp. 90-110.

Bathurst, R.J. and Cai, Z. (1994), "In-Isolation Cyclic Load-Extension Behavior of Two Geogrids", Geosynthetics *International*, Vol. 1, No. 1, pp. 1-19.

Bender, D.A. and Barenberg, E.J. (1978), "Design and Behavior of Soil-Fabric-Aggregate Systems", In *Transportation Research Record 671*, TRB, National Research Council, Washington, DC, 1978, pp. 64-75.

Berg R.R., Christopher, B.R. and Perkins, S.W. (2000), *Geosynthetic Reinforcement of the Aggregate Base Course of Flexible Pavement Structures, GMA White Paper II*, Geosynthetic Materials Association, Roseville, MN, USA, 130p.

Budiman, J., (1994), "Effects of Temperature on Physical Behaviour of Geomembranes", *Proceedings of the Fifth International Conference on Geotextiles, Geomembranes and Related Products*, Singapore, pp. 1093-1096.

Bush, D.I. (1990), "Variation of Long Term Design Strength of Geosynthetics in Temperatures up to 40° C", *Proceedings of the Fourth International Conference on Geotextiles, Geomembranes and Related Products*, The Hague, Netherlands, pp.673-676.

Calhoun, C.C. (1972), "Development of Design Criteria and Acceptance Specifications for plastic Filter Cloths", Army Engineer Waterways Experiment Station, Vicksburg, Mississippi. Technical Report No. S-72-7.

Cazzuffi, D. and Sacchetti, M. (1999), "Temperature Effects on Tensile-Creep behavior of High-Strength Geosynthetics", *Proceedings: Geosynthetics' 99 Conference*, 723-733.

Elias, V., Yuan, A., Swan, R. and Bachus, R. (1998), *Development of Protocols for Confined Extension/Creep Testing of Geosynthetics for Highway Applications*, U.S. Department of Transportation, Federal Highway Administration, Washington, D.C., Report No. FHWA-RD-97-143, 211p.

Hibbitt, Karlson and Sorensen (2002), *ABAQUS Standard User's Manuals*, Version 6.3-1, Pawtucket, RI, USA.

Hsuan, Y.G. (1998), "Temperature Effect on the Stress Crack Resistance of High Density Polyethylene Geomembranes", *Proceedings: Sixth International Conference on Geosynthetics*, Denver, CO, pp. 371-374.

Kinney, T.C. and Barenberg, E.J. (1982),"The Strengthening Effect of Geotextiles on Soil-Geotextile-Aggregate Systems", *Proceedings of the Second International Conference on Geotextiles*, Las Vegas, NV, USA, Vol. 2, 1982, pp. 347-352.

McGown, A. and Kupec, J. (2004), "A New Approach to the Assessment of the Behavior of Geogrids Subject to Biaxial Loading", *Proceedings of the Third European Geosynthetics Conferenc, EuroGeo 3*, Munich, Germany, March 2004.

McGown, A., Msukwa, T. and Jenner, C. (2002), "A Reassessment of the Contribution of Mesh Elements to the Load Carrying Capacity of Soil-Mesh Element Mixtures", *Proceedings of the Seventh International Conference on Geosynthetics*, 7 ICG, Nice, France, Vol. 4, pp. 1261-1264.

McGown, A., Andrawes, K.Z. and Yeo, K.C. (1985), "The Load-Strain-Time Behaviour of Tensar geogrids", *Proceedings: Polymer Grid Reinforcement*, pp. 11-17.

McGown, A. Andrawes, K.Z. and Kabir, M.H. (1982), "Load-Extension Testing of Geotextiles Confined In-Soil", *Proceedings of the Second International Conference on Geotextiles*, Las Vegas, NV, USA, Vol.3, pp. 793-798.

Moghaddas-Nejad, F. and Small, J.C. (2003), "Resilient and Permanent Characteristics of Reinforced Granular Materials by Repeated Load Triaxial Tests", *ASTM Geotechnical Testing Journal,* Vol. 26, No. 2, pp. 152-166.

NCHRP (2003), NCHRP Project 1-37A, *Development of NCHRP 1-37A Design Guide, Using Mechanistic Principles to Improve Pavement Design*, http://www.NCHRP 1-37A Designdesignguide.com/.

NCHRP (2000), *Harmonized Test Methods for Laboratory Determination of Resilient Modulus for Flexible Pavement Design, Volume 1, Unbound Granular Material*, NCHRP Project 1-28a Draft Report, 198p.

Perkins, S.W. (2002), *Evaluation of Geosynthetic Reinforced Flexible Pavement Systems Using Two Pavement Test Facilities*, U.S. Department of Transportation, Federal Highway Administration, Washington, DC, Report No. FHWA/MT-02-008/20040, 120 p.

Perkins, S.W. and Edens, M.Q. (2002), "Finite Element and Distress Models for Geosynthetic-Reinforced Pavements", *International Journal of Pavement Engineering*, Vol. 3, No. 4, NCHRP 1-37A Design, pp. 239-250.

Perkins, S.W. (1999), *Geosynthetic Reinforcement of Flexible Pavements: Laboratory Based Pavement Test Sections*, Montana Department of Transportation, Helena, Montana, Report No. FHWA/MT-99/8106-1, 140 p.

Perkins, S.W. and Cuelho, E.V. (1999) "Soil-Geosynthetic Interface Strength and Stiffness Relationships From Pullout Tests", *Geosynthetics International*, V. 6, No. 5, pp. 321-346.

Raumann, G. (1979), "A Hydraulic Tensile test with Zero Transverse Strain for Geotechnical Fabrics", *Geotechnical Testing Journal*, Vol. 2, No.2, pp. 69-76.

Schwartz, C.W. (2003), "Effect of Stress-Dependent Base Layer Behavior on the Superposition of Two-Dimensional Flexible Pavement Solutions", *International Journal of Geomechanics,* Vol. 2, No. 3, pp. 331-352.

Skoglund, K.A. (2002), *A Study of Some Factors in Mechanistic Railway Track Design*, Ph.D. Thesis, NTNU, Trondheim, Norway, March.

Soong, T.Y. and Lord, A.E. (1998), "Slow Strain Rate Modulus Assessment Via Stress Relaxation Experiments", *Proceedings: Sixth International Conference on Geosynthetics*, Denver, CO, pp. 711-715.

Soong, T.Y., Lord, A.E. and Koerner, R.M. (1994),"Stress Relaxation Behavior of HDPE Geomembranes", *Proceedings of the Fifth International Conference on Geotextiles, Geomembranes and Related Products*, Singapore, pp. 1121-1124.

Tseng, K. and Lytton, R. (1989), "Prediction of Permanent Deformation in Flexible Pavement Materials", ASTM STP 1016, pp. 154-172.

Tsuboi, M., Imaizumi, S. and Miyaji, H. (1998), "Effect of the temperature on Tensile Behavior of Geomembranes", *Proceedings: Sixth International Conference on Geosynthetics*, Denver, CO, 1998, pp. 201-204.

Van Zanten, (1986), "Geotextiles and Geomembranes in Civil Engineering", A.A. Balkema.

Yau, A.Y.Y. (1999), "Plasticity Characterization of Unbound Pavement Materials," unpublished Master of Science thesis, Department of Civil and Environmental Engineering, University of Maryland, College Park, MD.

14.0 APPENDIX A: UMAT FOR ISOTROPIC NON LINEAR ELASTIC WITH TENSION CUTOFF MATERIAL MODEL

```
      SUBROUTINE UMAT(STRESS,RWPTA,DDSDDE,SSE,SPD,SCD,
     1  RPL,DDSDDT,DRPLDE,DRPLDT,
     2  STRAN,DSTRAN,TIME,DTIME,TEMP,DTEMP,PREDEF,DPRED,CMNAME,
     3  NDI,NSHR,NTENS,NSTATV,PROPS,NPROPS,COORDS,DROT,PNEWDT,
     4  CELENT,DFGRD0,DFGRD1,IEL,NPT,LAYER,KSPT,KSTEP,KINC)
C
      INCLUDE 'ABA_PARAM.INC'
C
C
C  PURE INCREMENTAL VERSION, NO EQUILIBRIUM CHECK
C
C  ISOTROPIC
C
C  CUT ONLY THE ACTUAL TENSILE PRINCIPAL STRESS COMPONENTS
C  THE VARIABLE <<METHOD = 0>>
C
C     user routine name INC_ISO_CUT0_UMAT.for
C
C
      CHARACTER*80 CMNAME
      DIMENSION STRESS(NTENS),RWPTA(NSTATV),
     1  DDSDDE (NTENS,NTENS),
     2  DDSDDT(NTENS), DRPLDE(NTENS),
     3  STRAN(NTENS),DSTRAN(NTENS),TIME(2),PREDEF(1),DPRED(1),
     4  PROPS(NPROPS),COORDS(3),DROT(3,3),DFGRD0(3,3),DFGRD1(3,3)
C
      DIMENSION DT(6,6),DTP(4,4),CC(6,6),CCP(4,4)
      DIMENSION STRESP(6) , STRAIN(6), EPSINC(6) ,DMDSTM(6)
      DIMENSION SDEV(6),SDEV0(6),DSTRES(6),SI(6),PS(3),AN(3,3)
      DIMENSION STREST(6)
      DIMENSION ISGND(7), NINTPT(2),NINTPD(2)
      DIMENSION RMDIFF(2),RMMADF(2),RMPROC(2),RMMAPR(2)
      DIMENSION KELD(2),KELP(2)
            DIMENSION SMODTR(2),SMODUS(2)
C
      CHARACTER ROUTIN*6
C
      DIMENSION SIGA(3)
      LOGICAL EXTREM,SOLVED
      PARAMETER (SMALL=1.0D-8)
      PARAMETER (TOLER=1.0D-8)
      PARAMETER (TOLERM=1.0D-8)
      PARAMETER (ZERO=0.0D0 , HALF=0.5D0 , ONE=1.0D0 , TWO=2.0D0)
      PARAMETER (THREE=3.0D0)
      PARAMETER (THTMX=0.01D0)
C
      DATA ROUTIN/'AASHT4'/
      DATA ISGND / 1 , 1 , 1 , -1 , 1 , 1 , 1/
      DATA IFILOP /0/
      DATA IFILO2 /0/
      DATA IEL1, NPT1, LAYERS / 0,0,1/
      DATA ITERN /0/
      DATA KSTEP0, KINC0 /0,0/
      DATA METHOD /0/
      DATA INPTST,INPTS2 / 1 , 1 /
      DATA LSTFND /0/
      DATA NINTPT /0,0/
      DATA NINTPD /0,0/
            DATA ICOWRI /0/
            SAVE ICOWRI
      SAVE IFILOP
      SAVE IFILO2
      SAVE IEL1,NPT1,IELLST,NPTLST,LSTFND
      SAVE ITERN, KSTEP0, KINC0
```

```
      SAVE INPTST , INPTS2, LAYERS
      SAVE RK11,RK1PRE,RK1LST
      SAVE RMDIFF,RMMADF,RMPROC,RMMAPR
      SAVE KELD,KELP
            SAVE SMODTR,SMODUS
C
      TTIME=TIME(2)+DTIME
      STIME=TIME(1)+DTIME
      THETAC=STRESS(1)+STRESS(2)+STRESS(3)
      SOLVED = .FALSE.
      IF (NDI.LT.3) THEN
        WRITE(6,1212)ROUTIN
        STOP
      ENDIF
 1212 FORMAT(///'ERROR RETURN FROM UMAT',
     +   /,' Material routine ',A5,' not implemented for'
     +   /, ' less than 3 normal stresses',////)
C
C
C      ENTRY SECTION
C
C
      NPARS=6
C
C -- CHECK OF INPUT
C
      IF (INPTST.EQ.1   .and.  NPROPS.LT.5) THEN
         WRITE(6,1010)
         STOP
      ENDIF
 1010 FORMAT(///'**************************************************',
     +        /'*                                                *',
     +        /'*   TOO FEW INPUT PARAMETERS FOR UMAT            *',
     +        /'*   MINIMUM: 5 parameters                        *',
     +        /'*                                                *',
     +        /'**************************************************')
      RK1   = PROPS(1)
      RK2   = PROPS(2)
      RK3   = PROPS(3)
      PAAA  = PROPS(4)
      RNU   = PROPS(5)
C
C     EPTOET= PROPS(5)
C     GTTOET= PROPS(6)
C     RNUTP = PROPS(7)
C     RNUP  = PROPS(8)
C
      P_MIN = 0.01D0
      IF (NPROPS.GT.5)  P_MIN = PROPS(6)
      IF (DABS(P_MIN).LT.0.0001D0) P_MIN=0.01D0
C
      IF ( DABS(RK1-RK1PRE).GT.0.2D0  .AND.   INPTST.EQ.0
     +             .AND.INPTS2.EQ.1 )  THEN
          INPTS2=0
          INPTST=1
          LAYERS=2
      ENDIF
      RK1PRE=RK1
      IF (INPTST.EQ.1) THEN
       WRITE(6,1020)RK1,RK2,RK3,PAAA,RNU,P_MIN
 1020   FORMAT(///'**************************************************',
     +        /'*                                                *',
     +        /'*   MATERIAL MODEL INC_ISO_CUT0_UMAT             *',
     +        /'*                                                *',
     +        /'*   ABAQUS WILL BE RUN FOR THE FOLLOWING UMAT    *',
     +        /'*   INPUT PARAMETERS:                            *',
     +        /'*     K1    =',F11.3,'                           *',
     +        /'*     K2    =',F11.3,'                           *',
     +        /'*     K3    =',F11.3,'                           *',
     +        /'*     Pa    =',F11.3,'                           *',
```

```
   +        /'*     nu    =',F11.3,'  (Poissons ratio)      *',
   +        /'*     p_min =',F11.3,'  (tensile strength)    *')
 1024   FORMAT( '*                                          *',
   +        /'**************************************************')
 1022   FORMAT( '*                                          *',
   +        /'*     Monitor elements:                       *')
 1023   FORMAT( '*                  ',  I8,'                 *')
      IF (NPROPS.GT.NPARS) THEN
        WRITE(6,1022)
        DO 45 I=NPARS+1,NPROPS
  45       WRITE(6,1023) NINT(PROPS(I))
      ENDIF
      WRITE(6,1024)
      IF (RNU.GE.0.4999D0  .OR.  RNU.LT.ZERO) THEN
        WRITE(6,1030)
        STOP
      ENDIF
 1030 FORMAT(///'**************************************************',
   +        /'*                                          *',
   +        /'*   ILLEGAL POSSIONS RATIO                     *',
   +        /'*   Legal: 0 <= nu < 0.5                    *',
   +        /'*                                          *',
   +        /'**************************************************')
     ENDIF
     INPTST=0
C
     RNUP  = RNU
     EPTOET= 1.0D0
     GTTOET= 1.0D0 / (TWO*(ONE+RNUP))
     RNUTP = RNUP
     RNUPT = EPTOET*RNUTP
C
C -- THETA must remain a compressive stress,
C     in ABAQUS this means it must remain negative.
C     It is tested against THTMAX = 1 kPa
C
     THTMAX = -THTMX*PAAA
C
     RKW=ZERO
     NPAR=7
     ITR=0
C
C -- Define iteration number ITERN
C
     IF (KINC.NE.KINC0 .OR. KSTEP.NE.KSTEP0) THEN
        ITERN=1
             ICOWRI=2
     ELSEIF(IEL.EQ.IEL1  .AND.  NPT.EQ.NPT1
    +            .AND. DABS(RK11-RK1).LT.0.01D0 ) THEN
        ITERN=ITERN+1
        LSTFND=1
     ENDIF
     KSTEP0=KSTEP
     KINC0=KINC

     IF (KINC.EQ.1  .AND.   KSTEP.EQ.1 .AND.IEL1.EQ.0) THEN
       IEL1=IEL
            ICOWRI=1
       NPT1=NPT
       RK11=RK1
     ENDIF
     IF (LSTFND .EQ. 0) THEN
       IELLST = IEL
       NPTLST = NPT
       RK1LST = RK1
     ENDIF
C
C
C     MR = RK1*PAAA*(3*sig_mean/PAAA)^RK2 *(TAUoct/PAAA)^RK3
C     RNY = POISSONS RATIO
```

```
C
C FOR    A B A Q U S
C
C    INSERT STRESSES
C
      DO 30 I=1,6
      STRAIN(I)=0.0
            EPSINC(I)=0.0
   30 STRESP(I)=0.0
C
       STRESP(1)=STRESS(1)
       STRESP(2)=STRESS(2)
       STRESP(3)=STRESS(3)
       STRAIN(1)=STRAN(1)
       STRAIN(2)=STRAN(2)
       STRAIN(3)=STRAN(3)
       EPSINC(1)=DSTRAN(1)
       EPSINC(2)=DSTRAN(2)
       EPSINC(3)=DSTRAN(3)
      IF (NSHR.EQ.3) THEN
       STRESP(4)=STRESS(NDI+1)
       STRESP(5)=STRESS(NDI+2)
       STRESP(6)=STRESS(NDI+3)
       STRAIN(4)=STRAN(NDI+1)
       STRAIN(5)=STRAN(NDI+2)
       STRAIN(6)=STRAN(NDI+3)
       EPSINC(4)=DSTRAN(NDI+1)
       EPSINC(5)=DSTRAN(NDI+2)
       EPSINC(6)=DSTRAN(NDI+3)
      ELSE
       STRESP(4)=STRESS(NDI+1)
       STRAIN(4)=STRAN(NDI+1)
       EPSINC(4)=DSTRAN(NDI+1)
      ENDIF
C
      IF (KINC.EQ.1  .AND.   KSTEP.EQ.1) THEN
        DO 5 I=1,6
    5   SI(I)=STRESP(I)
      ELSE
        DO 6 I=1,6
    6   SI(I)=RWPTA(I)
      ENDIF
C
      PMEAN0 = (SI(1)+SI(2)+SI(3))/3.0D0
      SDEV0(1)=SI(1)-PMEAN0
      SDEV0(2)=SI(2)-PMEAN0
      SDEV0(3)=SI(3)-PMEAN0
      SDEV0(4)=SI(4)
      SDEV0(5)=SI(5)
      SDEV0(6)=SI(6)
      TAUOC0=SDEV0(1)**2 + SDEV0(2)**2 + SDEV0(3)**2+
     +      2*( SDEV0(4)**2 + SDEV0(5)**2 + SDEV0(6)**2 )
      TAUOC0=SQRT(TAUOC0/3.0D0)
C .
C . Minimum stiffness
C
      THTMIN = 3*PMEAN0
C     RMRMIN = RK1*PAAA*(-THTMIN/PAAA)**RK2*(TAUOC0/PAAA+1.0D0)**RK3
            RMRMIN = 100.0

C
      PMEAN = (STRESP(1)+STRESP(2)+STRESP(3))/3.0D0
      SDEV(1)=STRESP(1)-PMEAN
      SDEV(2)=STRESP(2)-PMEAN
      SDEV(3)=STRESP(3)-PMEAN
      SDEV(4)=STRESP(4)
      SDEV(5)=STRESP(5)
      SDEV(6)=STRESP(6)
      TAUOCT=SDEV(1)**2 + SDEV(2)**2 + SDEV(3)**2+
     +      2*( SDEV(4)**2 + SDEV(5)**2 + SDEV(6)**2 )
```

```
      TAUOCT=SQRT(TAUOCT/3.0D0)
              THETA=3*PMEAN
              IF (THETA .GT. THTMAX) THEN
                THETA=THTMAX
              ENDIF
      RMR = RK1*PAAA*(-THETA/PAAA)**RK2*(TAUOCT/PAAA+1.0D0)**RK3
              IF (RMR.LT.RMRMIN) RMR=RMRMIN
C
C

C     ELEMENTS TO THE ELASTIC CONSTITUTIVE TENSOR
C
C ------------------------------
C For Unit Stiffness
C ------------------------------

      ET = 1.0D0
      EP = ET*EPTOET
      GT = ET*GTTOET
      GP = EP/(2*(1+RNUP))
      DO 230 I=1,6
      DSTRES(I)=ZERO
      DO 230 J=1,6
  230 DT(I,J)=ZERO
C
C
      IF (NSHR.EQ.3) THEN
C
C .. The model is developed for cross anisotropic elasticity
C    and the general expressions are used,
C    but for isotropic elasticity the parameters are set so
C    as to give isotropic elasticity
C
C .. The following sequence in full 3D ::
C
C   s_11    S_22     S_33     S_12  S_13  S_23
C   plane  plane  transverse
C
C
      DT(1,1)=EP*(ONE-RNUTP*RNUPT)/((1+RNUP)*(ONE-RNUP-2*RNUTP*RNUPT))
      DT(1,2)=EP*(RNUP+RNUTP*RNUPT)/((1+RNUP)*(ONE-RNUP-2*RNUTP*RNUPT))
      DT(1,3)=EP*RNUTP/(ONE-RNUP-2*RNUTP*RNUPT)
      DT(2,1)=DT(1,2)
      DT(2,2)=DT(1,1)
      DT(2,3)=DT(1,3)
      DT(3,1)=ET*RNUPT/(ONE-RNUP-2*RNUTP*RNUPT)
      DT(3,2)=DT(3,1)
      DT(3,3)=ET*(ONE-RNUP)/(ONE-RNUP-2*RNUTP*RNUPT)
      DT(4,4)=GP
      DT(5,5)=GT
      DT(6,6)=GT
      ENDIF
C
      IF (NSHR.EQ.1) THEN
C
C .. The following sequence in PLANE STRAIN
C
C    s_11      S_22     S_33     S_12
C   plane  transverse    plane
C
C
C
      DT(1,1)=EP*(ONE-RNUTP*RNUPT)/((1+RNUP)*(ONE-RNUP-2*RNUTP*RNUPT))
      DT(1,2)=EP*RNUTP/(ONE-RNUP-2*RNUTP*RNUPT)
      DT(1,3)=EP*(RNUP+RNUTP*RNUPT)/((1+RNUP)*(ONE-RNUP-2*RNUTP*RNUPT))
      DT(2,1)=DT(1,2)
      DT(2,2)=ET*(ONE-RNUP)/(ONE-RNUP-2*RNUTP*RNUPT)
      DT(2,3)=ET*RNUPT/(ONE-RNUP-2*RNUTP*RNUPT)
      DT(3,1)=DT(1,3)
      DT(3,2)=DT(2,3)
```

```
      DT(3,3)=DT(1,1)
      DT(4,4)=GT
      ENDIF
C
C
C IF STRAIN=0.0 SKIP TANGENT STIFFNESS CALC
C
      ISKIP = 1
      DO 40 I=1,6
      IF (STRAIN(I).GT.SMALL  .OR.
     +    STRAIN(I).LT.-SMALL) ISKIP=0
   40 CONTINUE
      IF (ISKIP.EQ.1)GOTO 7500
C
C
C  .. CALC OF QUASI TANGENT RMR; COMPRESSION POSITIVE
C
 6900 THETA=3*PMEAN
            IF (THETA .GT. THTMAX) THEN
              THETA=THTMAX
            ENDIF
      RMR = RK1*PAAA*(-THETA/PAAA)**RK2*(TAUOCT/PAAA+1.0D0)**RK3
      THETA = -THETA
      SIGAA = THETA/THREE+SQRT(TWO)*TAUOCT
      SIGRR = THETA/THREE-SQRT(TWO)*TAUOCT/TWO
      SIGA0 = -SI(3)
            IF (NSHR.EQ.1) SIGA0 = -SI(2)
      SIGR0 = -SI(1)
      EPSAA = (SIGAA-SIGA0-RNUPT*2*(SIGRR-SIGR0))/RMR
C
C
      COMPLI = RK2/THETA + SQRT(2.0)*RK3/ (3.0*(TAUOCT+PAAA))
            COMPLI = 1/RMR - EPSAA*COMPLI
C
      RMR  = ONE/COMPLI
            IF (RMR.LT.RMRMIN) RMR=RMRMIN
C
C
C
 7500 ET = RMR
      EP = ET*EPTOET
      GT = ET*GTTOET
      GP = EP/(2*(1+RNUP))
C
C
 7000 CONTINUE
C
C -- END OF STIFFNESS CALCULATION FOR CURRENT STRESS
C
C  ----------------------------------
C
C  Compute incremental stress
C
C  ----------------------------------
C

      DO 240 I=1,3
              DSTRES(I+3)=DT(I+3,I+3)*EPSINC(I+3)*RMR
      DO 240 J=1,3
  240   DSTRES(I)=DSTRES(I)+DT(I,J)*EPSINC(J)*RMR
C
CC    ENDIF
C
C
            NPSTNS=0  ! Number of tensile principal stresses
      DO 205 I=1,6
  205 STRESP(I)=STRESP(I)+DSTRES(I)
C
C
      DO 550 I=1,6
```

```
 550 STREST(I)=STRESP(I)
C
C -- Check if tension is violated
C
      IF ((PMEAN + 1.414213*TAUOCT) .LT. P_MIN ) GOTO 190
C
     CALL CTTENS(STRESP,PS,AN,P_MIN,METHOD,NDI,NSHR,NPSTNS)
C
CCCCCCCCCCCCCCCCCCCCCCCCCCCCCCCCCCCCCCCCCCCCCCCCCCCCCCC
C
 190 CONTINUE
C
C .. Compute new invariants
C
        PMEAN = (STRESP(1)+STRESP(2)+STRESP(3))/THREE
        SDEV(1)=STRESP(1)-PMEAN
        SDEV(2)=STRESP(2)-PMEAN
        SDEV(3)=STRESP(3)-PMEAN
        SDEV(4)=STRESP(4)
        SDEV(5)=STRESP(5)
        SDEV(6)=STRESP(6)
        TAUOCT=SDEV(1)**2 + SDEV(2)**2 + SDEV(3)**2+
    +        2*( SDEV(4)**2 + SDEV(5)**2 + SDEV(6)**2 )
        TAUOCT=SQRT(TAUOCT/3.0D0)
             THETA = 3*PMEAN
             IF (THETA .GT. THTMAX) THEN
               THETA=THTMAX
             ENDIF
     RMRNEW = RK1*PAAA*(-THETA/PAAA)**RK2*(TAUOCT/PAAA+1.0D0)**RK3
C -- It was found that the soultion was unstable
C    if RMRNEW was used, so it was not used.
C
C    The stiffness is based on conditions at beginning
C    of the loadstep
C
C
C
C -- INSERT INTO  ABAQUS STRESS AND JACOBI
C
C
C
       DO 340 I=1,NTENS
              STRESS(I)=STRESP(I)
       DO 340 J=1,NTENS
 340       DDSDDE(I,J)=DT(I,J)*RMR
C
C

       NPRT=0
       IF (NPROPS.GT.NPARS) THEN
         DO 677 I=NPARS+1,NPROPS
           IF(NINT(PROPS(I)).EQ.IEL) NPRT=1
 677       CONTINUE
       ENDIF
      IF ((NPRT.EQ.1.AND.NPSTNS.GT.0).or. NPSTNS.EQ. 3) THEN
        WRITE(6,*)'Before tension cut-off'
        WRITE(6,1243)STREST,TTIME,IEL,NPT,ITERN
        CALL SPRIND(STREST,PS,AN,LSTR,NDI,NSHR)
        WRITE(6,1245)'Princ.stress & direction',PS(1),(AN(1,I),I=1,3)
        WRITE(6,1245)'Princ.stress & direction',PS(2),(AN(2,I),I=1,3)
        WRITE(6,1245)'Princ.stress & direction',PS(3),(AN(3,I),I=1,3)
        WRITE(6,*)'After tension cut-off'
        IF(NPSTNS.EQ.3) THEN
          DO 680 I=1,3
            AN(I,1)=ZERO
            AN(I,2)=ZERO
            AN(I,3)=ZERO
            AN(I,I)=ONE
            PS(I)=P_MIN
 680       CONTINUE
```

```
        ELSE
          CALL SPRIND(STRESP,PS,AN,LSTR,NDI,NSHR)
        ENDIF
        WRITE(6,1244)STRESP,RMR
        WRITE(6,1245)'Princ.stress & direction',PS(1),(AN(1,I),I=1,3)
        WRITE(6,1245)'Princ.stress & direction',PS(2),(AN(2,I),I=1,3)
        WRITE(6,1245)'Princ.stress & direction',PS(3),(AN(3,I),I=1,3)
              CALL PRINC(STRESP,SIG1,SIG2,SIG3)
           WRITE (6,1244)SIG1,SIG2,SIG3
        WRITE(6,*)'a'
       ENDIF
 1243 FORMAT(7F11.4,/'El.No ',I5,'Int.pt ',I5,' Iter.No ',I5)
 1244 FORMAT(6F11.4,F10.1)
 1245 FORMAT(A,F11.4,3F10.6)
      IF (NPSTNS.EQ.3) THEN
        WRITE(6,'(a,I3/)')'All stresses in tension, Element No ',IEL
CCC         STOP
      ENDIF
C
C -------------------------------------------------
C        UPDATING THE INTEGRATION POINT WORK ARRAY
C -------------------------------------------------
C
      DO 360 I=1,6
  360 RWPTA(I)=SI(I)
CCC test    WRITE(6,*)'ElNr= ',IEL,' mod ',RMR
C
      RETURN
      END
      SUBROUTINE TINVM(A,B,N,EPS,REGUL)
      IMPLICIT DOUBLE PRECISION (A-H,O-Z)
      DIMENSION A(N,N),B(N,N)
      LOGICAL REGUL
      DIMENSION IPERM(200)
      CALL TTRIM(A,IPERM,N,EPS,REGUL)
      IF(.NOT.REGUL) GO TO 99
      IF (N-1) 99,2,3
    3 CONTINUE
      N1=N-1
      DO 1 I=1,N1
      B(I,I)=1.0
      J=I+1
      DO 1 K=J,N
      B(I,K)=0.0
    1 B(K,I)=0.0
    2 B(N,N)=1.0
      CALL TTRIEM(A,B,IPERM,N,N)
   99 RETURN
      END
      SUBROUTINE TTRIEM(A,H,IPERM,N,M)
      IMPLICIT DOUBLE PRECISION (A-H,O-Z)
      DIMENSION A(N,N),H(N,M)
      DIMENSION IPERM(N)
      IF (N-1) 8,7,9
    9 CONTINUE
      N1=N-1
      DO 2 I=1,N1
      J=IPERM(I)
      IF(J-I)2,2,10
   10 CONTINUE
      DO 1 K=1,M
      E=H(I,K)
      H(I,K)=H(J,K)
    1 H(J,K)=E
    2 CONTINUE
      DO 6 K=1,M
      H(1,K)=H(1,K)/A(1,1)
      DO 4 I=2,N
      J=I-1
      D=H(I,K)
```

```
      DO 3 L=1,J
    3 D=D-A(I,L)*H(L,K)
      F=D
    4 H(I,K)=F/A(I,I)
      DO 6 N2=1,N1,1
      I=N1+1-N2
      J=I+1
      D=H(I,K)
      DO 5 L=J,N
    5 D=D-A(I,L)*H(L,K)
    6 H(I,K)=D
      GO TO 8
    7 H(1,1)=H(1,1)/A(1,1)
    8 RETURN
      END
      SUBROUTINE  TTRIM(A,IPERM,N,EPS,REGUL)
      IMPLICIT DOUBLE PRECISION (A-H,O-Z)
      DIMENSION A(N,N)
      DIMENSION SKALER(200),B(200)
      DIMENSION IPERM(N)
      LOGICAL REGUL
      IF(N.LE.1) GO TO 100
      DO 2 I=1,N
      E=0.0
      DO 1 J=1,N
    1 E=E+A(I,J)*A(I,J)
      IF(E.LE.0.) GO TO 99
    2 SKALER(I)=1/SQRT(E)
      J=1
      E=SKALER(1)*DABS(A(1,1))
      DO 3 I=2,N
      F=SKALER(I)*DABS(A(I,1))
      IF(F.LE.E) GO TO 3
      E=F
      J=1
    3 CONTINUE
      IF(E.LE.0.) GO TO 99
      IF(J.LE.1) GO TO 5
      E=SKALER(1)
      SKALER(1)=SKALER(J)
      SKALER(J)=E
      DO 4 I=1,N
      E=A(J,I)
      A(J,I)=A(1,I)
    4 A(1,I)=E
    5 IPERM(1)=J
      E=A(1,1)
      DO 101 I=2,N
  101 A(1,I)=A(1,I)/E
      N1=N-1
      IF(N.EQ.2) GO TO 14
      DO 12 I=2,N1
      J1=I-1
      E=0.0
      DO 7 J=I,N
      D=A(J,I)
      DO 6 K=1,J1
    6 D=D-A(J,K)*A(K,I)
      B(J)=D
      F=DABS(B(J))*SKALER(J)
      IF(F.LE.E) GO TO 7
      E=F
      M=J
    7 CONTINUE
      F=SKALER(M)*DABS(A(M,I))*EPS
      IF(E.LE.F) GO TO 99
      DO 8 J=I,N
    8 A(J,I)=B(J)
      IF(M.LE.I) GO TO 10
      E=SKALER(I)
```

```
      SKALER(I)=SKALER(M)
      SKALER(M)=E
      DO 9 J=1,N
      E=A(M,J)
      A(M,J)=A(I,J)
    9 A(I,J)=E
   10 IPERM(I)=M
      K1=I+1
      E=A(I,I)
      DO 12 J=K1,N
      D=A(I,J)
      DO 11 K=1,J1
   11 D=D-A(I,K)*A(K,J)
      F=D
   12 A(I,J)=F/E
   14 D=A(N,N)
      DO 13 K=1,N1
   13 D=D-A(N,K)*A(K,N)
      B(N)=D
      E=DABS(B(N))
      F=DABS(A(N,N))*EPS
      IF(E.LE.F) GO TO 99
      A(N,N)=B(N)
      REGUL=.TRUE.
      GO TO 100
   99 REGUL=.FALSE.
  100 RETURN
      END
      SUBROUTINE TMCON(T,B,C,M,N)
C
C .. USE STATMAT ROUTINNE     MCON
C    USAGE :
C                                       T
C          MCON(T,B,C,M,N) : RESULT    C = T * B * T
C
C                                   T (1:M,1:N)
C                                   B (1:M,1:M)
C                                   C (1:N,1:N)
C
      IMPLICIT DOUBLE PRECISION (A-H,O-Z)
      DIMENSION T(M,N),B(M,M),C(N,N),E(20)
      IF(M.LE.20) GOTO 10
      WRITE(6,1000) M
1000  FORMAT(//
     +' ARRAY  <E> IN ROUTINE MCON MUST BE EXTENDED TO E(',I3,')')
      STOP
10    CONTINUE
      DO 4 K=1,N
      DO 2 L=1,M
      D=B(L,1)*T(1,K)
      DO 1 J=2,M
    1 D=D+B(L,J)*T(J,K)
    2 E(L)=D
      DO 4 L=K,N
      D=T(1,L)*E(1)
      DO 3 J=2,M
    3 D=D+T(J,L)*E(J)
      C(L,K)=D
    4 C(K,L)=D
      RETURN
      END
C
      SUBROUTINE PRINC(STRESP,SIG1,SIG2,SIG3)
C
      INCLUDE 'ABA_PARAM.INC'
      DIMENSION STRESP(6),SIGA(3)
      LOGICAL EXTREM
      FX(SIG,RI,RII,RIII)=SIG**3-RI*SIG*SIG+RII*SIG-RIII
      DFDX(SIG,RI,RII)=3*SIG**2-2*RI*SIG+RII
      PARAMETER (SMALL=1.0D-14)
```

```
      PARAMETER (TOLER=1.0D-8)
      PARAMETER (TOLERM=1.0D-8)
      PARAMETER (ZERO=0.0D0 , HALF=0.5D0 , ONE=1.0D0 , TWO=2.0D0)
      PARAMETER (THREE=3.0D0)
      EXTREM=.FALSE.
CCCCCCCCCCCCCCCCCCCCCCCCCCCCCCCCCCCCCCCCCCCCCCCCCCCCCCCCCCCCC
C                                                            C
C BEGIN PROGRAM SEQUENCE FOR CALCULATION OF PRINCIPAL STRESSES  C
C                                                            C
C ( THIS SEQUENCE WILL BE REPLACED BY CALLS TO STANDARD        C
C   ABAQUS FUNCTIONS)                                        C
C                                                            C
CCCCCCCCCCCCCCCCCCCCCCCCCCCCCCCCCCCCCCCCCCCCCCCCCCCCCCCCCCCCC
C
C  . INPUT: "Stress vector" STRESP
C  - OUTPUT: PRINCIPAL STRESSES, SIG1, SIG2, SIG3
C
C
C
C .. Find the invariants:
C
C
C
C -BEGIN--ABAQUS STRESS SEQUENCE
      S11 = STRESP(1)         !
      S22 = STRESP(2)         !
      S33 = STRESP(3)         !
      S12 = STRESP(4)         !
      S13 = STRESP(5)         !
      S23 = STRESP(6)         !
C -END----ABAQUS STRESS SEQUENCE
C
C
C -BEGIN--GEOnac STRESS SEQUENCE
CC    S11 = STRESP(1)         !
CC    S22 = STRESP(2)         !
CC    S33 = STRESP(3)         !
CC    S12 = STRESP(4)         !
CC    S23 = STRESP(5)         !
CC    S13 = STRESP(6)         !
C -END----GEOnac STRESS SEQUENCE
C
      RI = S11+S22+S33
      RII= S12**2 + S23**2 + S13**2
      RII = S11**2 + S22**2 + S33**2 + 2*RII
      RII = (RI*RI-RII)/2.0
      RIII=S11*S22*S33
      RIII=RIII - S11*S23*S23 - S22*S13*S13 - S33*S12*S12
      RIII=RIII + 2*S12*S23*S13
      IF (DABS(RI) .LT. SMALL  .AND.
     +    DABS(RII) .LT. SMALL .AND.
     +    DABS(RIII) .LT. SMALL) THEN
            SIG1=ZERO
            SIG2=ZERO
            SIG3=ZERO
            GOTO 310
      ENDIF
      S11D = S11 - RI/3
      S22D = S22 - RI/3
      S33D = S33 - RI/3
      RIID= S12**2 + S23**2 + S13**2
      RIID = S11D**2 + S22D**2 + S33D**2 + 2*RIID
      RIID = RIID/2.0
      SIGCHR=SQRT(RIID)
      IF (SIGCHR .LT. SMALL) SIGCHR = 0.00001D0
      IF (DABS(RIII).LT.SMALL) THEN
            SIGA(3)=ZERO
            ROOTI=RI*RI-4*RII
            IF (ROOTI.LT.-SMALL)THEN
              SIGA(1)=1/SMALL
```

```
                SIGA(2)=1/SMALL
         ELSE
                IF (ROOTI.LT.ZERO)ROOTI=ZERO
                SIGA(1) = (RI+SQRT(ROOTI))/2
                SIGA(2) = (RI-SQRT(ROOTI))/2
         ENDIF
               GOTO 300
      ENDIF
C
C
C -- Determine the extremal points
C
      ROOTI = 4*RI*RI-12*RII
      IF (ROOTI.GT.-SMALL) THEN
        EXTREM = .TRUE.
              IF (ROOTI.LT.ZERO) ROOTI=ZERO
              EXT1=(2*RI-SQRT(ROOTI))/6
              EXT2=(2*RI+SQRT(ROOTI))/6
      ELSE
              EXTREM = .FALSE.
      ENDIF
C
C -- VENDETANGENT
C
      VEND = RI/3
      IF (.NOT.EXTREM) THEN
              EXT1=VEND
              EXT2=VEND
      ENDIF
C
C .. test to see if root at extremals
C
      SIGA(3)=EXT1
      YY = FX(EXT1,RI,RII,RIII)
      IF (DABS(YY).LT.SMALL) GOTO 130
      SIGA(3)=EXT2
      YY = FX(EXT2,RI,RII,RIII)
      IF (DABS(YY).LT.SMALL) GOTO 130
C
C -- see if
              IF (FX(EXT1,RI,RII,RIII).GT.ZERO) THEN
                SIG=EXT1
                ISIG3=1
                DO 10 I=1,1000
                 SIG=SIG-SIGCHR
                 IF  (FX(SIG,RI,RII,RIII).LT.ZERO) GOTO 11
  10      CONTINUE
  11      CONTINUE
         ELSE
                SIG=EXT2
                ISIG3=-1
                DO 20 I=1,1000
                 SIG=SIG+SIGCHR
                 IF  (FX(SIG,RI,RII,RIII).GT.ZERO) GOTO 21
  20      CONTINUE
  21      CONTINUE
              ENDIF
C
C -- SEARCH FIRST ROOT
C
      DO 100 I=1,1000
              SIGA(3) = SIG - FX(SIG,RI,RII,RIII)/DFDX(SIG,RI,RII)
              IF (I.LT.5)GOTO 99
              IF ( DABS(SIGA(3)-SIG) .LT. SIGCHR*SMALL) GOTO 110
  99   SIG=SIGA(3)
 100 CONTINUE
 110 CONTINUE
C
 130 ROOTI = (RI-SIGA(3))**2-4*RIII/SIGA(3)
      IF (ROOTI.GT.-TOLER*SIGCHR) THEN
```

```
           IF (ROOTI .LT. ZERO) ROOTI = ZERO
           SIGA(1)=(RI-SIGA(3)+SQRT(ROOTI))/2
           SIGA(2)=(RI-SIGA(3)-SQRT(ROOTI))/2
      ELSE
           SIGA(1)=1/SMALL
           SIGA(2)=1/SMALL
      ENDIF
  300 I1=1
      I2=1
      I3=1
      IF (SIGA(2).LT.SIGA(I1)) I1=2
      IF (SIGA(3).LT.SIGA(I1)) I1=3
      IF (SIGA(2).GT.SIGA(I3)) I3=2
      IF (SIGA(3).GT.SIGA(I3)) I3=3
      IF (I2.EQ.I1 .OR. I2.EQ.I3)I2=2
      IF (I2.EQ.I1 .OR. I2.EQ.I3)I2=3
      SIG1=SIGA(I3)
      SIG2=SIGA(I2)
      SIG3=SIGA(I1)
  310 CONTINUE
      END
C
C
C
      SUBROUTINE CTTENS(STRESP,PS,AN,P_MIN,METHOD,NDI,NSHR,NPSTNS)
C
C -- ROUTINE FOR CUTTING TENSION
C
      INCLUDE 'ABA_PARAM.INC'
      DIMENSION STRESP(6),PS(3),AN(3,3)
      DIMENSION TT(3,3),TCUTP(3,3),TCUTS(3,3)
          PARAMETER (ZERO=0.0D0)
C
C    CALL PRINC(STRESP,SIG1,SIG2,SIG3)
C -- Get the prinicpal stress PS and direction vector AN
      LSTR = 1   ! ABAQUS routine call for stresses
      CALL SPRIND(STRESP,PS,AN,LSTR,NDI,NSHR)
C
C -- NOTE: TENSION IS POSITIVE, SO MINOR PRINCIPAL STRESS
C        IN GETECHNICAL SENSE IS SIG1
C
CCCCCCCCCCCCCCCCCCCCCCCCCCCCCCCCCCCCCCCCCCCCCCCCCCCC
C                                 C
C PRINCIPAL STRESSES HAVE BEEN CALCULATED;          C
C CONTINUE WITH TENSION CHECK                       C
C                                 C
CCCCCCCCCCCCCCCCCCCCCCCCCCCCCCCCCCCCCCCCCCCCCCCCCCCC
C
C
      NPSTNS=0
C
      IF (METHOD.EQ.1) GOTO 595
C
C  VERSION FOR CUTTING ACTUAL PRINCIPAL STRESS COMPONENTS STARTS
C
      DO 560 I=1,3
        DO 560 J=1,3
 560  TCUTP(I,J)=ZERO
      DO 565 I=1,3
        IF (PS(I).GT.P_MIN) THEN
           TCUTP(I,I)=P_MIN
           NPSTNS=NPSTNS+1
        ELSE
           TCUTP(I,I)=PS(I)
        ENDIF
 565  CONTINUE
      IF (NPSTNS.GT.0) THEN
         IF(NPSTNS.LT.3) THEN
            DO 570 I=1,2
            DO 570 J=1,3
```

```
 570        TT(I,J)=AN(I,J)
          TT(3,1)=AN(1,2)*AN(2,3)-AN(1,3)*AN(2,2)
          TT(3,2)=AN(1,3)*AN(2,1)-AN(1,1)*AN(2,3)
          TT(3,3)=AN(1,1)*AN(2,2)-AN(1,2)*AN(2,1)
          N=3
          M=3
          CALL TMCON(TT,TCUTP,TCUTS,M,N)
          STRESP(1)=TCUTS(1,1)
          STRESP(2)=TCUTS(2,2)
          STRESP(3)=TCUTS(3,3)
          STRESP(4)=TCUTS(1,2)
          IF (NSHR.GT.1) THEN
            STRESP(5)=TCUTS(1,3)
            STRESP(6)=TCUTS(2,3)
          ENDIF
        ELSE
          DO 576 I=1,3
           STRESP(I)=P_MIN
           STRESP(3+I)=ZERO
 576        CONTINUE
        ENDIF
      ENDIF
C
C  VERSION FOR CUTTING ACTUAL PRINCIPAL STRESS COMPONENTS ENDS
C
C
      GOTO 605
 595  CONTINUE
C
C  VERSION FOR CUTTING MEAN STRESS STARTS
C
      SIG1=PS(1)
      IF (PS(2).GT.SIG1)SIG1=PS(2)
      IF (PS(3).GT.SIG1)SIG1=PS(3)
      IF (SIG1.LT.P_MIN) GOTO 190
C
C - MEAN STRES TENSION CUT-OFF
CCCC
      PDIFF=SIG1-P_MIN
      STRESP(1)=STRESP(1)-PDIFF
      STRESP(2)=STRESP(2)-PDIFF
      STRESP(3)=STRESP(3)-PDIFF
CCC
      NPSTNS=1
C
C  VERSION FOR CUTTING MEAN STRESS ENDS
C
 605 CONTINUE
C
 190 CONTINUE
      RETURN
      END
```

15.0 APPENDIX B: IMPLEMENTATION ACTIVITIES

This appendix contains a list of activities undertaken in this project to facilitate implementation of this work.

15.1 Liaison Activities

- The former AASHTO Subcommittee on Materials Technical Section 4E Task Group on Geogrids/Geotextiles has been disbanded and will not be reinstated. AASHTO has indicated that they will consider forming a new committee to review the results of this project for possible modification of existing standards once results are available. At the appropriate time, AASHTO should be contacted and requested to form a committee to carry out this action.
- It will be suggested to AASHTO through subcommittee A2K07(2) that a questionnaire on implementation to assist in identifying obstacles and agency needs to facilitate implementation be developed through AASHTO and circulated to state and federal transportation agencies via e-mail.
- A plan for liaison with geosynthetic manufacturers and European road agencies serving as sub-sponsors to the project has been developed. This plan describes the level of involvement of the sub-sponsor and the level of information sharing during the course of the project.
- Participation and contribution by WTI and other project team members as international observers to the European COST Transport program on Reinforcement of Pavements with Steel Meshes and Geosynthetics (REIPAS), COST-348. Financing for time and travel will be borne by the participants and not by FHWA.
- A task force as part of the ASTM Committee on Geosynthetics D35 has been established to evaluate test methods for developing property requirements for this application.

15.2 Presentations

Presentations have been made at various professional meetings (e.g., TRB, AASHTO, Regional State and Federal Highway design group meetings, Manufacuturers' association meetings). These presentations have been used to introduce the project to potential users and general interest groups so that they are aware of the project and the anticipated use of the results before completion of the work. Specific actions have included:

- A presentation package was developed for use by project team members and others desiring to present the goals and approaches of the project. The package is a short (15 to 20 minutes) general overview power point presentation of the project including the anticipated use of the results. Handouts have been prepared from the presentation.
- The presentation was given at the following venues:
  - 2002 TRB to the A2K05, A2K07 and A2K07(2) committees.
  - COST 348 committee meeting on January 24, 2002.
  - Sixth Annual Minnesota Pavement Conference, February 21, 2002.
  - Annual Meeting of the Norwegian Geotechnical Society, Trondheim, Norway, March 11, 2002
  - Joint ASCE/NAGS Workshop on Geosynthetic Reinforcement, Spokane, WA, May 3, 2002.
  - Geosynthetics 2003 Conference, Atlanta, GA, February 11, 2003.
  - Part of "Innovations in Geosynthetics in Transportation Applications", Alaska Department of Transportation, March 10-14.
  - Part of FHWA/NHI course on Geosynthetics in Transportation Engineering, Arizona and California Departments of Transportation.
- Papers have been presented at the following conferences:
  - Perkins, S.W., Cuelho, E.V., Eiksund, G., Hoff, I., Svanø, G., Watn, A., Christopher, B.R. and Schwartz, C.W. (2002) "Mechanistic-Empirical Models for Reinforced Pavements", *Proceedings of the Seventh International Conference on Geosynthetics*, Nice France, Vol. 3, pp. 951-954.
  - Eiksund, G., Hoff, I., Svanø, G., Watn, A., Cuelho, E.V., Perkins, S.W., Christopher, B.R. and Schwartz, C.S. (2002) "Material Models for Reinforced Unbound Aggregate", *Proceedings of the Sixth International Conference on the Bearing Capacity of Roads, Railways and Airfields*, Lisbon, Portugal, Vol. 1, pp. 133-143.
  - Perkins, S.W. and Watn, A. (2002) "Scandinavian and US Research and Design Experience with Geosynthetic Reinforced Flexible Pavements", *Proceedings of the*

  - *Fourth International Conference and Exhibition on Road and Airfield Pavement Technology*, Kunming China, Vol. 1, pp. 278-287.
  - Eiksund, G., Hoff, I. and Perkins, S.W. (2004) "Cyclic Triaxial Tests on Reinforced Base Course Material", Accepted for Publication, EuroGeo 3, Munich, Germany, March.
- Presentations were given at the following venues:
  - "A Roadmap for Base Reinforcement Research and Implementation", North American Geosynthetics Society (NAGS) Past President Seminar, Austin, Texas, November 7, 2002.
  - "Current Design Model Development Research", North American Geosynthetics Society (NAGS) Past President Seminar, Austin, Texas, November 7, 2002.
  - "What Do We Know About Base Reinforcement", TRB 2003 Panel Session on "Design and Performance of Base Reinforcement in Flexible Pavements", January 15, 2003.
  - "Evaluation of Base-Reinforced Pavements Using a Heavy Vehicle Simulator", Perkins, S.W. and Cortez, E.R., TRB 2004 Technical Session, January 15, 2003.

15.3 Publications

- A one-paragraph press-release article was prepared and submitted to the following trade magazines and periodicals for publication.
  - AASHTO Quarterly
  - Engineering News-Record
  - Hot-Mix Asphalt Technology
  - Public Roads
  - Public Works
  - Roads and Bridges
  - Routes and Roads
- A public-interest article was prepared and submitted to the following trade magazines and periodicals for publication:
  - FHWA Federal Focus
- A news item was published in the Western Transportation Institute Newsletter (May 2002, Issue 1, Vol. 6).
- Papers have been published as:

- Perkins, S.W., Cuelho, E.V., Eiksund, G., Hoff, I., Svanø, G., Watn, A., Christopher, B.R. and Schwartz, C.W. (2002) “Mechanistic-Empirical Models for Reinforced Pavements”, *Proceedings of the Seventh International Conference on Geosynthetics*, Nice France, Vol. 3, pp. 951-954.
- Eiksund, G., Hoff, I., Svanø, G., Watn, A., Cuelho, E.V., Perkins, S.W., Christopher, B.R. and Schwartz, C.S. (2002) “Material Models for Reinforced Unbound Aggregate”, *Proceedings of the Sixth International Conference on the Bearing Capacity of Roads, Railways and Airfields*, Lisbon, Portugal, Vol. 1, pp. 133-143.
- Perkins, S.W. and Watn, A. (2002) “Scandinavian and US Research and Design Experience with Geosynthetic Reinforced Flexible Pavements”, *Proceedings of the Fourth International Conference and Exhibition on Road and Airfield Pavement Technology*, Kunming China, 2002,Vol. 1, pp. 278-287.

- Anticipated papers for future conferences and journals include:
  - “Assessment of Interface Shear Growth from Measured Geosynthetic Strains in a Reinforced Pavement Subject to Repeated Loads”, Perkins, S.W. and Svanø, G., *Geotextiles and Geomembranes*, planned for submission.
  - “Evaluation of Base-Reinforced Pavements Using a Heavy Vehicle Simulator”, Perkins, S.W. and Cortez, E.R., *Geosynthetics International*, planned for submission.
  - “Shear Interaction Modulus from Cyclic Pullout Tests”, Cuelho, E.V., Perkins, S.W. and Christopher, B.R., *Geotextiles and Geomembranes*, planned for submission.
  - “Small Strain Tensile Modulus from Cyclic Tension Tests”, Cuelho, E.V., Perkins, S.W. and Christopher, B.R., *Geosynthetics International*, planned for submission.
  - “Geosynthetic Reinforced Large Scale Repeated Load Triaxial Tests”, Eiksund, G. and Perkins, S.W., *ASTM Geotechnical Testing Journal*, planned for submission.
  - “Equivalency of Isotropic and Orthotropic Linear Elastic Properties for Geosynthetics”, Perkins, S.W., *Geosynthetics International*, planned for submission.
  - “A Mechanistic-Empirical Model for Base-Reinforced Flexible Pavements”, Perkins, S.W., Eiksund, G., Hoff, I., Svanø, G., Watn, A., Cuelho, E.V., Christopher, B.R. and Schwartz, C.S., *Transportation Research Record, Transportation Research Board Annual Meeting*, planned for submission.

15.4 Workshops

- Two meetings/workshops were given for the sub-sponsors of the project. The first meeting took place on February 28, 2002. The second meeting took place on June 17-18, 2003.

15.5 WEB Pages

- A WEB page (http://www.coe.montana.edu/wti/wti/display.php?id=89) was developed for dissemination of information on the status of the program. The web page is part of WTI's pages. FHWA has been requested to include a link to this page from their web pages.
- A WEB page (http://www.geotek.sintef.no/georepave) was developed specifically for the sponsor and subsponsors of the project. The page contains agendas and minutes of project meetings, progress reports, presentations, implementation plans, articles and publications, agenda and minutes of project subsponsors meetings and feedback from subsponsors.